The Role of mDia1/3 Formins and the Actin Cytoskeleton in Synaptic Vesicle Endocytosis

Inaugural-Dissertation

to obtain the academic degree
Doctor rerum naturalium (Dr. rer. nat.)

submitted to the Department of Biology, Chemistry, Pharmacy
of Freie Universität Berlin

by

Britta Kristine Oevel

Berlin, March 2024

This study was conducted under the supervision of Prof. Dr. Volker Haucke from July 2018 to March 2024 at the Leibniz-Forschungsinstitut für Molekulare Pharmakologie, Berlin.

1st reviewer:	Prof. Dr. Volker Haucke
2nd reviewer:	Prof. Dr. Helge Ewers
Date of defense:	09.07.2024

So I start a revolution from my bed

'Cause you said the brains I had went to my head.

Noel Gallagher

Acknowledgements

I extend my sincere appreciation to the people who accompanied me on this doctoral journey. I express my special gratitude to Volker Haucke for giving me the opportunity to conduct my doctoral thesis within his group, for shaping this project and for sharing his expertise and passion for science. I thank Tolga Soykan for his continuous support, reassuring and calming presence and his expert guidance, as well as our extended subgroup of Svenja Bolz, Guan-Ting Liu and Agata Witkowska for our synergies and fruitful discussions on both professional and personal matters. I am grateful to Gresy Bregu and Hannah Gelhaus for the privilege of supervising them and for their contributions to this work. My appreciation extends to Svea Hohensee and Heike Stephanowitz for their expert facility support in sample preparation and analysis. I sincerely thank Delia Löwe for her immense help with all cell preparations and culture, as well as Silke Zillmann, Maria Mühlbauer, Claudia Bahnik, Marcus Wietstruk, Uwe Fink, and Sabine Hahn for their excellent technical support. I would like to thank Martin Lehmann and Christopher Schmied for providing state-of-the art microscopy and analysis tools, as well as Michael Krauß, Tanja Maritzen, and Noa Lipstein for their interest and constructive feedback. My heartfelt thanks to all present and former members of the group for fostering a compassionate and collaborative culture: Kerem Akkaya, Domenico Azarnia Tehran, Gabrielle Capin, Gillian Leigh Dornan, Michael Ebner, Paula Samsó Ferré, Marine Gil, Hannes Gonschior, Manuel Hessenberger, Lennart Hoffmann, Maria Jäpel, Mudassar Khan, Gaga Kochlamazashvili, Kinga Konkel, Marijn Kuijpers, Wen-Ting Lo, Tania López Hernández, Wonyul Jang, Philipp Koch, Klaudia Kosieradzka, Max Lucht, Fabian Lukas, Albert Mackintosh, Charles Malek, Sravanthi Nadiminti, Vini Natalia, Catherina Nordgaard, Phuong Nguyen, Amirreza Ohadi, Christoph Ott, Dymtro Puchkov, York Posor, Shalini Rawat, Julia Riedlberger, Sila Rizalar, Dorien Roosen, Giulia Russo, Linda Sawade, Yanwei Su, Miaomiao Tian, Rozemarijn van der Veen, Dennis Vollweiter, Haibin Wang, Alexander Wallroth, Klaas Yperman and Chen Xu. A warm hug goes to all colleagues I now call friends. For the night shifts, sub-group meetings, scientists with bikes, karaoke sessions, smoke breaks, lunches, querns, pickles, sass, gossip, frechness, beer hours, and inevitable hangovers, I will forever cherish those memories. Further gratitude is owed to my fellow PhD representatives, members of the Green Initative and the Leibniz PhD/PostDoc Networks for shaping the person I am today. Finally, I am deeply thankful to my family, friends and my partner. You are my source of inspiration, love, and energy. Your unwavering support was the cornerstone of this journey. Thank you.

Statement of Authorship

I hereby declare that I alone am responsible for the content presented in this dissertation entitled "*The Role of mDia1/3 Formins and the Actin Cytoskeleton in Synaptic Vesicle Endocytosis"* and affirm that all used sources or references are cited within.

Berlin, March 2024

Table of Content

Abstract

Neurotransmission, essential for sensory perception, motor control, cognition, and behavior, occurs at synapses, where neurotransmitters are released from the presynaptic neuron into the synaptic cleft, triggering responses at the postsynaptic cell. At chemical synapses, neurotransmitter release involves the fusion of synaptic vesicles (SVs) with the presynaptic membrane, necessitating compensatory membrane retrieval, termed synaptic vesicle endocytosis, to reform and refill SVs for subsequent fusion cycles. Despite the recognized role of the Actin cytoskeleton in synaptic vesicle endocytosis, the precise mechanisms governing Actin polymerization and its function within presynaptic nerve terminals remain poorly understood.

Here, we delineate the pivotal role of Actin regulatory diaphanous-related formins mDia1/3 and small Rho GTPases, RhoA/B and Rac1, in orchestrating synaptic vesicle recycling at rodent central synapses. Employing optical recordings of presynaptic membrane dynamics, ultrastructural and proteomic analyses, in combination with genetic/pharmacological manipulations, we demonstrate that mDia1/3 localize to the presynaptic membrane, proximal to the endocytic machinery, and govern the formation of presynaptic filamentous Actin structures (F-Actin). Loss of F-Actin due to perturbation of mDia1/3 results in significant alterations in presynaptic architecture, impacting plasma membrane homeostasis. Furthermore, our findings highlight that in the absence of mDia1/3, downregulation of RhoA and activation of Rac1 drive a compensatory response to mitigate the disruption of formin-mediated Actin dynamics. Besides modulating Rho GTPase signaling, we find that mDia1/3 negatively regulate the complex signaling network mediated by the mechanistic target of rapamycin complex 2 (mTORC2). We identify mTORC2 activation to be inversely coupled to the kinetics of SV recycling, likely through the modulation of cytoskeletal dynamics.

In conclusion, our study elucidates that the endocytic cytoskeleton is governed by interdependent signaling pathways involving the small Rho GTPases RhoA/B and Rac1, as well as the action of mDia1/3 formins, operating within feed forward loops. The dynamics of the Actin cytoskeleton integrate mechanical regulation of synaptic membrane morphology with biochemical signaling mediated by mTORC2 and Rho GTPases to orchestrate the kinetics of synaptic vesicle endocytosis.

Zusammenfassung

Die Neurotransmission spielt eine essenzielle Rolle in der sensorischen Wahrnehmung, der motorischen Kontrolle, der Kognition und dem Verhalten. Sie erfolgt an Synapsen, wo Neurotransmitter von der präsynaptischen Zelle in den synaptischen Spalt freigesetzt werden und eine Reaktion der postsynaptischen Zelle auslösen. An chemischen Synapsen erfolgt die Freisetzung von Neurotransmittern durch die Fusion synaptischer Vesikel mit der präsynaptischen Membran. Diese Fusion erfordert eine kompensatorische Rückreaktion, die als Endozytose bezeichnet wird, um die Rückgewinnung synaptischer Vesikel für erneute Neurotransmission zu gewährleisten. Obwohl eine Rolle des Aktin-Zytoskeletts im Prozess der Endozytose an Synapsen beschrieben wurde, bleiben die genauen Mechanismen, insbesondere die Kontrolle der Aktin-Polymerisation durch Proteine, umstritten.

In dieser Arbeit beschreiben wir eine bedeutende Funktion der kleinen Rho-GTPasen RhoA/B und Rac1 und die Diaphanous-verwandten Formine mDia1/3, die das Aktin-Zytoskelett in der Endozytose synaptischer Vesikel in Mauszellen regulieren. Wir nutzen mikroskopische Methoden zur Verfolgung dynamischer Prozesse der Membranfusion und Endozytose sowie zur hochauflösenden Darstellung der Membranstruktur von Synapsen in Kombination mit massenspektrometrischen Analysen und genetischen/pharmakologischen Manipulationen. Unsere Ergebnisse zeigen, dass mDia1/3 an der präsynaptischen Membran, in der Nähe von der Endozytose-Apparatur, lokalisieren und zur Bildung von filamentösen Aktinstrukturen (F-Aktin) an der Membran beitragen. Die Reduktion von F-Aktin infolge der negativen Manipulation der mDia1/3-Funktionen, führt zu signifikanten Veränderungen der präsynaptischen Membranarchitektur und ihrer Homöostase. Des Weiteren verdeutlichen unsere Resultate, dass in Abwesenheit von mDia1/3 die Aktivität von RhoA herunter - und die Aktivierung von Rac1 hochreguliert wird, als kompensatorische Antwort, um formin-vermittelte Beeinträchtigungen des Zytoskeletts zu mildern. Neben der Modulation von Rho-GTPasen zeigen wir, dass mDia1/3 die komplexen Signalwege, die durch den mechanistischen Target of Rapamycin Komplex 2 (mTORC2) vermittelt werden, negativ regulieren. Wir identifizieren eine inverse Korrelation zwischen der Aktivität von mTORC2 und der Kinetik der Endozytose synaptischer Vesikel in Abhängigkeit vom Aktin-Zytoskelett.

Zusammenfassend verdeutlicht unsere Studie, dass das Aktin-Zytoskelett von diversen Signalwegen, die die kleinen Rho-GTPasen RhoA/B und Rac1 sowie die Formine

mDia1/3 umfassen, die gegenseitig in Wechselwirkung treten, gesteuert wird. Die Dynamik des Aktin-basierten Zytoskeletts integriert die mechanische Modulation der Morphologie der synaptischen Membran mit biochemischen Signalwegen, die durch mTORC2 und kleine Rho-GTPasen vermittelt werden, um zuverlässig die Endozytose synaptischer Vesikel und damit die Neurotransmission zu regulieren.

1. Introduction

1.1. Neurotransmission at Chemical Synapses

The brain functions as the central processing unit, orchestrating vital physiological processes such as cognition, emotion, and behavior, facilitated by a complex network of nerve and glial cells. Information processing and storage in the brain requires efficient communication among nerve cells called neurons, which are specialized to receive and transmit cellular inputs. Neurons are highly polarized cells and consist of a neuronal soma (cell body) surrounding the nucleus, extensively branched dendrites that are able to receive synaptic signals, and a single axon that creates numerous synaptic connections (Figure 1).

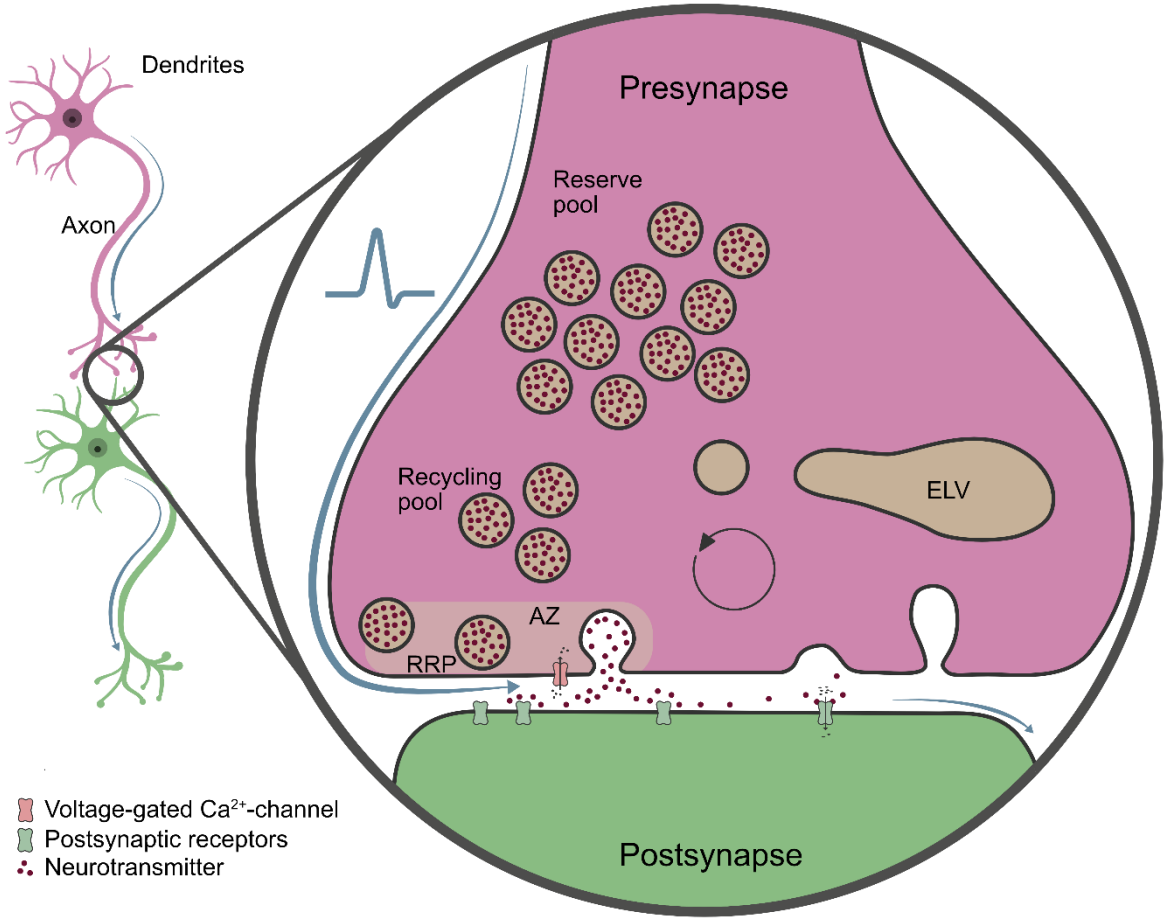

Figure 1: The Synaptic Vesicle Cycle.
Neurons are highly polarized cells, consisting of a soma surrounded by dendrites and a long axon forming connections, the chemical synapses, with the neighboring neuron. Upon arrival of an action potential, voltage-gated Calcium (Ca^{2+})-channels open and synaptic vesicles (SV) of the ready-releasable pool (RRP) fuse with the presynaptic membrane at the active zone (AZ) to release neurotransmitters into the synaptic cleft. At excitatory synapses, neurotransmitters diffuse and bind to receptors to give rise to an action potential through depolarization of the postsynaptic membrane via ion influx. In the presynaptic cell, excess membrane and SV proteins are recycled by endocytic membrane retrieval at the peri-active zone and SV reformation from transient endosome like vacuoles (ELVs) to replenish SV recycling and reserve pools.

These connections, known as chemical synapses, are intercellular junctions that facilitate the conversion of electrical stimuli into chemical signals. For neurotransmission, information has to be transferred from the axon terminals of one cell (presynaptic neuron) to the dendrite of a consecutive one (postsynaptic neuron) across the synaptic cleft (Figure 1). At chemical synapses, this is achieved by means of various neurotransmitters (e.g., glutamate, gamma-aminobutyric acid (GABA), etc.), which are packaged in lipid bilayer enclosed vesicles to allow their timed and rapid release in quanta (Katz, 1950) (Figure 2).

1.1.1. The Synaptic Vesicle

In the healthy brain, synaptic vesicles (SVs) are uniform in size, approximately 40 nm (Van der Kloot, 1991), share a common set of essential transmembrane proteins including Synaptophysin, Synaptotagmin and Synaptobrevin, and can contain approximately 1800 neurotransmitter molecules (Takamori et al., 2006) (Figure 2). Neurotransmitter loading is mediated by vesicular neurotransmitter transporters such as vesicular glutamate transporter 1 (vGLUT1) or vesicular GABA transporter (vGAT), which operate within an acidic environment (Farsi et al., 2017).

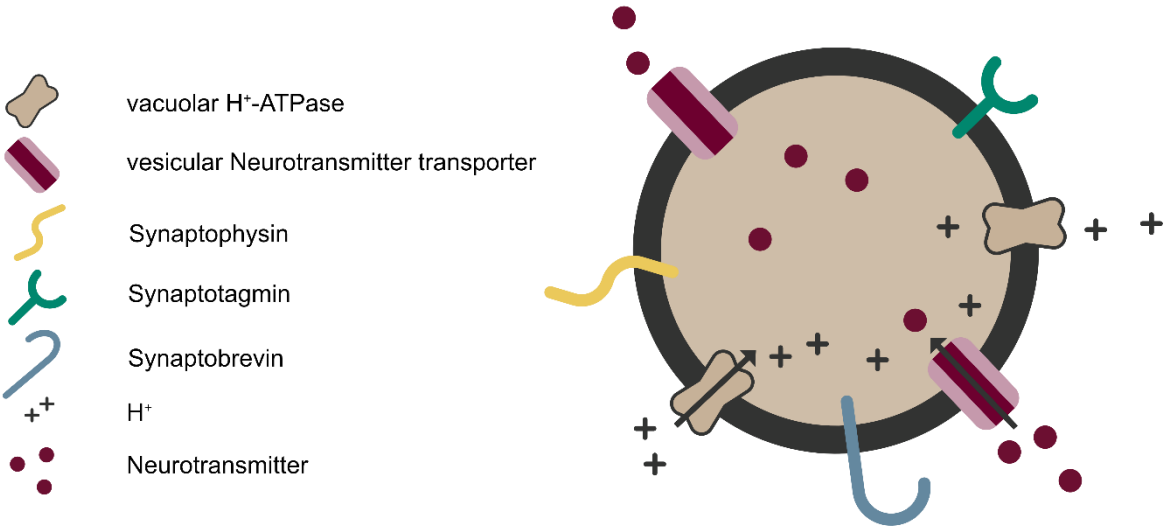

Figure 2: The Synaptic Vesicle.
A synaptic vesicle (SV) is composed of synaptic vesicle proteins that span its membrane, such as Synaptophysin, Synaptotagmin and Synaptobrevin. For neurotransmitter loading, the lumen of SV has to be acidified by the action of vacuolar H^+-ATPase. Following acidification, neurotransmitters are pumped into the SV through vesicular neurotransmitter transporters, such as vesicular glutamate transporter 1 (vGLUT1) or vesicular GABA transporter (vGAT) depending on the synapse type.

This process involves vacuolar H^+-ATPase (vATPase) pumping protons into the SV lumen through ATP hydrolysis (Toei et al., 2010), establishing an electrochemical

gradient that is utilized by the neurotransmitter transporters to shuttle neurotransmitter molecules into the SV (Figure 2).

1.1.2. Neurotransmitter Release

Chemical neurotransmission, the process of signal transduction between nerve cells, is based on the fusion of neurotransmitter-filled synaptic vesicles (SV) with the plasma membrane at specialized release sites within the active zone (AZ) (Figure 3). Upon fusion, neurotransmitters are released into the synaptic cleft, where they bind to specific receptors on the surface of the postsynaptic cell (Figure 1). Depending on the type of neurotransmitter released, postsynaptic signaling can either be excitatory (e.g. by glutamate) or inhibitory (e.g. by GABA).

At excitatory synapses, the binding of neurotransmitters to postsynaptic receptors mediates the influx of Na^+ ions into the cell, causing local depolarization of the neuronal membrane and disruption of its resting potential. This depolarization gives rise to an action potential (AP), the unit for stimuli of neurotransmitter release (Figure 1). Subsequently, the AP propagates unidirectionally along the neuronal axon towards the synapses, causing the opening of voltage-gated Ca^{2+}-channels (Figure 1). Increased Ca^{2+} ion concentration at the presynaptic bouton triggers the fusion of synaptic vesicles (SV) and the release of neurotransmitter, facilitating repeated neurotransmission (Kennedy, 2016) (Figure 3).

The process of synaptic vesicle fusion with the presynaptic membrane causing the release of neurotransmitters is termed SV exocytosis. Exocytosis is facilitated by the assembly of Soluble *N*-ethylmaleimide sensitive factor attachment protein receptor (SNARE) protein complexes that promote the fusion of the two distinct lipid bilayer compartments. The SNARE complex comprises the SV protein Synaptobrevin2 (VAMP-2) along with Synaptosomal-associated protein of 25 kDa (SNAP-25A) and syntaxin1A anchored in the AZ. Synaptotagmin1 (Syt1), another synaptic vesicle protein, clamps the SNARE complex at steady-state but acts as the neuronal Ca^{2+} sensor upon the arrival of an action potential, triggering neurotransmitter release (Brunger et al., 2018) (Figure 3).

To ensure time-locked fusion coinciding with AP arrival, a small subset of SVs, known as the ready-releasable pool (RRP) is docked at the plasma membrane and primed for synchronous fusion within milliseconds of calcium elevation (Holderith et al., 2012; Neher & Brose, 2018; Südhof, 2013) (Figure 3).

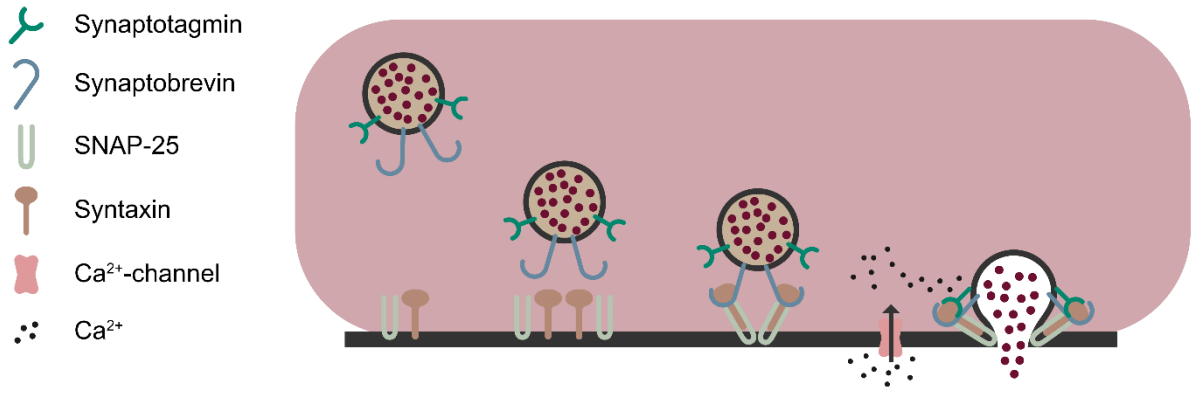

Figure 3: Synaptic Vesicle Exocytosis.
Exocytosis is initiated by synaptic vesicles docking at release sites in the active zone. Next, vesicles are primed via the formation of the Soluble N-ethylmaleimide sensitive factor Attachment protein Receptor (SNARE) complexes including vesicle protein Synaptobrevin and plasma membrane anchored Synaptosomal-associated protein of 25 kDa (SNAP-25) and Syntaxin, to enter the ready-releasable pool. Local increase in Ca^{2+} concentration is sensed by synaptotagmin1, which promotes fusion of synaptic vesicle and active zone membranes to release neurotransmitters into the synaptic cleft. Following action potentials, SVs fuse and release neurotransmitter either in a time-locked, synchronous or a delayed, asynchronous, manner. Additionally, SVs can fuse spontaneously in the absence of action potentials (Kavalali, 2015). Recent studies have shown that distinct molecular compositions of SV determine their fusion characteristics, with specific proteins governing synchronous (e.g. distinct Synaptotagmin and Synaptobrevin isoforms (Bacaj et al., 2013; Chanaday & Kavalali, 2018a; Südhof, 2013) fusion.

The RRP, constituting approximately 4% of SVs, requires constant replenishment. This replenishment occurs through mobilization from SV storage reservoirs, including the recycling (10-20%) and the immobile reserve pool (80-90% of all SVs; Review Wu 2018), or via direct recycling mechanisms in a compensatory manner (Guo et al., 2015) (Figure 1).

1.1.3. The Molecular Endocytic Machinery

Chemical neurotransmission is based on neurotransmitter release from SVs that fuse with the plasma membrane. To sustain high rates of release, neurotransmitter-filled SVs have to be regenerated, as the *de novo* synthesis in the soma coupled with axonal transport of new SVs would be insufficient to support the demand for release (Chanaday & Kavalali, 2018c). This resupply is based on retrieving excess membrane and synaptic vesicle proteins from the presynaptic membrane in a process called endocytosis, followed by cargo sorting via transient endosomal intermediates and the rapid refilling of newly reformed SVs with neurotransmitter (Figure 1).

Synaptic vesicle endocytosis occurs after collapse and lateral diffusion of SV components to the peri-active zone and requires membrane remodeling that is mediated by phospholipids present in the inner leaflet of the presynaptic membrane and protein complexes that form the endocytic machinery (Binotti et al., 2021) (Figure 4).

1.1.3.1. The Presynaptic Plasma Membrane

The recycling of SVs involves the retrieval of excess lipid bilayers from the plasma membrane after SV fusion to be reformed into vesicles. This process relies on the fine-tuned interactions of proteins with membranes to mediate membrane deformation and vesicle scission, facilitated by the tight coupling of signaling molecules such as phosphoinositides (PI), phosphorylated derivates of the membrane phospholipid phosphatidylinositol. PIs are present in the cytosolic leaflet of membranes and serve as spatiotemporal cues for membrane trafficking (Posor et al., 2022) under the control of the opposing functions of kinases and phosphatases (Hunter, 1995) (Figure 4).

At the presynaptic plasma membrane, the predominant PI is phosphatidylinositol-4,5-bisphosphate ($PI(4,5)P_2$), which forms nanoclusters of approx. 70 nm (Van Den Bogaart et al., 2011). Many effector proteins bind this phospholipid, including the SV release machinery (Lauwers et al., 2016; Martin, 2012; Walter et al., 2017). $PI(4,5)P_2$ presents the crucial signaling molecule and rate-limiting step to induce synaptic vesicle endocytosis through its endocytic effectors and its synthesis scales with synaptic activity (Bolz et al., 2023). Consequently, membrane trafficking processes during the SV cycle are closely linked to the interconversion of PI species (Wenk & De Camilli, 2004).

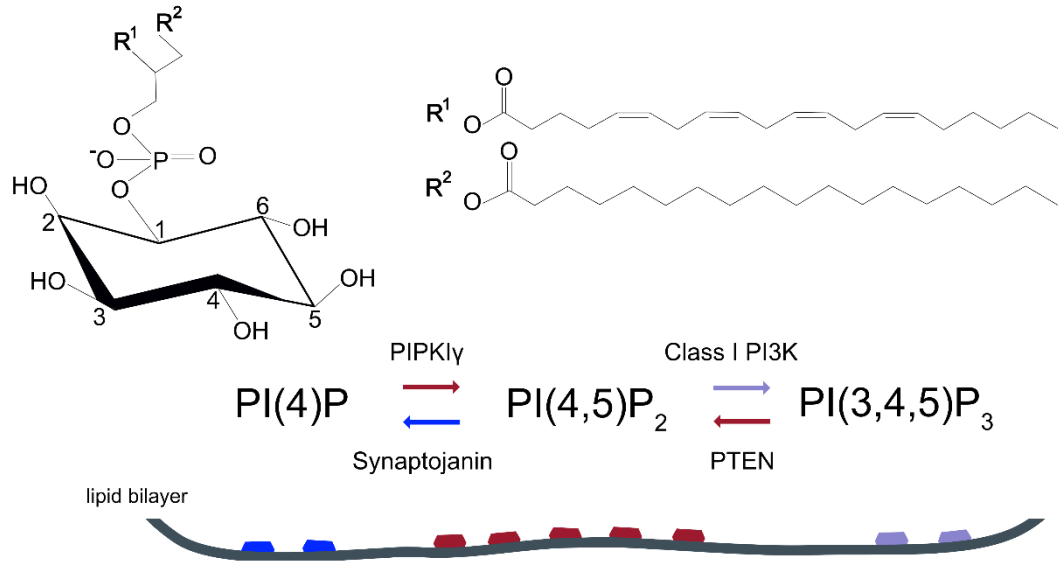

Figure 4: Interconversion of Phosphatidylinositol-4,5-bisphosphat.
Phosphatidylinositols contain a myo-inositol head group that can be modulated at different positions of the ring by lipid phosphatases and kinases and two lipid tails (R^1: 2-arachidonyl; R^2: 1-stearoyl chains) present in the lipid bilayer. Phosphatidylinositol-4,5-bisphosphat ($PI(4,5)P_2$) is the most abundant phosphoinositide of the plasma membrane and is generated by phosphatidylinositol 4-phosphate 5-kinase type I gamma (PIPKIγ) upon neuronal activity (Bolz et al., 2023). Synaptojanin converts $PI(4,5)P_2$ to phosphatidylinositol-4-phosphat (PI(4)P), a crucial step during synaptic vesicle recycling. PI(4)P is the phospholipid identity of synaptic vesicles. $PI(4,5)P_2$ can be phosphorylated at the 3'Hydroxyl (OH)-position by class I phosphoinositide 3-kinases (class I PI3K) to yield phosphatidylinositol-3,4,5-trisphosphat ($PI(3,4,5)P_3$). The inverse reaction is catalyzed by phosphatase and tension homolog (PTEN). At synapses, the balance between $PI(4,5)P_2$ and $PI(3,4,5)P_3$ crucially mediates neurotransmission, plasticity and cytoskeletal remodeling (Tariq & Luikart, 2021).

1.1.3.2. Coupling of Synaptic Vesicle Fusion and Endocytosis

The retrieval of SV membranes and proteins plays a crucial role in regulating the total amount of SVs, clearing release sites in the AZ by disassembly of SNARE complexes for consecutive fusion (Haucke et al., 2011), and maintaining plasma membrane homeostasis. Typically, endocytosis in neurons is compensatory, meaning endocytosed material matches the number of fused membranes and proteins during exocytosis. This requires mechanisms that initiate endocytosis spatiotemporally linked to fusion via mechanical and biochemical coupling (Maritzen & Haucke, 2018): The initiation can be triggered by multiple factors, including increased Ca^{2+} concentration, which activates signaling cascades, proteins that sense changes in membrane architecture upon addition of excess membrane following fusion, and/or adaptor proteins that detect surface-stranded synaptic vesicle proteins and facilitate cargo sorting (L. G. Wu et al., 2014).

Coupling via Calcium

Upon AP arrival, Ca^{2+}-influx not only acts on the SV fusion machinery but also stimulates the activity of the phosphatase calcineurin (CaN) (X. S. Wu et al., 2014). Calcineurin dephosphorylates multiple structurally diverse endocytic proteins, collectively referred to as dephosphins, including adaptor proteins Epsin and AP180, membrane-binding proteins Amphiphysins, the GTPase Dynamin, and the lipid phosphatase Synaptojanin1. The phosphorylation state of the dephosphins regulates their localization through protein-protein or protein-lipid interactions (Cousin & Robinson, 2001).

Coupling via Membrane Architecture

In addition, fusion of SV with the presynaptic membrane during exocytosis alters the lipid packaging of the membrane. Packaging defects result in changes in membrane tension that can be sensed by various proteins that drive endocytosis. For example, proteins with amphipathic helices can insert into membranes with packaging defects (Baumgart et al., 2011), while scaffolding proteins with intrinsic shapes that sense tension can deform underlying membranes, both serving as endocytic initiation hubs. Notably, the bin-amphiphysin-rvs (BAR) domain family proteins are pivotal for endocytosis and contain a crescent BAR domain of varying curvature that induces membrane invagination via oligomerization. F-BAR proteins, with a shallow BAR domain curvature, are recruited during the early phases of endocytosis, while N-BAR proteins, with increased curvature and carrying an N-terminal amphipathic helix are required at later stages (Figure 5). In addition, BAR proteins bind Dynamin, which catalyzes the final step of endocytosis, thereby coupling changes in membrane tension upon exocytosis with endocytic membrane invagination and vesicle scission.

Coupling via Adaptor Proteins

Following SV exocytosis, synaptic vesicle proteins are stranded on the presynaptic membrane, where they are captured by adaptor proteins (Figure 5). Different adaptor proteins recognize different cargo; for example, Epsin1/2 binds to ubiquitinated cargo, while AP180 and Stonin2 capture Synaptobrevin and Synaptotagmin, respectively. Adaptor proteins then recruit further endocytic machinery to drive the retrieval of SV proteins (Figure 5).

1.1.4. Pathways of Synaptic Vesicle Endocytosis

Although it has been recognized for over 50 years that SVs are locally recycled at presynaptic terminals (Ceccarelli et al., 1973; Heuser & Reese, 1973), the precise mechanisms underlying SV reformation remain a matter of debate. Currently, four distinct modes of endocytic membrane retrieval at synapses have been identified that occur on various timescales ranging from milliseconds to tens of seconds (Soykan et al., 2017) (Figure 6). The prevalence of these modes is contingent upon factors such as the synapse type, stimulus intensity, and temperature.

1.1.4.1. Clathrin-mediated Endocytosis

The most common cellular mechanism for vesicle formation is mediated by protein complexes that assemble into coat-like structures, like COPI/II or Clathrin. These coat proteins capture cargo proteins to be incorporated into vesicles, while simultaneously inducing and promoting underlying membrane curvature that drives vesicle formation (Robinson, 2015). Clathrin-mediated membrane invagination and endocytic retrieval (CME) is highly conserved across evolution, with homologous key proteins expressed from yeast to mammalian cells. Additionally, its molecular components are highly abundant at nerve terminals, and their depletion causes severe SV recycling defects at rodent central synapses at room temperature (Granseth et al., 2006).

At synapses, CME is initiated by the capture of surface-stranded SV proteins by adaptor proteins that are recruited to the plasma membrane by binding to $PI(4,5)P_2$ (Figure 5). Adaptor proteins bind Clathrin molecules that form polyhedral lattices that drive endocytic pit formation, facilitated by membrane-bending N-BAR proteins, such as Amphiphysin and Endophilin (Figure 5). Vesicle scission is mediated by Dynamin, followed by Clathrin coat disassembly through $PI(4,5)P_2$ hydrolysis via the phosphatase Synaptojanin1 (Figure 5). The SV cycle mediated by CME operates on a timescale of 10-20 s (Smith et al., 2008).

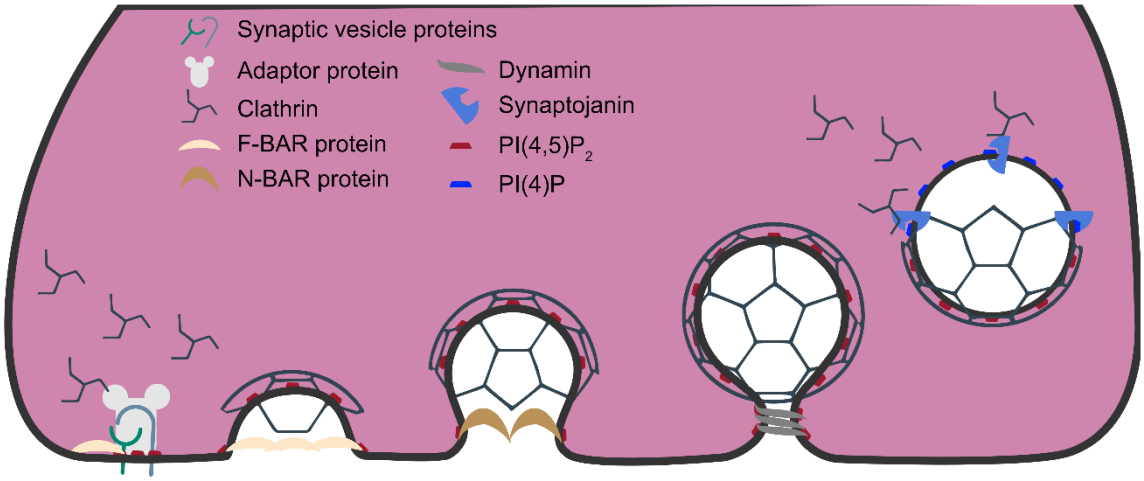

Figure 5: Coordination and Time course of Clathrin-mediated Endocytosis.
Initiation of Clathrin-mediated endocytosis is based on nucleation modules containing F-BAR proteins of the FCHO family, Epidermal growth factor receptor (EGFR) pathway substrate 15 (EPS15) and Intersectins, which serve as recruitment hubs for adaptor proteins. These adaptor proteins selectively capture specific cargo, like surface-stranded SV proteins following exocytosis. Adaptor proteins recruit Clathrin light and heavy chains, forming triskelia that polymerize into polyhedral lattices. Consequently, the underlying membrane is bent to form a deeply invaginated coated pit. High membrane curvature recruits N-BAR proteins Amphiphysin and Endophilin, which bind Dynamin. The GTPase Dynamin oligomerizes as a collar around the neck of the pit and catalyzes vesicle fission. The phosphatase Synaptojanin1 is recruited by Endophilin and hydrolyses $PI(4,5)P_2$ to PI(4)P on the released coated vesicles resulting in the dissociation of the adaptor proteins (Milosevic et al., 2011). The Clathrin coat is disassembled through the concerted activity of the ATPase Hsc70 and Auxilin. Newly retrieved uncoated vesicles may either fuse with transient endosome-like structures (ELVs) (Heuser & Reese, 1973), or directly transition into the distinct vesicle pools (Takei et al., 1996).

Historically, CME has been regarded as the primary pathway of synaptic vesicle retrieval; however, this view has been progressively challenged. Numerous studies have underlined that endocytic membrane retrieval and SV reformation are at least partially distinct processes (Kononenko et al., 2014; Soykan et al., 2017), and have indicated that fast Clathrin-independent endocytosis (CIE) is the predominant pathway for the initial membrane retrieval at physiological temperatures at mammalian synapses.

1.1.4.2. Clathrin-independent Endocytosis

Over the years, several Clathrin-independent and fast pathways of SV endocytosis have been described that can be distinguished by the size of endocytic intermediates as well as their kinetics.

The fastest pathway of vesicle regeneration is the Clathrin-independent kiss-and-run mode, as it omits the full collapse of the vesicle into the membrane. Kiss-and-run is based on the generation of a transient fusion pore that allows neurotransmitter release

followed by direct closure (Figure 6), resulting in fast kinetics of vesicle reacidification (400 – 860 milliseconds) (Gandhl & Stevens, 2003). Kiss-and-run is the predominant mechanism in neuroendocrine cells (Burgoyne et al., 2001) and potentially dopaminergic synapses (Staal et al., 2004), but has also been reported at mammalian central synapses (Chanaday & Kavalali, 2018b; Q. Zhang et al., 2009). However, its physiological relevance remains contentious (He & Wu, 2007), as newly exocytosed and subsequently retrieved SV proteins are largely non-identical (Gimber et al., 2015). Conversely, other Clathrin-independent mechanisms occur after the full collapse of SVs during exocytosis. Their prevalence depends on the intensity of the stimulus, leading to the distinction of different modes of CIE based on the size of endocytic intermediates and their time course. An ultrafast mode, termed ultrafast endocytosis (UFE), generates compensatory intermediates at the peri-active zone of approximately 60-80 nm in diameter, which are delivered to endosome-like vacuoles (ELVs) within a timescale of 50 ms – 1 s (Delvendahl et al., 2016; S. Watanabe, Rost, et al., 2013) (Figure 6). UFE is the predominant pathway at rodent central synapses at 37°C following brief periods of activity (S. Watanabe et al., 2014).
While fast components of SV endocytosis are also observed under high-frequency stimulation (Soykan et al., 2017), the main route of endocytosis following prolonged bursts of intense activity is based on the retrieval of larger membrane invaginations, approx. 150 nm in size, occurring on a slower timescale of 1 – 2 s, a pathway termed activity-dependent bulk endocytosis (ADBE) (Clayton & Cousin, 2009; Kononenko & Haucke, 2015; Körber et al., 2012) (Figure 6). ADBE is induced upon mobilization of the reserve pool, which is typically inactive under physiological conditions (Denker & Rizzoli, 2010), and is therefore considered an emergency backup pathway to recover vesicle pools over a timescale of minutes (Clayton & Cousin, 2009; Richards et al., 2000) .

Both UFE and ADBE are based on the retrieval of endocytic intermediates that exceed the size of SVs. Consequently, the complete course of SV regeneration relies on the fusion of intermediates with transient endosome-like vacuoles (ELVs). Studies have demonstrated that this reformation is based on the Clathrin machinery (Kononenko et al., 2014; S. Watanabe et al., 2014) and likely includes cargo selection mediated via adaptor proteins (AP1-3; (Kononenko et al., 2014; Onoa et al., 2010; Silm et al., 2019)) to ensure distinct molecular identities of SVs ((Morgan et al., 2013) e.g., for synchronous, asynchronous, or spontaneous release (Crawford & Kavalali, 2015).

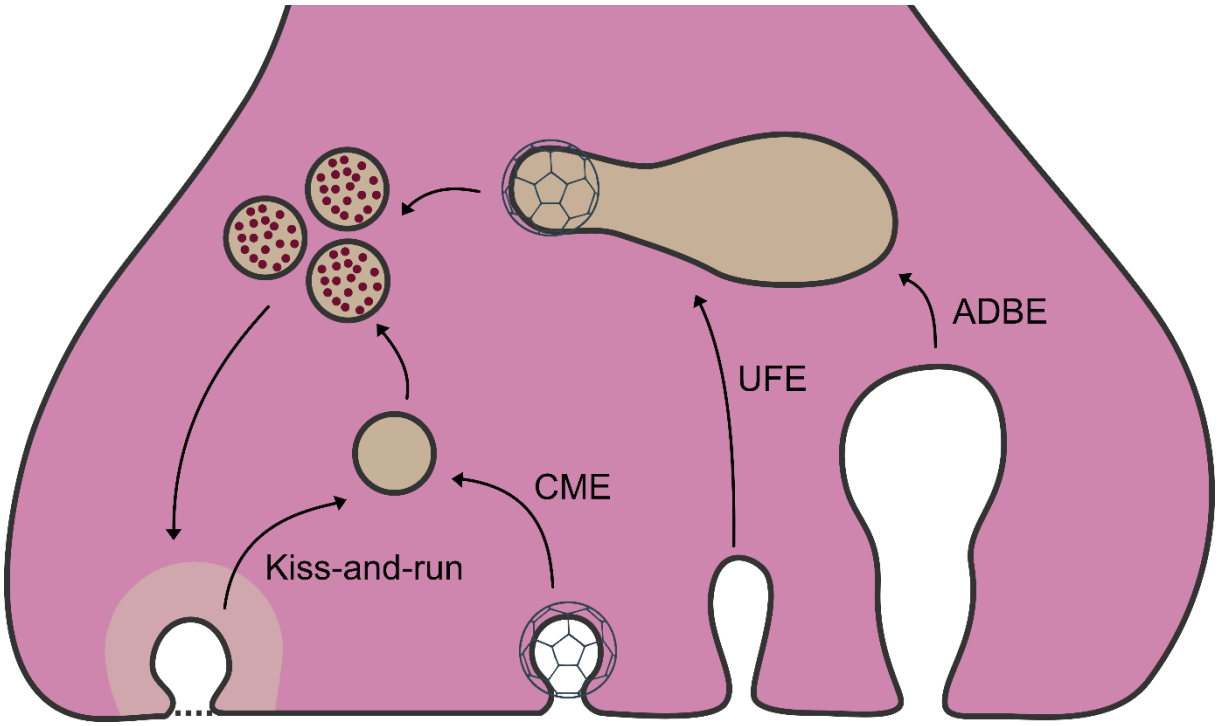

Figure 6: Pathways of Synaptic Vesicle Endocytosis.
Endocytosis can follow differential pathways at rodent central synapses, apart from Clathrin-mediated endocytosis (CME). In the kiss-and-run mode a transient fusion pore is formed to release neurotransmitters from synaptic vesicles. The predominant pathway following low stimulation at 37°C is ultrafast endocytosis (UFE), while strong stimulation stimulates activity-dependent bulk endocytosis (ADBE). Endocytic intermediates following UFE and ADBE fuse with transient endosome-like vacuoles (ELVs) from which vesicles are reformed via Clathrin-mediated budding.

Newly formed SVs are acidified and refilled with neurotransmitters and can either replenish the recycling pool or be captured and sorted to the reserve pool (Pieribone et al., 1995). In the reserve pool, SVs are clustered by the highly abundant phosphoprotein synapsin, which interacts with SVs and the Actin cytoskeleton (Gitler et al., 2008), and mobilizes SVs based on neuronal activity.

Consequently, no universal model of SV endocytosis exists and multiple pathways may be employed depending on activity level at individual synapses to meet the specific demands of recycling. At physiological temperature, fast CIE is responsible for immediate membrane retrieval following fusion (Delvendahl et al., 2016; Kononenko et al., 2014; Soykan et al., 2017), while Clathrin-mediated budding is required for sorting and complete recycling over a slower timescale (Chanaday & Kavalali, 2018a; S. Watanabe et al., 2014; Zhu et al., 2009).

In CME, vesicle formation is facilitated by the spontaneous assembly of proteinaceous membrane-binding scaffolds that assemble into curved structures that include BAR

proteins, the Clathrin coat, and Dynamin. The driving force for the vesicular membrane bending can be attributed to the rigidity and polyhedral shape of Clathrin coatamers. While several Clathrin-independent pathways share multiple molecular players with CME, for example, Endophilin-A (Milosevic et al., 2011), Synaptojanin1 (Verstreken et al., 2003; S. Watanabe et al., 2018) and Dynamin (S. Watanabe, Liu, et al., 2013; S. Watanabe, Rost, et al., 2013), a distinct molecule capable of providing force to deform membranes as a substitute for Clathrin remains elusive.

An emerging candidate for force generation and membrane trafficking in synaptic vesicle endocytosis is the Actin cytoskeleton, as most endocytic routes display sensitivity to Actin perturbation (Ogunmowo et al., 2023; S. Watanabe, Rost, et al., 2013). Moreover, numerous endocytic proteins, such as Protein kinase C and casein kinase substrate in neurons (PACSINs) and Dynamin, are known to interact and recruit regulatory proteins of the Actin cytoskeleton (Ferguson et al., 2009; Kessels & Qualmann, 2004; McMahon & Boucrot, 2011; Merrifield et al., 2005; Renard et al., 2015; Schafer, 2004), suggesting a significant interplay between SV endocytosis and the dynamics of the Actin cytoskeleton.

1.2. The Actin Cytoskeleton

The Actin cytoskeleton can exert mechanical forces and orchestrates numerous essential cellular processes, including locomotion, cytokinesis, morphogenesis, and vesicular trafficking (Blanchoin et al., 2014). To accomplish this diversity of tasks, the cytoskeleton undergoes constant remodeling by dynamically producing Actin filaments (F-Actin). F-Actin constitutes a semi-flexible polar polymer of monomeric globular Actin (G-Actin) that undergoes *treadmilling* (Bugyi & Carlier, 2010; Pollard, 1986), a process characterized by rapid growth at the barbed end and simultaneous disassembly at the pointed end (Figure 7).

Actin is one of the most abundant proteins in eukaryotic cells, with concentrations ranging from 70 to 150 μM (Isogai & Danuser, 2018). Hence, cellular *treadmilling* requires tight regulation in both space and time, facilitated by a myriad of signaling, scaffolding, and Actin-binding proteins that facilitate filament nucleation (Figure 8, Figure 11), elongation (Figure 12), capping (Figure 13), severing (Figure 7), depolymerization (Figure 7), crosslinking (Figure 16), and monomer sequestration (Figure 7) (Rafelski & Theriot, 2004).

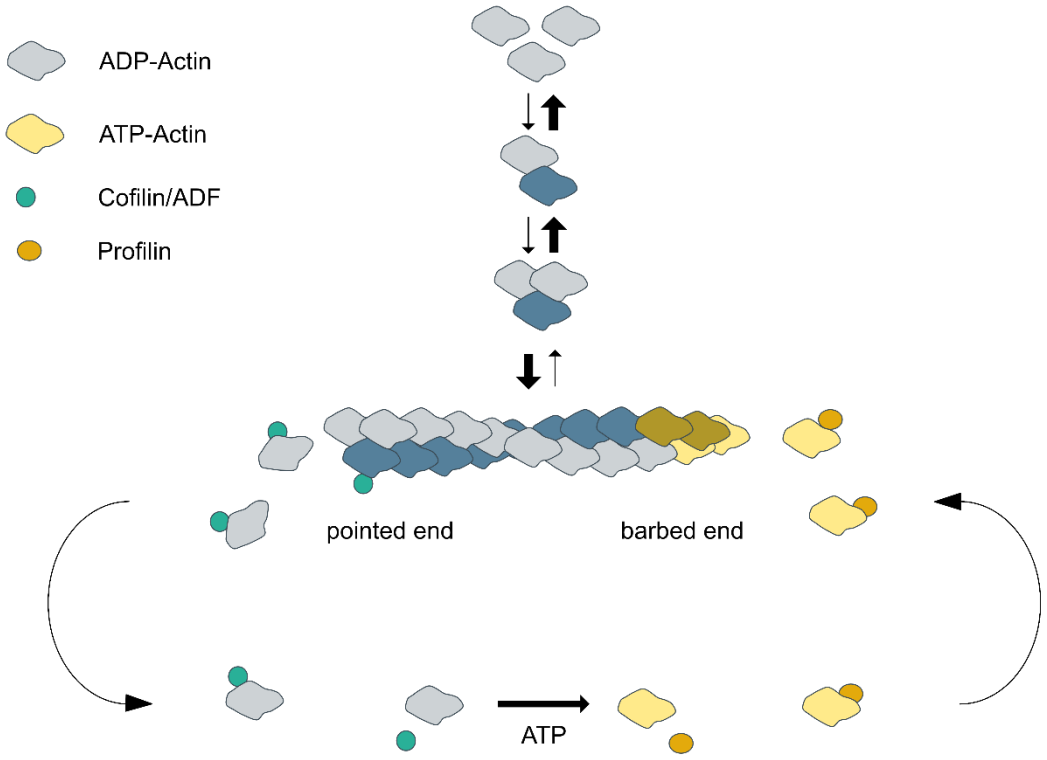

Figure 7: Filamentous Actin Nucleation and Treadmilling.
Monomeric globular Actin above the critical concentration of 0.1 µM spontaneously polymerizes by head-to-tail interactions to form short-lived dimers and trimers in vitro (I. Fujiwara et al., 2007). Once the kinetic barrier of tetramerization is overcome, Actin polymerization proceeds as long as the monomer concentration remains above the critical concentration. The resulting double-stranded helical filaments exhibit distinct polarity, characterized by plus and minus ends, ATP-bound Actin is enriched at the barbed end and exhibits less dissociation compared to ADP-bound Actin at the pointed end. Elongation of the filament at the barbed end is up to 10-fold faster compared to the minus or pointed end, with a rate of 11.6 $\mu M^{-1}s^{-1}$ (Pollard, 1986). In a steady-state (below the critical concentration of the monomer pool), a balance is reached wherein ATP-bound Actin is constantly added at the plus and ADP-bound Actin dissociates from the minus end, a phenomenon known as treadmilling (Ni & Papoian, 2019). Disassembly of F-Actin is additionally mediated by the Actin depolymerizing factor (ADF)/cofilin, that binds Actin monomers at the minus ends and causes filament severing and dissociation of ADP-bound Actin, which is sequestered by binding to cofilin (Tanaka et al., 2018). Conversely, binding of profilin catalyzes the ATP loading of Actin monomers and facilitates barbed-end elongation by the assistance of elongation factors (Goldschmidt-Clermont et al., 1992).

1.2.1. F-Actin Assembly

In cells, the rate-limiting step in F-Actin assembly, the formation of a stable multimer (Rosenbloom et al., 2021), is overcome by various Actin-nucleating proteins and promoting factors. For example, the Arp2/3 complex nucleates branched Actin networks by binding to the sides of existing filaments serving as a template for elongation. Formins and tandem-monomer-binding nucleators (e.g., Spire, Cobl, APC, JMY, LMOD) bind to multiple Actin monomers to initiate linear filaments (Campellone & Welch, 2010; M. A. Chesarone & Goode, 2009). Once nucleated, filaments are rapidly elongated by proteins from the ENA/VASP and formin families.

ENA/VASP proteins form tetramers bound to the plasma membrane, elongating parallel Actin bundles against the plasma membrane (Krause et al., 2003), while formins processively move along filament barbed ends incorporating profilin-bound Actin monomers (Figure 12).

1.2.1.1. The Arp2/3 Complex

The Arp2/3 complex comprises Actin-related proteins 2 (Arp2) and 3 (Arp3) along with additional subunits ARPC1-5 (Goley & Welch, 2006) (Figure 8). Upon activation, it serves as a nucleation seed for branched daughter filaments from the sides of pre-existing mother filaments at a 70° angle to form a Y-branched dendritic network (Figure 8). The complex possesses little biochemical activity on its own; thus, branching has to be promoted by nucleation-promoting factors (NPFs). Mammalian cells express several NPFs, including Wiskott-Aldrich Syndrome protein (WASP), neural WASP (N-WASP), three WASP and verprolin homologs (WAVEs), WASP homolog associated with Actin, membranes, and microtubules (WHAMM), WASP and Scar homolog (WASH), junction mediating regulatory (JMY) protein, and WAVE homology in membrane protrusions (WHIMP) protein (Kabrawala et al., 2020).

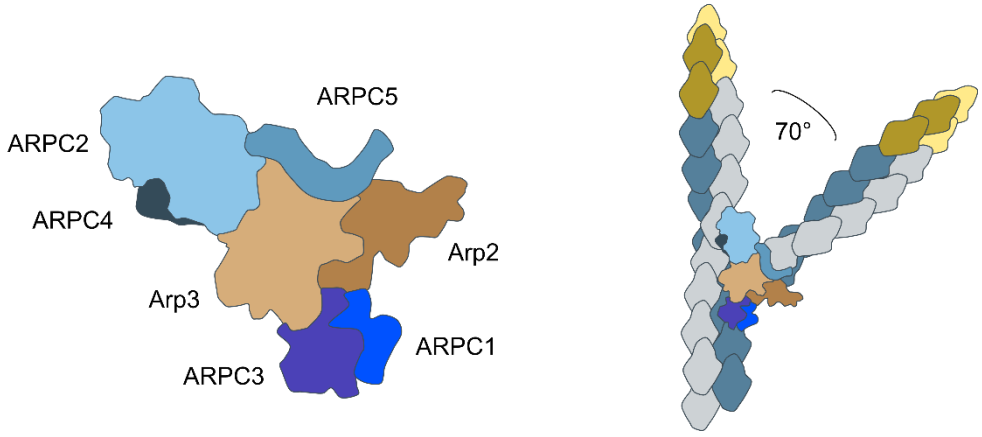

Figure 8: Arp2/3-mediated branched Actin Filament Nucleation.
Actin-related proteins 2 (Arp2) and 3 (Arp3), together with Actin related protein 2/3 complex subunit 1-5 (ARPC1-5) form the Arp2/3 complex, acting as a nucleation seed for filament branching in a 70° angle.

These NPFs share C-terminal WCA domains comprised of a G-Actin binding verpolin homology (WH2) domain and an Arp2/3 binding connector and acidic region (CA). At basal state, the WCA domain is sequestered by an intramolecular (cis), in WASP/N-WASP (Derivery & Gautreau, 2010), or through intermolecular (trans)

interactions within protein complexes as in WAVE, WASH, and WHAMM (Jia et al., 2010; Kim et al., 2000) (Figure 9).

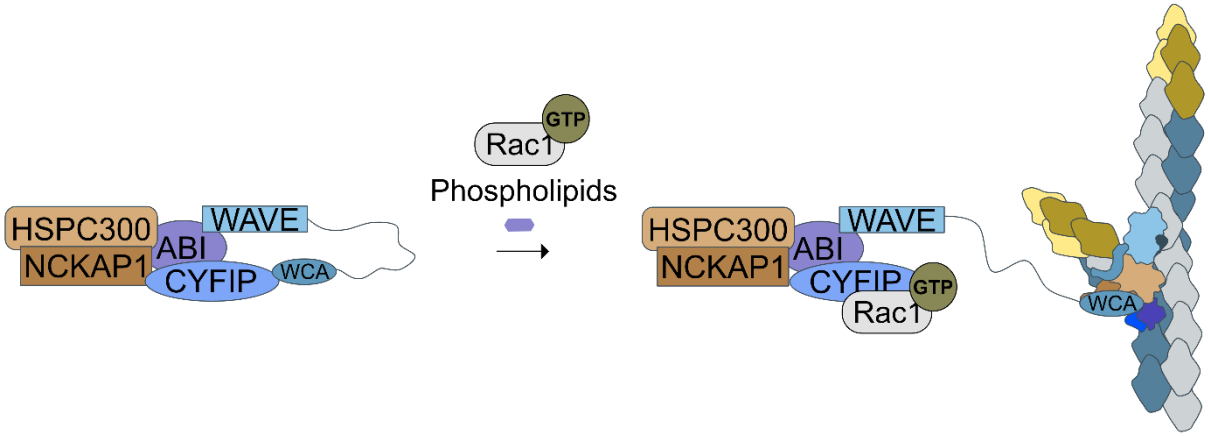

Figure 9: Arp2/3 Complex Activation through the WAVE Regulatory Complex.
Wiskott-Aldrich syndrome and verprolin homologous proteins (WAVE) associate with a multimeric protein complex containing abelson interactor (ABI), non-catalytic region of tyrosine kinase adaptor protein 1 (NcK)-associated protein (NckAP1) and cytoplasmic fragile X messenger ribonucleoprotein 1 (FMR1) interacting protein (CYFIP) as well as a 9 kDa- peptide Brick1 (HSPC300) (Eden et al., 2002; Stradal et al., 2004; Takenawa & Suetsugu, 2007). Those components are expressed by multiple genes (Dubielecka, Cui, et al., 2010) to form a diversity of WAVE complexes containing either ABI1/ABI2/ABI3; NckAP1/NckAPL; CYFIP1/ CYFIP2; and WAVE1/WAVE2/WAVE3 (Stovold et al., 2005). WAVE contains a C-terminal Actin-binding WASP homology-2 motif (WH2), a Central helix domain, and an Acidic Arp2/3-binding motif (WCA) that mediates an inhibitory interaction with the subunit CYFIP. Binding of small Ras homologous (Rho) GTPase Rac1 and phospholipids ($PI(3,4,5)P_3$) releases autoinhibition and initiate Arp2/3-mediated branched Actin nucleation (Campellone & Welch, 2010).

Autoinhibition can be relieved by integrating various upstream signals, including small Ras homologous (Rho) GTPases and phospholipids (Campellone & Welch, 2010), which stimulate the nucleation activity of Arp2/3 (Figure 9).

1.2.1.2. Formins

Formins were initially identified in mice as genes implicated in limb deformation upon mutation (Maas et al., 1990). In mammals, this family encompasses 15 genes, while *Saccharomyces cerevisiae, Saccharomyces pombe*, and *Drosophila melanogaster* express two, three, and six formin genes, respectively. The 15 mammalian formins are categorized into seven subfamilies (Courtemanche, 2018): Diaphanous (DIAPH/mDia), Dishevelled-associated activator of morphogenesis (DAAM), Formin-related proteins identified in leukocytes (FMNL), Formin Homology Domain-containing Protein (FHOD), Inverted Formin (INF), Formin (FMN) proteins, and Delphilin families (Kovar, 2006) (Figure 10).

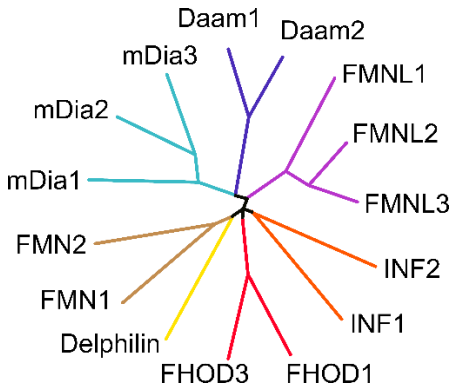

Figure 10: Phylogenetic Tree of Mammalian Formins.
15 formins from 7 subfamilies are expressed in eukaryotic cells: mammalian Diaphanous-related (mDia) formins mDia1, mDia2, and mDia3; Dishevelled-associated activator of morphogenesis (DAAM) DAAM1 and DAAM2; Formin-like proteins (FMNL) FMNL1, FMNL2, and FMNL3; Inverted formin (INF) INF1 and INF2; Formin homology domain containing protein (FHOD) FHOD1 and FHOD3; Delphilin; and Formin proteins (FMN) FMN1 and FMN2.

Formins exhibit triple functionality in modulating the Actin cytoskeleton: nucleation of linear F-Actin (Figure 12), profilin-dependent acceleration of filament elongation through processive movement (Figure 12), and the protection of growing barbed ends from capping proteins (Figure 13). These functions are mediated by the highly conserved formin homology 1 (FH1) and formin homology 2 (FH2) domains. The FH1 domain, which is extended and unstructured, contains multiple proline-rich motifs that bind Profilin-Actin complexes (Imamura et al., 1997) (Figure 12). The FH2 domain forms a donut-shaped antiparallel dimer, flexibly tethered by interactions of *lasso* and *post* segments (Xu et al., 2004), with a high affinity for Actin filament barbed ends (Pruyne et al., 2002) (Figure 12).

Nucleation

The precise mechanism of formin-mediated filament nucleation has remained elusive. Initially, it was suggested that formins stabilize and capture spontaneously formed Actin di- and trimers (Pring et al., 2003) to overcome the kinetic hurdle of spontaneous Actin nucleation (Sept & McCammon, 2001). However, FH2-mediated nucleation is notably inefficient when utilizing profilin-bound Actin monomers, the primary substrate in cells (M. A. Chesarone et al., 2010). *In vivo*, the profilin barrier to formin-mediated Actin nucleation is thought to be surmounted through cooperation with NPFs that compete with profilin for monomer binding and organize multiple Actin monomers in proximity to FH2 domains (Moseley et al., 2004) (Figure 11). Following nucleation, NPFs remain at the nucleation site, while formins move processively along the growing barbed end to elongate the filament and protect it from capping (Breitsprecher & Goode, 2013) (Figure 11).

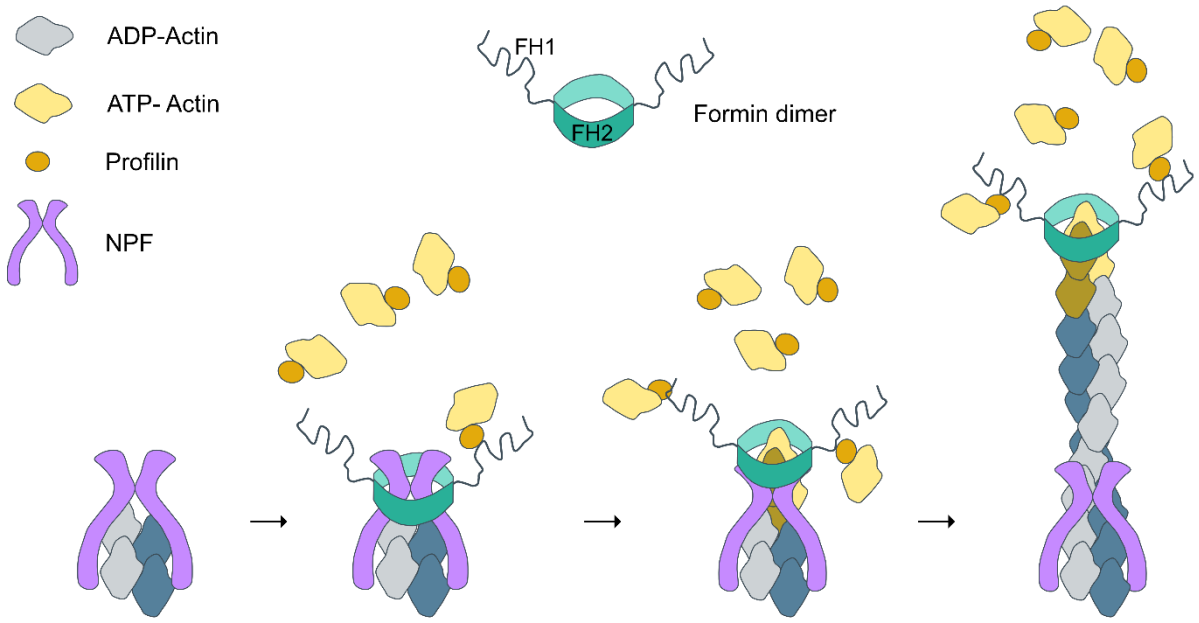

Figure 11: Formin-mediated F-Actin Nucleation.
Nucleation-promoting factors (NPFs) capture multiple Actin monomers and recruit formins. Individual formin isoforms have specific NPFs including adenomatous polyposis coli protein (APC) for mDia1 (Okada et al., 2010), Spire for FMN family formins (Quinlan et al., 2007) and Bud site selection factor 6 (Bud6) for yeast Bin1 (Graziano et al., 2011). The formin homology 1 domains (FH1) of formin dimers capture Profilin-Actin monomers through proline rich stretches that transport the subunits to the formin homology 2 (FH2) domains that processively move along Actin filament barbed ends.

Elongation

Following filament nucleation, the dimeric FH2 domain encircles and tracks the growing barbed end, facilitating the addition of Profilin-Actin subunits. Formins can enhance the barbed-end elongation rate, reaching up to 90 $\mu M^{-1}s^{-1}$ (Higashida et al., 2004; Kovar, 2006; Kozlov & Bershadsky, 2004; Mizuno et al., 2011; Romero et al., 2004; Vidali et al., 2009). This process involves transient, alternating contacts of the two halves of the FH2 dimer with the two terminal Actin subunits of the filament (Breitsprecher & Goode, 2013) (Figure 12). The FH1 domain recruits Profilin-Actin complexes through its proline-rich repetitive stretches, arranged in ascending affinity towards the FH2 domain (Courtemanche & Pollard, 2012), ensuring monomer transport to the barbed end (Figure 12). During elongation, the FH2 dimer switches between an *open* and a *closed* state in a stair stepping mechanism (Maufront et al., 2023), representing monomer incorporation and capped states of the filament, respectively (Kozlov & Bershadsky, 2004; Zigmond et al., 2003) (Figure 12).

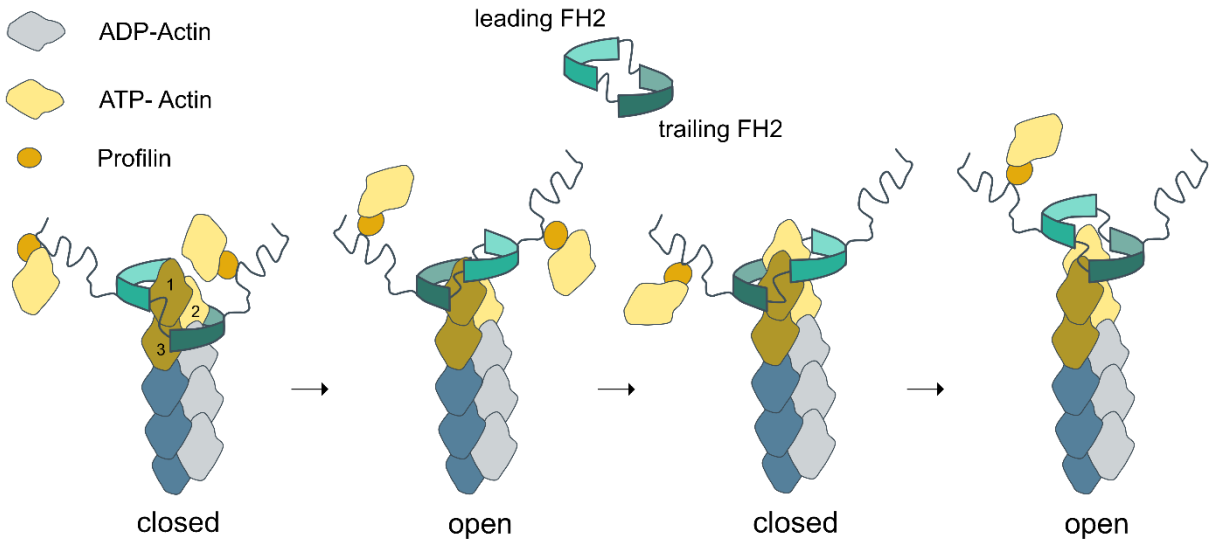

Figure 12: Stair-Stepping Model of Formin-mediated F-Actin Assembly.
The formin homology 2 (FH2) dimer switches between an open and closed configuration facilitating the incorporation of Actin monomers or capping the filament, respectively. In the closed state, the leading FH2 subunit is attached to the two terminal Actin monomers, while the trailing FH2 domain engages the second and third monomers. Transitioning to the open state involves disengagement of the trailing FH2 subunit, followed by a stepping motion to partially attach to the terminal barbed end monomer. In the open configuration the now leading FH2 is partially exposed, facilitating Actin monomer addition to re-enter the closed state (Paul & Pollard, 2009). Surprisingly, this movement does not necessitate Profilin or nucleotide hydrolysis but is believed to be linked to the release of free energy accompanying monomer incorporation (Paul & Pollard, 2009).

Due to their processive elongation availability, formins can produce over 50 µm-long Actin filaments in *in vitro* experiments (Breitsprecher et al., 2012; Kovar, 2006). However, in cells filaments are limited to 1 µm in length (Pollard T.D. & Kholodenko, 2003), indicating precise regulatory mechanisms to control formin-mediated Actin assembly. This regulation involves proteins that a) bind the FH2 domain (M. Chesarone et al., 2009; M. A. Chesarone & Goode, 2009), b) interfere with Profilin-Actin recruitment by binding the FH1 domain (Mason et al., 2011) or c) capping proteins that compete for association with filament barbed ends (Bartolini et al., 2012).

Stabilization

Formins compete with capping proteins, such as capping protein (CapZ) or Adducins, for binding to filament barbed ends (Shekhar et al., 2015), to shield filaments from depolymerization (Ulrichs et al., 2023) (Figure 13). This protective function is achieved through formins' leaky cap activity, allowing processive elongation in a Profilin-rich environment, or serving as capping proteins, that stabilize Actin filaments in a profilin-free environment (Harris et al., 2004; Kovar, 2006) (Figure 13). The capping ability of formins is expressed as its gating factor, describing the time a formin spends in the *open* versus *closed* state during elongation (Paul & Pollard, 2009).

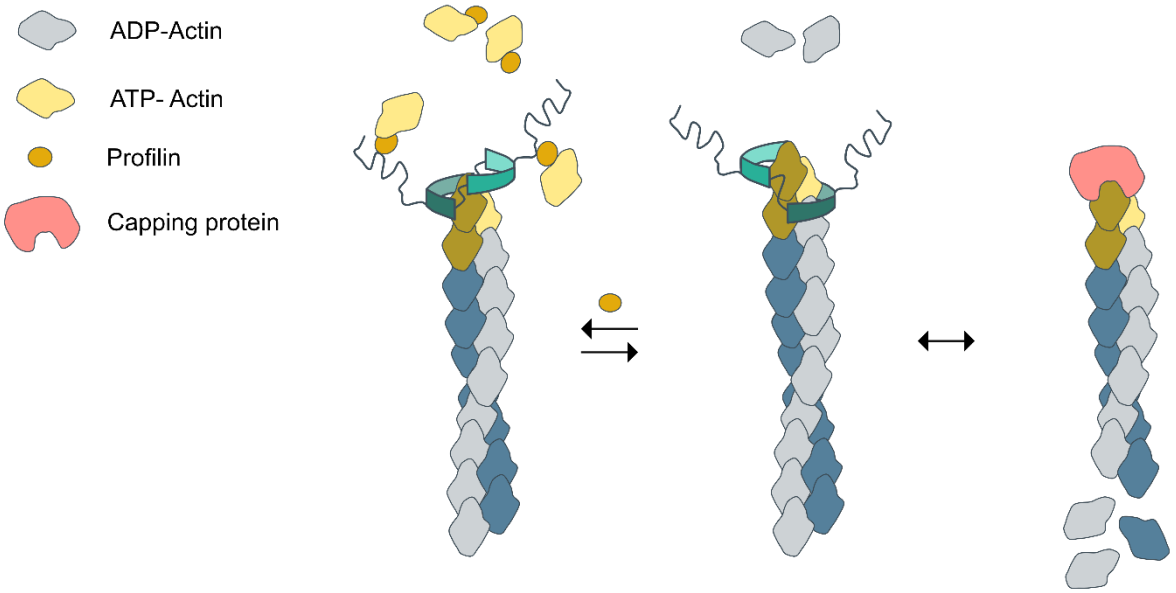

Figure 13: Formin-mediated Stabilization of Actin Filaments.
In a profilin-free environment formins can serve as capping proteins. This capping ability is described as its gating factor determined by the time spent in the open or close configuration during Actin assembly. Gating factors vary among formins, ranging from almost 0 (indicating a capped filament) for *S. pombe* Cdc12 to nearly 1 (signifying uninhibited elongation) for mDia1 (Kovar, 2006). Furthermore, formins compete with capping proteins for barbed end association, resulting in the stimulation of pointed end disassembly (Blanchoin et al., 2000).

Distinct formins exhibit varying degrees of impediment to elongation and depolymerization due to differences in gating factors and nucleation efficiency (Harris et al., 2004; Kovar et al., 2006; Neidt et al., 2009). As a result, cells can selectively employ individual formins to fulfill specialized functions such as fast nucleation, elongation, or stabilization of existing filaments (Shemesh & Kozlov, 2007).

Regulation of Formin-mediated Actin Assembly

The Actin functions of most mammalian formins are regulated through autoinhibition, mediated by an intramolecular interaction between an N-terminal diaphanous inhibitory domain (DID) and a C-terminal diaphanous autoregulatory domain (DAD) flanking the FH1 and FH2 domains (Figure 14). While the domain architecture of formins is highly conserved, autoinhibition is released by individual factors, including proteins (Brenig et al., 2015) and/or lipids (Ramalingam et al., 2010). For example, binding of the active small Rho GTPase RhoA to an N-terminal Rho binding domain (RBD) triggers the release of mammalian diaphanous 1 (mDia1) autoinhibition (Otomo et al., 2005; Rose et al., 2005), resulting in its dimerization followed by Actin assembly (Figure 14).

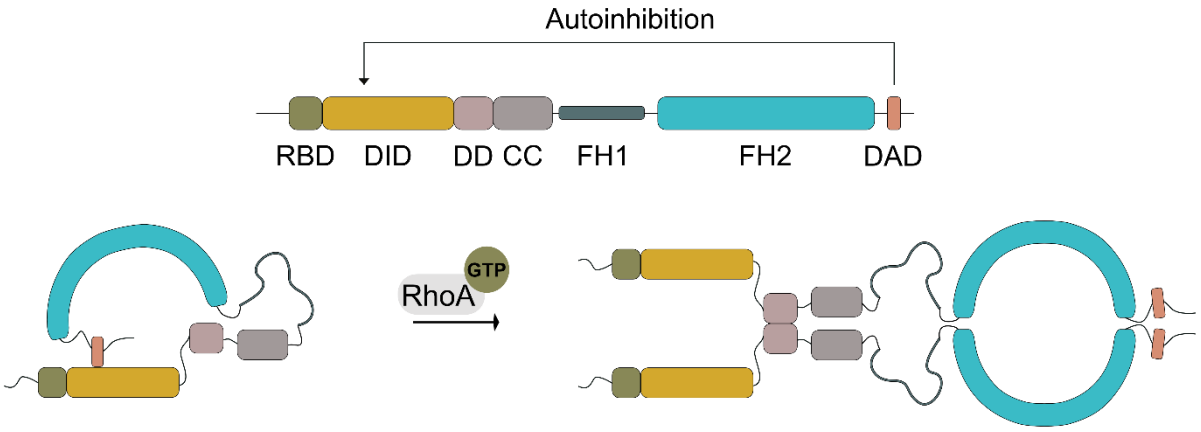

Figure 14: Domain Organization and Regulation of mDia1.
Diaphanous-related formin 1 (mDia1) contains an N-terminal GTPase-binding domain (GBD), an adjacent diaphanous inhibitory domain (DID), followed by a dimerization domain (DD), a coiled-coil (CC) and a C-terminal diaphanous autoregulatory domain (DAD) flanking the FH1 and FH2 domains. mDia1 is autoinhibited by an intramolecular interaction of its DID and DAD, hindering the FH2 domain to exert its F-Actin functions (Nezami et al., 2010; Otomo et al., 2010). mDia1 can be activated by the active small Rho GTPase RhoA, among other factors (Maiti et al., 2012).

1.2.2. Regulation of Actin Assembly by Rho GTPases

To tightly regulate Actin assembly, most nucleation-promoting factors (NPFs), including WASP family proteins and formins, are subject to autoinhibition. The release of autoinhibition is governed by signal transduction pathways through members of the Ras homologous (Rho) small GTPase family. Rho family GTPases serve as molecular switches (H. R. Bourne et al., 1990, 1991) that transduce extracellular signals to elicit cellular responses such as gene expression, cell morphology, and migration by specifically modulating rearrangements of the cytoskeleton (Chrzanowska-Wodnicka & Burridge, 1996; Machesky & Hall, 1997; Ridley et al., 1992; Ridley & Hall, 1992; Subauste et al., 2000). This family comprises 20 members, grouped into subfamilies based on sequence homology (Jaiswal et al., 2013): Cdc42 (Cdc42, G25K, TC10, TCL, WRCH1, and WRCH2); Rac (Rac1, Rac1b, Rac2, Rac3, and RhoG); Rho (RhoA, RhoB, and RhoC); RhoD (RhoD, and Rif); RhoH and Rnd (Rnd1, Rnd2, and Rnd3). As Rho GTPases are involved in dynamic cellular responses, their activities underlie tight spatiotemporal regulation through coordination of guanine nucleotide loading. The regulation of most Rho GTPases is based on the cycling between an active guanosine triphosphate (GTP) and an inactive guanosine diphosphate (GDP)-bound conformation. The switch cycle is mediated by three groups of regulatory proteins:

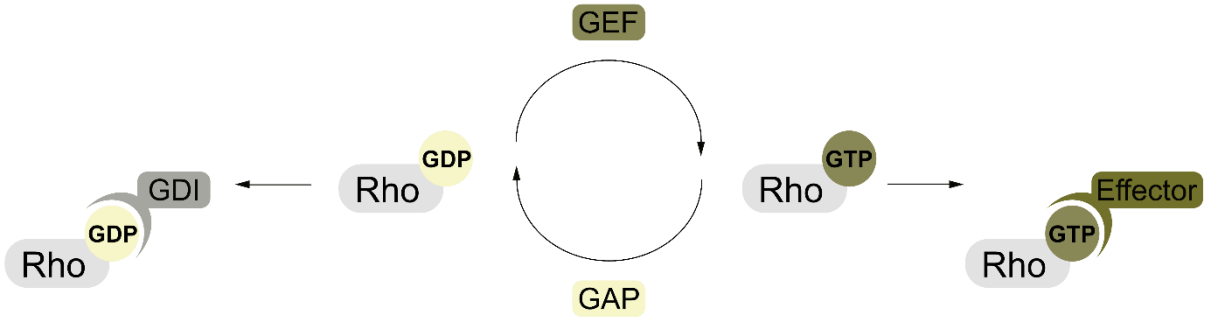

Figure 15: The Rho GTPase Switch Cycle.
GTPases feature a conserved nucleotide binding domain, known as the G-domain, comprising five sequence motifs (G1-G5) (Wittinghofer & Vetter, 2011). Activation of Rho GTPases is orchestrated by guanine exchange factors (GEFs), which stabilize the nucleotide-free state of GTPases (Lenzen et al., 1998) by displacing Mg^{2+} from the catalytic pocket. As cellular concentration of GTP is 10-fold higher than of the diphosphate (Bos et al., 2007), and GTPases have similar affinity for GDP/GTP, GEF binding stimulates loading of the more abundant GTP, which displaces the GEF and stimulates effector binding (Cherfils & Zeghouf, 2013). Rho GTPases exhibit an intrinsic, albeit inefficient, GTPase activity which is enhanced by over 4000-fold upon binding of GTPase-activating proteins (GAPs) (B. Zhang & Zheng, 1998). GAPs stimulate GTP hydrolysis by inserting water into the catalytic pocket (Moon & Zheng, 2003). Both GEFs and GAPs interact with similar binding interfaces (switch I (G2) and II (G3)) of the Rho GTPases (Fidyk & Cerione, 2002; Rossman et al., 2002) to confer conformational rearrangement (Dvorsky & Ahmadian, 2004). GDP-dissociation inhibitors (GDIs) negatively regulate Rho GTPases by impeding GDP replacement and sequestering prenylated forms in the cytosol (Garcia-Mata et al., 2011; Molnár et al., 2001).

Guanine nucleotide exchange factors (GEFs) activate Rho GTPases by catalyzing the exchange of GDP to GTP (Rossman et al., 2002), increasing affinity to bind effector proteins up to 100-fold (Fujisawa et al., 1996; Reid et al., 1996) (Figure 15). Conversely, GTPase-activating proteins (GAPs) stimulate the intrinsic hydrolysis rate of GTP, leading to GTPase inactivation (Bos et al., 2007; Gibbs et al., 1990) (Figure 15). Additionally, spatial localization and activity are modulated by post-translational lipid modification of a C-terminal CAAX (cysteine-aliphatic-aliphatic-X amino acid) motif that tethers Rho GTPases to membranes. Guanine nucleotide dissociation inhibitors (GDIs) can sequester GDP-loaded lipidated forms of Rho GTPases in the cytosol (Sasaki et al., 1993), preventing their membrane recruitment and binding of effectors (Garcia-Mata et al., 2011) (Figure 15).

Among the Rho GTPases, Cdc42, Rac1, and RhoA are the most studied canonical members (Burridge & Wennerberg, 2004), and their activities result in distinct Actin-based structures orchestrated by the actions of their main downstream effectors: Active Cdc42 governs the formation of filopodia, long, elongated rods of parallel Actin bundles important for cell motility and sensing the external environment (Nobes & Hall, 1995) (Figure 16). Filopodium formation is initiated by Cdc42-mediated stimulation of Arp2/3 Actin nucleation through the activation of WASP/N-WASP (Figure 16). Similarly, activation of Rac1 signals to the Arp2/3-mediated formation of

endocytic patches (Rotty et al., 2013) or lamellipodia, dense branched Actin networks involved in cell protrusion (Ridley et al., 1992), by means of the WAVE regulatory complex. Conversely, RhoA generates stress fibers, antiparallel Actin filaments crosslinked by non-muscle myosin II that mediate cellular mechanical responses.

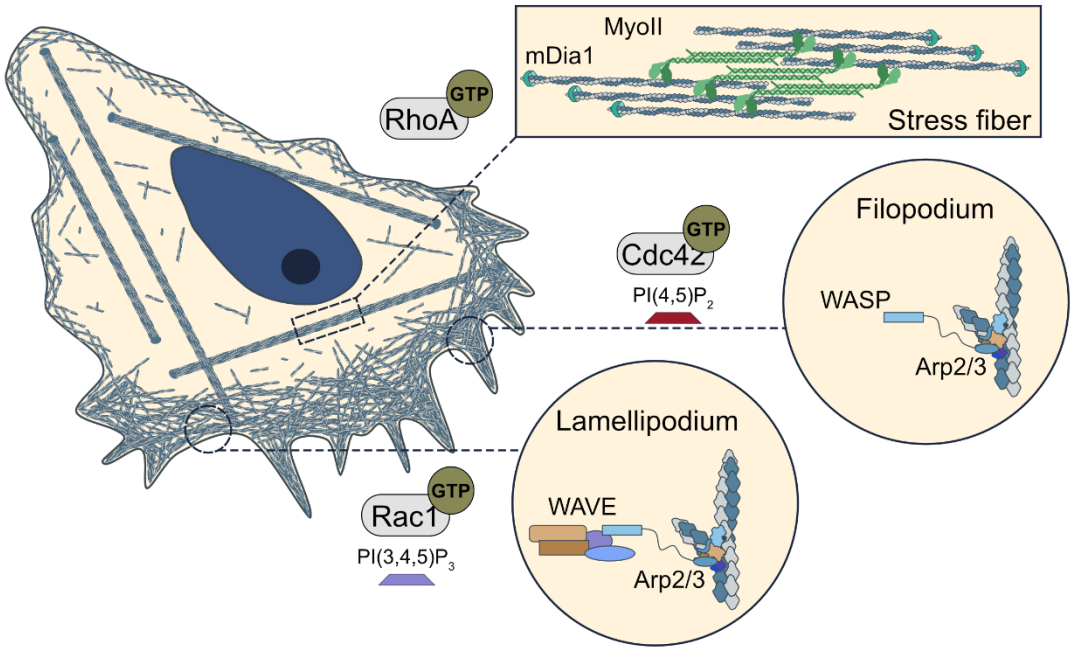

Figure 16: Small Rho GTPases form distinct Actin-based cellular Structures.
In migrating cells, the Actin cytoskeleton forms distinct structures downstream of Rho GTPases. RhoA activity mediates the formation of contractile stress fibers via mDia1-mediated linear filament assembly crosslinked by non-muscle myosin II bundles. Both Cdc42 and Rac1 stimulate Arp2/3-mediated Actin networks by releasing the autoinhibition of Wiskott-Aldrich Syndrome Protein (WASP) family members (Campellone & Welch, 2010) under spatial control of distinct phosphoinositide plasma membrane identities: While WASP/N-WASP activation requires simultaneous binding of Cdc42-GTP and $PI(4,5)P_2$ in the plasma membrane, prenylated Rac1-GTP (Chen et al., 2010; Ding et al., 2022) and $PI(3,4,5)P_3$ (Oikawa et al., 2004; Sossey-Alaoui et al., 2005) stimulate the activity of the WAVE regulatory complex to form filopodia and lamellipodia, respectively.

Myosins are molecular motors consisting of a head and tail region (Figure 17) that translocate along F-Actin through ATP hydrolysis towards barbed ends (Vicente-Manzanares et al., 2009). Their tails form bipolar filaments that tether F-Actin in an antiparallel manner, resulting in sliding of the filaments, a process fundamental to muscle contraction (Blanchoin et al., 2014) (Figure 18). RhoA stimulates actomyosin contractility via the concerted activities of its effectors mDia1 and Rho-associated protein kinase (ROCK) (N. Watanabe et al., 1999) (Figure 17). ROCK stimulates myosin contractility via phosphorylation cascades (Kaibuchi et al., 1999) triggering filament formation and bundling F-Actin into stress fibers (Figure 17).

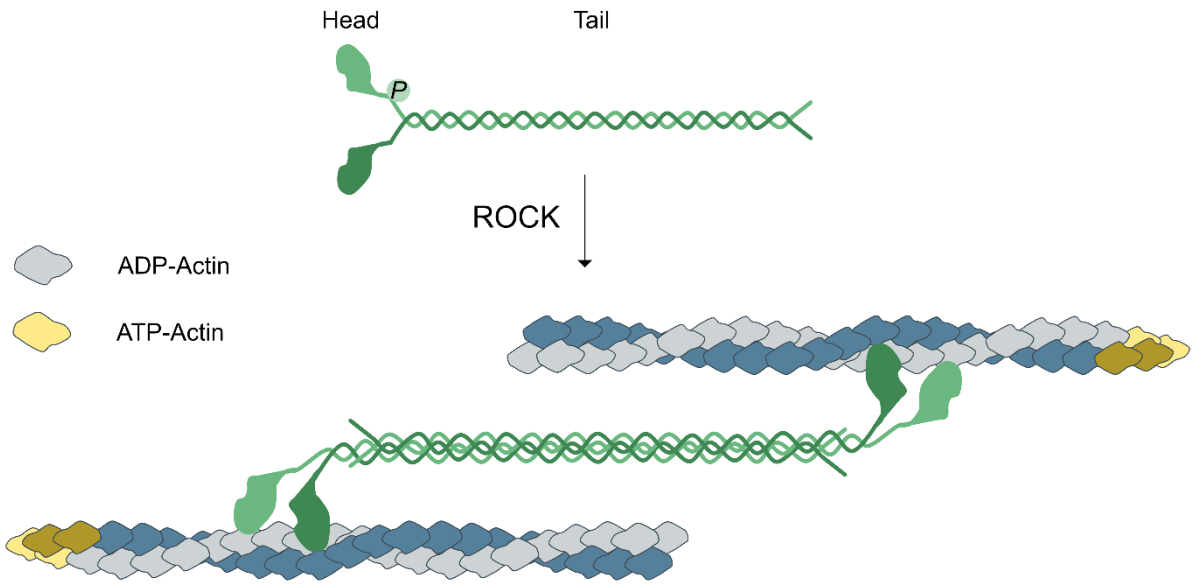

Figure 17: Actomyosin-based Stress Fibers.
Non-muscle myosin II forms dimers via its tail domain and contains a globular head with an Actin-binding region and the ATPase motor (Vicente-Manzanares et al., 2009). Upon RhoA activation, its effector Rho-associated kinase (ROCK) phosphorylates and inhibits myosin light chain phosphatase (N. Watanabe et al., 1999). Increased non-muscle myosin phosphorylation simulates its assembly into bipolar bundles that crosslink Actin filaments in an anti-parallel orientation. Through its ATPase activity non muscle myosin II can move towards the barbed ends of Actin filaments.

While all three canonical members, Cdc42, Rac1, and RhoA, are implicated in modulating distinct signaling pathways, all of them differentially regulate endocytosis in non-neuronal cells via various actions of their effectors (W. S. Garrett et al., 2000; Khandelwal et al., 2010; Lamaze et al., 1996). In particular, Cdc42 and Rac1 have been implicated in fast Endophilin-mediated endocytosis (FEME) (Boucrot et al., 2015; Renard et al., 2015), a process closely resembling endocytic pathways observed at synapses.

1.3. The Role of the Presynaptic Actin Cytoskeleton in Neurotransmission

Neurotransmission relies on the retrieval of lipids and proteins and the reformation of synaptic vesicles through endocytic pathways following neurotransmitter release. The principle underlying endocytosis involves the process of membrane invagination, wherein a flat membrane undergoes transformation through bending to generate oval or round vesicles (Shin et al., 2022). This budding process is facilitated by mechanical force, often induced by proteins like Clathrin, that assemble into cage-like structures as a multimeric coat (Lacy et al., 2018). In neurons, the involvement of Clathrin in SV

endocytosis is a subject of debate, suggesting a limited role in the initial retrieval of endocytic intermediates from the presynaptic membrane at physiological temperature (Kononenko et al., 2014; Soykan et al., 2017). Alternatively, Actin polymerization at the cell cortex paired with myosin contractility can provide mechanical properties for bending the underlying membrane (Figure 18).

1.3.1. Force Generation by the Actomyosin Cytoskeleton

The dynamics of the actomyosin cytoskeleton can exert mechanical forces (Blanchoin et al., 2014). Forces are generated by the directed assembly of F-Actin, e.g., towards the plasma membrane, as well as myosin-movement-based contractility resulting in pushing and pulling action, respectively (Figure 18). Thereby, actomyosin dynamics tightly couple biochemical and mechanical properties to drive a multitude of cellular processes that necessitate membrane deformation.

For example, the ability of actomyosin to deform the underlying membrane is a crucial determinant of endocytosis in *Saccharomyces cervisiae* (Ayscough, 2000; Engqvist-Goldstein & Drubin, 2003; Kaksonen et al., 2006). While disruption of Actin dynamics fully arrests endocytosis in yeast, similar pharmacological treatments only partially affect endocytic pathways in mammalian cells (Miya Fujimoto et al., 2000). Hence, many studies have reached different conclusions as to whether and at which step Actin is involved in endocytosis in eukaryotic cells (Boulant et al., 2011; Ferguson et al., 2009; Merrifield et al., 2005; Saffarian et al., 2009; Soulet et al., 2005; Yao et al., 2013). As the pattern of molecular events, as well as the involved proteins themselves, seem to be conserved between mammalian cells and yeast, the varying requirements for Actin have remained controversial. One potential explanation arises from higher energy barriers to deform the plasma membrane in yeast due to their higher turgor pressure (Dmitrieff & Nédélec, 2015). Hence, under high tension Actin polymerization and myosin contractility (Figure 18) provide the additional force needed for endocytic membrane deformation (Aghamohammadzadeh & Ayscough, 2009; Galletta et al., 2010; Hassinger et al., 2017; Thottacherry et al., 2018).

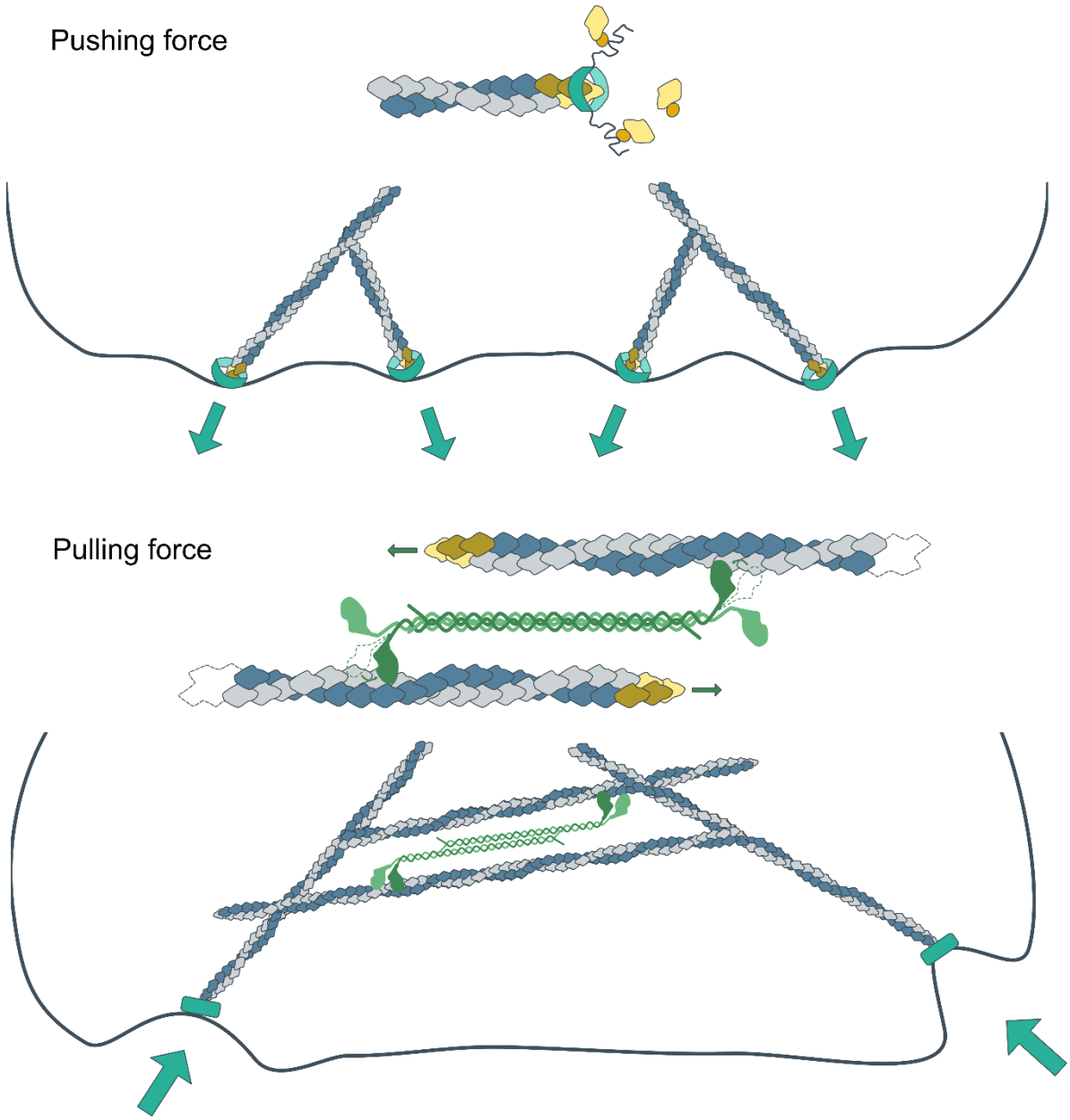

Figure 18: Force Generation by the Actomyosin Cytoskeleton.
When F-Actin barbed end assembly is directed towards the plasma membrane, Actin polymerization exerts a pushing force on the order of 1 pN per filament (Clarke & Martin, 2021). Conversely, the Actin cytoskeleton can also produce pulling forces by concerted action of non-muscle myosin II (MyoII) bundles, that crosslink multiple Actin filaments. Through ATP-hydrolysis MyoII moves along F-Actin towards barbed ends. This movement results in sliding F-Actin strands in opposing directions, producing contractility. If F-Actin is anchored to the plasma membrane via integral membrane proteins, a single myosin molecule can generate a force on the order of 3-5 pN (Finer et al., 1995; Molloy et al., 1995).

Accordingly, under conditions of high membrane tension, CME is also Actin-dependent in mammalian cells (Boulant et al., 2011; Kaur et al., 2014). The tension of the plasma membrane not only controls endocytosis through Actin dynamics but also additionally regulates the recruitment of BAR proteins (Riggi et al., 2019),

Clathrin pit formation (Saleem et al., 2015), and membrane fission by Dynamin (Morlot et al., 2012).

1.3.2. Cytoskeletal Contributions to Plasma Membrane Tension

Cellular membranes represent lipid bilayers under tension deriving from the in-plane force required to counteract hydrostatic pressure and surface expansion. Tension of the cellular plasma membrane is further modulated by contributions from cortical tension originating from adhesive forces of the underlying Actomyosin cytoskeleton (Dai & Sheetz, 1995; Waugh & Bauserman, 1995). Factors such as peripheral protein binding, transmembrane, and membrane-to-cortex attachment proteins contribute to cortical tension and constrain perturbations, including area changes to specific regions of the plasma membrane. Fluctuations in tension have to be accommodated through various mechanisms to prevent rupture of the plasma membrane (Lieber et al., 2013; Roffay et al., 2021): To counteract membrane perturbations, cells can generate or flatten membrane reservoirs like folds, wrinkles, caveolae, vacuole-like invaginations, and blebs as a first response to low or high tension, respectively (Gauthier et al., 2011; Sinha et al., 2011). Apart from modulating membrane architecture according to tension changes, cells can further translate biophysical cues into biochemical signaling by adjusting cytoskeletal assembly, cell adhesion, and/or membrane trafficking like exo- and endocytic coupling.

Plasma membrane tension bidirectionally regulates the balance between exocytosis and endocytosis in a wide range of cell types (Apodaca, 2002; Boulant et al., 2011). Similarly in neurons, raising plasma membrane tension inhibits both rapid and slow endocytic pathways (X. S. Wu et al., 2017) and acts as a global inhibitor of Actin assembly (Houk et al., 2012), while reducing tension triggers SV endocytosis in an Actin-dependent manner (Orlando et al., 2019), likely via facilitated tubulation activity of N-BAR proteins like Endophilin (Renard et al., 2015; Shi & Baumgart, 2015).

Consequently, most processes that are induced by perturbations in tension cause inverted effects downstream of their signaling cascades. Such reciprocal interactions between biochemical signals and physical forces form negative feedback circuits (Houk et al., 2012) that enable tension homeostasis in the range of minutes (Lieber et al., 2013). Similar tension homeostasis was found in neurons during SV cycling: Synaptic vesicle exocytosis results in a drop of plasma membrane tension, which recovers over the time course of endocytosis (20 s) (Perez et al., 2022).

The proper mechanoadaption requires a cellular tension-sensing mechanism that initiates the homeostatic remodeling of the plasma membrane by controlling Actin dynamics and exo- and endocytic coupling.

1.3.3. Regulation of Membrane Homeostasis by mTORC2

A known signaling network that couples Actin dynamics and endocytosis is mediated by the mechanistic target of rapamycin (mTOR) kinase (Jacinto et al., 2004; Riggi et al., 2019), an evolutionarily conserved serine and threonine kinase. Structurally, the mTOR kinase is an indispensable catalytic subunit for two functionally distinct subcomplexes, namely mTOR complex 1 (mTORC1) and mTOR complex 2 (mTORC2), that differ in their subunit composition (Figure 19) and sensitivity to the drug rapamycin (Loewith et al., 2002).

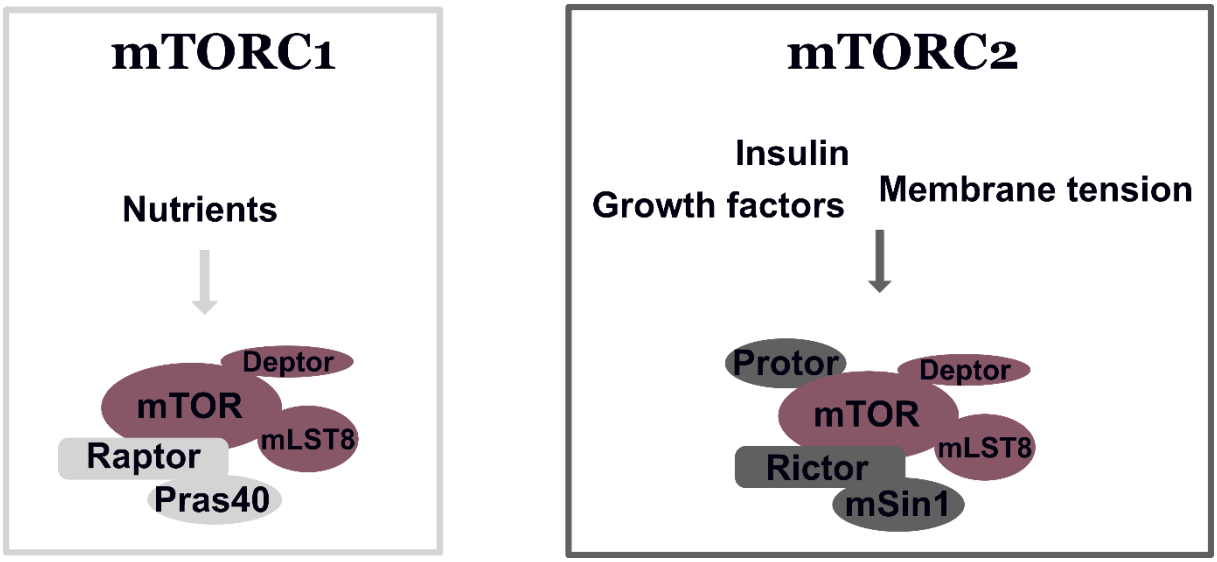

Figure 19: Structure and Regulation of mTORC1 and mTORC2.
mTORC1 and 2 share the catalytic mTOR kinase and mammalian lethal with SEC13 protein 8 (mLST8) as essential core proteins. Regulatory-associated protein of mTOR (RAPTOR) and proline-rich AKT substrate of 40 kDa (Pras40) are specific subunits of mTORC1, while rapamycin-insensitive companion of mTOR (RICTOR), mammalian stress-activated Map kinase-interacting protein 1 (mSIN1) and protein associated with Rictor (Protor) are unique to the core of mTORC2. Rictor is supposed to play a scaffolding role, while mSIN1 likely contains substrate binding sites and controls subcellular localization. Recent high resolution crystallization studies, determine mTORC2 as a homodimer. In contrast to mTORC1, the C-terminal domain of RICTOR masks the FKBP-rapamycin motif in mTOR resulting in the rapamycin-insensitive nature of mTORC2 (Scaiola et al., 2020). Deptor is a suppressor of both mTORC1 and mTORC2 activity.

Both complexes sense cellular physiologic cues but with different specificities to ensure cell growth, motility and metabolism. mTORC1 is activated by amino acids or nutrients to stimulate protein synthesis via p70 S6 Kinase (S6K) at threonine$_{398}$. Conversely, mTORC2 activity is regulated by plasma membrane tension, but also growth factor and

insulin signaling to control cell survival (Brazil et al., 2004), cytoskeletal rearrangements (Dos et al., 2004), as well as endocytosis (Riggi et al., 2019).

mTORC2 can bidirectionally sense membrane tension (Figure 20) and catalyzes compensatory modulation of membrane composition or cortical tension as a feedback mechanism conserved from yeast (Berchtold et al., 2012) to mammalian cells (Diz-Muñoz et al., 2016; Kippenberger et al., 2005; Sedding et al., 2005). Its tension-sensing mechanism is well described in yeast, where TORC2 gets activated by redistribution of $PI(4,5)P_2$ in response to increasing tension (Olivera-Couto & Aguilar, 2012; Walther et al., 2006) (Figure 20). Active TORC2 resolves membrane stress by modulating the Actin cytoskeleton and endocytosis, resulting in its own inactivation (Jacinto et al., 2004; Niles & Powers, 2012) (Figure 20).

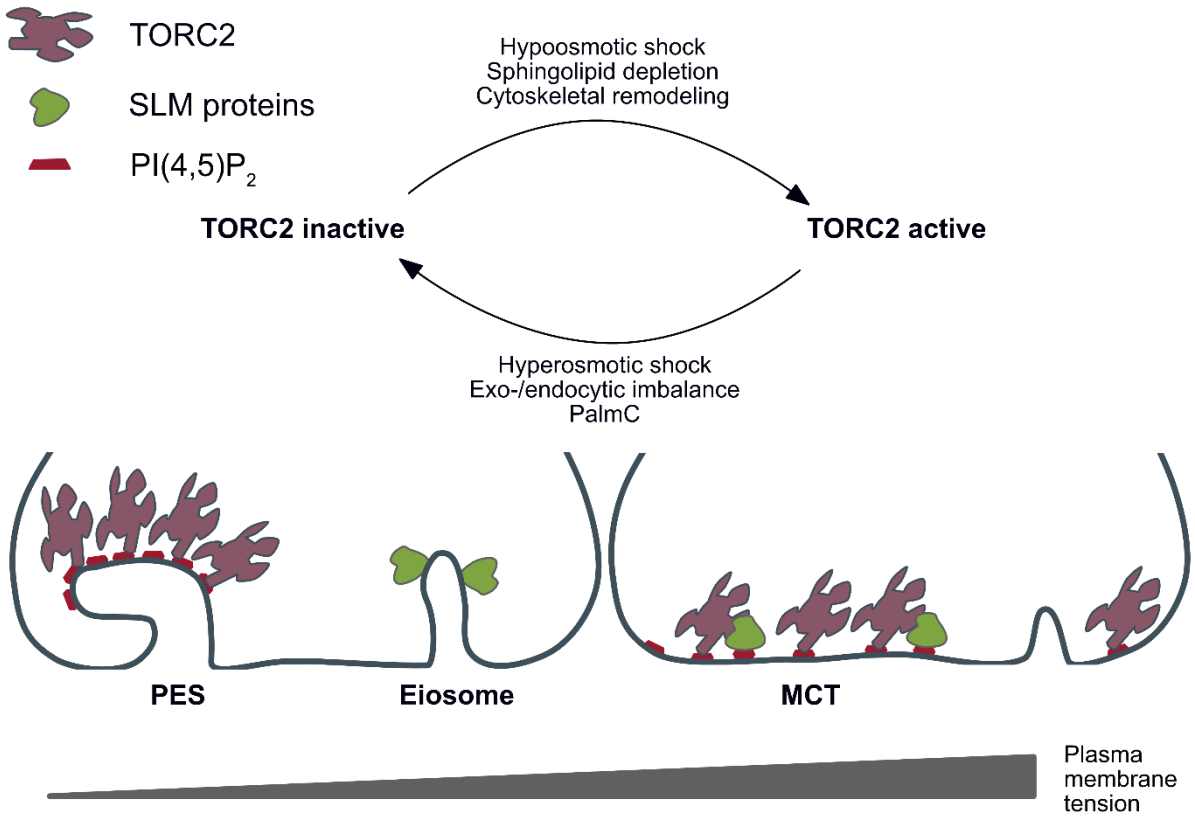

Figure 20: Tension Regulation of TORC2.
In Saccharomyces cerevisiae increases in membrane tension redistribute $PI(4,5)P_2$ binding proteins (SLM proteins), that are liberated from distinct plasma membrane domains, furrow-like invaginations organized by BAR proteins called eiosomes (Olivera-Couto & Aguilar, 2012; Walther et al., 2006), to membrane compartments containing TORC2 (MCT, (Berchtold & Walther, 2009). Therein, SLM proteins bind and activate TORC2, while facilitating recruitment of the serine/threonine kinase Ypk1 (the yeast homolog of AKT) for its consequent phosphorylation and activation by TORC2. Activated Ypk1 promotes biosynthesis of sphingolipids (Aronova et al., 2008), which in turn resolves membrane stress and causes TORC2 inactivation (Niles & Powers, 2012). Conversely, TORC2 inhibition by reduced membrane tension is triggered by reorganization of pre-existing $PI(4,5)P_2$ into discrete membrane invaginations (PES) that sequester TORC2 by membrane lipid phase-separation (Riggi et al., 2018).

In mammalian cells, active mTORC2 phosphorylates and consequently activates a number of downstream substrates, mainly AGC kinases, including protein kinase B (AKT) and protein kinase C (PKC) among others (Figure 21).

The mTORC2-dependent transient phosphorylation of the serine$_{473}$ residue of AKT1 is often used as the hallmark of mTORC2 activity in experimental studies (p-AKT1; (Bayascas & Alessi, 2005)) (Figure 21).

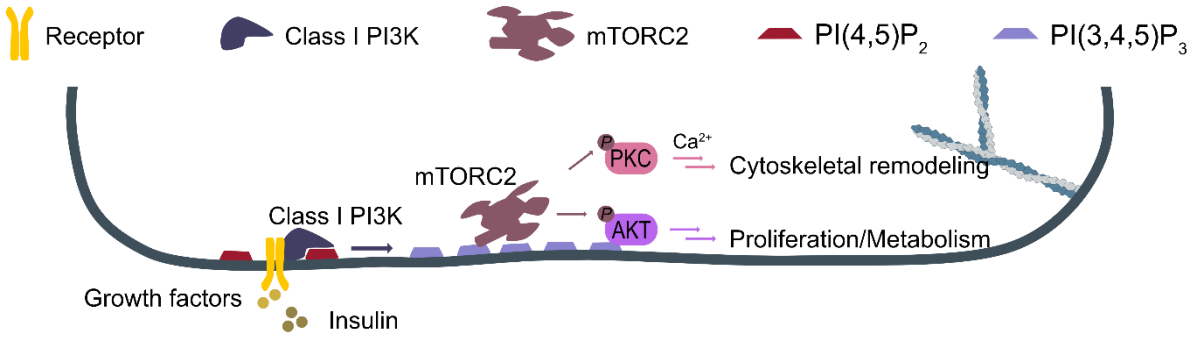

Figure 21: mTORC2-mediated Phosphorylation of Protein kinases B and C.
Upon stimulation of class I PI3K activity by growth factors or insulin, increased PI(3,4,5)P_3 levels recruit mTORC2 substrate protein kinase B (AKT) and 3-phosphoinositide dependent kinase 1 (PDK1) to the plasma membrane, resulting in AKT phosphorylation at threonine$_{308}$ in the activation loop (Bellacosa et al., 1998). This phosphorylation event primes AKT for a consecutive phosphorylation in its hydrophobic motif at serine$_{473}$ (p-AKT) (Bayascas & Alessi, 2005), which is mediated by mTORC2. In turn, active p-AKT phosphorylates downstream targets that control cell survival, growth, proliferation and cell metabolism, e.g. by downregulating the activity of inhibitors (PRAS40) of mTORC1 signaling (Manning & Cantley, 2007). In addition, mTORC2 phosphorylates protein kinase C (PKC) in a constitutive manner (Newton, 2018). Mature phosphorylated PKC is autoinhibited via a pseudosubstrate (Leonard et al., 2011) and gets activated by the binding of Ca^{2+} and diacylglycerol (DAG) inducing the remodeling of the Actin cytoskeleton (Jacinto et al., 2004).

Studies in nerve cells have shown that AKT is phosphorylated in an activity-dependent manner and controls Dynamin activity via downstream phosphorylation cascades (Smillie & Cousin, 2012). Furthermore, the mTORC2 substrate PKC acts as a synaptic Ca^{2+} sensor and modulates SV endocytosis (Jin et al., 2019) through phosphorylation of endocytic proteins, including the F-BAR protein PACSIN1 (Plomann et al., 1998) or the regulation of the cytoskeleton. Regulation of the cytoskeleton includes the modulation of membrane composition via its phospholipid identity that affects membrane-to-cortex attachments or the direct phosphorylation of Actin regulatory proteins (Ono et al., 2022).

Through its bidirectional sensing of membrane tension and compensatory activity to modulate membrane architecture via the control of the Actin cytoskeleton, mTORC2 plays a key role in regulating membrane homeostasis, a principal factor of SV endocytosis. Accordingly, recent studies have underlined the importance of mTORC2 in the brain (Carson et al., 2013; Siuta et al., 2010) in shaping neuronal morphology

(Thomanetz et al., 2013) and regulating plasticity by controlling the rearrangements of the Actin cytoskeleton (Huang et al., 2013).

1.3.4. Distinct Actin Pools Modulate the SV Cycle.

Decades of research have yielded a detailed description of the molecular components of presynaptic terminals (Wilhelm et al., 2014). Yet, the nanoscale organization of the presynaptic Actin cytoskeleton has largely remained elusive, due to the occlusion of the presynaptic signal in diffraction-limited microscopy (Jung et al., 2020) by the apposed enriched Actin network of the postsynapse (Allison et al., 1998) (Figure 22). Recent advances in super-resolution microscopy have identified distinct pools of presynaptic Actin, a mesh located at the active zone, rails connecting the active zone and the reserve SV pool, and an Actin corral spanning the presynaptic compartment (Bingham et al., 2023) (Figure 22).

These Actin pools have been shown to serve contrasted roles at different steps of the SV cycle (Bleckert and Photowala, 2012): The cytoskeleton acts as a scaffold to surround the reserve (Sankaranarayanan et al., 2003), the ready-releasable pool of SVs (Guzman et al., 2019) and the endocytic zone (Ogunmowo et al., 2023) (Figure 22). At the reserve pool, SVs are clustered by crosslinks with synapsins that connect vesicles to F-Actin. Actin rails connect the reserve pool with the active zone (Cingolani & Goda, 2008) (Figure 22) and facilitate RRP replenishment (Sakaba & Neher, 2003; X. S. Wu et al., 2016) by SV transport through myosin activity (González-Forero et al., 2012; Maschi et al., 2018; A. Peng et al., 2012; G. Srinivasan et al., 2008). Actin also participates in clustering of the AZ machinery and limits SV fusion and neurotransmitter release through a barrier function (Glebov et al., 2017) (Figure 22). This barrier function is likely mediated by a branched Actin network mediated by Rac1 signaling, which negatively regulates synaptic strength and release probability via synaptic vesicle priming (Keine et al., 2022; O'neil et al., 2021).

1.3.4.1. The Role of Presynaptic Actin in Synaptic Vesicle Endocytosis

Presynaptic Actin is highly dynamic (Colicos et al., 2001) and the abundance of F-Actin is increased following continuous neuronal activity (Job & Lagnado, 1998). Furthermore, impairing endocytosis, e.g. by loss of Dynamins, results in the accumulation of Actin filaments at stalled endocytic intermediates (Ferguson et al., 2009).

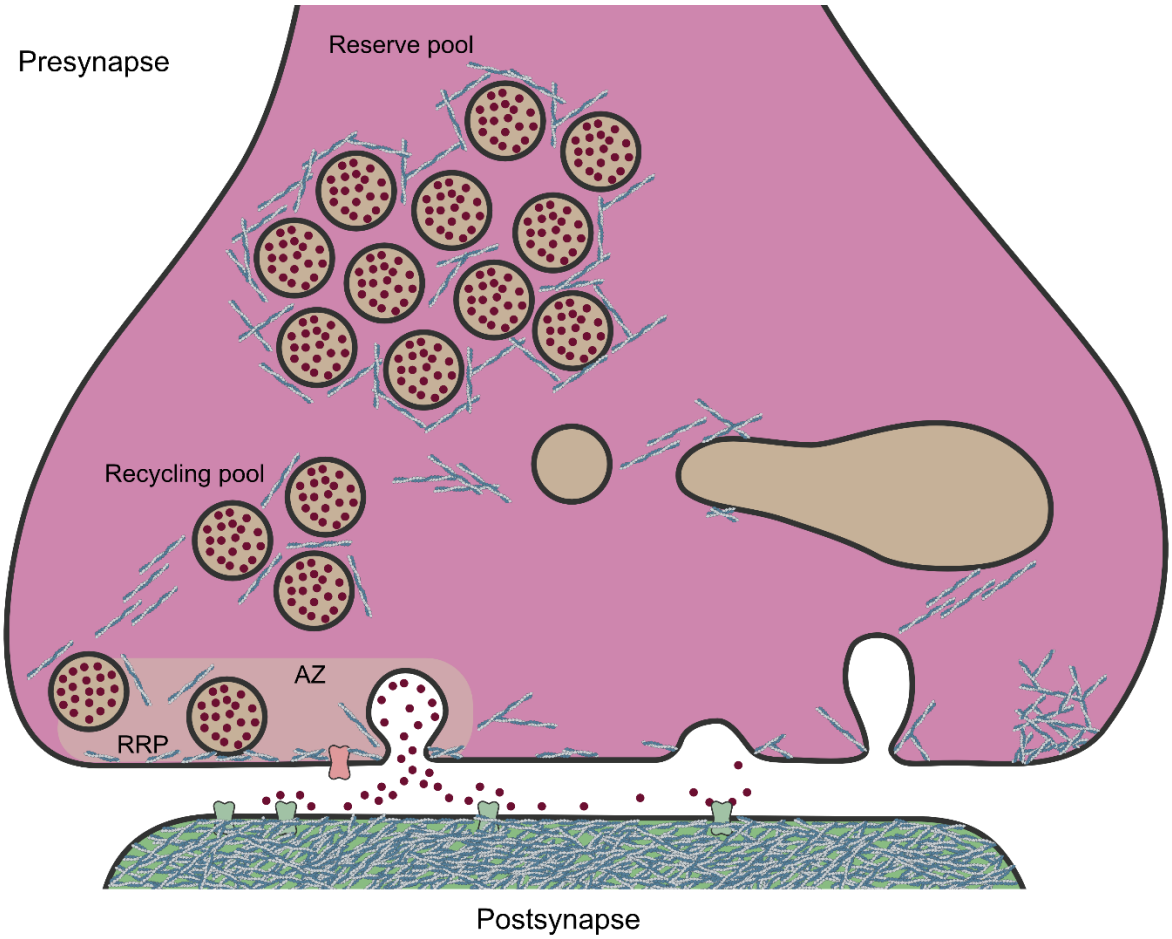

Figure 22: Presynaptic Actin Pools modulate the Synaptic Vesicle Cycle.
Actin filaments act as scaffolds to cluster the reserve, recycling and ready-releasable pool (RRP) of synaptic vesicles. An Actin mesh at the active zone (AZ) modulates AZ architecture and acts as a barrier to limit SV fusion. Cytoskeletal dynamics facilitate the formation of endocytic intermediates by pushing forces via direct assembly and/or by forming a corral-like rigid diffusion barrier. Rails of Actin filaments connect the endocytic zone, synaptic vesicles pools and the active zone driving SV transport dependent on non-muscle myosin activity.

Similar to endocytosis in non-neuronal cells, the role of the Actin cytoskeleton in SV endocytosis has been highly debated. Genetic depletion of Actin monomers fully arrests all forms of endocytosis at several synapse types (X. S. Wu et al., 2016). However, pharmacological perturbations of Actin organization utilizing the same drugs have yielded inconclusive, often conflicting results depending on the model system and experimental conditions used (Babu et al., 2020; Bleckert et al., 2012; J. Bourne et al., 2006; Delvendahl et al., 2016; Eguchi et al., 2017; Holt et al., 2003; Z. Hua et al., 2011; Z. Li & Murthy, 2001; Richards et al., 2004; Sankaranarayanan et al., 2003; Soykan et al., 2017; D. Wang et al., 2010; S. Watanabe et al., 2014; W. Zhang & Benson, 2001). Based on recent studies, two models have diverged on how the Actin cytoskeleton might contribute to SV endocytosis. In a passive mode, rigid Actin networks surround the endocytic zone, forming a diffusion barrier that enhances

tension at the periphery of the bouton, facilitating endocytic membrane invagination. In this model, membrane compression during SV exocytosis drives endocytic pit formation through mechanical coupling (Ogunmowo et al., 2023). Here, Actin acts as a restrictive membrane scaffold that promotes Dynamin-mediated fission by keeping invaginations under longitudinal tension (Roux et al., 2006). Conversely, in the active participation model, membrane invagination is achieved via active pushing and pulling forces generated by *de novo* localized Actin polymerization coupled with myosin contractility. Here, Actin polymerization helps with the initiation of the membrane pit, while contractile forces become essential for the later progression of vesicle formation (Carlsson & Bayly, 2014) (Figure 22). In this model, Actin regulatory factors are actively recruited through, e.g., the action of BAR proteins.

Recent studies have indicated a novel and significant role for Actin-regulatory proteins of the formin family in synaptic vesicle endocytosis, using pharmacological perturbation. In contrast to Arp2/3-mediated processes (Ganguly et al., 2015), formin activity mediates the retrieval of SV proteins at rodent central synapses (Soykan et al., 2017). From this family, the isoform mammalian diaphanous 1 (mDia1) has emerged as a potential candidate to orchestrate endocytosis as an effector of the small Rho GTPase RhoA by modulating cytoskeletal rearrangements driving presynaptic membrane architecture (Deguchi et al., 2016).

2. Aims of the Study

Following the controversy surrounding Actin manipulation in synaptic vesicle endocytosis, we aimed to further elucidate the components of the synaptic cytoskeleton that drive endocytic pathways at mouse hippocampal boutons. Through a combination of pharmacological and genetic perturbation, we assessed the effects of the manipulation of cytoskeletal nucleators and regulatory proteins utilizing live-cell tracking of synaptic vesicle dynamics as well as super-resolution techniques such as stimulated emission depletion and electron microcopy. We designed strategies to pinpoint what nucleator drives Actin assembly at presynaptic boutons, building on the previous identification of the formin candidate mDia1, and investigating how Actin nucleators aid the retrieval of endocytic intermediates (e.g., via active directed force generation or a passive scaffolding role in setting cortical tension, etc.). We further intended to identify signaling networks that regulate such neuronal cytoskeletal dynamics, e.g., by means of the canonical members of the small Rho GTPase family, Cdc42, Rac1, and RhoA, known to mediate distinct Actin-assembly mechanisms. Finally, we intended to address what connects synaptic activity and neurotransmitter release to cytoskeletal remodeling and endocytosis induction by elucidating coupling mechanisms (e.g. plasma membrane tension, calcium/mTORC2 signaling, etc.).
In sum, we aimed to clarify and reconcile previous conflicting data to further define a model for the role of the Actin cytoskeleton in facilitating synaptic vesicle endocytosis.

3. Materials and Methods

3.1. Materials

3.1.1. Animals

Primary neurons were obtained from either wild-type C57BL/6J (Charles River, RRID: IMSR_JAX:000664) or mDia1 KO mice (J. Peng et al., 2003, 2007). All animal experiments were reviewed and approved by the ethics committee of the *Landesamt für Gesundheit und Soziales* (LAGeSo) Berlin or the Committee on the Ethics of Animal Experiments of Columbia University and conducted according to the committees' guidelines (LAGeSo) or the Guide for the Care and Use of Laboratory Animals of the National Institutes of Health (for mDia1 KO mice). At the facilities, animal care officers monitored compliance with all regulations. Mice were group-housed under 12/12 h light/dark cycle with access to food and water *ad libitum*. Mice from both genders were used and cultures were randomly allocated to experimental groups (e.g., different treatments). Multiple independent experiments using several biological replicates were carried out as indicated in the Figure legends.

3.1.2. Antibodies

Antibodies and their working dilutions used in this study are denoted in Table 1/Table 2 (IB: Immunoblot; IC: Immunocytochemistry; IP: Immunoprecipitation). Antibodies were stored according to the manufacturer's recommendations. All secondary antibodies were species-specific (highly cross-adsorbed).

Table 1: Primary Antibodies used in this Study.

Antigen	Clone	Species	Source Identifier	IB	IC	IP
β-Actin	6L12	mouse, monoclonal	Sigma-Aldrich Cat# A5441 RRID:AB_476744	1:5000		
AKT		rabbit, polyclonal	Cell Signaling Technology Cat# 9272 RRID:AB_329827	1:2000		
phospho-AKT1 ($Serine_{347}$)	D9E	rabbit, monoclonal	Cell Signaling Technology Cat#4060 RRID:AB_2315049	1:1000	1:100	
Bassoon	Gp179 H11A2	guinea pig, monoclonal	Synaptic Systems Cat# 141 318 RRID:AB_2927388		1:100	
Cdc42		rabbit, polyclonal	Abcam Cat# ab64533 RRID:AB_1310067	1:1000	1:100	

Dynamin1*	DG1	rabbit, polyclonal	Detlev Grabs and Pietro D. Camilli (Shupliakov et al., 1997)	1:2000		
GAPDH	Clone 71.1	mouse, monoclonal	Sigma-Aldrich Cat# G8795 RRID:AB_1078991	1:5000		
GFP	3E6	mouse, monoclonal	Thermo Fisher Scientific Cat# A-11120 RRID:AB_221568		1:2500	
Homer1	2G8	mouse, monoclonal	Synaptic Systems Cat# 160 011 RRID:AB_2120992		1:200	
Homer1		rabbit, polyclonal	Synaptic Systems Cat# 160 003 RRID:AB_887730		1:200	
LAMP1	D2D11	rabbit, monoclonal	Cell Signaling Technology Cat# 9091 RRID:AB_2687579	1:1000		
mDia1	Clone 51	mouse, monoclonal	BD Biosciences Cat# 610848 RRID:AB_398167	1:500		2 µg
mDia1	EPR7948	rabbit, monoclonal	Abcam Cat# ab129167 RRID:AB_11143749		1:100	
mDia3		rabbit, polyclonal	Sigma-Aldrich Cat# HPA005647 RRID:AB_1078657	1:1000		
Myosin IIb	3H2	mouse, monoclonal	Abcam Cat# ab684 RRID:AB_305661		1:100	
Myosin IIb		rabbit, polyclonal	Cell Signaling Technology Cat# 3404 RRID:AB_126421	1:2000		
PACSIN1		rabbit, polyclonal	GeneTex Cat# GTX108567 RRID:AB_1951092	1:1000		
vGAT (cytosolic domain)		rabbit, polyclonal	Synaptic Systems Cat# 131 013 RRID:AB_2189938		1:100	
vGAT (luminal domain)		rabbit, polyclonal	Synaptic Systems Cat# 131 103C3 RRID:AB_887867		1:100	
vGLUT1 (cytosolic domain)		rabbit, polyclonal	Synaptic Systems Cat# 135 302 RRID:AB_887877		1:100	
vGLUT1 (luminal domain)		guinea pig, polyclonal	Synaptic Systems Cat# 135 304 RRID:AB_887878		1:100	
Rac1	Clone 102	mouse, monoclonal	BD Biosciences Cat# 610650 RRID:AB_397977	1:1000	1:50	
Raptor	24C12	rabbit, monoclonal	Cell Signaling Technology Cat# 2280 RRID:AB_561245	1:1000	1:200	
Rictor	D16H9	rabbit, monoclonal	Cell Signaling Technology Cat# 9476 RRID:AB_10612959	1:1000		

Rictor	H11	mouse, monoclonal	Santa Cruz Biotechnology Cat# sc-271081 RRID:AB_10611167		1:50
RFP		rabbit, polyclonal	Takara Bio Cat# 632496, RRID:AB_10013483		1:500
RhoA	67B9	rabbit, monoclonal	Cell Signaling Technology Cat# 2117 RRID:AB_10693922	1:1000	
Synapsin1	46.1	mouse, monoclonal	Synaptic Systems Cat# 106 011 RRID:AB_2619772		1:400
Synapsin1		rabbit, polyclonal	Synaptic Systems Cat# 106 103 RRID:AB_11042000		1:400
Synaptojanin1*	Sj1	mouse, monoclonal	Ottavio Cremona and Pietro D. Camilli (Cremona et al., 1999)	1:1000	
Synaptotagmin1 (cytosolic domain)	41.1	mouse, monoclonal	Synaptic Systems Cat# 105 011 RRID:AB_887832		1:100
Synaptotagmin1 (luminal domain)		rabbit, polyclonal	Synaptic Systems Cat# 105 103C3 RRID:AB_887829		1:100
α-Tubulin	DM1A	mouse, monoclonal	Sigma-Aldrich Cat# T9026 RRID:AB_47759	1:5000	

* Antibody was a kind gift of Pietro D. Camilli (New Haven, USA).

Table 2: Secondary Antibodies used in this Study.

Fluorophore conjugate	Raised in	IgG species recognized	Source Identifier	IB	IC
Alexa Fluor™ 488	goat	mouse	Thermo Fisher Scientific Cat# A-11029 RRID:AB_2534088		1:400
Alexa Fluor™ 488	goat	rabbit	Thermo Fisher Scientific Cat# A-11034 RRID:AB_2576217		1:400
Atto542	donkey	mouse	Martin Lehmann (Gonschior et al., 2022)		1:400
Atto542	donkey	rabbit	Martin Lehmann (Gonschior et al., 2022)		1:400
Alexa Fluor™ 568	goat	guinea pig	Thermo Fisher Scientific Cat# A-11075 RRID:AB_2534119		1:400
Alexa Fluor™ 568	goat	mouse	Thermo Fisher Scientific Cat# A-11004; RRID:AB_2534072		1:400
CF568	donkey	rabbit	Biotium Cat# 20098-1 RRID:AB_10853318		1:400

Alexa Fluor™ 594	goat	mouse	Thermo Fisher Scientific Cat# A-11032 RRID:AB_2534091		1:200
Alexa Fluor™ 594	goat	rabbit	Thermo Fisher Scientific Cat# A-11037 RRID:AB_2534095		1:200
Atto647N	camelid	guinea pig	Thermo Fisher Scientific Cat# N0602-S RRID:AB_2744576		1:200
AlexaFluor™ 647	goat	mouse	Thermo Fisher Scientific Cat# A-21235 RRID:AB_2535804		1:400
CF647	goat	rabbit	Biotium Cat# 20047-1 RRID:AB_10853792		1:400
IRDye 680RD	goat	mouse	LI-COR Biosciences Cat# 925-68070 RRID:AB_2651128	1:10000	
IRDye 680RD	goat	rabbit	LI-COR Biosciences Cat# 926-68071 RRID:AB_10956166	1:10000	
IRDye 800CW	goat	mouse	LI-COR Biosciences Cat# 926-32210 RRID:AB_621842	1:10000	
IRDye 800CW	goat	rabbit	LI-COR Biosciences Cat# 926-32210 RRID:AB_621842	1:10000	

For visualization of Actin filaments at synapses, Phalloidin-Alexa Fluor™594 (1:1000; AAT Bioquest; Cat# ABD-23158) was utilized. To stain for biotinylated proteins, Streptavidin CF®647 conjugates (1:500; Biotium/VWR; Cat# BT29039) were applied during secondary antibody incubation. For detection of biotinylated proteins following immunoblotting, biotinylated proteins were bound by Streptavidin-Horseradish peroxidase (HRP) conjugates (1:20000; Abcam; Cat# ab7403) and visualized through the application of the SuperSignal™ West Pico PLUS Chemiluminescence kit (Thermo Fisher Scientific; Cat# 34579) according to the manufacturer's manual.

3.1.3. Cell Lines

Human embryonic kidney 293T (HEK293T) cells were obtained from the American Type Culture Collection (Cat# CRL-3216; RRID: CVCL_0063). Cells were cultured in Dulbecco's modified Eagle's medium supplemented with glucose (DMEM; 4.5 g/L; Thermo Fisher Scientific) and 10% heat-inactivated fetal bovine serum (FBS; Gibco), penicillin (100 U/ml; Gibco), and streptomycin (100 µg/ml; Gibco) at 37°C and 5% CO_2. Cells were routinely tested for mycoplasma contamination.

3.1.4. Chemicals

Compounds were dissolved in dimethyl sulfoxide (DMSO), unless indicated otherwise, and diluted 1:1000 to their working concentrations (Table 3). For acute pharmacological treatment (in pHluorin/CypHer assays), drugs were added to the imaging buffer. For longer incubations, the conditioned cell media was supplemented with the chemicals (s. (Table 3). for incubation time).

For silencing neuronal network activity, sodium channels were inhibited by the addition of tetrodotoxin (TTX; in 10 mM sodium acetate, pH 5.3) to the neuronal culture medium at day in vitro (DIV) 12 for 36 h. As a control, cells from the same preparation were treated with equal volumes of 10 mM sodium acetate (annotated as Vehicle).

Table 3: Chemicals used in this Study.

Name	Target protein	Source Identifier	Working concentration	Incubation time	Application
AZD 3147	mTOR kinase	Cayman Chemical Cay22474-500	10 nM	2 h	pHluorin/ STED/ Immunoblot
Dynasore	pan-Dynamin	Sigma-Aldrich Cat# D7693	80 µM	10 min	STED
EHT 1864	pan-Rac family	MedChemExpress Cat# HY-16659	10 µM	acute	STED/ CypHer/ pHluorin/ Immunoblot
			10 µM	2 h	EM/ STED
IMM-01	pan-mDia	Sigma-Aldrich Cat# SML1064	10 µM	acute	pHluorin
Jasplakinolide	F-Actin	Sigma-Aldrich Cat# J4580	8 µM [JLY]	acute	CypHer/ pHluorin
			1 µM	30 min	pHluorin/ STED
Latrunculin A	β-Actin	Cayman Chemical Cat# CAY10684	5 µM [JLY]	acute	CypHer/ pHluorin
MK 2206	pan-AKT	MedChemExpress Cat# HY- 10358	10 µM	acute	pHluorin
ML141	Cdc42	MedChemExpress Cat# HY-12755	10 µM	acute	CypHer/ Immunoblot
PalmC	-	MedChemExpress Cat# HY-101017	10 µM	acute	pHluorin/ Immunoblot
Rapamycin	mTORC1	MedChemExpress Cat# HY-10219	200 nM	2 h	
Rhosin	pan-Rho	MedChemExpress Cat# HY-12646	10 µM	2 h	Immunoblot
SMIFH2	pan-formin (FH2)	MedChemExpress Cat# HY-16931	30 µM	acute	pHluorin/ Immunoblot
Tetrodotoxin	Sodium channels	Carl Roth Cat# 6973.1	1 µM	36 h	EM
Y-27632	pan-Rho-Kinase (ROCK)	Tocris Cat# 1254	1 µM [JLY]	acute	CypHer/ pHluorin

3.1.5. Plasmids

All recombinant DNA reagents used for protein expression are listed in Table 4: Synaptophysin-pHluorin was a kind gift from Leon Lagnado (Univ. of Sussex, UK), vGLUT1-pHluorin was generated in-house by Svenja Bolz as previously described (Bolz et al., 2023). mDia1-WT-TurboID and RhoA-CA were generated by Tolga Soykan. Cytosolic TurboID (TurboID CTR) was kindly provided by Noa Lipstein. All other expression vectors were generated for this study. Vectors based on pGEX were used for recombinant expression of GST-tagged proteins under an inducible tac promotor. Plasmids based on pEGFP-C1, pmCherry-N1, pCAG and pcDNA3 utilizing a CMV or CAG promotor (Table 4) were used for overexpression based on transfection of neuronal cells, while pFUGW vectors carrying a human Synapsin1 promotor (hSyn1) were used for the generation of lentiviral particles for the transduction of neurons.

Table 4: Plasmids used for Protein Expression in this Study.

Name in Study	Species	Tag	Promotor	Backbone	Source Identifier
Synaptophysin-pHluorin	rat	2x pHluorin (Asn_{183} – Thr_{184})	CMV	pEGFP-C1	Leon Lagnado
vGLUT1-pHluorin	rat	pHluorin (Gly_{99}-Gly_{100})	hSyn1	pFUGW	Svenja Bolz
mCherry	-	mCherry	CMV	pmCherry-N1	Clontech Cat# 632523
mDia1-WT	mouse	mCherry (C-terminal)	CMV	pmCherry-N1	This study
mDia1-ΔN	mouse	mCherry (C-terminal)	CMV	pmCherry-N1	This study
mDia1-VN	mouse	mCherry (C-terminal)	CMV	pmCherry-N1	This study
mDia1-ML	mouse	mCherry (C-terminal)	CMV	pmCherry-N1	This study
mDia1-VNML	mouse	mCherry (C-terminal)	CMV	pmCherry-N1	This study
mDia1-WT-SNAP	mouse	SNAP (C-terminal)	hSyn1	pFUGW	This study
mDia1-K994A-SNAP	mouse	SNAP (C-terminal)	hSyn1	pFUGW	This study
mDia1-VN-SNAP	mouse	SNAP (C-terminal)	hSyn1	pFUGW	This study
mDia1-ML-SNAP	mouse	SNAP (C-terminal)	hSyn1	pFUGW	This study
mDia1-VNML-SNAP	mouse	SNAP (C-terminal)	hSyn1	pFUGW	This study
mDia1-WT-TurboID	mouse	TurboID (C-terminal)	hSyn1	pFUGW	Tolga Soykan
mDia1-VN-TurboID	mouse	TurboID (C-terminal)	hSyn1	pFUGW	This study
TurboID CTR	-	TurboID	hSyn1	pFUGW	Noa Lipstein
Dynamin1-WT	mouse	SNAP (C-terminal)	hSyn1	pFUGW	This study
Dynamin-K44A	mouse	SNAP	hSyn1	pFUGW	This study

CIP4	mouse	(C-terminal) mCherry	CMV	pmCherry-N1	Christian Merrifield RRID:Addgene_27685
Endophilin-A1	rat	(C-terminal) eGFP	CMV	pEGFP-N1	Martin Lehmann
FBP17	human	(C-terminal) eGFP	CMV	pEGFP-C1	Pietro D. Camilli RRID:Addgene_22229
FCHO1	mouse	(N-terminal) mCherry	CMV	pmCherry-N1	Christian Merrifield RRID:Addgene_27690
FCHO2	mouse	(C-terminal) mCherry	CMV	pmCherry-N1	Christian Merrifield RRID:Addgene_27686
PACSIN1	mouse	(C-terminal) eGFP	CMV	pEGFP-N1	Katharina Branz
PACSIN2	mouse	(C-terminal) eGFP	CMV	pEGFP-N1	Katharina Branz
RhoA-CA	human	(C-terminal) 3 x HA	CMV	pcDNA3.1	Tolga Soykan
GST-mDia1 (FH1-FH2-DAD)	mouse	(N-terminal) GST (C-terminal) His	tac	pGEX-6P-1	Antoine Jégou & Guillaume Romet-Lemonne RRID:Addgene_85822
GST	-	(N-terminal) GST	tac	pGEX-4T-1	Volker Haucke

In the course of this study several approaches to deplete mDia1 have been carried out and are annotated in the figure legends: For knockdown of mDia1, RhoA, and RhoB by transfection, commercially available lentiviral small hairpin RNA (shRNA) vectors based on the pLKO.1 backbone (Table 5; annotated in figure legends as *transfected*) were purchased from Sigma-Aldrich. To reduce the amount of DNA needed for transfection to perform pHluorin assays, vectors expressing shRNA embedded into a microRNA (miRNA) context for mDia1 together with Synaptophysin-2x-pHluorin as a reporter were cloned based on pRRLsinPPT-emGFP-miR Control, a kind gift of Dr. Peter S. McPherson (Montreal, Canada). Finally, lentiviral vectors for knockdown of mDia1, mDia3, Raptor, and Rictor (annotated in figure legends as *transduced*) were generated based on the backbone f(U6) sNLS-RFPw shCTR, a kind gift from Christian Rosenmund (Berlin, Germany). All vectors used for genetic depletion via RNA interference are listed in Table 5 and express gene-specific shRNA under a U6 promotor that either targets the coding sequence (CDS) or the 3'-untranslated region (3'-UTR).

Table 5: Plasmids used for shRNA-mediated Knockdown in this Study.

Name	Target	Species	Reporter	Promoter	Vector	Source
shCTR	none	-	-	-	pLKO.1	Sigma-Aldrich Cat# SHC016

shmDia1	3'UTR of mDia1	mouse	-	-	pLKO.1	Sigma-Aldrich Cat# TRCN0000108685 NM_007858
shRhoA	CDS of RhoA	mouse	-	-	pLKO.1	Sigma-Aldrich Cat# TRCN0000302388 NM_016802
shRhoB	CDS of RhoB	mouse	-	-	pLKO.1	Sigma-Aldrich Cat# TRCN0000294874 NM_007483
shCTRmiR	none	mouse	Synaptophysin-2x-pHluorin	CMV	pRRLsinPPT	This study
shmDia1miR	mDia1	mouse	Synaptophysin-2x-pHluorin	CMV	pRRLsinPPT	This study
shCTR	none	-	NLS-RFP	hSyn1	pFUGw	Christian Rosenmund (S. Watanabe et al., 2014)
shmDia1	3'UTR of mDia1	mouse	NLS-RFP	hSyn1	pFUGw	This study
shmDia3	CDS of mDia3	mouse	NLS-RFP	hSyn1	pFUGw	This study
shRaptor	CDS of Raptor	mouse	NLS-RFP	hSyn1	pFUGw	This study
shRictor	3'UTR of Rictor	mouse	NLS-RFP	hSyn1	pFUGw	This study

3.1.6. Oligonucleotides

Plasmids generated for this study were cloned using oligonucleotides (BioTez GmbH, Berlin, Germany) and are listed in Table 6 (lower case denotes nucleotides that do not anneal to the backbone; underlined nucleotides denote sense and antisense sequences of shRNA).

Table 6: Oligonucleotides used in this Study.

Plasmid	Forward primer [5'-3']	Reverse primer [5'-3']
pSNAP-N1	tataaccggtcaccATGGACAAAGACTGCG	tatagcggccgctTTAACCCAGCCCAGGC
pFUG_hSyn_MCS	CCGGTatttaaatggatcccctgcagggcggccgcttaattaatctagatgtacag	AATTCtgtacatctagattaattaagcggccgccctgcaggggatccatttaaata
mDia1-ΔN	aatagatctatgAACTCCTCTGCATCGTACGGAGATG	gcgaccggTCCAGATCCGC
mDia1-K994A	TCGAGACACCgcGTCTGCAGATC	AGTTTACAAAGGAAGCTG
Dynamin1-K44A	GAGCGCCGGCgcGAGCTCGGTGCTGG	TGGCCGCCTACCACGGCG
shCTRmiR (Syph-pH)	caccgactctagaggatctaccggtcgccacc ATGGACGTGGTGAATCAGCTGGTG	ccactggtcgactcaCTACCTC
shmDia1miR	TGCTGaatgcttgaccctaccatcaaGTTTTGG CCACTGACTGACttgatggtggtcaagcatt	CCTGaatgcttgaccctaccatcaaGTCAGTCA GTGGCCAAAACttgatggtggtcaagcattC
f(U6) BFP shCTR	tccagTTTTTGGAAATTAATTAACAGAG GGCCCTGCGTAT (for hSyn1) AAAAGAAGAGAAAGGTAATGagcgagctg attaaggagaaca (for BFP)	tccttaatcagctcgctCATTACCTTTCTCTTC TTTTTTGGATCTACCT (for hSyn1) tgatatcgaattaattctagTCAGTTaagcttgtgccc cagtttgctaggga (for BFP)

shmDia1	GATCCCCgcctaaatggtcaaggagataTTCAA GAGAtatctccttgaccatttaggcTTTTTGGAA ATTAAT	TAATTTCCAAAAAgcctaaatggtcaaggagat a TCTCTTGAAtatctccttgaccatttaggcGGG
shmDia3	GATCCCCgccctaatccagaatcttgta TTCAAGAGAtacaagattctggattagggcTTTT TGGAAATTAAT	TAATTTCCAAAAAGccctaatccagaatcttgta TCTCTTGAAtacaagattctggattagggcGGG
shRaptor	GATCCCCcctcatcgtcaagtccttcaaTTCAAG AGAttgaaggacttgacgatgaggTTTTTGGAA ATTAAT	TAATTTCCAAAAAcctcatcgtcaagtccttcaa TCTCTTGAAttgaaggacttgacgatgaggGGG
shRictor	GATCCCCcgagactttgtctgtctaattTTCAAG AGAAattagacagacaaagtctcgTTTTTGGAA ATTAAT	TAATTTCCAAAAAcgagactttgtctgtctaattT CTCTTGAAaattagacagacaaagtctcgGGG

lower case – Nucleotides that do not anneal to the backbone
Underline – sense and antisense sequence of shRNA

3.1.7. Commercial Kits

Commercial kits that were used in this study are annotated in Table 7.

Table 7: Commercial Kits used in this Study.

Kit	Source	Identifier	Additional information
Rhotekin-Rho binding domain (RBD) beads	Cytoskeleton Inc.	Cat# RT02	60 µg/reaction
PAK-p21 binding domain (PBD) beads	Cytoskeleton Inc.	Cat# PAK02	20 µg/reaction
ProFection Mammalian Transfection System – Calcium Phosphate	Promega	Cat# E1200	
Q5 site-directed mutagenesis kit	New England Biolabs Inc.	Cat# E0552S	

3.1.8. Software and Code

Software and code used in this study are listed in Table 8.

Table 8: Software and code used in this Study.

Name	Source	Identifier
Affinity Designer	Serif Ltd	Version 1.10.6.1665
Fiji	National Institutes of Health (NIH)	RRID:SCR_002285
Image Lab Software	Bio-Rad	RRID:SCR_014210 Version 6.0.1
Image Studio Lite	LI-COR Biosciences	RRID:SCR_013715 Version 5.2.5
Macro plot Lineprofile multicolor	Kees Straatman	(Gerth et al., 2019)
MaxQuant	Jürgen Cox	https://www.maxquant.org/maxquant/ Version 1.6.1.0
Perseus	Jürgen Cox	https://www.maxquant.org/perseus/ Version 1.6.7.0

pHluorin ROI selector	Github	RRID:SCR_002630
Prism	GraphPad	RRID:SCR_002798 Version 9.5.1.
SynActJ	Martin Lehmann	(Schmied et al., 2021)

3.2. Methods

3.2.1. Molecular Biology Methods

To generate expression (Table 4) vectors, primers (Table 6) were designed for the specific amplification of a target sequence with overlaps containing restriction sites for enzymatic digestion and subsequent insertion into the target vector. For site-directed mutagenesis, primers containing the altered base sequences were utilized (Table 6). For knockdown strategies (Table 5), oligonucleotides containing sense, antisense, a linker sequence, and restriction overhangs (Table 6) were annealed and ligated into backbones cut with restriction enzymes.

3.2.1.1. Generation of Expression Plasmids

Expression plasmids generated for this study were cloned by polymerase chain reaction (PCR) amplification (Phusion™ High-Fidelity DNA polymerase) and restriction enzyme (Thermo Fisher Scientific; Fast digest) digest according to the manufacturers' manual.

pSNAP-N1 was generated in-house by Hannes Gonschior by sub-cloning pSNAP$_f$ (New England BioLabs Inc., Cat#N9183S) via PCR and the restriction enzymes *AgeI* and *NotI* into pmCherry-N1.

pFUG_hSyn_MCS was cloned by Amirreza Ohadi to enable simple insertion of SNAP-tagged proteins by inserting a multiple cloning site (MCS) on annealed oligonucleotides into a pFUG_hSyn1 backbone (a gift from Christian Rosenmund, Berlin, Germany) cut by *AgeI* and *EcoRI*.

To generate mDia1-WT-mCherry, the coding sequence of mDia1 was cut from mDia1-mEmerald-N1 (Addgene, Cat#54157) and pasted into pmCherry-N1 by *AgeI* and *XhoI* digestion.

mDia1-WT-SNAP was cloned by cutting out the coding sequence of mDia1 from mDia1-mEmerald-N1 and pasting it into pSNAP-N1 by *AgeI* and *NheI* digest of both vector and insert.

To subclone mDia1-SNAP into a lentiviral vector the coding sequence of mDia1-SNAP was pasted from mDia1-WT-SNAP-N1 into pFUG_hSyn1_MCS utilizing common cut sites for *NheI* and *NotI* digest.
The mDia1-ΔN truncation variant was generated by introducing a new start codon on a primer shifted by 60 amino acids (Table 6), PCR amplifying the truncated DNA and subcloning the template into pmCherry-N1 by *BglII* and *AgeI* digest.
For generating mDia1-VNML-mCherry, its coding sequence was first extracted from GFP-CA-mDia1 (Addgene, Cat#45583) using restriction digest by *BsiWI* and *AgeI*, and subcloned into mDia1-WT-mCherry cut with the same enzymes.
mDia1-WT-mCherry and mDia1-VNML-mCherry were digested with *NheI* and *Esp3I* yielding short fragments encoding the N-terminal sequence and larger fragments containing the C-terminal coding sequence and the rest of the backbone. Fragments were then swapped and ligated to yield mDia1-VN-mCherry and mDia1-ML-mCherry.
The subcloning of mDia1 variants into pFUG backbones for the generation of lentiviral particles, followed the extraction of the coding sequence from mCherry/SNAP vectors into pFUG mDia1-WT-SNAP through restriction digest using enzymes *NheI* and *AgeI*.
For the generation of a lentiviral vector expressing Dynamin-WT, the coding sequence of Dynamin1 was first extracted from Dynamin1-pmCherry-N1 (Addgene; Cat#27697) by *EcoRI* and *XmaI* digestion and cloned into pSNAP-N1 with the same enzymes. Subsequently, Dynamin1-SNAP was isolated by *NheI* and *NotI* digest and transformed into pFUG_hSyn1_MCS.
For introducing point mutations in mDia1 (Lysine-994 to Alanine; K994A) and Dynamin1 (Lysine-44 to Alanine; K44A), the Q5 site-directed mutagenesis kit (New England Biolabs Inc.; E0552S) was used according to the manufacturer's manual and oligonucleotides listed in Table 6.

3.2.1.2. Generation of shRNA-carrying Plasmids

Knockdown of proteins was achieved through RNA interference either by $CaCl_2$ transfection of gene-specific shRNA encoding vectors (pLKO.1; Sigma-Aldrich or shRNAmiR) on DIV 7 or by transduction of cells with lentiviral particles harboring the gene-specific shRNA on DIV 2. The respective method is indicated in the Figure legends as *transfected* or *transduced*. To reduce the amount of DNA needed for transfection and to improve neuronal health, shRNAmiRs were expressed from the 3'UTR of Synaptophysin-pHluorin based on (Ritter et al., 2017): The reporter

protein/synthetic cassette was generated by PCR amplifying Synaptophysin-2x-pHluorin with oligos (Table 6) harboring *XbaI* and *SalI* sites. The eGFP in the RRLsinPPT-eGFP-miRCTR plasmid (a kind gift from Dr. Peter S. McPherson, McGill University, Canada) was replaced by the PCR product through similar restriction digest to yield shCTRmiR. miRmDia1 (start position 4892, targeting sequence matches open-reading frame) was designed with BLOCK-iT™ (Thermo Fisher Scientific) and subcloned into shCTRmiR to yield shmDia1miR following protocol in (Ritter et al., 2017).

As both transfection strategies were limited by low efficiency, lentiviral knockdown was carried out: Lentiviral particles were based on a shuttle vector (pFUGw) driving the expression of a nuclear-targeted red fluorescent protein (NLS-RFP) under a human Synapsin1 (hSyn1) promotor to monitor infection efficiency in neurons and a scrambled mouse shRNA against Clathrin without any murine targets, which was used as the control virus (f(U6) sNLS-RFPw shCTR). To knockdown mDia1, a shRNA sequence based on 5'-GCCTAAATGGTCAAGGAGATA-3' as the sense nucleotide corresponding to the 3'UTR of mouse mDia1 (NM_007858.4; Sigma-Aldrich, Cat# TRCN0000108685) was designed as an oligonucleotide with overhangs (Table 6) and annealed into the f(U6) sNLS-RFPw shCTR backbone cut with *BamHI* and *PacI* to yield the vector f(U6) sNLS-RFPw shmDia1. For mDia3 shRNA, a sense sequence based on 5'-GCCCTAATCCAGAATCTTGTA-3' corresponding to nucleotides 2473-2493 of mouse mDia3 (DIAPH2; NM_172493; Sigma-Aldrich, Cat# TRCN0000108782) was used to construct f(U6) sNLS-RFPw shmDia3 as described above.

For genetic perturbation of mTORC1 activity, the sense sequence 5'-CCTCATCGTCAAGTCCTTCAA-3' corresponding to the coding nucleotides 1505-1525 of Raptor (rptor; NM_028898; Sigma-Aldrich, Cat# TRCN0000077471) was designed as an oligonucleotide (Table 6) and annealed into the f(U6) sNLS-RFPw shCTR backbone cut with *BamHI* and *PacI* to yield the vector f(U6) sNLS-RFPw shRaptor. To interfere with mTORC2, a sense sequence based on 5'-CGAGACTTTGTCTGTCTAATT-3' targeting the 3'UTR of mouse Rictor (NM_030168; Sigma-Aldrich, Cat# TRCN0000123394) was used to construct f(U6) sNLS-RFPw shRictor as described above.

All vectors were confirmed by Sanger sequencing (LGC Genomics, Berlin, Germany) and amplified by self-made chemically competent TOP10 *E. coli* before purifying

respective endotoxin-free DNA by 2-propanole precipitation (NucleoBond Xtra Midi EF kit; Macherey-Nagel).

3.2.2. Cell Biology Methods

3.2.2.1. Production of Lentiviral Particles

Production of lentiviral particles was conducted using the second-generation packaging system: In brief, HEK293T were co-transfected with lentiviral shRNA constructs and the packaging plasmids psPAX2 (Addgene; Cat# 12260) and MD2.G (Addgene; Cat# 12259) using $CaCl_2$. After 12 h, the cell media was replaced. Virus-containing supernatants were collected at 48 and 72 h after transfection, filtered to remove cell debris, and particles were concentrated (30-fold) via low-speed centrifugation (Amicon Ultra-15, Ultracel-100; Merck Millipore; Cat# UFC9100) before aliquoting and storage at -70°C. For all experiments, an infection rate of over 95% was achieved at DIV 14-16.

3.2.2.2. Isolation, Culture and Transfection of Primary Neurons

Neuronal hippocampal cell cultures were prepared as described (López-Hernández et al., 2022; Soykan et al., 2017). In short, hippocampi from postnatal mice (p0-p3) were surgically isolated and dissociated into single cells by trypsin (5 g/L, Sigma-Aldrich) digestion. Neurons (100000 cells/ well of a 6-well) were plated onto poly-L-lysine-coated coverslips and grown in modified Eagle medium (MEM; Thermo Fisher) supplemented with 5% FCS and 2% B-27 (Gibco) and maintained at 5% CO_2 and 37°C in humidified incubators. In addition, 2 µM cytosine β-D-arabinofuranoside (AraC) was added to the cell culture media in the first 2 days in vitro (DIV) to limit glial proliferation. For transient protein expression, neurons were transfected on DIV 7-9 utilizing a Calcium phosphate transfection kit (Promega; Cat# E1200): In brief, 1-6 µg plasmid DNA (per well of a 6-well plate) were mixed with 250 mM calcium phosphate ($CaCl_2$) in ultrapure nuclease-free water. The resulting solution was added to equal volumes of 2x 4-(2-hydroxyethyl)-1-piperazineethanesulfonic acid buffered saline (2x HEPES; 100 µL) and incubated at room temperature for 20 min. Resulting precipitates were added dropwise to cells that had been transferred to osmolarity-adjusted Neurobasal-A (NBA; Gibco) media to induce starvation. After incubation at 37°C and 5% CO_2 for 30 min, neurons were washed thrice with osmolarity-adjusted Hank's

balanced salt solutions (HBSS; Gibco) and transferred back to their original conditioned media.

3.2.3. Biochemical Methods

3.2.3.1. Protein Quantification

To analyze protein levels in cellular lysates, proteins are separated according to their weight by a combination of sodium dodecyl sulfate polyacrylamide gel electrophoresis (SDS-PAGE), followed by binding and visualization of proteins by antibodies (Table 2) detecting immunoreactive bands following immunoblotting. Quantification of protein bands via immunoblotting requires equal loading of sample proteins, necessitating quantification of total protein levels prior to electrophoresis. For this purpose, a colorimetric detection assay, utilizing the *Biuret* reaction, known as the bicinchoninic acid (BCA) assay was used.

3.2.3.2. BCA Assay

To perform the BCA assay (Thermo Fisher Scientific; Cat#23227), lysate samples (1 µL) were diluted in MQ water (9 µL) and replicated in a microtiter well (Pierce 96-Well Plates). Bicinchoninic acid/copper sulfate (BCA/$CuSO_4$) solution (190 µL; 50/1) was added and incubated at 37°C for 30 min. The absorbance of the formulated complex was measured at 482 nm with the SpectroStar^{Nano} (BMG Labtech, Software Version 5.50). As calibration, a series of bovine serum albumin (BSA) dilutions of known concentrations (10 µL each; 2000, 1500, 1000, 750, 500, 250, 125, 25, 0 µg/mL) were assayed alongside the unknown samples. Concentrations of the unknown samples were then calculated by fitting the resulting calibration curve, with a sample to working reagent ratio of 1:10 (v/v).

3.2.3.3. Immunoblotting

To compare protein levels between experimental conditions, immunoblotting was performed: Protein concentrations in lysates were measured by BCA assay (Thermo Fisher Scientific; Cat#23227) and equal protein amounts were diluted in Laemmli sample buffer [final (1 x) concentration: 31.5 mM 2-Amino-2-(hydroxymethyl)propane-1,3-diol (Tris), 1 % (w/v) sodium dodecyl sulfate (SDS), 10 %

(v/v) glycerol, 0.001% (w/v) 3,3-Bis(3,5-dibromo-4-hydroxyphenyl)-2,1λ⁶-benzoxathiole-1,1(3*H*)-dione (bromophenol blue), 5 % (v/v) 2-mercaptoethanol; pH 6.8] and denatured at 55°C for 20 min (unless indicated otherwise).
Samples were resolved by SDS-PAGE with self-made Bis(2-hydroxyethyl)amino-tris(hydroxymethyl)methan (BisTris; 250 mM) based 4-20 % polyacrylamide (Rotiphorese Gel 30; Carl Roth) gradient gels and run (80-120 V; 90 min) in NuPAGE MOPS SDS running buffer (Thermo Fisher Scientific; Cat#NP000102) using Mini-PROTEAN Tetra Vertical Electrophoresis Cells (Bio-Rad, Cat#1658004).
For RhoA-binding analysis and membrane fractionation experiments, RFP-fluorescence of mDia1 variants in respective fractions was imaged in-gel on a ChemiDoc XRS+ (Bio-Rad) controlled by the Image Lab software (version 6.0.1) utilizing the Alexa546 preset (605/50 Filter3; Light Green Epi illumination).
Separated proteins were wet-blotted (110 V; 90 min; 4°C) on fluorescence-optimized polyvinylidene difluoride (PVDF) membranes (Immobilon-FL; Merck; IPFL00010) in transfer buffer (25 mM Tris (pH 7.6), 192 mM glycine, 20% (v/v) methanol, 0.03% (w/v) SDS). Subsequently, membranes were blocked with blocking buffer [5 % bovine serum albumin (BSA), in Tris-buffered saline (TBS) containing 0.01% Tween 20 (TBS-T)] for 1 h at RT and incubated (4 °C; overnight) with primary antibodies under constant agitation at indicated dilutions (Table 1) in blocking buffer. Membranes were washed thrice with TBS-T and incubated with corresponding pairs of IRDye 680RD- or 800CW-conjugated secondary antibodies in TBS-T for 1 h at RT. After three wash cycles with TBS-T, bound antibodies were visualized by the Odyssey Fc Imaging System (LI-COR Biosciences) controlled and analyzed by Image Studio Lite (Version 5.2.5). For colorimetric analysis of protein levels, the intensity of immunoreactive bands was measured by assigning shapes of equal size to all lanes at similar heights and subtracting the individual background for each shape. Signals were normalized to controls on the same blot. The PageRuler Prestained (Thermo Fisher Scientific; Cat#26616) was used as a ladder to control for protein size.

3.2.3.4. Pulldown of BAR Family Proteins by recombinant mDia1

To express a glutathione S-transferase (GST) fusion protein of mDia1 (FH1-FH2-DAD), a preculture of 100 mL lysogeny broth (LB; 1.0 % (w/v) Yeast extract, 0.5 % (w/v) sodium chloride (NaCl), 0.5 % (w/v) Trypton; pH 7.4) of the *Escherichia coli* BL21 strain was transformed with GST-mDia1-FH1-FH2-DAD and grown overnight in

ampicillin (100 µg/mL) at 37°C. The following day, 50 mL of the overnight culture was added to 500 mL of growth media (2x YT; 1.0 % (w/v) Yeast extract, 0.5 % (w/v) NaCl, 1.6 % (w/v) Trypton; pH 7.4) supplemented with ampicillin (100 µg/mL) and grown at 23 °C under agitation at 180 rpm until an optical density OD_{600} of 0.7 was reached. Subsequently, protein expression was induced by the addition of 0.5 mM isopropyl thiogalactoside (IPTG), and cells were incubated at 16°C for 12 h under agitation at 180 rpm. Bacteria were harvested by centrifugation (4000 g; 20 min; 4°C) and the resulting pellets were resuspended in 35 mL of ice-cold PBS.

To purify GST-mDia1 proteins, proteins were first extracted by incubation with 1 mM phenylmethylsulfonyl fluoride (PMSF), 125 units benzonase (DNase) and 35 mg of lysozyme for 15 min, followed by sonification (Sonoplus; Bandelin, 70 %) at 4°C. Subsequently, cells were lysed by the addition of 1 % (v/v) TritonX-100. After 10 min incubation at 4°C, supernatants were extracted by centrifugation (35000g; 15 min; 4°C) and incubated with 500 µL of PBS-washed immobilized glutathione resin (GST-bind™ resin Novagen, Millipore, Cat# 70541) for 1 h at 4°C under agitation. Resin was pelleted by centrifugation (3000 g; 5 min; 4°C), in between three washes with ice-cold PBS, to remove unbound proteins.

For the pulldown of BAR proteins, HEK293T cells were transfected with various constructs expressing proteins of the BAR protein family (Table 4) using $CaCl_2$. After 48 h of transfection, cells were washed with ice-cold PBS and harvested in lysis buffer (50 mM HEPES, 150 mM NaCl, 2 mM magnesium chloride ($MgCl_2$), 1 % TritonX-100, protease inhibitor cocktail (PIC), Phosphatase inhibitors II/III; pH 7.4). Supernatants were collected by centrifugation (15000 g; 15 min; 4°C) and protein concentration was measured with the BCA method. Volumes of lysates containing 500 µg of protein were loaded onto 50 µg of resin-bound GST-mDia1 fusion proteins and incubated for 1 h at 4°C with agitation. Subsequently, unbound proteins were removed by five wash steps with lysis buffer. Bound proteins were eluted and denatured (20 min; 55°C) in 2x Laemmli buffer, resolved by SDS-PAGE, and analyzed by immunoblotting.

3.2.3.5. Analysis of Membrane-association of mDia1 Variants

To characterize the membrane association of mDia1 variants, HEK293T cells were transfected with wild-type or mutant mDia1 vectors using $CaCl_2$. 48 h after transfection, cells were washed with ice-cold PBS and harvested in ice-cold resuspension buffer (20 mM HEPES, 130 mM NaCl, PIC; pH 7.4). Cells were lysed by

forcing the suspension through 18-gauge syringes to crack the plasma membrane in between three freeze-thaw cycles in liquid nitrogen. Nuclei were removed by centrifugation at 1000 g for 5 min at 4°C. The supernatant (total lysate) was sedimented at 100000 g for 30 min at 4°C to yield the membrane fraction as the pellet and the cytosolic fraction as the high-speed supernatant. The pellet was resuspended in resuspension buffer to the same volume as the cytosolic fraction. Equal volumes of all fractions were analyzed by SDS-PAGE and immunoblotting to allow interpretation of protein enrichment in cytosolic or membrane fractions with respect to the total lysate.

3.2.3.6. Analysis of RhoA-association of mDia1 Variants

To characterize the interaction of mDia1 variants with RhoA, HEK293T cells were transfected with either wild-type or mutant mDia1 along with constitutively active HA-tagged RhoA (RhoA-CA; Q63L) using $CaCl_2$. After 48 h of transfection, cells were washed with ice-cold PBS and harvested in ice-cold lysis buffer (50 mM HEPES, 150 mM NaCl, 1 % 3-[Dimethyl[3-(3α,7α,12α-trihydroxy-5β-cholan-24-amido)propyl] azaniumyl] propane-1-sulfonate (CHAPS), PIC, Phosphatase inhibitors II/III; pH 7.4). Supernatants were collected by centrifugation (15000 g; 15 min; 4°C) and protein concentration was measured with the BCA method. Volumes of lysates containing 500 µg of protein were loaded onto 20 µL of prewashed Pierce™ Anti-HA Magnetic Beads (Thermo Fisher Scientific; Cat# 88837) and incubated for 1 h at 4°C with agitation. Subsequently, unbound proteins were removed by two wash steps with lysis buffer. Bound proteins were eluted and denatured (20 min; 55°C) in 1x Laemmli buffer, resolved by SDS-PAGE and analyzed by in-gel fluorescence and immunoblotting.

3.2.3.7. Analysis of Rho GTPase Activity via Effector Pulldown Assays

To analyze the activity of small Rho GTPases, pulldowns utilizing effector protein domains that exclusively bind to their GTP-bound forms were performed: Neurons (200 000 cells) were washed with ice-cold PBS and harvested in GTPase lysis buffer (50 mM HEPES, 500 mM NaCl, 10mM $MgCl_2$, PIC, phosphatase Inhibitor cocktails II/ III; pH 7.4). Cells were lysed for 5 min under repetitive mixing before centrifugation (15000 g; 5 min; 4°C). Cleared lysates were incubated with Rhotekin-Rho binding domain (RBD) beads (60 µg; Cytoskeleton Inc.) or with PAK-p21 binding domain (PBD) beads (20 µg; Cytoskeleton Inc.) at 4°C under constant rotation to bind active

RhoA or Cdc42 and Rac1, respectively. After 2 h, the beads were pelleted by centrifugation (1000 g; 1 min; 4°C) and washed with washing buffer (50 mM HEPES, 150 mM NaCl, 10 mM $MgCl_2$; pH 7.4). After repeated centrifugation, unbound proteins were discarded with the supernatant, while bound proteins were eluted from the beads by the addition of 2 x Laemmli buffer and boiling (10 min; 95°C). Finally, the activity of small Rho GTPases was resolved by SDS-PAGE and analyzed by immunoblotting input and pulldown samples.

3.2.3.8. Identification of Proximal Protein Neighbors

The characterization of molecular interactions between proteins is essential for understanding their biological function at specific subcellular localizations. Traditional approaches, such as immunoprecipitation-based affinity purification, can isolate bait proteins via specific immobilized antibodies (Figure 23). However, immunoprecipitation methods face limitations concerning low abundantly expressed proteins, restricting the identification of transient or low-affinity interactions. In recent years, proximity labeling (PL) has emerged as a powerful complementary method to map the molecular protein environment in live cells. PL relies on an enzyme tag, such as TurboID, which catalyzes the conversion of an inert substrate (biotin and ATP) into a reactive intermediate (biotin-AMP), which labels endogenous proteins in a proximity-dependent manner (Cho et al., 2020). This labeling can occur within intact cells, preserving the spatial relationships and interaction networks in their native state (Branon et al., 2018). The covalent modification introduced by PL provides a chemical handle for the selective isolation and subsequent identification of labeled proteins by mass spectrometry (Cho et al., 2020).

In this study, we utilized complementary proteomic analysis of a) the mDia1 interactome isolated by immunoprecipitation from synaptosomes and b) the proximal protein environment of synaptic mDia1 following TurboID-mediated biotinylation.

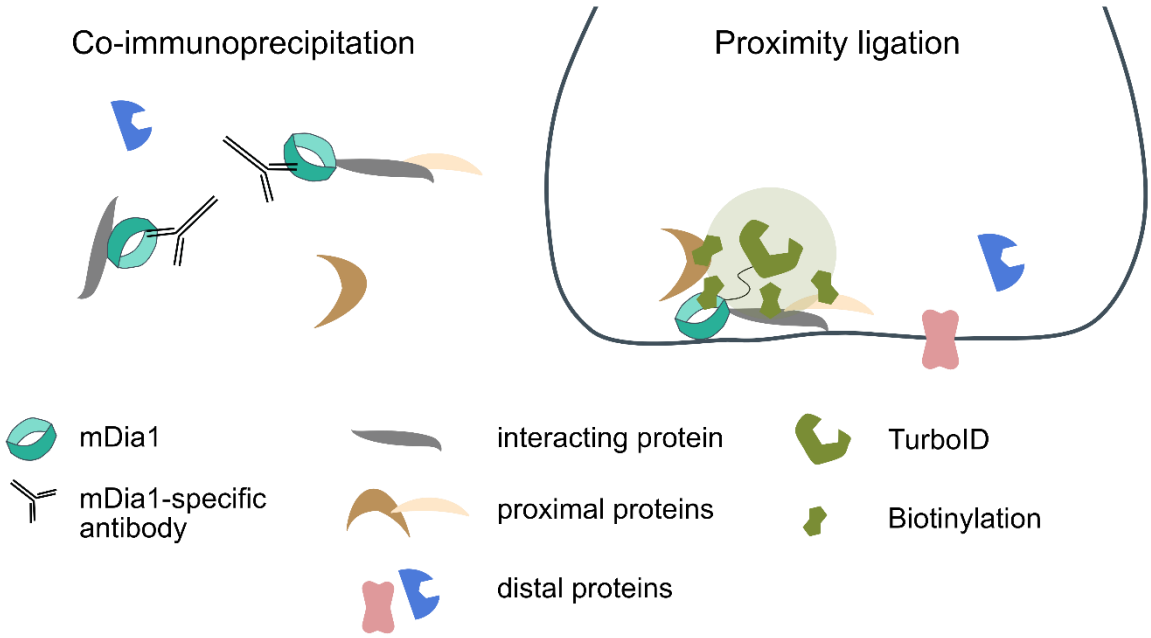

Figure 23: Identification of Proximal Protein Neighbors.
Co-immunoprecipitation enables the isolation of the immediate proximal environment of proteins through the affinity purification of bait proteins utilizing immobilized specific antibodies. This analysis is complemented by proximity labeling of the native protein environment following exogenous expression of fusion proteins tagged with TurboID. The TurboID tag encodes an engineered biotin ligase that biotinylates proximal proteins within a range of 10 nm in the presence of ATP and biotin. By expressing mDia1-TurboID fusion constructs, spatial relationships between proteins can be labeled and identified within their cellular environment. To differentiate specific labeling events attributed to mDia1 proximity, a non-selective cytosolic TurboID is employed to profile proteins in the reference compartment, the neuronal cytosol.

Immunoprecipitation from Synaptosomes

To immunoprecipitate synaptic mDia1, synaptosomes (P2') were prepared as follows: One mouse brain (p28) was homogenized (900 rpm; 12 strokes with glass-teflon homogenizer) in 7 mL of ice-cold homogenization buffer [(320 mM sucrose, 4 mM HEPES; pH 7.4) supplemented with mammalian protease inhibitor cocktail (PIC)] at 4°C. Large cellular debris and nuclei were sedimented by centrifugation at 900 g for 10 min at 4°C. The supernatant was further centrifuged at 12500 g for 15 min at 4°C. The resulting pellet (P2) was resuspended in 15 mL of homogenization buffer and pelleted at 12500 g for 15 min at 4°C yielding the crude synaptosomal fraction P2'. Subsequently, the pellet was resuspended in 2 mL of immunoprecipitation buffer [20 mM HEPES, 130 mM NaCl, 2 mM $MgCl_2$, 1 % (w/v) CHAPS, PIC, phosphatase inhibitor cocktail II and III (Sigma-Aldrich); pH 7.4] and lysed for 30 min at 4°C under light agitation. The lysate was cleared by centrifugation at 15000 g at 4°C for 15 min and protein concentration was measured using the BCA assay. For identification of the

protein environment of mDia1, P2' lysate (2 mg; 2 g/L) was incubated with either 2 µg of anti-mDia1 antibody (BD Biosciences, Cat# 610848) or equal amounts of immunoglobulin G (IgG) isotype control mouse antibody (Thermo Fisher Scientific; Cat# 31903; RRID:AB_10959891) for 1 h at 4°C before the addition of 25 µL of Pierce Protein A/G Magnetic Beads (Thermo Fisher Scientific) for an additional 2 h under constant rotation. Subsequently, unbound proteins were removed from the beads by three consecutive wash cycles with immunoprecipitation buffer. Bound proteins were eluted and boiled (10 min; 95°C) in 2x Laemmli buffer, resolved by SDS-PAGE, and analyzed by immunoblotting and mass spectrometry.

Proximity-ligation Analysis by Expression of TurboID Fusion Proteins

To investigate the proximal protein environment of synaptic mDia1, primary neuronal cultures (8 x 10^6 cells) were transduced with lentiviral vectors encoding cytosolic TurboID control (CTR), wild-type mDia1 (mDia1-WT-TurboID), or a Rho-binding deficient variant of mDia1 (mDia1-VN-TurboID) fused to TurboID on DIV2. Neurons were supplemented with 100 µM biotin in their culture media. After 12 h of incubation, cells were placed on ice and subjected to five washes with ice-cold PBS. Subsequently, cell lysis was conducted for 30 min at 4°C under gentle agitation by the addition of 1 mL of lysis buffer [50 mM Tris, 150 mM NaCl, 0.1% (w/v) SDS, 1% (v/v) Triton X-100, PIC, phosphatase inhibitor cocktail II and III (Sigma-Aldrich); pH 7.4]. Following centrifugation at 15000 g at 4°C for 15 min, supernatants were collected, and protein content was quantified calorimetrically using the BCA assay. For the isolation of biotinylated proteins, we followed the protocol described in (Cho et al., 2020). In short, respective volumes of lysates containing 500 µg of protein were incubated with 50 µg of lysis buffer-washed Pierce™ Streptavidin magnetic beads (Thermo Fisher Scientific; Cat# 88816) for 12 h with agitation at 4°C. Thereafter, unbound proteins were removed from the beads through consecutive wash cycles with lysis buffer (2 x for 2 min), 1 M potassium chloride (KCl) (for 2 min), 0.1 M sodium hydrogencarbonate ($NaHCO_3$) (for 10 s) and 2 M urea (for 10 s). Bound proteins were then eluted and boiled (10 min; 95°C) in 2x Laemmli buffer, resolved by SDS-PAGE, and analyzed by immunoblotting and mass spectrometry.

Mass Spectrometric Analysis

Mass spectrometry (MS) was employed for the comprehensive examination of protein interactions and the environment surrounding mDia1 within the synaptic context,

following the isolation of mDia1 immunoprecipitates from synaptosomes as well as the isolation of its proximal proteome using biotinylation facilitated by TurboID tags.

Eluted proteins were reduced (5 mM dithiothreitol; 30 min at 55°C), alkylated (15 mM iodoacetamide; 20 min at RT in the dark), and submitted to MS analysis: Proteins were subjected to SDS-PAGE following excision of 3 bands per lane and in-gel digestion of proteins by trypsin (1:100 (w/w); overnight at 37°C). Resulting tryptic peptides were separated by reverse-phase high-performance liquid chromatography (RP-HPLC; Ultimate™ 3000 RSLCnano system; Thermo Scientific) using a 50 cm analytical column (in-house packed with Poroshell 120 EC-C18; 2.7 µm; Agilent Technologies) with a 120 min gradient. RP-HPLC was coupled on-line to an Orbitrap Elite mass spectrometer (Thermo Fisher Scientific) that performed precursor ion (MS1) scans at a mass resolution of 60000, while fragment ion (MS2) scans were acquired with an automatic gain control (AGC) target of 5×10^3 and a maximum injection time of 50 ms. To dissect phosphorylation patterns, lysates were subjected to MS analysis before and after the enrichment of phospho-peptides via immobilized iron nitrilotriacetate (Fe-NTA, HighSelect™ Phosphopeptide enrichment kit, Thermo Fisher Scientific, Cat# A32992) according to the manufacturer's manual.
Data analysis, including label free quantification, was performed with MaxQuant (version 1.6.1.0) using the following parameters: The initial maximum mass deviation of the precursor ions was set at 4.5 parts per million (ppm), and the maximum mass deviation of the fragment ions was set at 0.5 Da. Cysteine carbamidometyl and propionamide, methionine oxidation and N-terminal acetylation were set as variable modifications. For the identification of proteins, data were searched against the SwissProt murine database. False discovery rates were < 1 % at the protein level based on matches to reversed sequences in the concatenated target-decoy database. The statistical analysis was done with Perseus (Version 1.6.7.0).

3.2.4. Microscopic Methods

3.2.4.1. Live-imaging of Synaptic Vesicle Recycling

Neurotransmission involves the packaging of neurotransmitters within synaptic vesicles, facilitating their controlled release in quanta. Transporter proteins (such as vGAT or vGLUT1) actively pump neurotransmitters into newly formed vesicles driven

by an electrochemical gradient (Farsi et al., 2017), resulting in an acidic environment (pH ~ 5.6) within the vesicle lumen (Miesenböck et al., 1998). Upon exocytosis, the luminal surface of the vesicles is rapidly exposed to the extracellular neutral pH (~ 7.4) of the synaptic cleft. This cycling between distinct pH environments has facilitated the study of the exo- and endocytic kinetics of synaptic vesicle recycling through pH-sensitive probes.

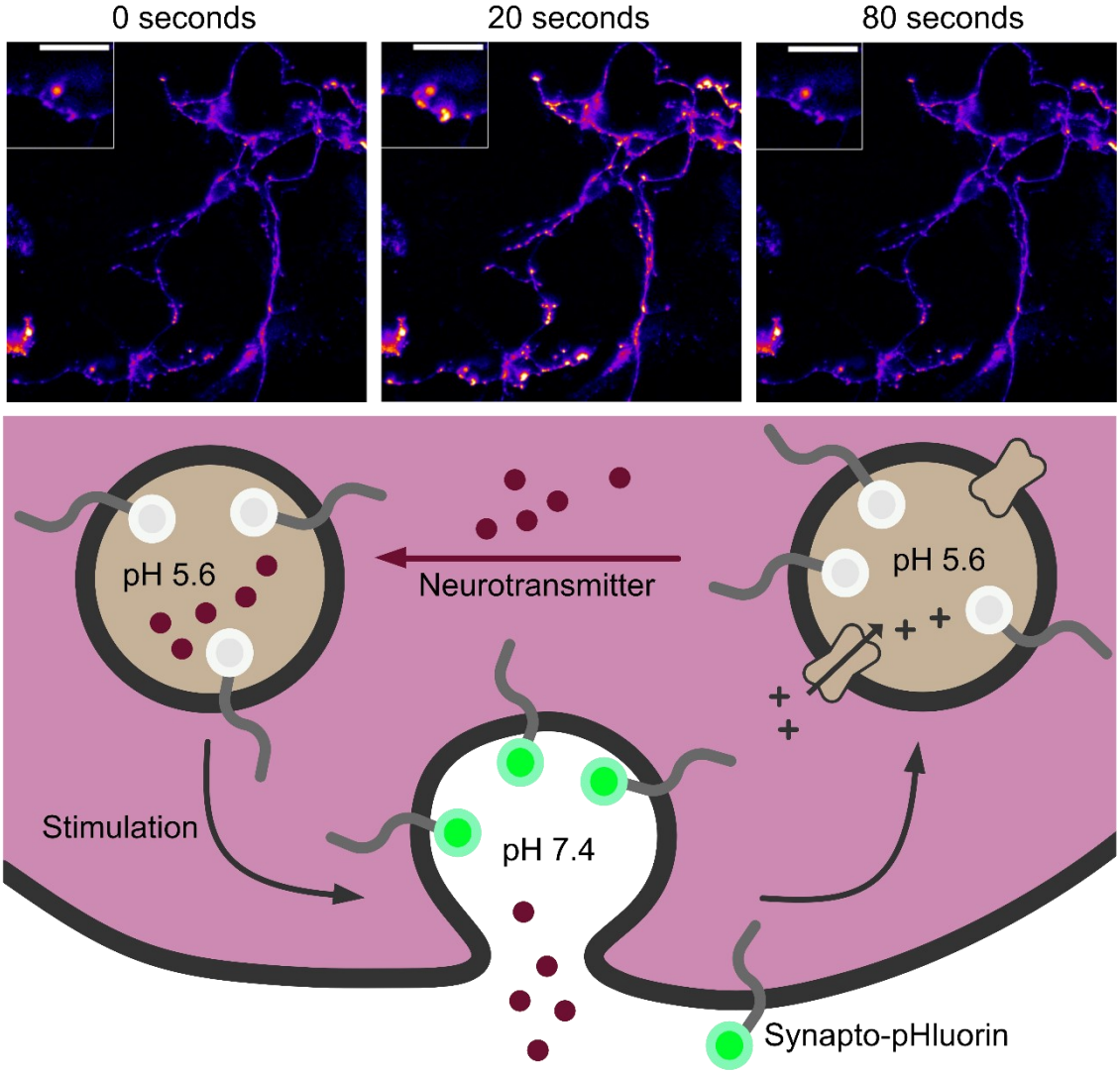

Figure 24: A pH-sensitive Tool to Measure Kinetics of Synaptic Vesicle Cycling. Mutagenesis (F64L/S65T/Q80R/S147D/N149Q/V163A/S175G/S202F/Q204T/A206T) alters the spectral properties of GFP, rendering it pH-sensitive (pHluorin). When pHluorin is fused to the luminal domain of an SV protein and expressed in neurons, its signal is suppressed within the acidic vesicle lumen. Upon stimulation with action potential trains, vesicles undergo fusion with the presynaptic membrane causing pHluorin molecules to emit fluorescence due to neutralization of their environment, which can be visualized by fluorescence microscopy. Subsequently, after endocytosis and acidification of newly formed endocytic intermediates, pHluorin fluorescence is re-quenched. Monitoring pHlourin fluorescence over time post-stimulation enables the observation of exo- and endocytic cycling. Scale bar, 2.5 µm.

The green fluorescent protein (GFP), adopts a barrel-shaped structure that shields its chromophore core, an aromatic ring formed by the cyclization of three neighboring amino acid residues (serine$_{65}$, tyrosine$_{66}$, and glycine$_{67}$) (F. Yang et al., 1996), which absorbs blue light and emits it as green fluorescence. The protonation of tyrosine$_{66}$ alters the excitation characteristics of GFP and is constrained by a proton relay network comprised of surrounding amino acid residues within its cylinder. Mutations in GFP core residues enhance the sensitivity of its spectral properties to pH alterations by affecting the protonation state of tyrosine$_{66}$, eclipsing its signal at acidic pH levels below 6.0, which is reversible within 20 ms after returning to neutral pH (Miesenböck et al., 1998). This superecliptic pH-sensitive GFP variant (pHluorin), exhibits a pK_a of 7.1 (Sankaranarayanan et al., 2000) and can be fused to the luminal domain of synaptic vesicle proteins (yielding Synapto-pHluorin).

Upon exogenous expression, Synapto-pHluorin molecules undergo dequencing during exocytosis due to the exposure to the neutral pH of the synaptic cleft and are re-quenched upon vesicle recycling and re-acidification of endocytic intermediates (Figure 24). The endocytosis of synaptic vesicles occurs over a timescale exceeding 10 seconds following stimulation with action potential trains (López-Hernández et al., 2022; Soykan et al., 2017), enabling the determination of endocytosis kinetics by monitoring the decay of pHluorin fluorescence post-stimulation (Figure 24/ Figure 25). To mitigate artefacts from the exogenous expression of fusion proteins, pHluorin assays can be complemented by antibody uptake experiments. Therein, the internalization of endogenous SV proteins is tracked by fluorophore-coupled antibodies directed against the luminal domains of SV proteins. For example, the cyanine-based pH-sensitive dye CypHer5E can be employed, exhibiting bright fluorescence in its protonated state (Adie et al., 2003) within the acidic pH of the SV lumen. Upon exocytosis, its fluorescence is quenched and recovered upon endocytosis and re-acidification processes (Y. Hua et al., 2011; López-Hernández et al., 2022).

Consequently, the expression of Synapto-pHluorin or incubation with CypHer5E-coupled luminal domain antibodies enables the visualization of exo-endocytic cycling of exogenous and endogenous SV proteins, respectively, with opposite pH-dependence (Figure 24).

For live-imaging of Synaptophysin and vesicular glutamate transporter 1 (vGLUT1) recycling, SV proteins fused to the green-fluorescent protein-based pH-sensitive fluorescent reporter pHluorin at their luminal domain were overexpressed by plasmid

transfection (Synaptophysin-pHluorin; DIV 7) or lentiviral transduction (vGLUT1-pHluorin; DIV 2).

For following endogenous vesicular gamma-aminobutyric acid transporter (vGAT) recycling, spontaneously active synaptic boutons were labeled by incubating cells with CypHer5E-conjugated antibodies against the luminal domain of vGAT (1:500 from a 1 mg/ml stock; Synaptic Systems; Cat#131,103CpH) for 2 h in their respective conditioned culture media at 37 °C and 5% CO_2 prior to imaging.

To investigate kinetics of SV recycling, neurons at DIV 14-16 were placed into an RC-47FSLP stimulation chamber (Warner Instruments) in osmolarity-adjusted imaging buffer [170 mM NaCl, 20 mM N-Tris(hydroxyl-methyl)-methyl-2-aminoethane-sulphonic acid (TES), 5 mM Glucose, 5 mM $NaHCO_3$, 3.5 mM potassium chloride (KCl), 1.3 mM $CaCl_2$, 1.2 mM sodium sulfate (Na_2SO_4), 1.2 mM magnesium chloride ($MgCl_2$), 0.4 mM potassium dihydrogenphosphate (KH_2PO_4), 50 µM *(2R)*-amino-5-phosphonovaleric acid (AP5) and 10 µM 6-cyano-7-nitroquinoxaline-2,3-dione (CNQX); pH 7.4] at 37°C (Tempcontrol 37-2 digital). Cells were subjected to electrical field-stimulation (MultiStim System-D330; Digimeter Ltd.) with annotated stimulation trains to evoke action potentials (APs) [40 Hz, 5s (200 APs), 40 Hz, 2s (80 APs), 20 Hz, 2s (40 APs); at 100 mA] at 37.5°C. Following changes in fluorescence were tracked by an inverted Zeiss Axiovert 200M microscope, equipped with a 40x oil-immersion EC Plan Neofluar objective (NA 1.30), an EM-CCD camera (Evolve Delta 512) and a pE-300^{white} LED light source (CoolLED). The scanning format was set to 512 x 512 pixels with 16-bit sampling. eGFP (Excitation: BP470-40; Emission: BP535-50; Zeiss filter set 38) or Cy5 (Excitation: BP640-30; Emission: BP525-50; Zeiss filter set 50) filter sets were used for pHluorin or CypHer assays, respectively. Images were acquired at 0.5 Hz frame rate for 100 s with 50 (Syph-pHluorin) or 100 (vGLUT1-pH, vGAT-CypHer) ms exposure with an electron multiplying gain of 250 operated through Fiji-based MicroManager 4.11 software.

Analysis of responding boutons was performed through custom-written macros to identify regions of interest (ROIs) in an automated manner using SynActJ (Schmied et al., 2021). Such analysis averaged fluorescence for each time point (t) in an image series (video) of at least >20 responding boutons and corrected values for background fluorescence yielding raw background-corrected fluorescence (F) (Figure 25A). The fold increase of fluorescence after stimulation (F_{max}) can serve as a measure for exocytic fusion and is calculated by normalising F by the mean intensity of F before stimulation (Baseline/basal fluorescence (F_0) = mean intensity of first 5 frames for pHluorin; first

10 frames for CypHer) for each time point (surface normalisation = F/F_0 for pHluorin; $F_0 - F_{min}$ for CypHer) (Figure 25B). To account for boutons with varying pHluorin expression in one image series and to compare reacidification kinetics, the fluorescence of each time point was subtracted by the basal fluorescence (F_0) to yield ΔF ($F-F_0$), which was then normalised by its peak value (ΔF_{max}) (Figure 25C). The resulting peak normalised curves ($\Delta F/ \Delta F_{max}$) are annotated as norm. ΔF. Endocytic decay constants (τ) were calculated by averaging and then fitting the norm. ΔF ($\Delta F/\Delta F_{max}$) traces of all videos in one condition (N) to a mono-exponential decay curve [$y_0 + A*e^{(-t/\tau)}$] with the constraints of $y_0 = 1$ and offset = 0 in Prism 9 (Graphpad) (Figure 25C).

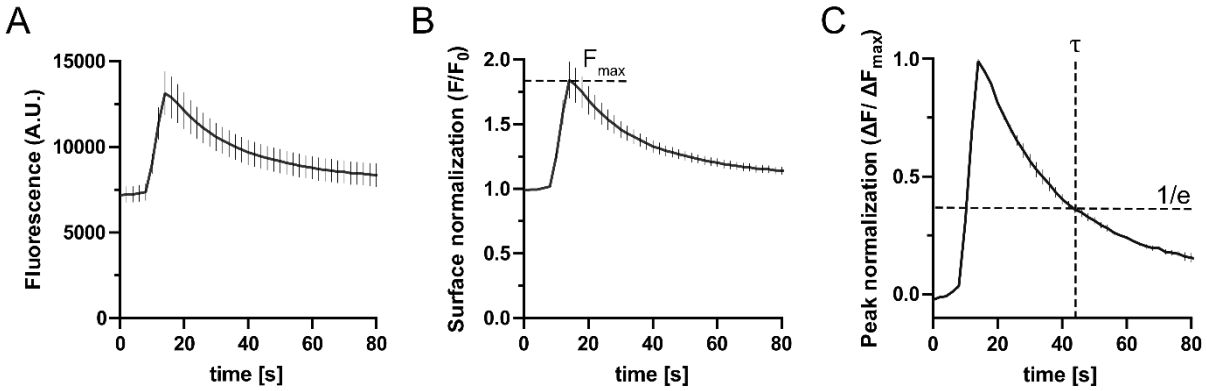

Figure 25: Analysis of SV Endocytosis Kinetics by following pHluorin Fluorescence.
A: The time course of pHluorin fluorescence traces of over 20 boutons is measured and background-corrected (F).
B: Fluorescence traces are surface normalized by dividing F by the mean intensity before stimulation (basal fluorescence F_0). The fold increase of fluorescence after stimulation F_{max} can serve as a measure for exocytosis.
C: The fluorescence of each time point is subtracted by F_0 and divided by the maximum value of that curve ($\Delta F/\Delta F_{max}$). Resulting peak normalized curves (norm. ΔF) are fitted to mono-exponential decay curves [$1 + A*e^{(-t/\tau)}$] to yield decay constants τ (time point for norm. $\Delta F = 1/e$).

CypHer-traces had to be corrected for photobleaching: The decay constant of the bleaching curve was determined by fitting the data points of the first 10 frames (20 s, prior to stimulation) to a mono-exponential decay curve. The corresponding value of the photobleaching curve at a given time *t* was added to the raw fluorescence intensity measured at each corresponding time point to correct for the loss of intensity due to bleaching.

3.2.4.2. Analysis of the Presynaptic Membrane Pool of SV Proteins

Synaptic vesicle proteins undergo cycling between vesicle pools and the presynaptic membrane. Inhibition of endocytosis leads to accumulations of synaptic vesicle proteins stranded on the plasma membrane (López-Hernández et al., 2022; Raimondi

et al., 2011). These stalled synaptic vesicle proteins can be visualized by antibodies targeting the exposed luminal domains on the plasma membrane surface under non-permeabilizing conditions (Figure 26). This technique complements live-imaging assays by distinguishing between presynaptic membrane and internalized pools, providing an indirect measure of stalled endocytic invaginations.

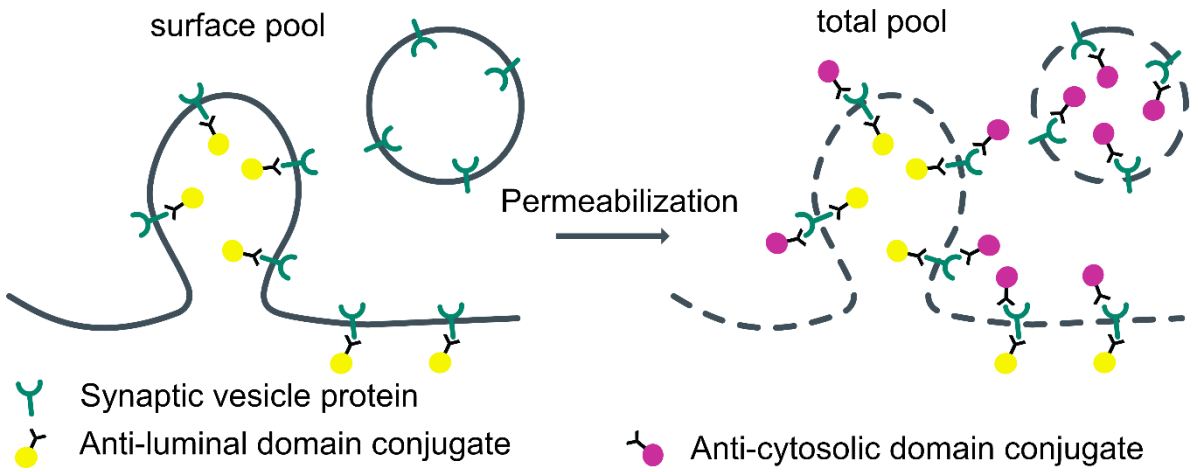

Figure 26: Analysis of the Presynaptic Membrane Pool of Synaptic Vesicle Proteins.
The presynaptic membrane (surface) pool of synaptic vesicle proteins, such as vGAT, vGLUT1, or Synaptotagmin1, can be accessed by the application of antibodies recognizing their luminal domains under non-permeabilizing conditions. Upon permeabilization of membranes, the total pool becomes accessible and can be visualized by fluorophore-coupled antibody conjugates targeting the cytosolic domains of SV proteins.

To assess the presynaptic membrane pool of synaptic vesicle proteins, hippocampal cultures were transferred to ice and washed with ice-cold phosphate-buffered saline (PBS). Neurons were then fixed using 4% p-formaldehyde (PFA) and 4% sucrose in PBS for 15 min at room temperature (RT). Following fixation, cells were washed thrice with PBS and were then incubated with antibodies targeting the luminal domain of synaptic vesicle proteins (vGAT, vGLUT1, Synaptotagmin1) in a buffer containing 10% normal goat serum (NGS) in PBS for 1 h at RT. Subsequently, unbound antibodies were removed by three PBS washes, while bound antibodies were labeled using corresponding fluorophore-coupled secondary antibodies in PBS supplemented with 10% NGS for 1 h at RT to visualize the surface pool of the respective SV protein. After three consecutive wash cycles with PBS, permeabilization buffer (10 % NGS and 0.3 % Triton X-100 in PBS) was applied for 30 min at RT to permeabilize membranes. Thereafter, the total pools of SV proteins, as well as Synapsin1 as a marker protein, were accessed by incubation with primary antibodies recognizing epitopes within cytosolic domains in permeabilization buffer at 4°C overnight. The subsequent day, unbound antibodies were removed through three washes with PBS, while bound

antibodies were decorated with differentially fluorescently labeled secondary antibodies in permeabilization buffer. Finally, neurons underwent three PBS washes, and coverslips were mounted in Immu-Mount™ (Thermo Fisher Scientific, Cat# 10622689).

Synaptic vesicle protein pools were imaged using a spinning disc confocal microscope (Zeiss Axiovert 200M) with a 63x oil objective (1.4 NA), equipped with the Perkin-Elmer Ultra View ERS system and a Hamamatsu C9100 EM-CCD camera under the control of Volocity software (Perkin-Elmer, v6.21).

For subsequent analysis, confocal images underwent Gaussian blur filtering (sigma = 2 pixels), and Synapsin1 labeling served as a mask to confine the quantified area to Synapsin1-positive boutons by applying thresholding using Otsu's method. Within the masked area, both surface and internal signals of SV proteins were analyzed and the ratio of surface to total pool was computed.

3.2.4.3. Stimulated Emission Depletion Microscopy

The optical resolution of fluorescence microscopy is constrained by the diffraction limit of light, achieving a maximum lateral resolution of 200 nm (Z. Wang et al., 2011). In order to resolve small structures like synapses (500 - 2000 nm) and their sub-synaptic structures (active zone: 200 - 400 nm; SV: 40-50 nm; (Nosov et al., 2020)), super-resolution fluorescence or electron microscopy must be applied.

Stimulated emission depletion (STED) microscopy offers a means to overcome the classical diffraction limit by suppressing spontaneous fluorescence emission centered around a focal spot (Figure 27). This is achieved through intense light pulses at the edge of the infrared spectrum, which prompt excited fluorophores to revert to the ground state (s_0) (Figure 27), inducing stimulated photon emission of a longer wavelength and depleting spontaneous fluorescence signal before reaching the detector (Vicidomini et al., 2018). In a STED microscope, the superimposition of the excitation laser with a shortly delayed red-shifted depletion laser in the shape of an overlapping donut cancels the emission of fluorophores distant from the center of excitation (Figure 27), resulting in a narrower point-spread function and enhanced spatial resolution (Yuan & Fang, 2014).

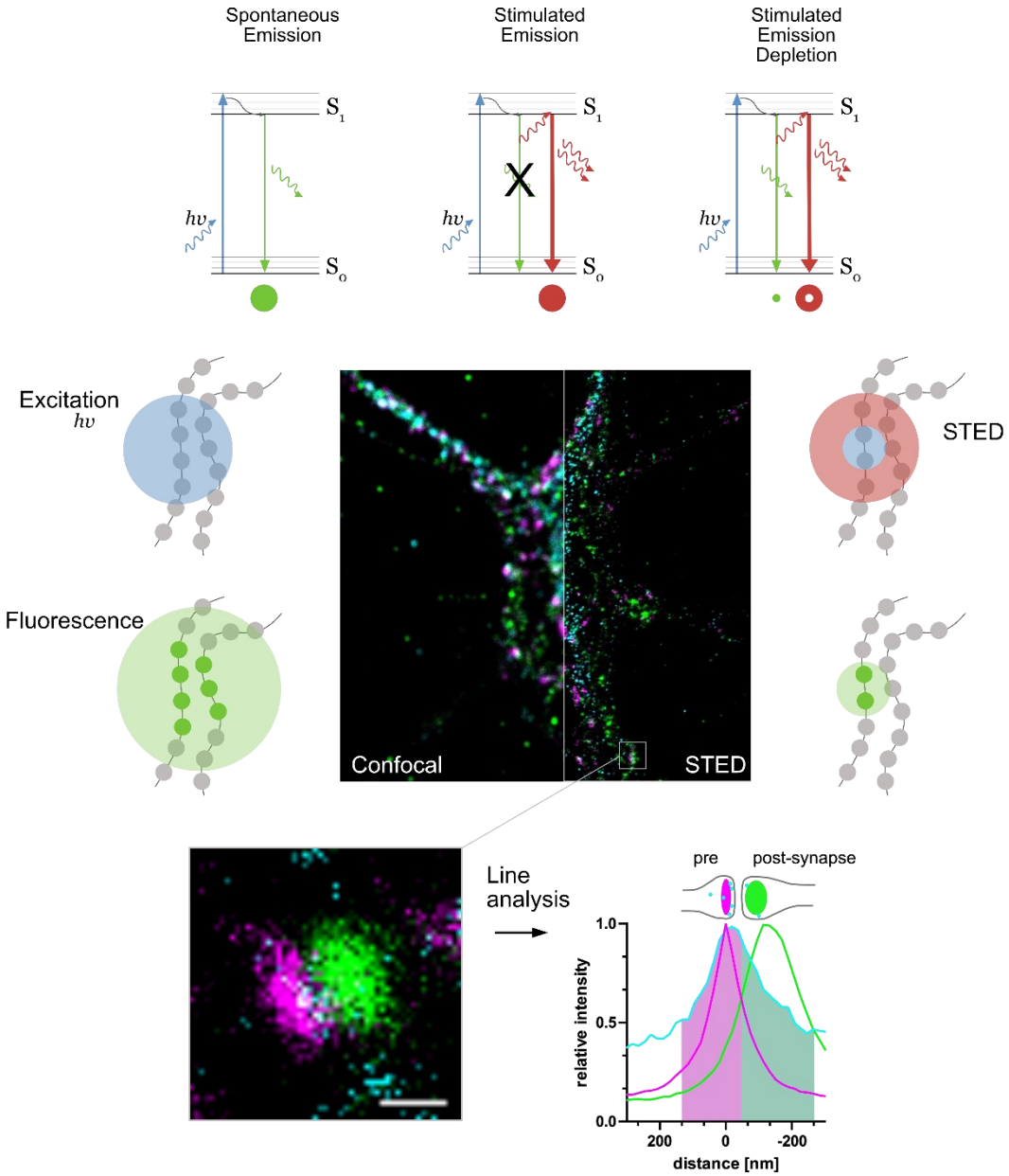

Figure 27: STED Microscopy for the Analysis of subsynaptic Protein Localization.
In confocal microscopy, fluorophores are excited (S_1) by the excitation laser (hv) and emit fluorescent photons (spontaneous emission) to return to the ground state (s_0). In structures of close vicinity all fluorophores are excited and cannot be distinguished by the detector. Spontaneous emission can be suppressed by additional light pulses inducing stimulated emission of photons at higher wavelengths. In STED microscopy, a donut-shaped beam is superimposed with the excitation spot. Within the region where excitation and STED lasers overlap, fluorophores are exited and stimulated to emit at the wavelength of the STED laser, which are omitted from reaching the detector through appropriate filter sets. This filtering results in a reduction of the effective fluorescent spot size to enhance spatial resolution. Consequently, pre-and postsynaptic regions can be distinguished via immunocytochemistry of respective marker proteins. Co-staining of proteins of interest enables the discrimination of their nanoscale localization and synaptic abundance.

STED microscopy facilitates the localization of synaptic proteins by immunocytochemistry with respect to pre- and postsynaptic marker proteins (Panatier et al., 2014) (Figure 27).

Immunocytochemistry

For immunostainings, neuronal cultures were chemically fixed on DIV 14-16 using 4% p-formaldehyde (PFA) and 4% sucrose in phosphate buffered saline (PBS) for 15 min at room temperature (RT). For experiments in Figure 39, cultures were stimulated with a 40 Hz train for 5 s in imaging buffer before immediate fixation. After fixation, cells were washed thrice with PBS and incubated with permeabilization buffer (10% normal goat serum, 0.3 % Triton X-100 in PBS) for 30 min at RT, followed by primary antibody incubation of proteins of interest in permeabilization buffer at indicated dilutions (Table 1) at 4°C overnight. Subsequently, unbound antibodies were removed by three PBS washes while bound antibodies were decorated by corresponding fluorophore-coupled secondary antibodies (Table 2) in permeabilization buffer for 1h at RT.

For F-Actin staining, Phalloidin-Alexa Fluor™ 594 (1:1000 stock; AAT Bioquest; Cat# ABD-23158) was added in the secondary incubation step. Finally, neurons were washed thrice with PBS, followed by two washes with ultra-pure water. Coverslips were dried for 2 h before mounting in ProLong™ Gold Antifade (Thermo Fisher Scientific; #P36934) on glass slides (Thermo Fisher Scientific; VWR; Cat#630-1985). The slides were cured for at least 72 h at RT before imaging.

Multicolor time-gated STED Imaging

STED images were acquired from fixed samples by a HC PL APO CS2 100 x oil objective (1.40 NA) on a Leica SP8 TCS STED 3x microscope (Leica Microsystems) equipped with a pulsed white-light excitation laser (WLL; ~ 80 ps pulse width, 80 MHz repetition rate; NKT Photonics) and a STED laser for stimulated emission (775 nm). The scanning format was set to 1024 x 1024 pixels, with 8-bit sampling, 4x line averaging, 4x frame accumulation and 6x optical zoom, yielding a final pixel size of 18.9 nm. Three-color imaging was performed by sequentially exciting the following fluorophores (excitation filter = Exf; emission filter = Emf): Atto647N (Exf: 640 nm; Emf: 650-700 nm); Alexa Fluor™ 594 (Exf: 590 nm; Emf: 600-640 nm) and Atto542 (Exf: 540 nm; Emf: 550-580 nm) operated by the Leica Application Suite X (Leica Microsystems, 2020). For stimulated depletion of the signal, the 775 nm STED laser was applied to all emissions. The detection of the resulting signal was time-gated by 0.3-6 ns to allow enough time for stimulated depletion and collected by two sensitive HyD detectors at appropriate spectral regions distinct from the STED laser wavelength. Settings in independent experiments were similar between conditions to allow

quantification of signals. Raw data, obtained from three-channel time-gated STED (gSTED) imaging, were analyzed with Fiji. For analysis, only synapses oriented in the xy-plane exhibiting a clear separation of Bassoon (presynapse) and Homer1 (postsynapse) clusters were taken into account. To determine synaptic localization and presynaptic levels of proteins of interest, multicolor line profiles were measured: A line (1.0 µm length, 0.4 µm width) perpendicular to the synaptic cleft (space between Bassoon & Homer1 cluster) was drawn (Gerth et al., 2019) and the fluorescence intensity of all three channels along this line was measured using a Fiji Macro (Macro_plot_lineprofile_multicolor; Dr. Kees Straatman, University of Leicester, UK). The resulting profiles were aligned to the maximum Bassoon intensity, which was set to 0 nm (Figure 27). For localization analysis, all three profiles were normalized to their maxima, which were set to 1. For quantification of presynaptic protein levels, only the fractions of the non-normalized line profiles of proteins of interest overlapping with the normalized averaged Bassoon distribution (between 151.4 and -37.8 nm, Figure 27) were integrated. Intensities were normalized to controls (DMSO, shCTR, WT) which were set to 100.

3.2.4.4. Transmission Electron Microscopy

Transmission electron microscopy (EM) enables the analysis of synaptic ultrastructure at nanometer resolution by visualizing electron-rich subcellular structures such as membranes (Deguchi et al., 2016; S. Watanabe, Rost, et al., 2013). In EM, beams of electrons are transmitted through ultrathin sections containing cellular components embedded in resin following post-fixation in osmium, which preserves lipid-rich membranes. Membranes impede the electron beam's passage through the section in proportion to their electron density. Contrast in EM relies on electron density; thus, stains composed of heavy metals like uranyl and lead are employed to bind to polar biological structures, particularly membranes, enhancing their visibility.
EM imaging of synapses provides visualization of endocytic phenotypes by enabling the quantification of membrane-bound compartments representing the intermediates of the SV cycle, including coated and non-coated vesicles, coated and non-coated invaginations, and transient endosome-like vacuoles (Figure 28).

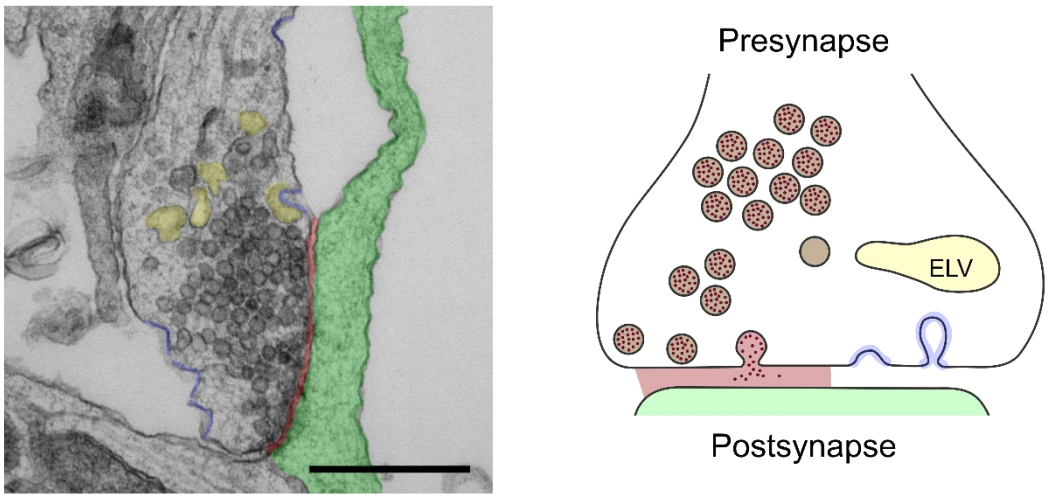

Figure 28: Electron microscopy enables Visualization of synaptic Ultrastructure.
Transmission electron microscopy utilizes electromagnets to concentrate an electron beam. This beam is transmitted through ultrathin sample sections, allowing electrons to traverse the entire tissue thickness and be detected. Electrons are repelled by heavy metals bound to lipid membranes and cannot fully cross the sections resulting in the composition of white (transmitted) and black (repelled electrons) images. In TEM images of synapses, subcompartments auch as the postsynapse (green) and the synaptic cleft underneath the active zone (marroon) can be identified. Additionally, intermediates of the synaptic vesicle cycle, such as invaginations (blue) and endosome-like vacuoles (ELVs, yellow) can be defined. Scale bar, 250 nm.

To investigate the synaptic effects of F-Actin manipulations at the ultrastructural level, cells on coverslips were chemically fixed with 2% glutaraldehyde in cacodylat buffer (CDB; 0.1 M sodium cacodylat) for 1 h at RT. Coverslips were washed thrice with CDB before osmification with 1% (w/v) osmium tetroxide (OsO_4) and 1.5% (w/v) potassium hexacyanoferrat ($K_3Fe(CN)_6$) in CBD for 1 h at 4°C. After post-fixation, cells were stained with 1% (w/v) uranyl acetate, dehydrated by methanol gradients and finally embedded by epoxy resin (Sigma Aldrich; Cat# 45359) infiltration. After polymerization (60°C, 30 h), coverslips were removed and ultra-thin (70 nm) sections were cut and contrasted with 2% (w/v) uranyl acetate and 80 mM lead citrate. 8-bit images were obtained on a Zeiss 900 transmission electron microscope equipped with Olympus MegaViewIII or Olympus Morada G2 digital cameras at 30000x magnification, yielding a pixel size of 1.07 nm. Subsequently, morphometry (density of synaptic vesicles, endosome-like vacuoles, Clathrin-coated vesicles, Clathrin-coated pits and non-coated invaginations) was analyzed from synaptic profiles with clearly distinguishable active zones and adjacent synaptic vesicles in a blinded manner.

3.2.5. Statistical Analysis

All data in this study are presented as the mean ± standard error of the mean (SEM) and were obtained from *N* independent experiments with a total sample number of *n* (e.g., number of images, videos, synapses, etc.) as annotated in the Figure legends. For analysis of protein levels in STED microscopy and synaptic structures in EM, statistical differences between groups were calculated considering *n*, while in all other experiments statistical differences were calculated between independent experiments *N* (In pHluorin/CypHer assays, at least 20 responding boutons/video were analyzed). For n > 100 or N > 5, data were tested for Gaussian distribution following D'Agostino-Pearson tests to determine parametric versus non-parametric statistical testing. The statistical significance between two groups was evaluated with either two-tailed unpaired student's t-tests for normally distributed data or two-tailed unpaired Mann-Whitney tests if the data did not follow a Gaussian distribution. In experiments that necessitated normalization (to 100 or 1) before analysis, one-sample t-tests or one-sample Wilcoxon rank tests were performed for normal and non-normal distributed data, respectively. The statistical significance between more than two experimental groups of normally distributed data was analyzed by one-way ANOVA, followed by a Tukey's post hoc test, while Kruskal-Wallis tests with post hoc Dunn's multiple comparison test were used when datasets did not follow Gaussian distribution.

Corresponding statistical tests are indicated in the Figure and significance levels are annotated as asterisks (*p < 0.05, **p < 0.01, ***p < 0.001, and ****p < 0.0001). Differences that are not significant are not stated or indicated as ns (p > 0.05). Statistical data evaluation was performed using GraphPad Prism 9.5.1 (733). All Figures were assembled using Affinity Designer (version 1.10.6.1665).

4. Results

Cytoskeletal Dynamics modulate Synaptic Vesicle Endocytosis

The cytoskeleton is the major cellular source of force generation and mediates vesicle trafficking and membrane deformation across various cell types (Aghamohammadzadeh & Ayscough, 2009; Hassinger et al., 2017; Thottacherry et al., 2018), suggesting a similar function in pit formation and membrane retrieval in endocytic pathways of synaptic vesicle (SV) recycling. In fact, the absence of Actin filaments (F-Actin) by genetic depletion of β/γ-Actin isoforms results in complete blockage of all forms of endocytosis at several synapses (X. S. Wu et al., 2016), underscoring their importance in synaptic processes. However, the precise contributions of cytoskeletal assembly, stability, and contractility remain elusive, as previous studies on SV recycling utilizing pharmacological manipulations of cytoskeleton dynamics have yielded inconclusive, often conflicting data (Babu et al., 2020; J. Bourne et al., 2006; Delvendahl et al., 2016; Z. Hua et al., 2011; Z. Li & Murthy, 2001; Ogunmowo et al., 2023; Richards et al., 2004; Sankaranarayanan et al., 2003; Soykan et al., 2017; S. Watanabe, Rost, et al., 2013; L. G. Wu & Chan, 2022).

To revisit the role of F-Actin dynamics in presynaptic endocytosis in hippocampal mouse neurons, the model system used in this study, we acutely treated cells with a pharmacological cocktail containing the G-Actin sequestering drug latrunculin A, F-Actin stabilizing compound jasplakinolide and Y-27632, an inhibitor of Rho-associated protein kinase (ROCK) signaling (Figure 29). This mixture has been shown to preserve the existing Actin-cytoskeleton architecture while blocking Actin assembly, disassembly and rearrangement, as well as the contractility of actomyosin strands through inhibition of ROCK (G. E. Peng et al., 2011).

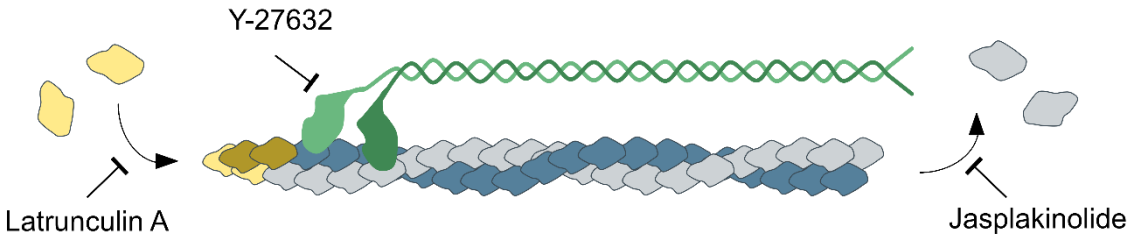

Figure 29: A pharmacological Cocktail to block Actin Dynamics
The combination of latrunculin A, to sequester Actin monomers (G-Actin), jasplakinolide, to stabilize Actin filaments (F-Actin) and Y-27632, an inhibitor of Rho-associated protein kinase (ROCK) blocking myosin movement arrests Actin dynamics.

We investigated the effects of perturbing F-Actin dynamics by optically monitoring the exo- and endocytosis of exogenously expressed Synaptophysin (Syph) fused to a pH-sensitive super-ecliptic green fluorescent protein (pHluorin) on its luminal domain. Following exocytosis, pHluorin molecules are de-quenched due to their exposure to the neutral pH of the synaptic cleft and are re-quenched upon vesicle recycling and reacidification (Figure 24). Exocytosis is induced by field stimulation of cultured neurons with trains of action potentials (APs) at physiological temperature (37.5°C). SV endocytosis occurs on a timescale exceeding 10 seconds following these conditions, which is slower than the re-quenching reaction of pHluorin upon SV reacidification (López-Hernández et al., 2022; Soykan et al., 2017). Hence, the decay of pHluorin fluorescence post-stimulation serves as a measure of the time course of SV endocytosis.

Blocking F-Actin dynamics by JLY application significantly impaired the endocytic retrieval of exogenously expressed Syph-pHluorin (Figure 30A/B), following 200 AP stimulation at physiological temperature in hippocampal synapses (Figure 30A/B). Interestingly, ROCK inhibition alone (Figure 30G/H), or the combined treatment of latrunculin A and jasplakinolide (Figure 30E/F) did not alter Syph-pHluorin endocytosis kinetics. Conversely, the co-application of Y-27632 and jasplakinolide resulted in a mild perturbation of endocytosis kinetics (Figure 30E/F).
To mitigate potential artefacts stemming from exogenous expression of pHluorin reporters, we additionally assessed the internalization of the endogenous vesicular γ-aminobutyric acid transporter (vGAT) using antibodies targeting its luminal domain coupled to the pH-sensitive fluorophore CypHer5E (Y. Hua et al., 2011; López-Hernández et al., 2022). This cyanine-based dye is quenched at neutral pH but exhibits bright fluorescence within the acidic lumen of SVs, serving as a marker for the exo- and endocytic cycling of endogenous SV proteins.
Perturbation of Actin dynamics by JLY cocktail incubation significantly delayed the endocytic retrieval of endogenous vGAT in response to train stimulation with 200 Aps (Figure 30D/E), consistent with the observations from exogenously expressed Syph-pHluorin.

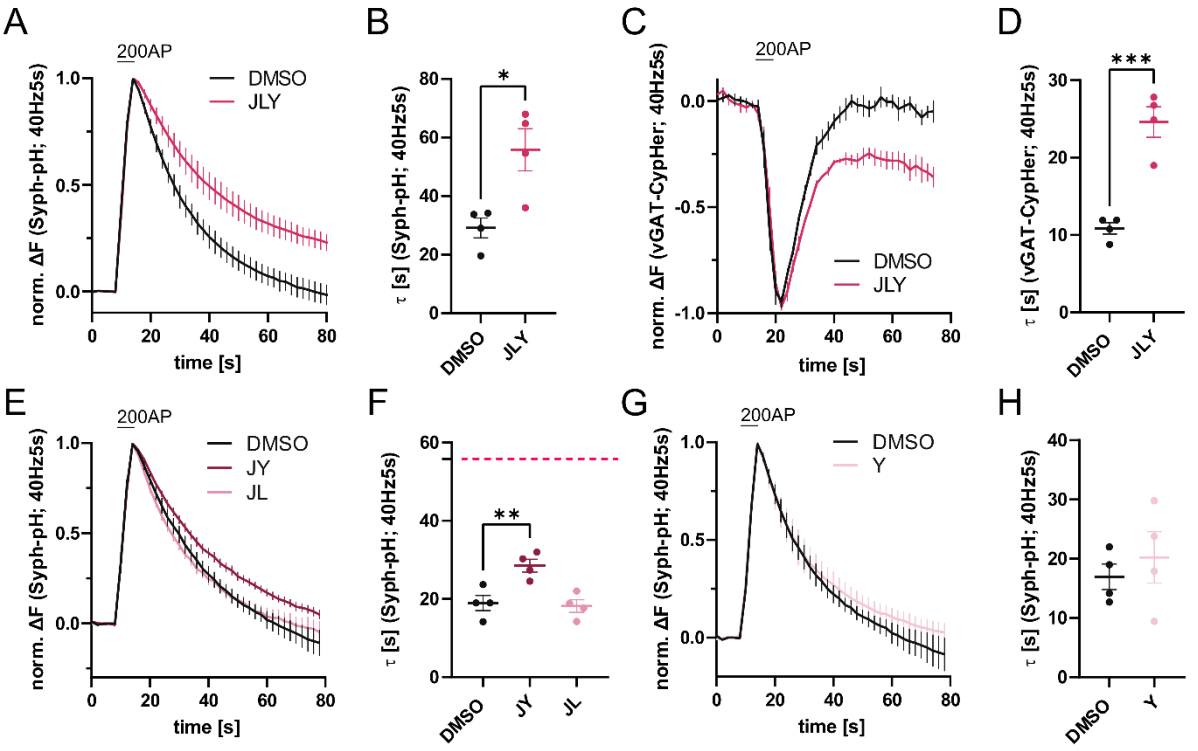

Figure 30: Perturbation of Actin Dynamics blocks Endocytosis of Synaptophysin and vGAT.
A: Averaged normalized Syph-pH fluorescence traces from transfected neurons stimulated with 200 APs (40 Hz, 5s) at physiological temperature (37.5°C). Neurons were treated with 0.1% DMSO or JLY cocktail (containing 8 µM Jasplakinolide, 5 µM Latrunculin A and 10 µM Y-27632). N = 4; n_{DMSO} = 23 videos; n_{JLY} = 36 videos.
B: Endocytic decay constants (τ) of Syph-pHluorin traces in A: τ_{DMSO} = 29.1 ± 3.4 s; τ_{JLY} = 55.8 ± 7.2 s; $p < 0.05$, two-tailed student's t-test.
C: Averaged normalized bleach-corrected vGAT-CypHer fluorescence traces from hippocampal neurons treated with DMSO or JLY cocktail in response to 200 AP (40 Hz, 5s) stimulation. N = 4; n_{DMSO} = 23 videos; n_{JLY} = 29 videos.**D:** Endocytic decay constants of vGAT-CypHer traces in C: τ_{DMSO} = 10.9 ± 0.7 s, τ_{JLY} = 24.6 ± 2.0 s; $p < 0.001$, two-tailed unpaired student's t-test.
E: Averaged normalized Syph-pH fluorescence traces from transfected hippocampal neurons treated with 0.1% DMSO, JY or JL combinations stimulated with 200 APs (40 Hz, 5s). N = 4; n_{DMSO} = 24 videos; n_{JY} = 19 videos; n_{JL} = 21 videos.
F: Endocytic decay constants (τ) of Syph-pHluorin traces in E: τ_{DMSO} = 19.0 ± 1.9 s; τ_{JY} = 28.5 ± 1.6 s; τ_{JL} = 18.2 ± 1.6 s; $p_{DMSO\ vs\ JY} < 0.01$, one-way ANOVA with Tukey's post-test. The dotted line indicates averaged τ from JLY treatments.
G: Averaged normalized Syph-pH fluorescence traces from transfected hippocampal neurons treated with 0.1% DMSO or 10 µM Y-27632 following 200 AP (40 Hz, 5s) stimulation. N = 4; n_{DMSO} = 25 videos; n_{Y} = 18 videos.
H: Endocytic decay constants (τ) of Syph-pHluorin traces in G: τ_{DMSO} = 17.0 ± 2.2 s; τ_{Y} = 20.2 ± 4.3 s. Data was generated together with Tolga Soykan.

Taken together, these findings suggest that the dynamic Actin cytoskeleton facilitates presynaptic endocytosis in hippocampal neurons.

4.1. mDia1/3 Formins drive Synaptic Vesicle Endocytosis via presynaptic Actin

The dynamics of F-Actin are tightly regulated by various protein classes, with filaments being rapidly assembled or severed in response to external stimuli (Rottner et al., 2017). However, studies into the involvement of such Actin mediators in presynaptic endocytosis have been limited. Recent data suggests that formins, a class of proteins capable of nucleating, polymerizing, and stabilizing Actin filaments, in particular diaphanous-related formin 1 (mDia1), may promote the recycling of Synaptophysin-pHluorin (Soykan et al., 2017), potentially by facilitating F-Actin assembly at the presynapse (Bingham et al., 2023; Ganguly et al., 2015).

4.1.1. mDia Formin Activity bidirectionally controls the Kinetics of SV Recycling

We confirmed that shRNA-mediated depletion of mDia1, targeting its 3'-untranslated region (3'-UTR), impaired Syph-pH endocytosis in response to 200 AP stimulation (Figure 31A/B) consistent with prior findings by (Soykan et al., 2017). This perturbation was rescued by reintroducing shRNA-resistant wild-type mDia1, as endocytosis kinetics were fully restored (Figure 31A/B).

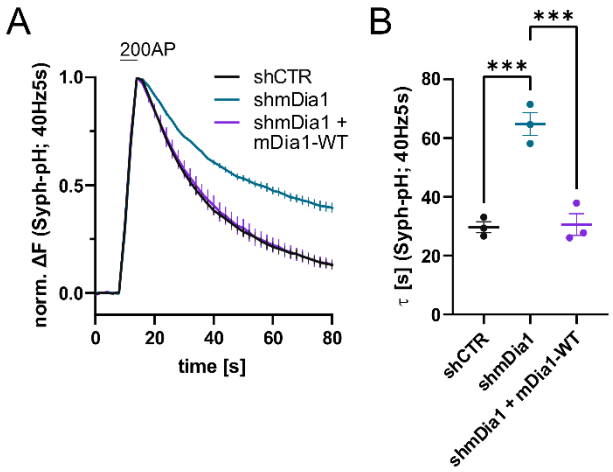

Figure 31: Loss of the Formin mDia1 impairs the Endocytosis of Synaptophysin.
A: Averaged normalized Syph-pHluorin fluorescence traces from neurons transfected with shRNA-encoding plasmids against no mammalian target (shCTR) or Diaph1 (shmDia1) in response to 200 AP (40 Hz, 5s) stimulation. Neurons were co-transfected with mDia1-mCherry (mDia1-WT) or mCherry alone (shCTR & shmDia1) to exclude artefacts from overexpression. N = 3; n_{shCTR} = 28 videos, $n_{shmDia1}$ = 21 videos, $n_{shmDia1 + mDia1\text{-}WT}$ = 21 videos.
B: Endocytic decay constants of Syph-pHluorin traces in E: τ_{shCTR} = 29.7 ± 1.9 s; $\tau_{shmDia1}$ = 64.7 ± 3.9 s; $\tau_{shmDia1 + mDia1\text{-}WT}$ = 30.6 ± 3.7 s; $p_{shCTR\ vs\ shmDia1}$ < 0.001, $p_{shmDia1\ vs\ shmDia1 + mDia1\text{-}WT}$ < 0.001, one-way ANOVA with Tukey's post-test.

Thus, these results underscore the critical involvement of the formin mDia1 in SV endocytosis.

However, we noted that the impairment of SV endocytosis by genetic ablation of mDia1 was less severe compared to the phenotypes observed following pharmacological inhibition of pan-formin activity by SMIFH2 application (Soykan et al., 2017). This discrepancy suggests potential compensatory mechanisms for the loss of mDia1 function involving closely related formins.

Based on domain architecture and function, the closest mDia1-related formins are the other isoforms of the diaphanous-related formin (DRF) family, namely mDia2 and mDia3. Previous studies on DRFs in the brain have indicated that mDia1 and mDia3 are expressed in the hippocampi of adult mice and share over-lapping functions. In contrast, mDia2 serves distinct roles in neuronal development and in other brain regions of adult mice (Shinohara et al., 2012).

Accordingly, we observed the expression of mDia1 and mDia3 in our hippocampal cultures (Figure 32A). To explore potential compensation between mDia1 and mDia3 in presynaptic endocytosis, we generated lentivirus carrying shRNA targeting mDia1 or mDia3. The combination of shmDia1+3 lentiviruses resulted in high transduction efficiency and depletion of both mDia1 and mDia3 levels in our hippocampal cultures 12 days post-infection (Figure 32A).

We further probed SV endocytosis by vesicular glutamate transporter 1 (vGLUT1)-pHluorin expressed by lentiviral particles in those cultures to minimize artifacts from plasmid expression. Retrieval of vGLUT1-pHluorin in response to 40 or 80 AP stimulation was perturbed upon loss of mDia1 (Figure 32B-E), and the co-depletion of mDia3 tended to further exacerbate this effect (Figure 32B-E), while exocytic fusion remained unaffected (Figure 80). Similarly, significant blockage of endocytosis upon loss of mDia1/3 was observed when assessing the recycling of endogenous vGAT (Figure 32F/G).

These findings suggest that mDia1/3 mediate SV endocytosis in both excitatory and inhibitory synapses, highlighting the overlapping functions of mDia1 and mDia3, consistent with previous studies (Deguchi et al., 2016; Litschko et al., 2019; Sakamoto et al., 2018; Shinohara et al., 2012; Thumkeo et al., 2011).

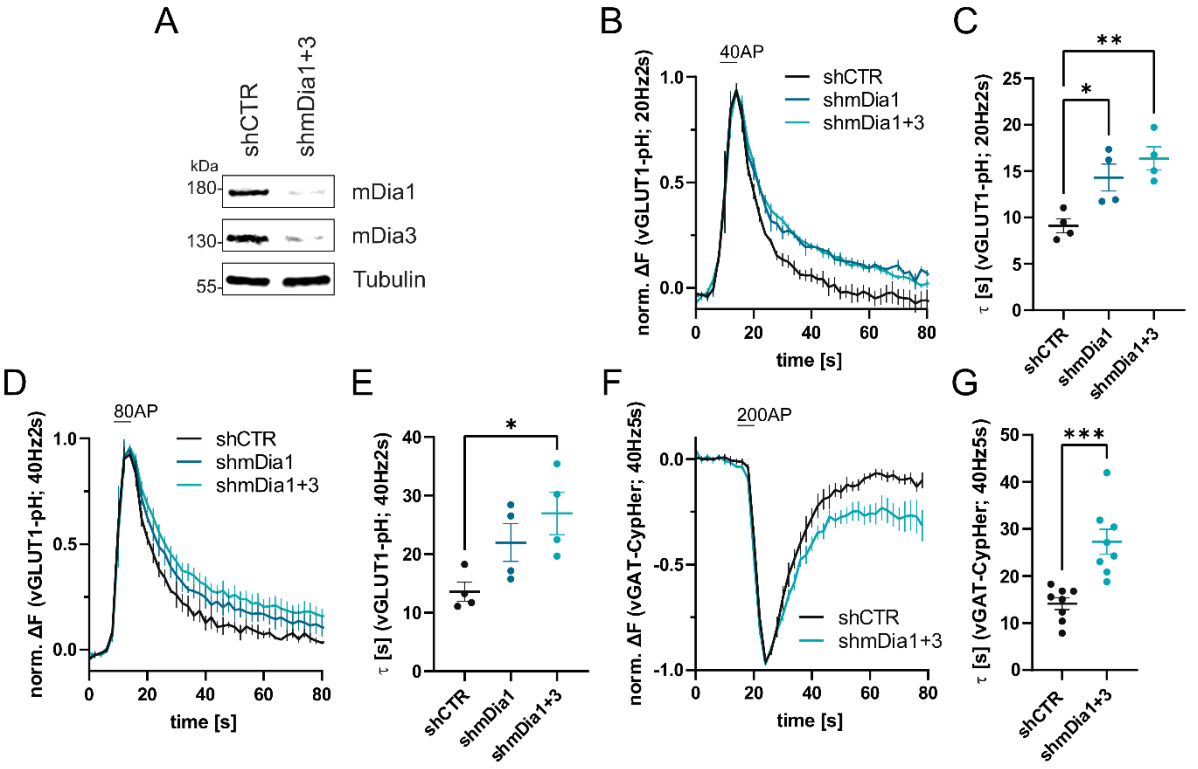

Figure 32: Loss of mDia1/3 impairs Kinetics of vGLUT1 and vGAT Recycling.
A: Knockdown efficiency of lentiviral particles carrying shRNA against no mammalian target (shCTR) or Diaph1 and Diaph2 genes (shmDia1+3) in mouse hippocampal cultures harvested 12 days after transduction. Protein abundance of mDia1, mDia3 and Tubulin was immunoblotted with specific antibodies.
B: Averaged normalized vGLUT1-pHluorin fluorescence traces from stimulated (40 APs; 20 Hz, 2 s) hippocampal neurons transduced with lentiviruses encoding shCTR, shmDia1 or both shmDia1 and shmDia3 combined (shmDia1+3). N = 4; n_{shCTR} = 17 videos, $n_{shmDia1}$ = 19 videos, $n_{shmDia1+3}$ = 18 videos. **C:** Endocytic decay constants of vGLUT1-pHluorin fluorescence traces in B: τ_{shCTR} = 9.1 ± 0.8 s; $\tau_{shmDia1}$ = 14.3 ± 1.5 s; $\tau_{shmDia1+3}$ = 16.4 ± 1.3 s; $p_{shCTR\ vs\ shmDia1}$ < 0.05, $p_{shCTR\ vs\ shmDia1+3}$ < 0.01, one-way ANOVA with Tukey's post-test.
D: Averaged normalized vGLUT1-pHluorin fluorescence traces for neurons transduced with shCTR, shmDia1 or shmDia1+3 in response to 80 AP stimulation (40 Hz, 2 s). N = 4; n_{shCTR} = 12 videos; $n_{shmDia1}$ = 15 videos; $n_{shmDia1+3}$ = 18 videos.
E: Endocytic decay constants of vGLUT1-pHluorin fluorescence traces in D: τ_{shCTR} = 13.6 ± 1.6 s; $\tau_{shmDia1}$ = 22.0 ± 3.2 s; $\tau_{shmDia1+3}$ = 26.9 ± 3.6 s; $p_{shCTR\ vs\ shmDia1+3}$ < 0.05, one-way ANOVA with Tukey's post-test.
F: Averaged normalized bleach-corrected vGAT-CypHer fluorescence traces from hippocampal neurons transduced with shCTR or shmDia1+3 in response to 200 AP (40 Hz, 5s) stimulation. N = 8; n_{shCTR} = 37 videos, $n_{shmDia1+3}$ = 35 videos.**G:** Endocytic decay constants of vGAT-CypHer traces in F: τ_{shCTR} = 14.1 ± 1.3 s; $\tau_{shmDia1+3}$ = 27.3 ± 2.6 s; p < 0.001, two-tailed unpaired student's t-test.

As blocking mDia1+3 activity by genetic ablation impaired SV endocytosis (Figure 32A/B), we were prompted to test the effects of artificially activating mDia function on endocytic membrane retrieval. DRFs are autoinhibited by an intramolecular interaction of their N-terminal diaphanous-inhibitory domain (DID) with their C-terminal diaphanous-autoregulatory domain (DAD) (Rose et al., 2005). *In vivo*, this autoinhibition is relieved by binding to GTP-bound forms of small Rho GTPases, converting biochemical signaling to mechanical output (Blanchoin et al., 2014).

Here, we modulated mDia formin activity by the application of IMM-01 (IMM), an intramimic compound that binds to the armadillo-repeat region, displacing the DAD from its binding pocket within the DID (Lash et al., 2013). Consequently, IMM binding to mDia formins prevents intramolecular association with the DAD domain, resulting in a continuously-accessible FH2 domain to associate with Actin. In NIH 3T3 cells, the application of IMM phenocopies the effects of overexpressing constitutively active forms of mDia formins, inducing the formation of filopodia-like structures and gradually increasing F-Actin abundance over time (Lash et al., 2013).
The acute treatment of neurons with IMM resulted in a moderate but significant acceleration of SV endocytosis, as monitored by vGLUT1-pHluorin (Figure 33), indicating that mDia activation facilitates SV kinetics.

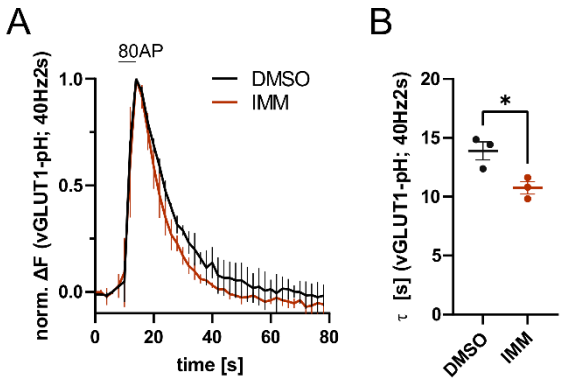

Figure 33: Activation of mDia1 facilitates vGLUT1 Endocytosis.
A: Averaged normalized vGLUT1-pHluorin fluorescence traces from transduced neurons in response to 80 AP (40 Hz, 2s) stimulation. Cells were treated with 0.1% DMSO or 10 µM mDia activator (IMM) in the imaging buffer. N = 3; n_{DMSO} = 18 videos; n_{IMM} = 16 videos.
B: Endocytic decay constants of vGLUT1-pHluorin traces in A: τ_{DMSO} = 14.9 ± 0.8 s; τ_{IMM}= 9.8 ± 0.5 s; $p < 0.05$, two-tailed unpaired student's t-test.

Taken together, these results indicate that the activities of mDia1/3 formins bidirectionally drive synaptic vesicle recycling, as their perturbation blocks (Figure 32), while stimulation accelerates (Figure 33) the kinetics of synaptic vesicle endocytosis.

4.1.2. mDia1/3 modulate Ultrastructure of presynaptic Membranes

The recycling of synaptic vesicles involves distinct and overlapping pathways that operate on different timescales depending on the initial stimulus and temperature. At physiological temperature, fast Clathrin-independent mechanisms drive the initial and immediate membrane retrieval to generate endocytic intermediates that are rapidly transported and fused to transient endosome-like vacuoles (ELVs) (Delvendahl et al.,

2016; Kononenko et al., 2014; Soykan et al., 2017). Subsequently, synaptic vesicles are then regenerated via Clathrin-mediated budding from ELVs (Chanaday & Kavalali, 2018a; S. Watanabe et al., 2014; Zhu et al., 2009).

We previously identified a role for mDia1/3 in SV cycling, as genetic ablation of those formins blocks the endocytic retrieval of exogenous and endogenous SV proteins monitored in pHluorin and CypHer assays. However, these assays are limited in determining the precise stage at which formins act on SV recycling. The observed acidification phenotypes could stem from a) the blockage of initial membrane retrieval, b) failed transport of endocytic intermediates to ELVs, or c) perturbed cargo sorting of the *v*-ATPase, the synaptic vesicle protein pump, into newly generated vesicles.

To elucidate the stages of the synaptic vesicle cycle in which formins are implicated, we investigated the ultrastructure of synaptic boutons upon genetic depletion of mDia1/3 using electron microscopy (EM). EM analysis allows the quantification of membrane-bound compartments representing intermediates of the SV cycle, including coated and non-coated vesicles, coated and non-coated invaginations and ELVs (Figure 28).
Synapses from mDia1/3-depleted neurons displayed drastic alterations of membrane-bound compartments (Figure 34A). However, Clathrin-coated intermediates, such as pits and vesicles, were rarely observed in both control and mDia1/3-depleted cells (Data not shown). Interestingly, the loss of mDia1/3 resulted in a mild increase in Clathrin-coated pits, while the number of Clathrin-coated vesicles was not significantly altered (Data not shown). Those results are consistent with predominant Clathrin-independent mechanisms of endocytic membrane retrieval and underscore that mDia1/3 are dispensable for vesicle uncoating mechanisms following budding from ELVs.

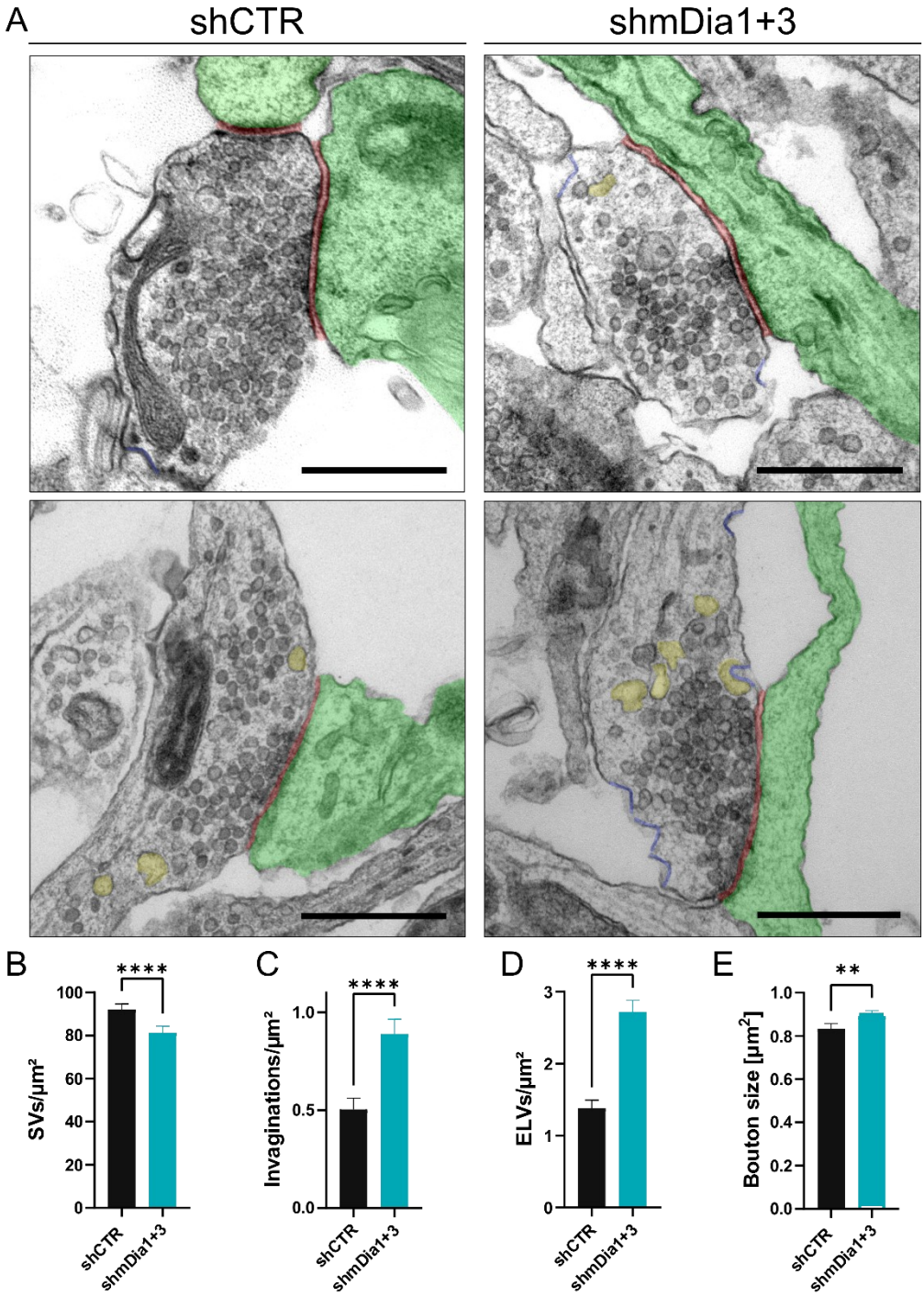

Figure 34: Loss of mDia1/3 alters Membrane Compartments and synaptic Ultrastructure.
A: Representative synaptic electron micrographs of hippocampal neurons transduced with lentiviral particles encoding shCTR or shmDia1+3. Invaginations and ELVs are colored in blue and yellow, while postsynapse and synaptic cleft are colored in green and maroon, respectively. Scale bar, 250 nm.
B-E: Averaged membrane compartments of boutons exemplified in **A**. [**B:** SVs/ µm² : shCTR (92.2 ± 2.5); shmDia1+3 (81.4 ± 2.9; $p < 0.0001$, Mann-Whitney test)]; [**C:** Invaginations/µm²: shCTR (0.5 ± 0.1); shmDia1+3 (0.9 ± 0.1; $p < 0.0001$, Mann-Whitney test)]; [**D:** ELVs/µm²: shCTR (1.4 ± 0.1); shmDia1+3 (2.7 ± 0.2; $p < 0.0001$, Mann-Whitney test); [**E:** Bouton size: shCTR (0.8 ± 0.0) and shmDia1+3 (0.9 ± 0.0; $p < 0.01$, Mann-Whitney test)]. N = 3; n_{shCTR} = 326 synapses, $n_{shmDia1+3}$ = 323 synapses.Experiments were performed together with Svea Hohensee.

Conversely, we found accumulations of non-coated plasma membrane invaginations both in the vicinity and distal of the active zone (Figure 34C).

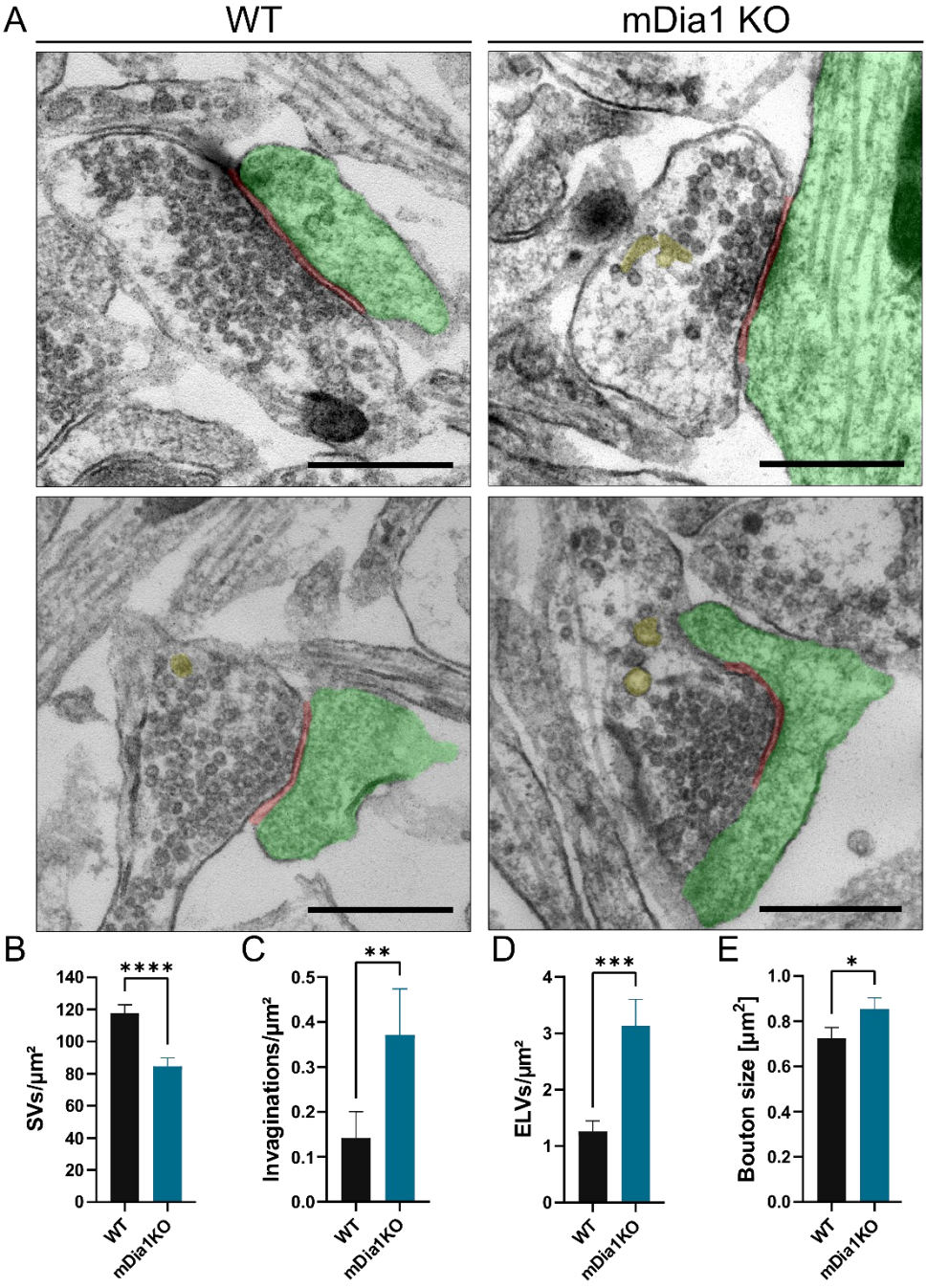

Figure 35: Knockout of mDia1 alters synaptic Ultrastructure.
A: Representative synaptic electron micrographs of hippocampal neurons from WT or mDia1 KO mice. Invaginations and ELVs are colored in blue and yellow, while postsynapse and synaptic cleft are colored in green and maroon, respectively. Scale bar, 250 nm.
B-E: Averaged membrane compartments of boutons exemplified in **A**. [**B:** SVs/ µm² : WT (117.6 ± 5.3); mDia1 KO (84.6 ± 5.2; $p < 0.0001$, Mann-Whitney test)]; [**C:** Invaginations/µm²: WT (0.1 ± 0.1); mDia1 KO (0.4 ± 0.1; $p < 0.01$, Mann-Whitney test)]; [**D:** ELVs/µm²: WT (1.3 ± 0.2); mDia1 KO (3.1 ± 0.5; $p < 0.001$, Mann-Whitney test)]; [**E:** Bouton size: WT (0.7 ± 0.0); mDia1 KO (0.9 ± 0.0; $p < 0.05$, Mann-Whitney test)]. N = 1; $n_{WT} = 103$, $_{nmDia1KO}= 96$ synapses.Experiments were performed together with Atul Kumar and Dmytro Puchkov.

Moreover, elevated numbers of ELVs (Figure 34D) were observed, suggesting a role as donor membranes for SV reformation (Kononenko & Haucke, 2015; S. Watanabe et al., 2014), as supported by the observed reduction in SV numbers in mDia1/3-depleted

neurons (Figure 34B). Notably, significant accumulations of plasma membrane invaginations (Figure 35A/C) and ELVs (Figure 35D) correlated with reduced numbers of SVs (Figure 35B) were similarly found in hippocampal neurons from mDia1 KO mice. Interestingly, both in mDia1-KO (Figure 35E) and mDia1+3-depleted neurons, presynaptic boutons (Figure 34E) were enlarged in size, a phenotype previously observed in mDia1/3-KO mice following neuronal inactivation (Deguchi et al., 2016).
Taken together, the loss of mDia formins significantly alters synaptic ultrastructure, characterized by the extension of bouton size, accumulations of endocytic intermediates such as invaginations and ELVs, and a reduction in SV density. Our observations suggest that mDia formins act at the early stages of endocytosis, specifically in the membrane retrieval step involving the deformation of membranes. In addition, formins mediate the reformation of synaptic vesicles from ELVs.

We conducted further analysis of ultrastructural changes in mDia1/3-depleted boutons upon induction of endocytosis following stimulation with 200 APs, as well as inactivation of network activity by silencing neurons through the application of tetrodotoxin (TTX), a voltage-gated sodium channel blocker, inhibiting AP propagation and evoked neurotransmission (Horvath et al., 2020).
Electrical stimulation exacerbated the accumulation of membrane invaginations and ELVs in the loss of mDia1/3 (Data not shown), in stark contrast to EM phenotypes observed in stimulated boutons after pharmacological inhibition of pan-formin activity by SMIFH2 (Soykan et al., 2017). Interestingly, the depletion of the synaptic vesicle pool upon mDia1/3 perturbation was rescued by blocking evoked and asynchronous release through TTX treatment (Figure 36A/B), indicating that the phenotype of SV reduction in mDia1/3-depleted neurons is activity-dependent. Conversely, silencing neuronal cultures for three days did not resolve the accumulations of membrane invaginations and endosome-like-vacuoles (Figure 36C/D), suggesting that the formation of those intermediates is not dependent on evoked neurotransmission.

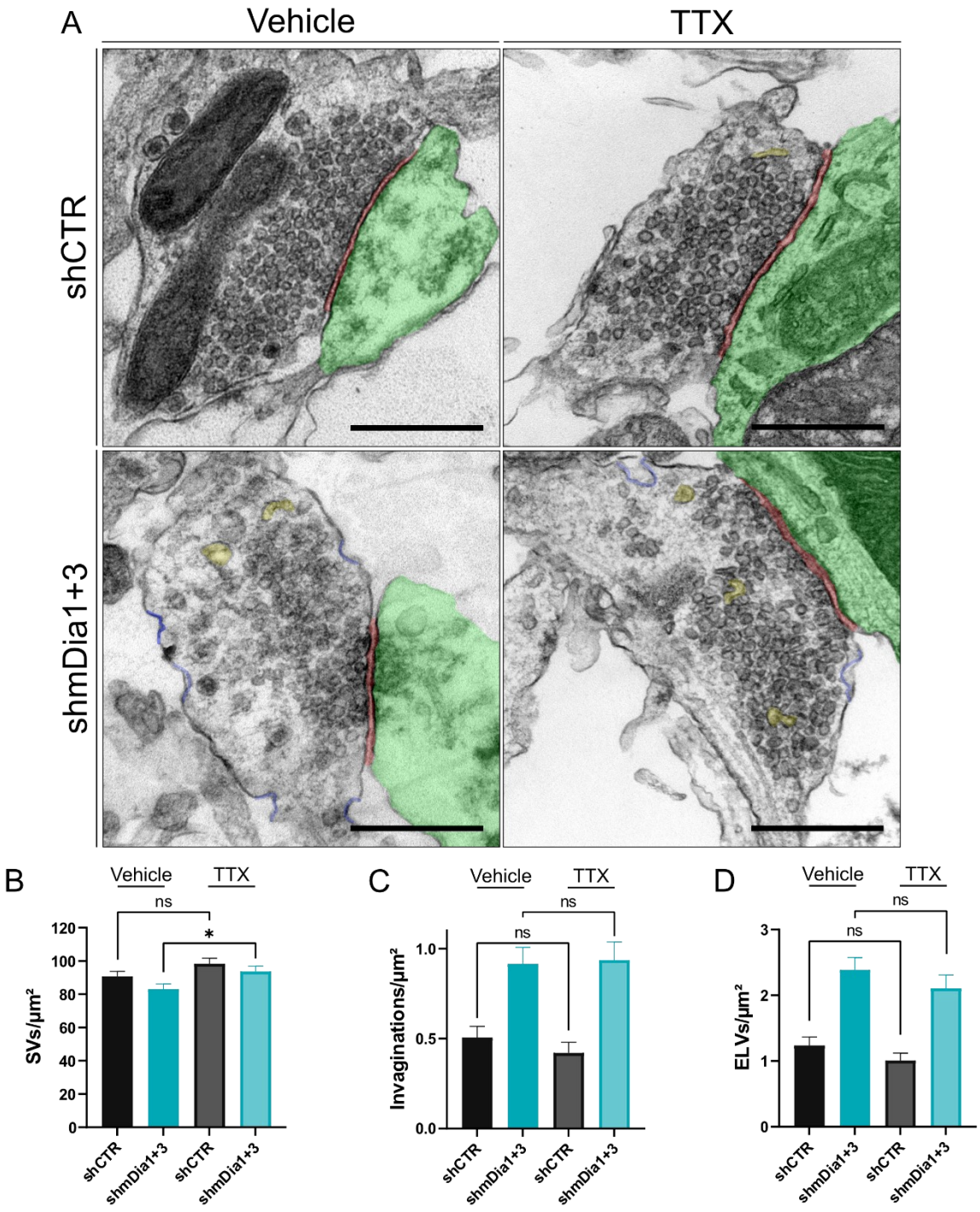

Figure 36: Neuronal Inactivation partially rescues ultrastructural Phenotypes upon mDia1/3 depletion.
A: Representative synaptic electron micrographs from neurons transduced with shCTR or shmDia1+3 and treated with 0.1% Vehicle or 1 µM TTX for 36 h before fixation. Invaginations and ELVs are colored in blue and yellow, postsynapse and synaptic cleft are colored in green and maroon, respectively. Scale bar, 250 nm.
B-D: Averaged membrane compartments of boutons exemplified in **A**. N = 2, $n_{shCTR + Vehicle}$ = 225 synapses, $n_{shmDia1+3 + Vehicle}$ = 225 synapses, $n_{shCTR + TTX}$ = 204 synapses, $n_{shmDia1+3 + TTX}$ = 221 synapses.
B: Averaged SVs/ µm² : shCTR + Vehicle (90.7 ± 3.1); shmDia1+3 + Vehicle (83.2 ± 2.9); shCTR + TTX (98.4 ± 3.3); shmDia1+3 + TTX (93.8 ± 3.1); $p_{shmDia1+3 + Vehicle \text{ vs } shmDia1+3 + TTX} < 0.05$, Kruskal-Wallis test with Dunn's post-test.
C: Averaged Invaginations/µm²: shCTR + Vehicle (0.5 ± 0.1); shmDia1+3 + Vehicle (0.9 ± 0.1); shCTR + TTX (0.4 ± 0.1); shmDia1+3 + TTX (0.9 ± 0.1). Legend continued on next page.

D: Averaged ELVs/µm²: shCTR + Vehicle (1.2 ± 0.1); shmDia1+3 + Vehicle (2.4 ± 0.2); shCTR + TTX (1.0 ± 0.1); shmDia1+3 + TTX (2.1 ± 0.2).
Experiments were performed together Svea Hohensee.

As the genetic perturbation of mDia1/3 results in accumulations of plasma membrane invaginations in an activity-independent manner, we questioned whether the observed undulations were of an endocytic nature. When endocytosis is drastically perturbed, SV proteins accumulate on stalled endocytic invaginations at the plasma membrane (López-Hernández et al., 2022; Raimondi et al., 2011) Stalled synaptic vesicle proteins can be visualized by antibodies recognizing exposed luminal domains on the plasma membrane surface under non-permeabilizing conditions. To determine if membrane deformations observed in our study can be classified as endocytic intermediates, we differentially accessed surface (stalled at the plasma membrane) and total (present at the plasma membrane and internalized) pools of SV proteins by performing immunostaining in non-permeabilized and detergent-permeabilized conditions (Figure 26).

Following confocal microscopy analysis of the total and surface pools of synaptic vesicle proteins Synaptotagmin1, vGLUT1, and vGAT, we found that Synaptotagmin1 surface levels remained unchanged in mDia1/3-depleted boutons marked by Synapsin1 staining (Figure 37A/B). In contrast, vGLUT1 and vGAT abundance on the plasma membrane was significantly reduced in neuronal cultures lacking mDia1/3, suggesting a potential endocytosis overshoot at steady-state (Figure 37C-F). These findings are in stark contrast to the loss of endocytic proteins such as AP-2 (López-Hernández et al., 2022) or Dynamin1/3 (Raimondi et al., 2011), indicating that mDia formins act on endocytosis via distinct mechanisms.

Hence, the accumulated membrane invaginations of the plasma membrane observed in electron microscopy (Figure 34/Figure 36) are not decorated with stalled SV proteins (Figure 37), indicating that they differ from activity-dependent endocytic pit formation.

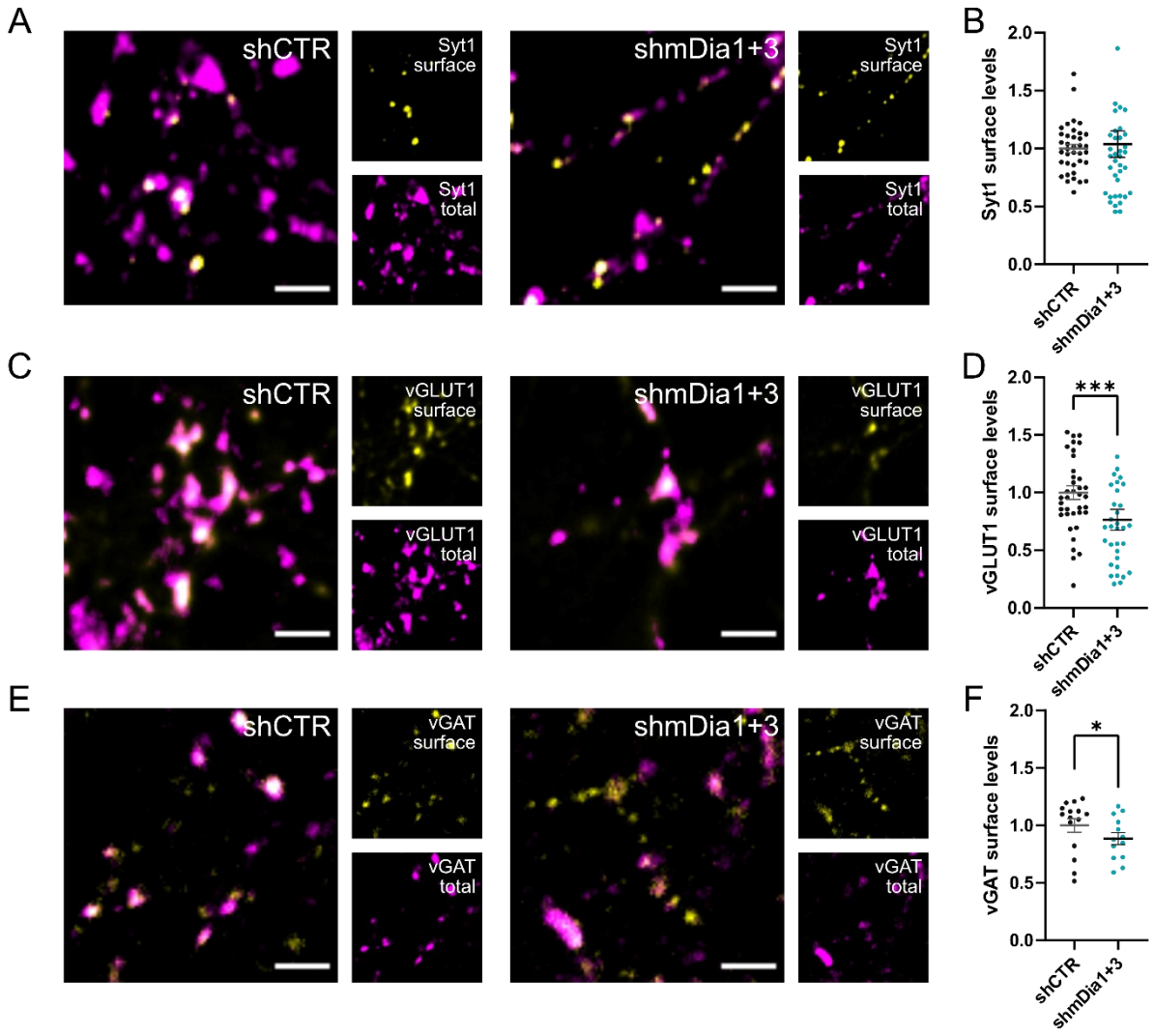

Figure 37: Depletion of mDia1/3 perturbs surface Levels of SV Proteins.
A: Representative confocal images of the surface (yellow) and total (magenta) pool of Synaptotagmin1 (Syt1) in hippocampal neurons treated with lentiviral particles against shCTR and shmDia1+3. Scale bar, 2.5 µm.
B: Analysis of surface levels of Synaptotagmin1 in shCTR (1.0 ± 0.0) and shmDia1+3 (1.0 ± 0.1) treated neurons in Synapsin1 positive boutons. Levels are expressed as the ratio of surface to total Synaptotagmin1 and are normalized to shCTR, which was set to 1. N = 5; n_{shCTR} = 37 images, $n_{shmDia1+3}$ = 38 images.
C: Representative confocal images of the surface (yellow) and total (magenta) pool of vGLUT1 in hippocampal neurons treated with lentiviral particles against shCTR and shmDia1+3. Scale bar, 2.5 µm.
D: Analysis of surface levels of vGLUT1 in shCTR (1.0 ± 0.1) and shmDia1+3 (0.8 ± 0.1) treated neurons in Synapsin1 positive boutons. Levels are expressed as the ratio of surface to total Synaptotagmin1 and are normalized to shCTR values, which was set to 1. N = 5; n_{shCTR} = 38 images, $n_{shmDia1+3}$ = 35 images.
E: Representative confocal images of the surface (yellow) and total (magenta) pool of vGAT in hippocampal neurons treated with lentiviral particles against shCTR and shmDia1+3. Scale bar, 2.5 µm.
F: Analysis of surface levels of vGAT in shCTR (1.0 ± 0.1) and shmDia1+3 (0.9 ± 0.1) treated neurons in Synapsin1 positive boutons. Levels are expressed as the ratio of surface to total Synaptotagmin1. Values were set to 1 for shCTR. N = 2; n_{shCTR} = 15 images, $n_{shmDia1+3}$ = 13 images.
Experiments were performed together with Hannah Gelhaus.

Taken together, mDia1/3 play a critical role in driving the replenishment of the SV pool by modulating endocytic membrane retrieval and reformation of SVs from transient endosomal intermediates (Figure 34). Furthermore, membrane accumulations in

mDia1/3-depleted neurons are present at steady-state and do not resolve under silencing conditions (TTX) (Figure 36), indicating an activity-independent non-endocytic nature (Figure 37). Hence, our data support a more general role for mDia formins in maintaining presynaptic membrane architecture and homeostasis.

4.1.3. mDia1 interacts with the presynaptic Membrane

Ultrastructural analysis of the genetic depletion of mDia1/3 revealed significant phenotypes on presynaptic membrane architecture. Building upon earlier findings implicating formins in mediating endocytosis kinetics, we argued that mDia formins must be targeted to membranes to drive SV retrieval. Interestingly, mDia1 harbors an unstructured N-terminal region that has been implicated in membrane association and insertion (Ramalingam et al., 2010). The membrane-binding region of mDia1 contains three stretches of basic amino acid sequences that mediate binding to negatively charged phospholipids such as $PI(4,5)P_2$ at the plasma membrane (Bucki et al., 2019). This architecture suggests that mDia1's function in SV retrieval involves the recruitment to and association with presynaptic membranes.

To test this hypothesis, we generated an N-terminal truncation mutant of mDia1 (mDia1-ΔN) lacking its first 60 amino acids (Figure 38A). Following membrane isolation through ultracentrifugation, we found that this truncation mutant displayed reduced association with the membrane fraction, marked by lysosomal associated membrane protein 1 (LAMP-1) enrichment in transfected HEK293T cells (Figure 38A/B). The perturbed membrane association rendered mDia1-ΔN unable to restore the kinetics of Syph-pHluorin endocytosis in comparison to the wild-type protein in neurons depleted of endogenous mDia1 using microRNA (Figure 38C/D).
Hence, our findings suggest that the N-terminal domain of mDia1 is crucial for SV endocytosis, likely through direct binding to membranes.

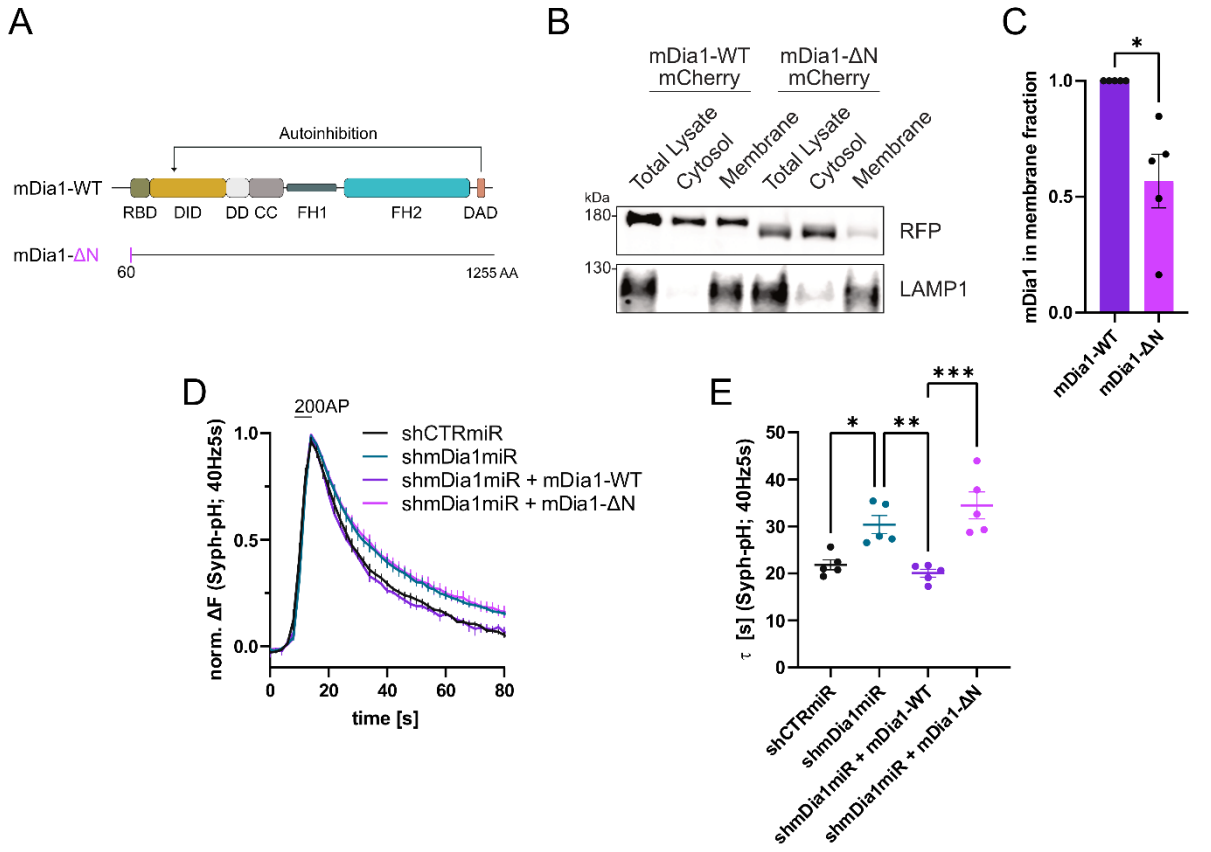

Figure 38: Membrane Association of mDia1 is mediated by its N-terminus to modulate SV Recycling.
A: Schematic representation of functional domains of mDia1. Rho-binding domain (RBD), Diaphanous inhibitory domain (DID), Dimerization domain (DD), Coiled coil domain (CC), Formin homology domain 1 (FH1), Formin homology domain 2 (FH2), Diaphanous autoinhibitory domain (DAD). The unstructured N-terminus (first 60 amino acids) contains three basic stretches and was truncated in the ΔN mutant.
B: Membrane levels of mDia1-WT-mCherry versus mDia1-ΔN-mCherry proteins overexpressed in HEK293T cells. Membrane and cytosolic cellular fractions were isolated by ultracentrifugation and analyzed by immunoblotting with specific antibodies (LAMP1) and in-gel fluorescence of mCherry tags.
C: Densitometric quantification of mDia1-WT versus mDia1-ΔN (0.6 ± 0.1; $p < 0.05$, one sample t-test) membrane-associated protein levels. Data shown are normalized to mDia1-WT (set to 1). N = 5 independent experiments.
D: Averaged normalized Syph-pHluorin fluorescence from stimulated (200 APs, 40 Hz, 5s) hippocampal neurons transfected with shCTRmiR or shmDia1miR. For rescue experiments, neurons were co-transfected with plasmids encoding mDia1-WT-mCherry, mDia1-ΔN-mCherry or mCherry alone (shCTRmiR & shmDia1miR). N = 5; $n_{shCTRmiR}$ = 41 videos, $n_{shmDia1miR}$ = 51 videos, $n_{shmDia1miR + mDia1\text{-}WT}$ = 35 videos, $n_{shmDia1miR + mDia1\text{-}\Delta N}$ = 37 videos.
E: Endocytic decay constants of Syph-pHluorin traces from D: $\tau_{shmDia1miR + mDia1\text{-}WT}$ = 20.0 ± 0.8 s; $\tau_{shmDia1miR + mDia1\text{-}\Delta N}$ = 34.5 ± 2.9 s; $\tau_{shCTRmiR}$ = 21.8 ± 1.1 s, $\tau_{shmDia1miR}$ = 30.4 ± 1.9 s; $p_{shCTRmiR \text{ vs } shmDia1miR} < 0.05$; $p_{shmDia1miR \text{ vs } shmDia1miR + mDia1\text{-}WT} < 0.01$; $p_{shmDia1miR + mDia1\text{-}WT \text{ vs } shmDia1miR + mDia1\text{-}\Delta N} < 0.01$, one-way ANOVA with Tukey's post-test).

As assaying the mDia1-ΔN mutant in pHluorin rescue experiments indicated a role of membrane binding of formins in SV endocytosis, we were prompted to analyze the nanoscale localization of mDia1. In order to resolve small structures like synapses (Nosov et al., 2020), super-resolution microscopy has to be applied. Here, we employed multicolor time-gated stimulated emission depletion (gSTED) microscopy

to investigate the distribution of synaptic mDia1 with respect to marker proteins of the pre- and postsynapse.

Hippocampal neurons were stained for mDia1, the presynaptic active zone marker Bassoon, and Homer 1, a scaffold protein of the postsynaptic density (PSD). Synapses were selected based on their orientation, i.e., synapses exhibiting a clear juxtaposition of Bassoon (presynapse) and Homer1 (postsynapse) punctae in the xy-plane were taken into account. Line profiles perpendicular to the synaptic cleft, representing the space between Bassoon and Homer1 clusters, were generated and analyzed to assess the distributions of the three proteins (Gerth et al., 2019) (Figure 27). This analysis revealed that endogenous mDia1 is primarily localized to the presynaptic compartment (Figure 39A/D), where it is concentrated at or very close to the plasma membrane, i.e., within 50 nm from the presynaptic membrane (Dani et al., 2010).

Hence, our findings underscore that at steady-state, mDia1 is concentrated at the presynaptic plasma membrane in hippocampal neurons.

Given the presence of mDia1 at putative endocytic sites under steady-state conditions (Figure 39), we were prompted to investigate alterations in the localization or distribution of mDia1 when endocytosis is induced or perturbed. To quantify the abundance of presynaptic mDia1, we integrated the individual absolute synaptic line profiles corresponding to the defined presynapse, delineated by the relative Bassoon distribution (Bolz et al., 2023) (Figure 27).

To investigate the dynamics of mDia1 when endocytosis is induced, we fixed and stained cultures after electrical stimulation with 200 AP trains. Interestingly, mDia1 levels at the presynaptic membrane were reduced at stimulated boutons (Data not shown), indicating the removal of mDia1 from sites of endocytosis following high activity. To block endocytosis, we utilized the pan-Dynamin inhibitor Dynasore, known to acutely induce accumulation of endocytic intermediates in electron microscopy studies (Macia et al., 2006), as a result of impaired membrane scission. Notably, Dynasore-treated synapses did not exhibit changes in mDia1 levels or localization under steady-state conditions (Data not shown).

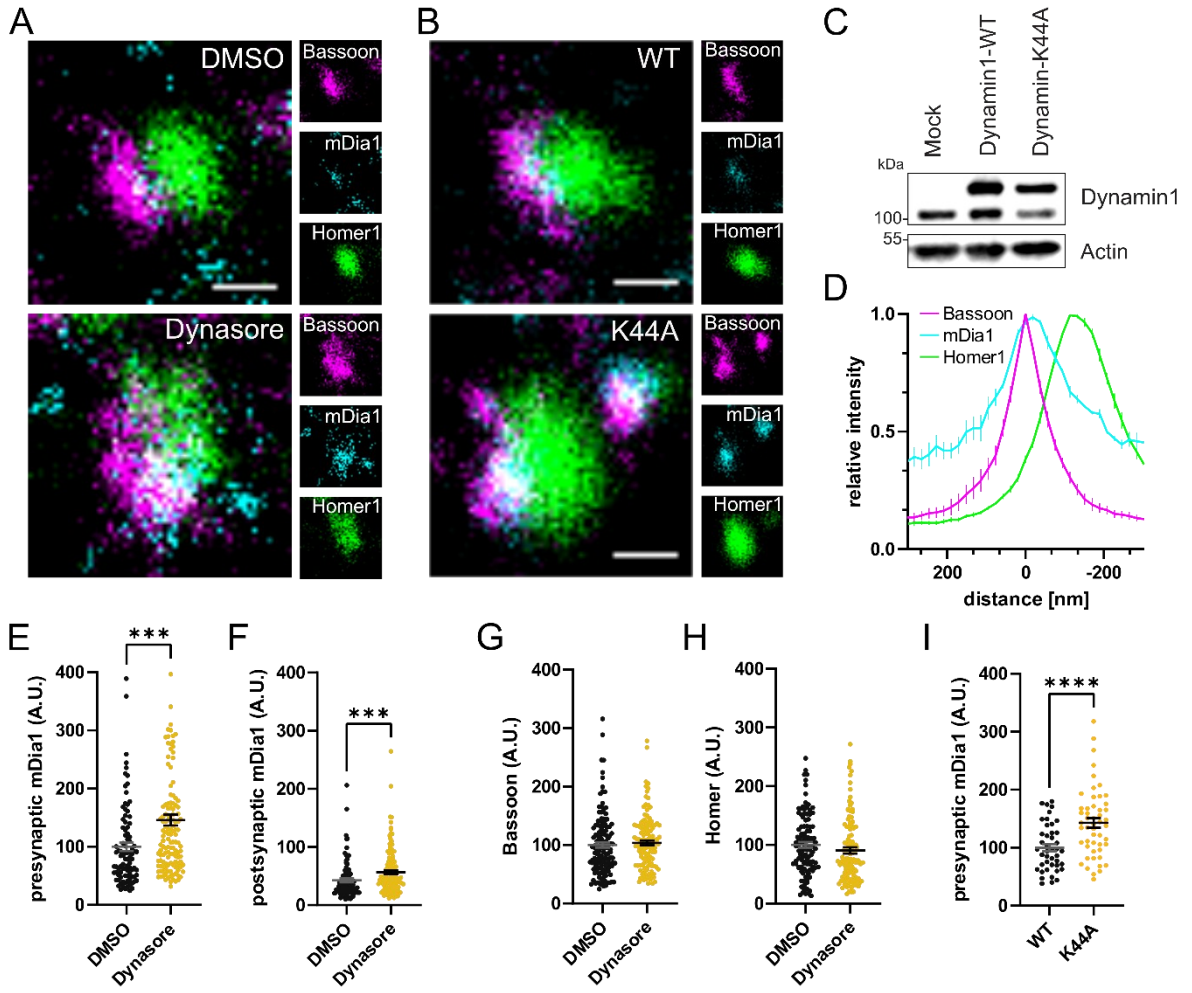

Figure 39: mDia1 is localized to endocytic Spots at the presynaptic Membrane.
A: Representative three-channel time-gated STED images of synapses from hippocampal cultures treated with 0.1% DMSO or 80 µM Dynasore for 10 min before fixation and immunostained for Bassoon (presynaptic marker, magenta), mDia1 (cyan) and Homer1 (postsynaptic marker, green). Scale bar, 250 nm.
B: Representative STED images of synapses from hippocampal cultures transduced with wildtype Dynamin1 (WT) or GTPase-deficient Dynamin1 (K44A) in response to 200 AP (40 Hz, 5s) stimulation. Cells were immunostained for Bassoon (magenta), mDia1 (cyan) and Homer1 (green). Scale bar, 250 nm.
C: Expression levels of Dynamin1 in neurons transduced with Dynamin1 WT or K44A for 12 days. Protein abundance of Dynamin1 and Actin were immunoblotted with specific antibodies.
D: Averaged normalized line profiles for synaptic distribution of mDia1 and Homer1 relative to Bassoon (Maximum set to 0 nm). N = 3; n = 235 synapses.
E/F: Presynaptic (**E**) and postsynaptic (**F**) mDia1 levels in synapses in A; presynaptic DMSO = 100 ± 7.3; presynaptic Dynasore = 145.8 ± 9.3; p = 0.0001; one sample Wilcoxon test; postsynaptic DMSO = 42.6 ± 3.4, postsynaptic Dynasore 56.5 ± 3.3; p < 0.001, Mann-Whitney test. Data shown are normalized to presynaptic DMSO (set to 100). N = 3; n_{DMSO} = 92 synapses, $n_{Dynasore}$ = 135 synapses.
G/H: Quantification of Bassoon (**G**) and Homer1 (**H**) levels in synapses from A: Bassoon DMSO 100.0 ± 4.5; Bassoon Dynasore 103.7 ± 4.1; Homer1 DMSO 100.0 ± 4.3; Homer1 Dynasore 98.6 ± 5.3.
I: Presynaptic mDia1 levels in synapses from B: Dynamin1-WT 100 ± 6.2; Dynamin1-K44A 142.9 ± 8.3, p < 0.0001, one sample Wilcoxon test. Data shown are normalized to Dynamin1-WT (set to 100). N = 2; n_{WT} = 43 synapses, n_{K44A} = 51 synapses.

However, if Dynasore was applied to cells additionally subjected to electrical stimulation with 200 APs, we observed a significant accumulation of mDia1 at presynaptic sites marked by Bassoon (Figure 39E). Similarly, Dynasore treatment

increased mDia1 levels at the postsynapse (Figure 39F); however, the abundance of Bassoon and Homer1 was unaffected (Figure 39G/H).
We further substantiated those findings, by lentivirally overexpressing dominant-negative Dynamin1 K44A, a GTPase inactive mutant, in hippocampal cultures (Figure 39C). Similarly, stimulated neurons expressing the mutant Dynamin1 K44A exhibited a significant increase in presynaptic mDia1 levels (Figure 39B/I) mirroring the effects observed following pharmacological pan-Dynamin inhibition.
Hence, our findings further underline the role of mDia1 in the early stages of SV endocytosis, as mDia1 accumulates on endocytic intermediates that are stalled when Dynamin function is impaired.

Taken together, these results indicate that mDia1 localizes at the presynaptic membrane (Figure 39) and this association is a crucial determinant for its role in mediating SV endocytosis (Figure 38).

4.1.4. mDia1 associates with Proteins of the Endocytic Machinery

We observed an accumulation of mDia1 at presynaptic sites upon disruption of endocytosis by interfering with Dynamin function (Figure 39). Previous studies have shown that genetic ablation of Dynamin isoforms results in the accumulation of endocytic machinery (Ferguson et al., 2009). Consequently, we hypothesized that mDia1 might associate with or directly interact with endocytic proteins to drive SV recycling. Hence, we were prompted to investigate the interactome of synaptic mDia1 to identify potential pathways involved in its role in endocytosis.

We discovered that mDia1 was localized in synaptosomes (P2') isolated by ultracentrifugation (Figure 40C), indicating its synaptic localization, consistent with our STED analysis (Figure 39). We further isolated synaptic mDia1 by immunoprecipitation from lysates using specific antibodies (Figure 40C/D).
We conducted an unbiased quantitative proteomic (MS) analysis of immunoprecipitates from detergent-extracted mouse synaptosomes to dissect the interactome of synaptic mDia1. In our analysis, we identified a total of 625 proteins in synaptic immunoprecipitates of mDia1, of which 318 were enriched (> 1-fold) compared to precipitates of a control (CTR) antibody (Figure 40A). Alongside the bait protein mDia1 and Actin itself, our analysis revealed the presence of various Actin-regulatory proteins, including Myosin IIB (MyoIIB) and the small GTPase Rac1, as confirmed by both MS analysis and immunoblotting (Figure 40B/C).

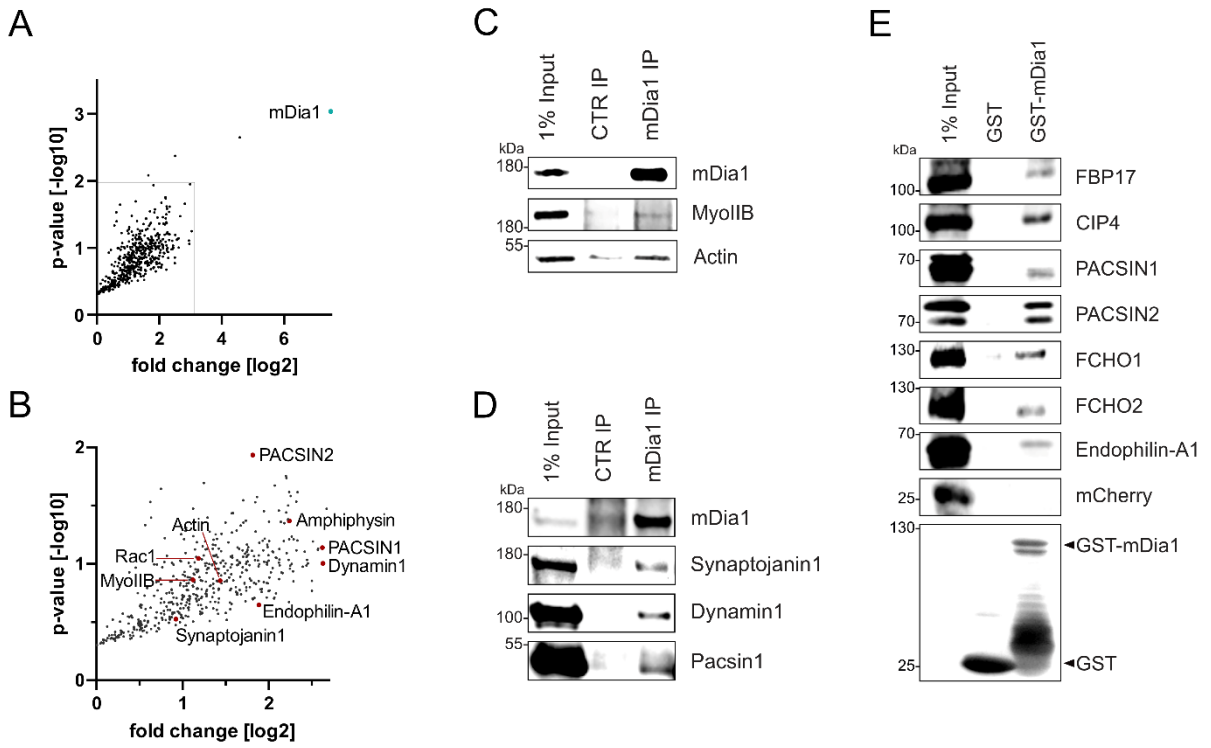

Figure 40: Synaptic mDia1 associates with cytoskeletal and endocytic Proteins.
A: Volcano plot of proteins associating with synaptic mDia1 analyzed by label-free proteomics of anti-mDia1 versus control (CTR) immunoprecipitates from detergent-extracted mouse synaptosomes (P2' fraction). The logarithmic ratios of protein intensities are plotted against negative logarithmic p-values derived from two-tailed student's t-test. The cyan dot shows the specific enrichment of mDia1 as the bait protein of the immunoprecipitation ($p < 0.001$, two-tailed student's t-test). N = 3 independent experiments.
B: Zoom into volcano plot in A highlighting specific proteins association with synaptic mDia1: Selected cytoskeletal hits include β/γ-Actin, Myosin IIB (MyoIIB) and Rac1. Selected endocytic hits include Amphiphysin ($p < 0.05$), Dynamin1, Endophilin-A1, PACSIN1, PACSIN2 ($p < 0.05$) and Synaptojanin1.
C: Endogenous immunoprecipitation of mDia1 from detergent-extracted mouse synaptosomes using mDia1-specific antibodies. Samples were analyzed by immunoblotting using specific antibodies against mDia1, MyoIIB and β-Actin.
D: Endogenous immunoprecipitation of endocytic proteins by mDia1 from detergent-extracted mouse synaptosomes (P2' fraction). Precipitates were analyzed by immunoblotting for mDia1, Synaptojanin1, Dynamin1 and PACSIN1.
E: Pulldown of overexpressed F- and N-BAR proteins from HEK293T cells by truncated mDia1 expressed from E. coli. Samples were analyzed by immunoblotting for GST and the respective protein tags of the BAR proteins.
Mass spectrometry was performed by Heike Stepahnowitz.

Interestingly, several proteins previously implicated in SV endocytosis were also enriched in mDia1 immunoprecipitates. These proteins include the lipid phosphatase Synaptojanin1, the bin-amphiphysin-rvs (BAR) domain proteins Amphiphysin, Endophilin-A1, and PACSIN1/2, and the GTPase Dynamin1 (Andersson et al., 2008; Raimondi et al., 2011; S. Watanabe et al., 2018) as confirmed by immunoblotting (Figure 40D). Proteins of the BAR family have previously been implicated in binding to formins and regulating their activity and localization (Aspenström, 2010; Echarri et al., 2019). It has been proposed that their direct interaction is mediated by the proline-

rich formin homology 1 (FH1) domain of mDia1 and the Src-homology 3 (SH3) domain found in BAR proteins (Wallar & Alberts, 2003).
Consistently, we narrowed down the interaction site of BAR proteins within mDia1 to a C-terminal fragment containing the FH1, FH2, and DAD domains (Figure 40E). This affinity-purified immobilized mDia1 fragment successfully isolated a myriad of different F-BAR proteins when overexpressed in HEK293T cells following pulldown experiments.
Taken together, the synaptic interactome of mDia1, enriched with endocytic and cytoskeletal machinery, underscores its potential role in synaptic vesicle endocytosis, likely through modulation of the Actin cytoskeleton.

Surprisingly, the number of identified proteins in the interactome of mDia1 was low, possibly limited by its reduced presynaptic abundance (Wilhelm et al., 2014). To complement our findings from the immunoprecipitation of mDia1, we additionally investigated the proximal protein environment of mDia1 using proximity labeling (PL) with TurboID. TurboID is an optimized biotin ligase that covalently biotinylates proximal proteins (within a range of 10 nm; (Cho et al., 2020)) in an ATP- and biotin-rich environment. When used as a protein tag, TurboID can enable the preservation of the native state of spatial relationships, as the isolation and analysis of labeled proximal neighbor proteins are straightforward.
To investigate the synaptic protein environment of mDia1, we compared proteins biotinylated by mDia1-TurboID with a non-specific cytosolic TurboID, which promiscuously biotinylates proteins in its reference compartment, the neuronal cytosol. This comparison allows us to identify proteins that are specifically proximal to mDia1 at synaptic sites.
To test the experimental setup, hippocampal neurons were transduced with lentiviral particles expressing cytosolic TurboID control (CTR) or mDia1-TurboID and biotinylation efficiency was analysed. Cells were treated with DMSO or exogenous biotin to increase substrate availability for the ligase tag. Biotinylated proteins were visualized by fluorophore-coupled Streptavidin alongside Synapsin1, serving as a synaptic marker. Synaptic levels of biotinylated proteins were increased when TurboID CTR was expressed and further enhanced by overnight treatment with exogenous biotin (Figure 41A).

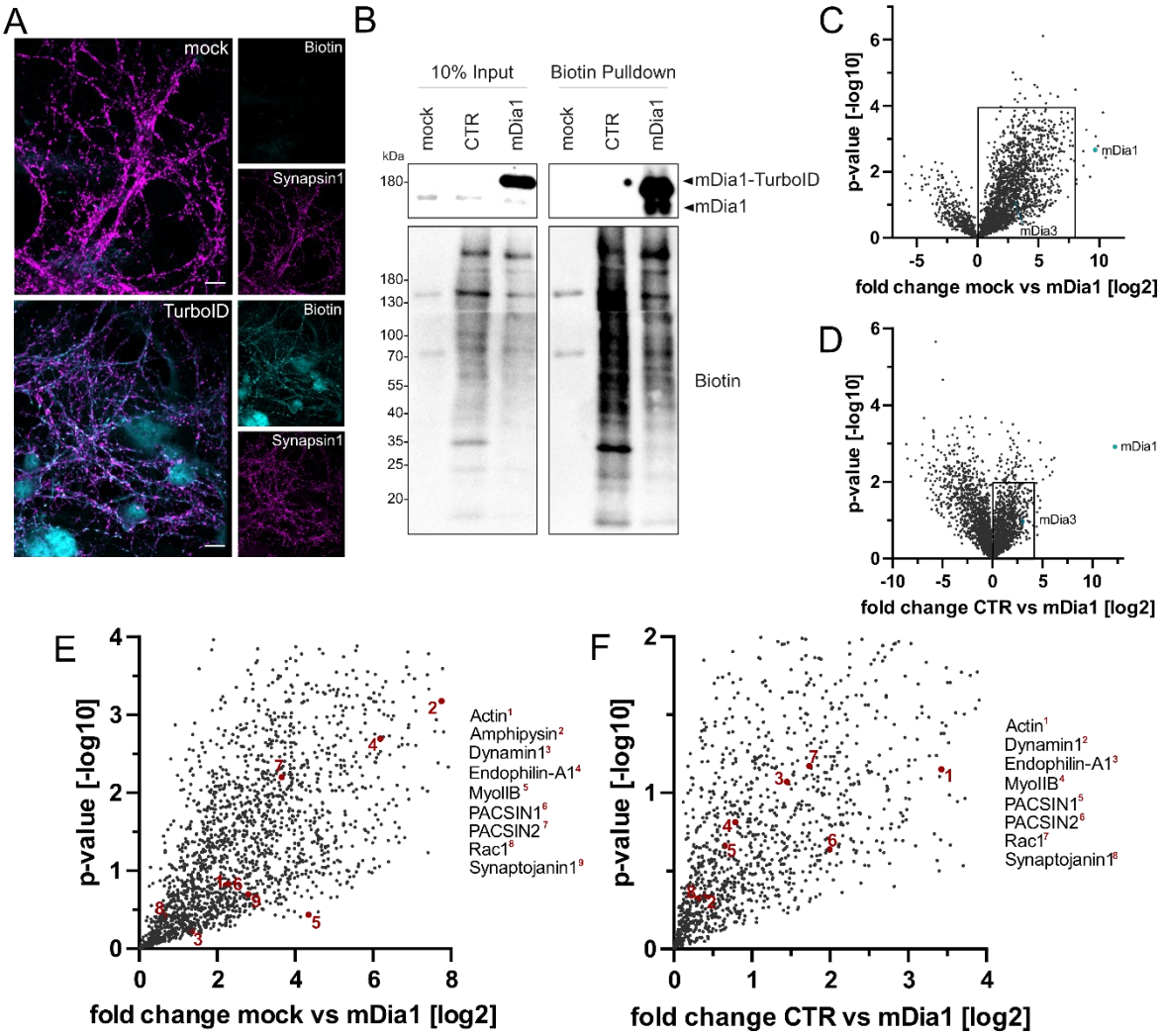

Figure 41: The proximal Protein Environment of neuronal mDia1.
A: Representative images of neurons transduced with the cytosolic biotin ligase TurboID, treated with 100 µM Biotin for 12 h and stained for Synapsin1 (magenta) and biotinylated proteins (cyan). Scale bar, 1 µm.
B: Analysis of biotinylated protein abundance in neurons transduced with cytosolic TurboID (CTR) or mDia1 fused to TurboID (mDia1-TurboID) and treated with 100 µM Biotin for 12 h. Biotinylated proteins were enriched by pulldown via immobilized Streptavidin and visualized by immunoblotting utilizing mDia1-specific antibodies and chemiluminescent Streptavidin.
C/E: Volcano plot of proteins in the proximal environment of neuronal mDia1 analyzed by label-free proteomics of biotinylated proteins in neurons transduced with mDia1-TurboID or mock-treated cells. The logarithmic ratios of protein intensities are plotted against negative logarithmic p-values derived from two-tailed student's t-test. Each dot represents one protein. The cyan dot shows the specific enrichment of mDia1 as the bait protein ($p < 0.01$, two-tailed student's t-test). Zoom-in on endocytic and cytoskeletal hits is presented in **E**. N = 3 independent experiments.
D/F: Volcano plot of proteins in the proximal environment of neuronal mDia1 analyzed by label-free proteomics of biotinylated proteins in neurons transduced with cytosolic CTR or mDia1-TurboID. The cyan dot shows the specific enrichment of mDia1 as the bait protein ($p < 0.01$, two-tailed student's t-test). Zoom-in on endocytic and cytoskeletal hits is presented in **F**. N = 3 independent experiments.
Experiments were performed together with Gresy Bregu and Heike Stepahnowitz.

As proximal biotinylation was successful, we further tested the isolation of biotinylated proteins by pulldown utilizing immobilised Streptavidin. Immunoblotting indicated the enrichment of biotinylated proteins in both the CTR and mDia1 conditions with respect to a non-infected control (mock) (Figure 41B). We further analysed the

respective isolated proteomes in three conditions: mock-treated (to exclude proteins non-specifically bound to immobilized Streptavidin), cytosolic TurboID as the control (CTR) and wild-type mDia1. This analysis identified 2750 proteins in eluates stemming from mDia1 alone, of which 2295 were specifically enriched with respect to the mock (Figure 41C/E), and 1370 proteins were specifically biotinylated by mDia1 compared to the promiscuous cytosolic CTR (Figure 41D/F). Significantly higher amounts of biotinylated proteins were identified in the CTR compared to mDia1, possibly due to the higher expression of the small ligase tag alone or the random localization in comparison to the directed localization of mDia1.
Hence, highly abundant neuronal proteins could be specific mDia1 neighbors but might not show significant enrichment over the CTR, prompting us to analyze both mock and CTR enrichment. TurboID-based proximity labeling coupled with proteomic identification of biotinylated proteins complemented the interactome analysis by direct immunoprecipitation of mDia1 from synaptosomes, as over 50% of proteins identified in the immunoprecipitates were also identified by proximity-labeling. Common hits included cytoskeletal components like Actin, MyoIIB and Rac1, as well as endocytic proteins like N-BAR proteins Amphiphysin, Endophilin, F-BAR proteins PACSIN1/2, Synaptojanin1 and Dynamin1 (Figure 41E/F). Interestingly, mDia3 was also highly biotinylated by mDia1, indicating the action of both isoforms in similar synaptic compartments, underscoring their compensation ability, as observed before (Figure 32).

Taken together, the MS analysis of the synaptic protein environment of mDia1 either by immunoprecipitation (Figure 40) or proximity-ligation (Figure 41) further substantiates the notion that mDia1 mediates endocytosis by modulating the cytoskeleton at endocytic sites, where additional endocytic factors are present.

4.1.5. mDia1/3 Formins control the presynaptic Actin Cytoskeleton

Among the most enriched proteins identified in the synaptic environment of mDia1, were β/γ-Actin isoforms, underlining that mDia1's role in SV endocytosis might be Actin-based. As mDia formins regulate various aspects of Actin dynamics including the nucleation, polymerization, and stabilization of filaments mediated by a conserved F-Actin binding surface within the dimeric FH2 domains, we were prompted to dissect whether these functions are crucial for the function of mDia1 in driving the kinetics of SV endocytosis.

To this end, we generated an Actin-null variant of mDia1 using site-directed mutagenesis of lysine$_{994}$ to alanine (K994A), a modification known to completely abolish Actin nucleation and polymerization functions of mDia1 (Daou et al., 2014), as well as perturbing its ability to protect F-Actin from barbed end capping (Xu et al., 2004).

In our experiments, we observed that the K994A variant failed to restore delayed vGLUT1-pHluorin endocytosis in mDia1-depleted hippocampal neurons in contrast to the wild-type (WT) protein (Figure 42A/B).

Hence, this suggests that the Actin-related functions of the mDia1-FH2 domain, including the nucleation, assembly and stabilization of filamentous Actin, facilitate SV endocytosis.

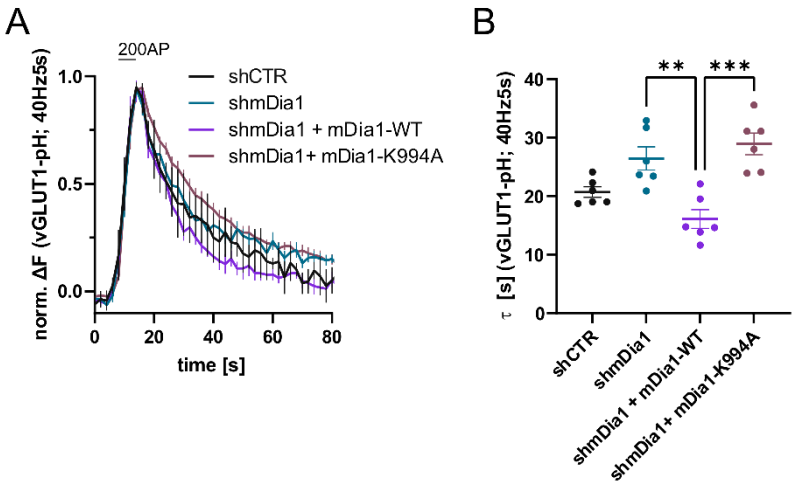

Figure 42: mDia1 modulates SV Endocytosis through its Actin Functions.
A: Averaged normalized vGLUT1-pHluorin fluorescence traces for neurons transduced with shCTR or shmDia1 in response to 200 AP (40 Hz, 5s) stimulation. For rescue purposes, cells were co-transduced with mDia1-WT-SNAP or mDia1-K994A-SNAP. N = 6; n_{shCTR} = 21 videos; $n_{shmDia1}$ = 21 videos; $n_{shmDia1 + mDia1\text{-}WT}$ = 16 videos; $n_{shmDia1 + mDia1\text{-}K994A}$ = 19 videos.
B: Endocytic decay constants of vGLUT1-pHluorin traces from A: τ_{shCTR} = 20.7 ± 0.9 s; $\tau_{shmDia1}$ = 26.4 ± 2.0 s; $\tau_{shmDia1 + mDia1\text{-}WT}$ = 16.1 ± 1.9 s; $\tau_{shmDia1 + mDia1\text{-}K994A}$ = 29.0 ± 1.9 s; $p_{shmDia1 \text{ vs } shmDia1 + mDia1\text{-}WT} < 0.01$; $p_{shmDia1 + mDia1\text{-}WT \text{ vs } shmDia1 + mDia1\text{-}K994A} < 0.001$, one-way ANOVA with Tukey's post-test.

To further study the relationship between mDia1 and the cytoskeleton in neurons, we investigated the synaptic nanoscale localization of F-Actin using phalloidin labeling. Multicolor gSTED imaging confirmed the high enrichment of F-Actin at the postsynapse (Korobova & Svitkina, 2010), with a dendritic density of around 200 nm thickness (Frost et al., 2010). However, Actin filaments were also detected, albeit at reduced levels, at presynaptic boutons marked by Bassoon. To quantify presynaptic F-Actin, we integrated absolute F-Actin line profiles that overlapped with the relative Bassoon distribution, stemming from the analysis of individual synapses. This

approach allowed us to assess the abundance of F-Actin specifically within the presynapse.

Induction of endocytosis in neuronal cultures by stimulation trains of 200 APs, did not alter F-Actin levels at presynaptic terminals (Data not shown). However, blocking endocytosis either through the application of Dynasore or the expression of Dynamin1-K44A resulted in a significant elevation in presynaptic F-Actin within the Bassoon-marked area both under steady-state conditions and at stimulated boutons (Figure 43).

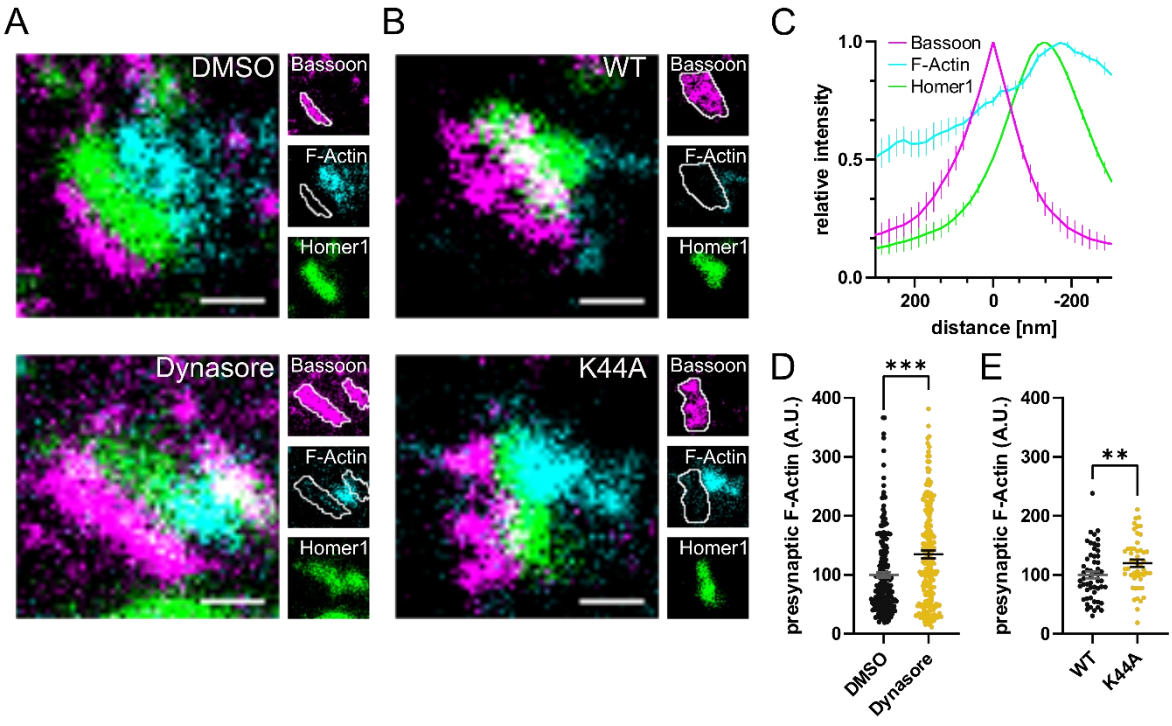

Figure 43: F-Actin accumulates at endocytic Sites upon impaired SV Endocytosis.
A: Representative three-channel time-gated STED images of synapses from hippocampal cultures treated with 0.1% DMSO or 80 µM Dynasore for 10 min. Cells were fixed and stained for Bassoon (magenta), F-Actin (cyan) and Homer1 (green). Scale bar, 250 nm.
B: Representative three-channel time-gated STED images of synapses from hippocampal cultures transduced with Dynamin1-WT or Dynamin1-K44A. Cells were fixed and stained for Bassoon (magenta), F-Actin (cyan) and Homer1 (green). Scale bar, 250 nm.
C: Averaged normalized line profiles for synaptic distribution of F-Actin and Homer1 relative to Bassoon (Maximum set to 0 nm). N = 4; n = 154 synapses.
D: Presynaptic F-Actin levels in synapses treated with 0.1% DMSO (100 ± 4.8) or 80 µM Dynasore (134.7 ± 6.8; p = 0.001, one sample Wilcoxon test) from A. Absolute line profiles of F-Actin overlapping with Bassoon (presynapse) distribution were integrated. Data shown are normalized to DMSO (set to 100). N = 3; n_{DMSO} = 207 synapses, $n_{Dynasore}$ = 211 synapses.
E: Presynaptic F-Actin levels in synapses from neurons transduced with Dynamin1-WT (100 ± 5.9) or Dynamin1-K44A (119.8 ± 6.2, p < 0.01, one sample Wilcoxon test) in B. Absolute line profiles of F-Actin overlapping with Bassoon (presynapse) distribution were integrated. Data shown are normalized to WT (set to 100). N = 1; n_{WT} = 54 synapses, n_{K44A} = 49 synapses.

Hence, these findings suggest a dynamic interplay between endocytic processes and the regulation of F-Actin dynamics at presynaptic sites.

Given that F-Actin was present at endocytic sites (Figure 43) and mDia1's role in SV endocytosis relies on its Actin regulatory activities mediated by the FH2 domain (Figure 42), we were prompted to investigate the impact of formin depletion on the abundance of presynaptic F-Actin in hippocampal neurons.

Utilizing gSTED microscopy, we observed a significant reduction in the detectable amount of F-Actin within the Bassoon area upon depletion of mDia1 (Data not shown) and co-depletion of mDia1/3 further exacerbated this phenotype (Figure 44A).

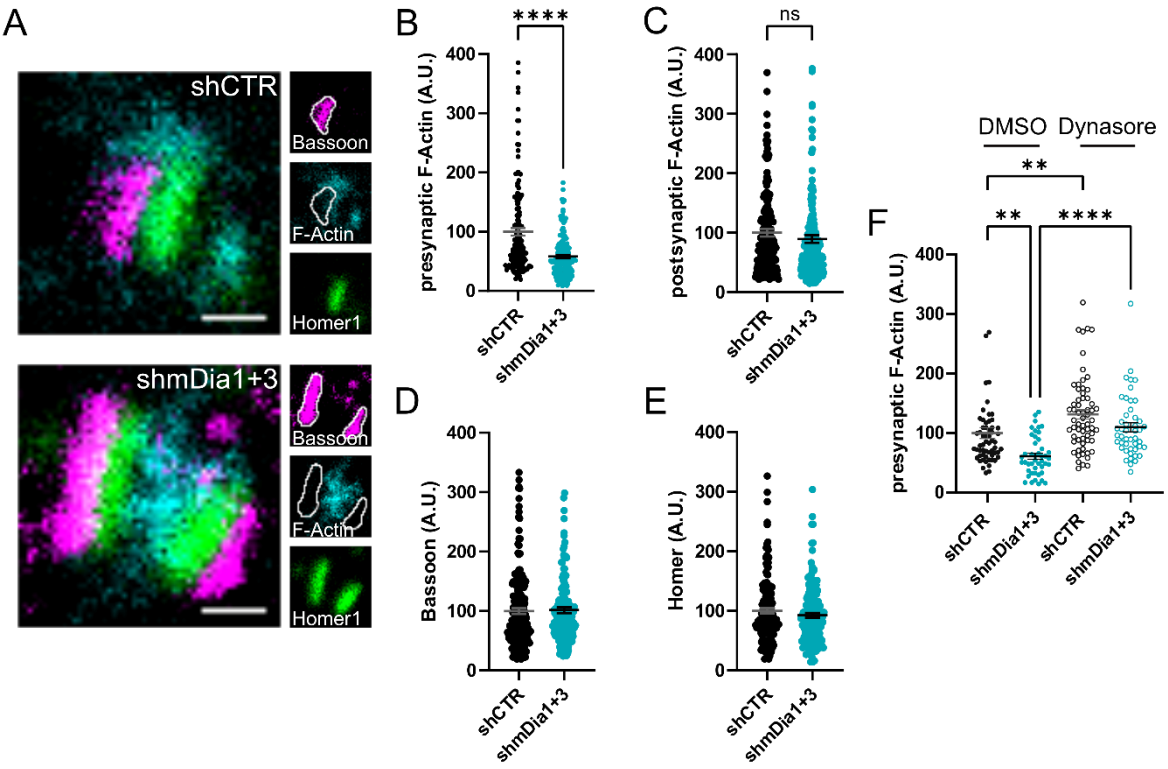

Figure 44: Depletion of mDia1/3 reduces presynaptic F-Actin.
A: Representative three-channel time-gated STED images of synapses from hippocampal cultures transduced with shCTR or shmDia1+3, fixed and immunostained for Bassoon (presynaptic marker, magenta), F-Actin (cyan) and Homer1 (postsynaptic marker, green). Scale bar, 250 nm.
B/C: mDia1 levels at the presynapse (**B**) and postsynapse (**C**) of neurons transduced with shCTR or shmDia1+3.
B: 100 ± 6.4 for shCTR; 58.1 ± 2.9 for shmDia1+3; $p < 0.001$, one sample Wilcoxon test.
C: 100.0 ± 6.4 for shCTR; 89.3 ± 6.4 for shmDia1+3. Data shown are normalized to shCTR (set to 100). N = 4; n_{shCTR} = 155 synapses, $n_{shmDia1+3}$ = 158 synapses.
D/E: Bassoon (**D**) and Homer1 (**E**) levels in synapses transduced with shCTR (100.0 ± 4.7 for Bassoon; 100.0 ± 4.5 for Homer1) or shmDia1+3 (101.4 ± 4.8 for Bassoon; 92.4 ± 4.0 for Homer1). Data shown are normalized to DMSO values (set to 100).
F: Presynaptic F-Actin levels in synapses from hippocampal cultures transduced with shCTR (100 ± 9.0) or shmDia1+3 (61.2 ± 4.9; $p_{shCTR + DMSO \text{ vs } shmDia1+3 + DMSO} < 0.01$) and treated with 0.1% DMSO or 80 µM Dynasore (131.4 ± 7.8 for shCTR + Dynasore; 109.7 ± 7.6 for shmDia1+3 + Dynasore; $p_{shCTR + DMSO \text{ vs } shCTR + Dynasore} < 0.01$, $p_{shmDia1+3 + DMSO \text{ vs } shmDia1+3 + Dynasore} < 0.0001$; Kruskal-Wallis test with Dunn's post-test) for 10 min before fixation. Cells were immunostained for Bassoon (magenta), F-Actin (cyan), and Homer1 (green). Absolute line profiles of F-Actin overlapping with Bassoon (presynapse) distribution were integrated. Data shown are normalized to DMSO (set to 100). N = 1; $n_{shCTR + DMSO}$ = 59 synapses, $n_{shmDia1+3 + DMSO}$ = 45 synapses, $n_{shCTR + Dynasore}$ = 63 synapses, $n_{shmDia1+3 + DMSO}$ = 47 synapses.

Interestingly, postsynaptic F-Actin abundance was not significantly altered by the loss of mDia1/3 (Figure 44C), similar to Bassoon and Homer1 distribution and abundance (Figure 44D/E), indicating mDia1/3 specifically modulate F-Actin levels at the presynapse.

Following our observations that inhibition of Dynamin function caused the accumulation of mDia1 and F-Actin at stimulated boutons (Figure 39 and Figure 43), we sought to determine if stalled mDia1 was causative of the increased F-Actin level upon Dynasore application. Surprisingly, Dynasore treatment still resulted in the accumulation of F-Actin at presynaptic sites co-localizing with Bassoon in the absence of mDia1/3 (Figure 44F).

The accumulation of F-Actin in an mDia-depleted background suggests the presence of additional compensation mechanisms to polymerize F-Actin upon stimulation in neurons lacking mDia1+3.

We reasoned that if the reduction of presynaptic Actin in mDia1/3-depleted neurons was causative for the observed defect in SV endocytosis, pharmacological stabilization of F-Actin might rescue this effect. Treatment of neurons lacking mDia1/3 with jasplakinolide indeed fully restored the kinetics of SV endocytosis monitored by vGLUT1-pHluorin (Figure 45A/B).

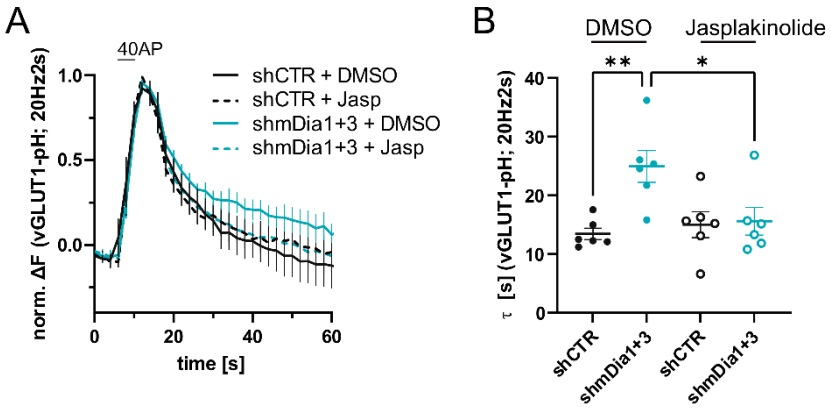

Figure 45: mDia1+3 drive SV Endocytosis by modulating synaptic F-Actin.
A: Averaged normalized vGLUT1-pHluorin fluorescence traces for neurons transduced with shCTR or shmDia1+3 in response to 40 AP (20 Hz, 2s) stimulation. Neurons were pre-incubated with 0.1 % DMSO or 1 µM Jasplakinolide (Jasp) for 30 min in the cell media before imaging. N = 6; $n_{shCTR + DMSO}$ = 32 videos, $n_{shmDia1+3 + DMSO}$ = 35 videos, $n_{shCTR + Jasp}$ = 33 videos; $n_{shmDia1+3 + Jasp}$ = 34 videos.
B: Endocytic decay constants of vGLUT1-pHluorin traces in A: $\tau_{shCTR + DMSO}$ = 13.4 ± 1.0 s, $\tau_{shCTR + Jasp}$ = 15.0 ± 2.2 s, $\tau_{shmDia1+3 + DMSO}$ = 25.0 ± 2.7 s, $\tau_{shmDia1+3 + Jasp}$ = 15.6 ± 2.4 s; $p_{shCTR\ vs\ shmDia1+3} < 0.01$; $p_{shmDia1+3 + DMSO\ vs\ shmDia1+3 + Jasp} < 0.05$, one-way ANOVA with Tukey's post-test). Data are expressed as mean ± SEM.

These results indicate that diminished F-Actin levels impair SV kinetics upon perturbation of mDia function.

Taken together, the formins mDia1/3 drive the kinetics of SV endocytosis by modulating presynaptic F-Actin abundance (Figure 44/Figure 45) mediated by the functions of their FH2 domains (Figure 42).

4.2. Crosstalk between Rho GTPase Signaling and mDia1/3 facilitates SV Endocytosis

4.2.1. Regulation of the Formin mDia1 by RhoA/B

Many formins, including the mDia subfamily are regulated by small Rho GTPases (Kühn & Geyer, 2014). For mDia1 it has been shown that in particular, RhoA, when bound to GTP, associates with the Rho-binding domain (RBD) in mDia1 and releases it from autoinhibition, resulting in the stimulation of its FH2 domain to perform its Actin functions (Otomo et al., 2005). As pharmacological activation of mDia1 by application of IMM facilitated SV membrane retrieval (Figure 33), we reasoned that synaptic RhoA activation could regulate mDia-mediated SV recycling at presynaptic nerve terminals in a similar manner.

Consistently, we found endogenous RhoA concentrated at the presynapse marked by Bassoon in multicolor gSTED imaging (Figure 46A/B). Surprisingly, genetic ablation of RhoA (Data not shown) or overexpression of dominant negative (GDP-locked) forms of RhoA (Oevel et al., 2024) did not hamper SV endocytosis monitored by Syph-pHluorin in hippocampal neurons. However, when RhoA was co-depleted with its closely-related isoform RhoB (Figure 46C/D) or dominant-negative variants of both proteins were co-expressed (Oevel et al., 2024), Syph-pHluorin retrieval in response to 200 AP stimulation was significantly impaired, suggesting a redundancy between RhoA and RhoB isoforms at presynaptic terminals.

These findings indicate the importance of Rho-mediated signalling in regulating the dynamic processes underlying neurotransmission at the synapse.

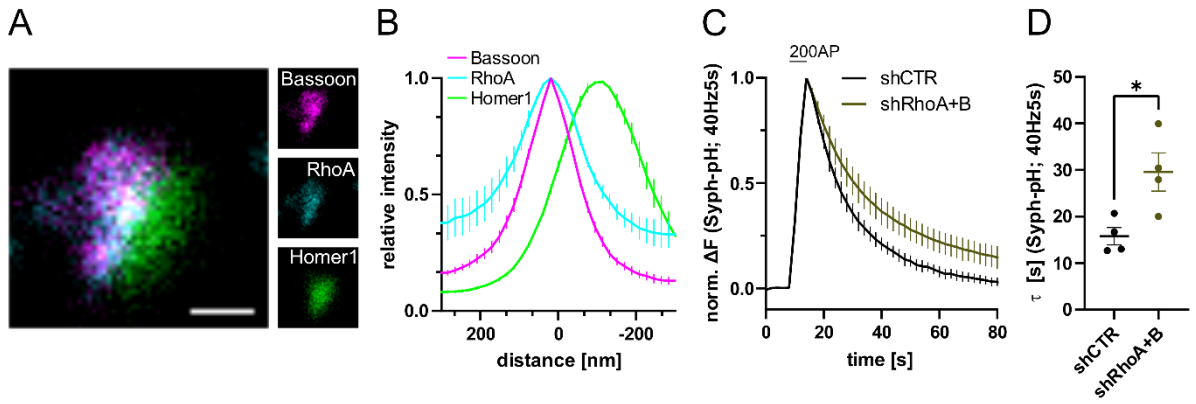

Figure 46: Presynaptic RhoA/B drive SV Endocytosis.
A: Representative three-channel time-gated STED image of a synapses from hippocampal cultures, fixed and immunostained for Bassoon (magenta), RhoA (cyan) and Homer1 (green). Scale bar, 250 nm.
B: Averaged normalized line profiles for synaptic distribution of RhoA and Homer1 relative to Bassoon (Maximum set to 0 nm). N = 5; n = 230 synapses.
C: Averaged normalized Synaptophysin-pHluorin fluorescence traces from stimulated (200 APs; 40 Hz, 5s) hippocampal neurons transfected with shRNA against no mammalian target (shCTR) or against RhoA and RhoB (shRhoA+B). N = 4; n_{shCTR} = 28 videos, n_{RhoA+B}= 27 videos.
D: Endocytic decay constants of Syph-pHluorin traces in C: τ_{shCTR} = 15.8 ± 1.9 s; $\tau_{shRhoA+B}$ = 29.6 ± 4.1; $p < 0.05$, two-tailed student's t-test.
Experiments from A/B were performed together with Gresy Bregu and Hannah Gelhaus. Experiments from C/D were performed together with Tolga Soykan.

Given the overlapping presynaptic distribution of endogenous RhoA and mDia1 (Figure 46A/B and Figure 39A/D), along with phenocopying of formin loss when interfering with Rho activity in pHluorin experiments (Figure 46C/D), we were prompted to test if mDia-related phenotypes were dependent on its activation by RhoA.

To this end, we investigated the molecular interaction between mDia1 and RhoA and its impact on their subcellular localization. mDia1 is autoinhibited by an intramolecular association of its C-terminal DAD with the N-terminal DID (Figure 14). Autoinhibition is relieved upon binding of RhoA-GTP to the RBD of mDia1, a domain that partially overlaps with the DAD binding site on the DID sequence (Otomo et al., 2010). We generated a double point mDia1 mutant, by replacing $valine_{161}$ and $asparagine_{165}$ with aspartate (V161D + N165D; mDia1-VN), within the overlapping region of the RBD and DID, known to be crucial for Rho association (Rose et al., 2005), while preserving DID-DAD auto-inhibitory binding (Lammers et al., 2005). We hypothesized that these modifications would render mDia1 deficient in Rho binding. To test this hypothesis, we co-expressed the mDia1 variants with constitutively active RhoA (RhoA-CA, Q63L, GTP-locked) in HEK293T cells and analyzed their interaction through co-immunoprecipitation. Unexpectedly, we did not observe mDia1-WT in immunoprecipitates of RhoA-CA (Figure 47A), limiting our ability to verify mDia1-VN

as a Rho-binding deficient mutant. Therefore, we generated a constitutively active variant of mDia1 (mDia1-ML) by mutating methionine$_{1182}$ and leucine$_{1185}$to alanine (M1182A + L1185A), critical residues involved in autoinhibition (Lammers et al., 2005; Nezami et al., 2010). Interestingly, this mutant exhibited strong interaction with RhoA-CA (Figure 47A), indicating that its conformation is facilitating Rho binding. We utilized the strong association of mDia1-ML and RhoA, to validate the role of valine$_{161}$ and asparagine$_{165}$ residues in RhoA binding, by introducing aspartate at those positions to generate mDia1-VNML (V161D +N165D and M1182A + L1185A). Overexpressed RhoA-CA failed to co-immunoprecipitate mDia1-VNML from HEK293T cells (Figure 47A) with respect to the efficient isolation of mDia1-ML.

These findings indicate that valine$_{161}$ and asparagine$_{165}$ are crucial residues mediating the interaction between RhoA and mDia1 in cells, rendering mDia1-VN a *bona fide* Rho-binding deficient variant, consistent with the characterized binding interface in crystallography studies (Lammers et al., 2008).

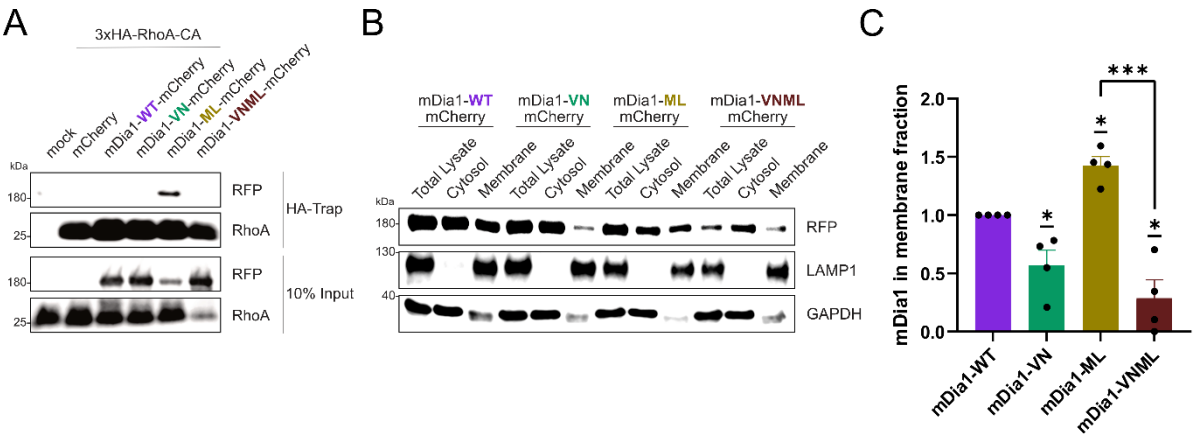

Figure 47: RhoA Association regulates Subcellular Localization of mDia1.
A: Co-immunoprecipitation of exogenously expressed mDia1 variants by constitutively-active RhoA (RhoA-CA). HEK293T cells were co-transfected with mDia1-mCherry constructs and HA-tagged RhoA-CA. Proteins were isolated by utilizing HA-traps and samples were analyzed by immunoblotting using specific antibodies against RFP and RhoA.
B: Membrane levels of mDia1-mCherry variants overexpressed in HEK293T cells together with constitutively-active RhoA. Membrane and cytosolic cellular fractions were isolated by ultracentrifugation and analyzed by immunoblotting with specific antibodies against LAMP1 and GAPDH, and in-gel fluorescence of mCherry tags.
C: Densitometric quantification of mDia1-WT versus mDia1-VN (0.6 ± 0.1; $p < 0.05$), mDia1-ML (1.4 ± 0.1; $p < 0.05$), and mDia1-VNML (0.3 ± 0.2; $p < 0.05$, one sample t-test) membrane-associated protein levels. $p_{mDia1\text{-}ML\ vs\ mDia1\text{-}VNML} < 0.001$, student's t-test. Data shown is normalized to mDia1-WT (set to 1). N = 4 independent experiments.

In non-neuronal cells, the RhoA-mDia1 interaction serves both regulatory functions (mDia1 activation through release of autoinhibition) and mediates the recruitment of mDia1 to specific sites of Actin polymerization (Colucci-Guyon et al., 2005; Higashi et al., 2008). Given the varied degrees to which our mutants associate with RhoA, we

investigated the impact of Rho binding on the subcellular localization of the mDia1 variants through biochemical assays.

To assess the impact of Rho binding on mDia1 localization, we expressed the mDia1 variants in HEK293T cells and isolated membrane and cytosolic fractions via ultracentrifugation. We found that exogenous wildtype mDia1 is primarily localized in the cytosol, as indicated by its co-fractionation with the cytosolic marker glyceraldehyde 3-phosphate dehydrogenase (GAPDH) (Figure 47A B/C). In contrast, enhanced association with RhoA in mDia1-ML leads to its recruitment to the membrane, evident from its enrichment in the membrane fraction alongside the membrane marker lysosome-associated membrane protein-1 (LAMP-1) (Figure 47A B/C). Conversely, impeding RhoA binding by the introduction of aspartate mutations in the binding surface of mDia1, reduces the association of both mDia1-VN and mDia1-VNML variants with membranes.

These results indicate that RhoA-binding of mDia1 plays a crucial role in its recruitment to cellular membranes, controlling its subcellular localization.

To examine the relationship between Rho-dependent recruitment and activation of mDia1 and its role in SV endocytosis, we tested whether strong RhoA-binding (mDia1-ML) versus RhoA-binding deficient mutants (mDia1-VN/VNML) could rescue impaired vGLUT1-pHluorin retrieval in mDia1-depleted synaptic boutons.

Surprisingly, altering the Rho-binding ability of mDia1 did not affect its role in mediating SV endocytosis in our assays, as both strong-binding (mDia1-ML) and binding-deficient mutants (mDia1-VN/VNML) were able to restore impaired SV kinetics in response to stimulation with 200 AP trains (Figure 48A/B). Although the association of synaptic mDia1 with RhoA does not directly impact SV endocytosis (Figure 48A/B), the synaptic environment of mDia1-VN significantly differed from that of the WT protein, as probed by proximity-ligation analysis (Figure 48C). Notably, early endocytic proteins including FCHO2, Intersectin1, Amphiphysin and Endophilin-A1 were significantly reduced in the proximity of mDia1-VN, proteins like Dynamin1/3 and Synaptophysin were enriched. Furthermore, mDia1-VN exhibited less association with actomyosin-regulators mDia3 and MyoIIB but was increasingly surrounded by cytoskeletal factors including Cdc42, IQGAP1, Protein kinase C (PKC) and ROCK2 (Figure 48C).

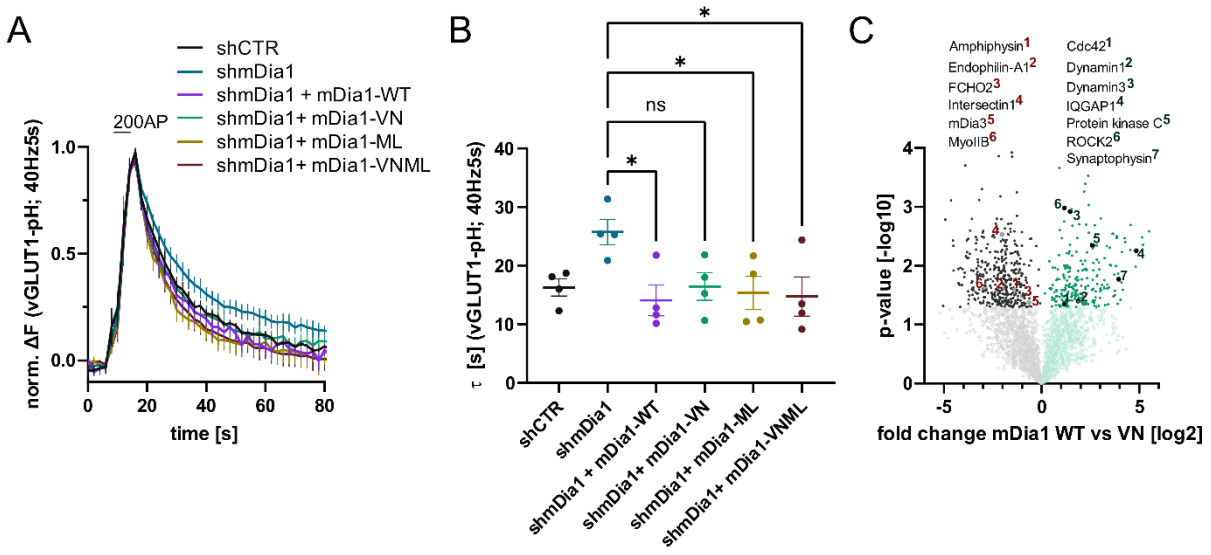

Figure 48: mDa1 mediates SV endocytosis independent of RhoA.
A: Averaged normalized vGLUT1-pHluorin fluorescence traces from hippocampal neurons transduced with lentiviral particles encoding shCTR or shmDia1 in response to 200 AP (40 Hz, 5s) stimulation. For rescue purposes, cells were co-transduced with mDia1-WT-SNAP, mDia1-VN-SNAP, mDia1-ML-SNAP, or mDia1-VNML-SNAP encoding lentivirus. N = 4; n_{shCTR} = 17 videos, $n_{shmDia1}$ = 21 videos, $n_{shmDia1 + mDia1-WT}$ = 12 videos, $n_{shmDia1 + mDia1-VN}$ = 13 videos, $n_{shmDia1 + mDia1-ML}$ = 13 videos, $n_{shmDia1 + mDia1-VNML}$ = 13 videos.
B: Endocytic decay constants of vGLUT1-pHluorin traces in A: τ_{shCTR} = 16.3 ± 1.5 s; $\tau_{shmDia1}$ = 25.7 ± 2.1 s; $\tau_{shmDia1 + mDia1-WT}$ = 14.1 ± 2.6 s; $\tau_{shmDia1 + mDia1-VN}$ = 16.4 ± 2.4 s; $\tau_{shmDia1 + mDia1-ML}$ = 15.4 ± 2.8 s; $\tau_{shmDia1 + mDia1-VNML}$ = 14.7 ± 3.3 s; $p_{shmDia1 vs shmDia1 + mDia1-WT} < 0.05$; $p_{shmDia1 vs shmDia1 + mDia1-ML} < 0.05$, $p_{shmDia1 vs shmDia1 + mDia1-VNML} < 0.05$ one-way ANOVA with Tukey's post-test.
C: Volcano plot of proteins proximal to neuronal mDia1 in dependence of RhoA. Neurons were transduced with lentiviral particles carrying mDia1-WT/VN-TurboID and treated with 100 µM Biotin for 12 h. Biotinylated proteins were enriched through immobilised Streptavidin and analyzed by label-free proteomics. Black and green dots present proteins specifically ($p < 0.05$, two-tailed student's t-test) surrounding wildtype (WT) and Rho-binding deficient (VN) mDia1, respectively. N = 3 independent experiments.
Experiments in A/B/C/F were performed together with Gresy Bregu.

These results indicate that RhoA regulation of synaptic mDia1 plays a subordinate role in its mediation of SV endocytosis, possibly by acting through RhoA-independent signaling that enables endocytic membrane retrieval (e.g. acting through Cdc42, ROCK2, IQGAP1, etc.).

Taken together, synaptic vesicle endocytosis is modulated by redundant RhoA/B signaling (Figure 46) that can act on the subcellular localization of mDia1 (Figure 47). However, at synapses mDia1 can act on SV endocytosis through RhoA-independent signaling cascades potentially involving proteins such as Cdc42, PKC, and ROCK2 (Figure 48).

4.2.2. mDia1/3 Formins regulate Rho GTPase Signaling

4.2.2.1. mDia1/3 regulate RhoA Activity in a positive Feedback Loop

The co-depletion of RhoA and RhoB significantly impairs the endocytic retrieval of Synaptophysin (Figure 46), suggesting that shared effectors of RhoA/B are vital for synaptic vesicle endocytosis. However, the direct association of RhoA with its effector mDia1 appears to play a secondary role in modulating SV endocytosis (Figure 48), possibly through unknown compensatory pathways that likely involve F-Actin dynamics. The cytoskeleton is known to be controlled by interdependent signaling networks characterized by feedback regulation between components within the same pathway and between the key regulatory switches of the small Rho GTPase family (Lawson & Ridley, 2018). Studies have also demonstrated that mDia1 can exert positive feedback on the nucleotide binding status of RhoA by stimulating the activity of the leukemia-associated RhoGEF (LARG) (Kitzing et al., 2007).

To investigate whether synaptic mDia1 similarly regulates RhoA activity, we conducted pulldown assays using immobilized Rhotekin, an effector protein that binds specifically to GTP-bound RhoA.

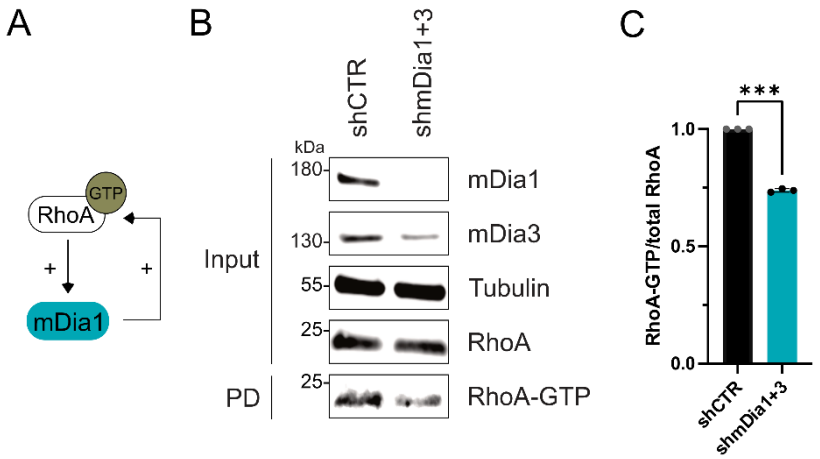

Figure 49: mDia1/3 regulate RhoA Activity.
A: Schematic representation of activation of mDia1 by RhoA-GTP and positive feedback loop of mDia1 on RhoA-GTP levels through GEF stimulation.
B: Analysis of RhoA activity by RhoA-GTP pulldown (PD) from whole-cell lysates (input) of mouse hippocampal neurons expressing shCTR or shmDia1+3 using immobilized Rhotekin as a bait. Samples were analyzed by immunoblotting for mDia1, mDia3, RhoA and Tubulin using specific antibodies. Input, 10% of material used for the pulldown.
C: Densitometric quantification of RhoA-GTP normalized to total RhoA levels (input) in lysates from neurons transduced with shCTR or shmDia1+3 (0.7 ± 0.0, $p < 0.001$, one sample t-test) from immunoblots exemplified in E. Values for shCTR were set to 1. N = 3 independent experiments.

Our results revealed a reduction in RhoA-GTP levels in lysates of mDia1/3-depleted neurons (Figure 49B/C), indicating that neuronal mDia1 activity is implicated in the upstream activation of RhoA in a positive feedback loop.

Hence, the loss of neuronal mDia1/3 results in the downregulation of RhoA activity.

4.2.2.2. RhoA-mDia1/3 Axis modulates Cdc42 and Rac1 Signaling

Cytoskeletal dynamics are regulated by a network of signaling pathways mediated by small Rho GTPases. The canonical members Cdc42, Rac1 and RhoA signal to distinct yet partially overlapping effectors, leading to the formation of various Actin structures, including filopodia, lamellipodia and stress fibers, respectively. Moreover, these signaling pathways are highly interconnected to facilitate coordinated control of cytoskeletal organization, resulting in crosstalk between Rho GTPases to additionally regulate one another (Müller et al., 2020).

In neurons depleted of mDia1/3 formins, RhoA activity is reduced. Multiple studies in non-neuronal cells have demonstrated that RhoA activity antagonizes the activation of other small GTPases like Rac1 (Chauhana et al., 2011; MacHacek et al., 2009; Nimnual et al., 2003; Ohta et al., 2006; Rottner et al., 1999), prompting us to assess the activities of closely related GTPases in conditions of mDia perturbation. Using immobilized PAK as a bait, we observed significantly elevated levels of active and GTP-bound forms of Rac1 and Cdc42 in hippocampal neurons depleted of mDia1+3 (Figure 50B/C).
To further validate if the increased Rac1 and Cdc42 activities are directly linked to diminished GTP-bound RhoA in cells lacking mDia1/3, we treated cells with pan-Rho inhibitor Rhosin, blocking association of Rho proteins with their GEF LARG (Shang et al., 2012). In the presence of Rhosin, a similar enhancement in Rac1-GTP levels was observed, while the activity of Cdc42 was unchanged (Figure 50E).
These results indicate that loss of mDia formins leads to hyperactivation of Rac1 and Cdc42 (Figure 50B/C), and the increased activity of Rac1 stems from decreased Rho-GTP levels (Figure 50E) in mDia1+3-depleted neurons (Figure 49).

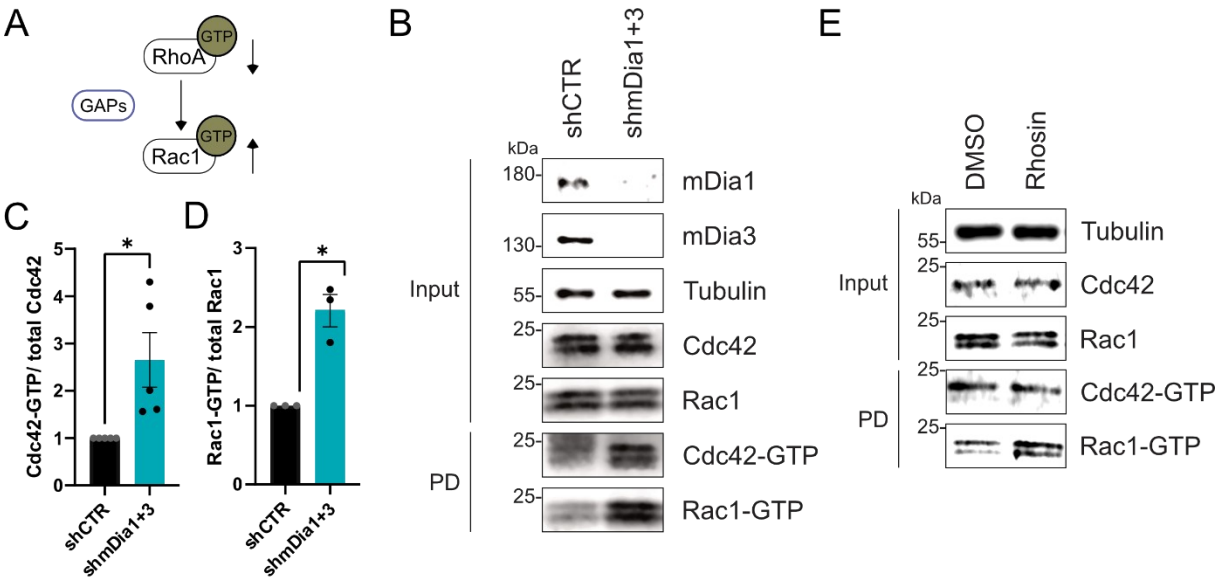

Figure 50: Loss of mDia1/3 activates Cdc42/Rac1 Signaling.
A: Schematic of the interplay between RhoA and Rac1 signaling via GTPase regulatory proteins (e.g. GTPase activating proteins (GAPs) among others).
B: Analysis of Cdc42 and Rac1 activity by Cdc42/Rac1-GTP pulldown (PD) from whole-cell lysates (input) of mouse hippocampal neurons expressing shCTR or shmDia1+3 utilizing immobilized PAK as a bait. Samples were analyzed by immunoblotting for mDia1, mDia3, Cdc42, Rac1 and Tubulin using specific antibodies. Input, 10% of material used for the pulldown. Contrast of pulldown and input blots was seperatly adjusted for visualisation purposes.
C: Densitometric quantification of Cdc42-GTP normalized to total Cdc42 levels (input) in lysates from shmDia1+3 transduced neurons (2.7 ± 0.6; $p < 0.05$, one sample t-test). Values for shCTR were set to 1. N = 5 independent experiments.
D: Densitometric quantification of Rac1-GTP normalized to total Rac1 levels (input) in lysates from neurons transduced with shCTR or shmDia1+3 (2.2 ± 0.2; $p < 0.05$, one sample t-test). Values for shCTR were set to 1. N = 3 independent experiments.
E: Analysis of Cdc42 and Rac1 activity by Cdc42/Rac1-GTP pulldown (PD) from whole-cell lysates (input) of mouse hippocampal cultures upon inhibition of Rho activity utilizing immobilized PAK as bait. Cells were treated with 0.1 % DMSO or 10 µM Rho Inhibitor (Rhosin) for 2 h before harvest. Samples were analyzed by immunoblotting for Rac1 and Tubulin using specific antibodies. Input, 10% of material used for the pulldown. Contrast of pulldown and input blots was seperatly adjusted for visualisation purposes.

4.2.3. Rac1 Signaling drives Synaptic Vesicle Endocytosis via presynaptic Actin

Following our observations of activation of Cdc42 and Rac1 signaling upon genetic depletion of mDia1/3, we hypothesized a potential compensatory role for Rho GTPase signaling in SV endocytosis.

To test this hypothesis we first examined the nanoscale localization of Cdc42 and Rac1 at synapses utilizing multicolor gSTED imaging. Microscopic analysis revealed that Cdc42 was concentrated at presynaptic boutons, while Rac1 was equally distributed between pre- and postsynaptic compartments in unperturbed hippocampal neurons

(Figure 51), consistent with its previously described functions at both pre-(Keine et al., 2022; O'neil et al., 2021) and postsynaptic sites (Duman et al., 2022; Oh et al., 2010).

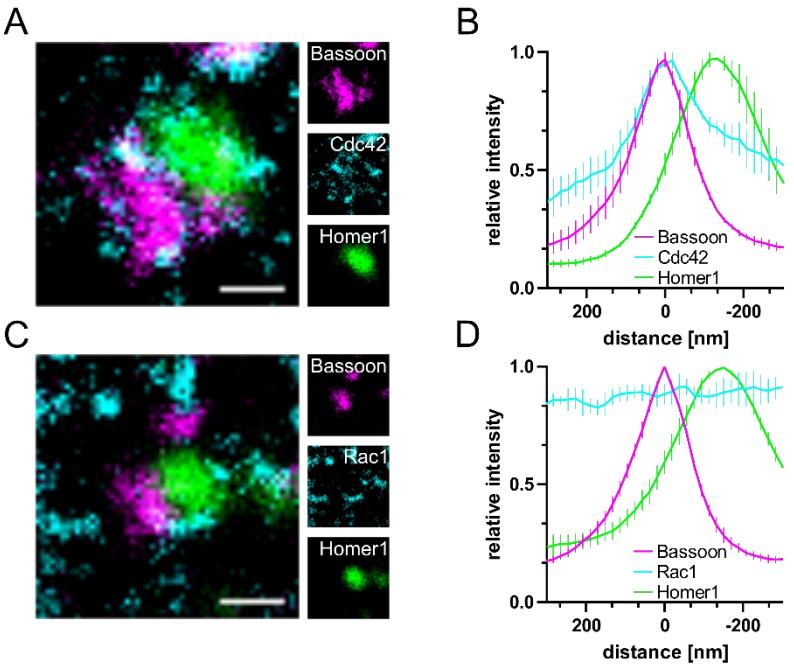

Figure 51: Cdc42 and Rac1 localize at presynaptic Boutons.
A: Representative three-channel time-gated STED image of a synapse from hippocampal mouse cultures, fixed and immunostained for Bassoon (magenta), Cdc42 (cyan) and Homer1 (green). Scale bar, 250 nm.
B: Averaged normalized line profiles for synaptic distribution of Cdc42 and Homer1 relative to Bassoon (Maximum set to 0 nm). N = 3; n = 96 synapses.
C: Representative three-channel time-gated STED image of a synapse from hippocampal cultures, fixed and immunostained for Bassoon (magenta), Rac1 (cyan) and Homer1 (green). Scale bar, 250 nm.
D: Averaged normalized line profiles for synaptic distribution of Rac1 and Homer1 relative to Bassoon (Maximum set to 0 nm). N = 3; n = 79 synapses.

Secondly, we investigated the role of presynaptic Cdc42 and Rac1 activity on SV endocytosis by assaying the action of specific pharmacological inhibitors in CypHer and pHluorin assays. Blocking Cdc42 activity by treating cultures with ML141, an inhibitor of GTP binding of Cdc42 (Surviladze et al., 2010), did not affect the recycling kinetics of neither vGAT nor vGLUT1 endocytosis (Figure 52). Conversely, we found that acute application of EHT 1864, a selective blocker of pan-Rac family activity through nucleotide displacement (Onesto et al., 2008; Raynaud et al., 2014), caused a delay in the endocytic retrieval of both endogenous vGAT and exogenously expressed vGLUT1 (Figure 53) in response to 200 AP or 40 AP stimulation trains, respectively. These results indicate that the activity of Rac1 but not Cdc42 drives synaptic vesicle endocytosis.

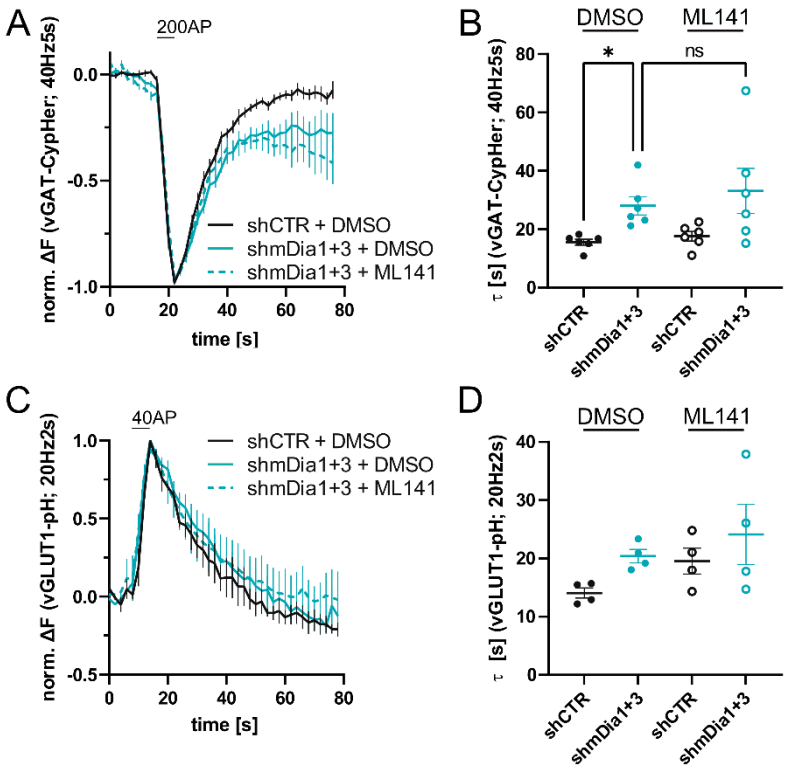

Figure 52: Cdc42 Activity does not affect Synaptic Vesicle Endocytosis.
A: Averaged normalized vGAT-CypHer fluorescence traces for neurons transduced with shCTR or shmDia1+3 in response to 200 AP (40 Hz, 5s) stimulation. Cells were acutely treated with 0.1 % DMSO or 10 µM Cdc42 Inhibitor (ML141) in the imaging buffer. N = 6; $n_{shCTR + DMSO}$ = 31 videos, $n_{shmDia1+3 + DMSO}$ = 33 videos, $n_{shmDia1+3 + ML141}$ = 32 videos.
B: Endocytic decay constants of vGAT-CypHer traces in A: $\tau_{shCTR + DMSO}$ = 15.6 ± 1.0 s, $\tau_{shmDia1+3 + DMSO}$ = 28.0 ± 3.1 s, $\tau_{shCTR + ML141}$ = 17.6 ± 1.6 s, $\tau_{shmDia1+3 + ML141}$ = 33.1 ± 7.7 s; $p_{shCTR + DMSO \text{ vs } shmDia1+3 + DMSO}$ < 0.01, Kruskal-Wallis test with Dunn's post-test.
C: Averaged normalized vGLUT1-pHluorin fluorescence traces for neurons transduced with shCTR or shmDia1+3 in response to 40 AP (20 Hz, 2s) stimulation. Cells were acutely treated with 0.1 % DMSO or 10 µM Cdc42 Inhibitor (ML141) in the imaging buffer. N = 4; $n_{shCTR + DMSO}$ = 22 videos, $n_{shmDia1+3 + DMSO}$ = 25 videos, $n_{shCTR + ML141}$ = 19 videos $n_{shmDia1+3 + ML141}$ = 19 videos.
D: Endocytic decay constants of vGLUT1-pHluorin traces in C: $\tau_{shCTR + DMSO}$ = 14.1 ± 0.9 s, $\tau_{shmDia1+3 + DMSO}$ = 20.4 ± 1.2 s, $\tau_{shCTR + ML141}$ = 19.5 ± 2.2 s, $\tau_{shmDia1+3 + ML141}$ = 24.1 ± 5.2 s.

Given the activation of Cdc42 and Rac1 in cultures depleted of mDia1/3 (Figure 50), we were prompted to test the impact of hyperactive Rac1 and Cdc42 on SV endocytosis phenotypes associated with mDia formin loss. While perturbation of Cdc42 in mDia1/3-depleted neurons had no effect on the kinetics of exogenous vGLUT1 or endogenous vGAT retrieval (Figure 52), inhibition of Rac activity further aggravated impaired vGAT and vGLUT1 endocytosis in neurons lacking mDia1+3 (Figure 53).

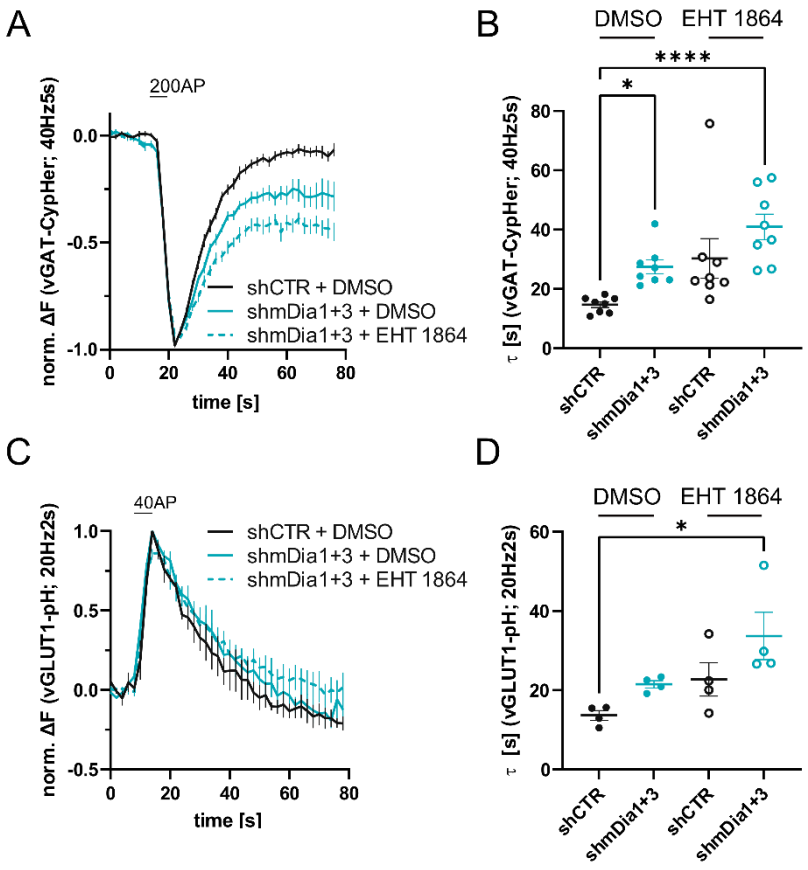

Figure 53: Rac1 Activity modulates Synaptic Vesicle Endocytosis.
A: Averaged normalized vGAT-CypHer fluorescence traces for neurons transduced with shCTR or shmDia1+3 in response to 200 AP (40 Hz, 5 s) stimulation. Cells were acutely treated with 0.1 % DMSO or 10 µM Rac1 Inhibitor (EHT 1864) in the imaging buffer. N = 8; $n_{shCTR + DMSO}$ = 46 videos, $n_{shmDia1+3 + DMSO}$ = 45 videos, $n_{shCTR + EHT\ 1864}$ = 42 videos, $n_{shmDia1+3 + EHT\ 1864}$ = 43 videos.
B: Endocytic decay constants of vGAT-CypHer traces in A: $\tau_{shCTR + DMSO}$ = 14.7 ± 0.9 s, $\tau_{shmDia1+3 + DMSO}$ = 27.5 ± 2.3 s, $\tau_{shCTR + EHT\ 1864}$ = 30.3 ± 6.7 s, $\tau_{shmDia1+3 + EHT\ 1864}$ = 41.0 ± 4.3 s; $p_{shCTR + DMSO\ vs\ shmDia1+3 + DMSO}$ < 0.05, $p_{shCTR + DMSO\ vs\ shmDia1+3 + EHT\ 1864}$ < 0.0001, Kruskal-Wallis test with Dunn's post-test.
C: Averaged normalized vGLUT1-pHluorin fluorescence traces for neurons transduced with shCTR or shmDia1+3 in response to 40 AP (20 Hz, 2 s) stimulation. Cells were acutely treated with 0.1 % DMSO or 10 µM Rac Inhibitor (EHT 1864) in the imaging buffer. N = 4; $n_{shCTR + DMSO}$ = 16 videos, $n_{shmDia1+3 + DMSO}$ = 19 videos, $n_{shCTR + EHT\ 1864}$ = 16 videos, $n_{shmDia1+3 + EHT\ 1864}$ = 15 videos.
D: Endocytic decay constants of vGLUT1-pHluorin traces in C: $\tau_{shCTR + DMSO}$ = 13.7 ± 1.2 s, $\tau_{shmDia1+3 + DMSO}$ = 21.5 ± 0.9 s, $\tau_{shCTR + EHT\ 1864}$ = 22.7 ± 4.2 s, $\tau_{shmDia1+3 + EHT\ 1864}$ = 33.7 ± 6.0 s; $p_{shCTR + DMSO\ vs\ shmDia1+3 + EHT\ 1864}$ < 0.05, one-way ANOVA with Tukey's post-test.

To substantiate those findings, we probed the effects of expressing constitutively active GTP-locked Rac1 (Rac1-CA; Q61L), incapable of GTP hydrolysis, or dominant-negative Rac1 (Rac1-DN; T17N), which sequesters Rac1-GEFs, thereby impairing endogenous Rac1 activation (Wong et al., 2006), on Synaptophysin-pHluorin endocytosis. The constitutive activation of Rac1 had no effect on Synaptophysin retrieval. Conversely, overexpression of dominant-negative Rac1 perturbed the kinetics of SV endocytosis (Figure 54) in line with findings from pharmacological inhibition (Figure 53).

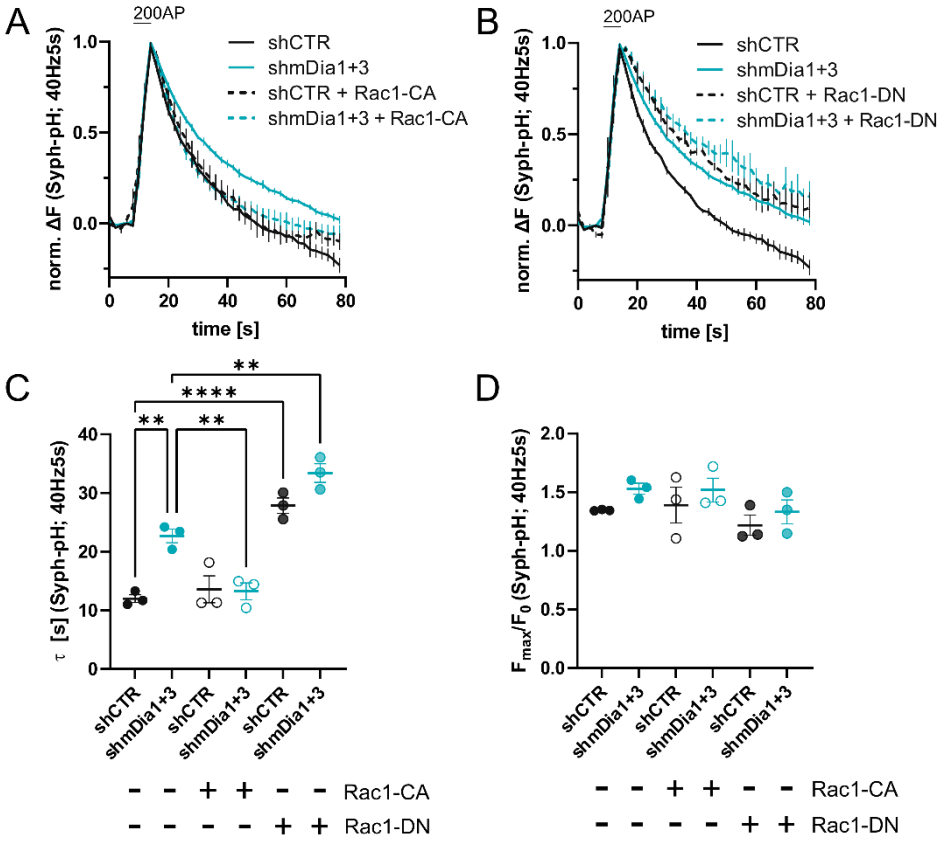

Figure 54: Rac1 Activity compensates for mDia1/3 to drive Synaptic Vesicle Endocytosis.
A/B: Averaged normalized Synaptophysin-pHluorin fluorescence traces from stimulated (200 APs; 40 Hz, 5s) hippocampal neurons transduced with lentiviruses encoding shCTR or shmDia1+3 and transfected with plasmids for expression of constitutively-active Rac1 (Rac1-CA; Q61L variant) or dominant-negative Rac1 (Rac1-DN; T17N variant). N = 3; n_{shCTR} = 12 videos, $n_{shmDia1+3}$ = 23 videos, $n_{shCTR + Rac1\text{-}CA}$ = 10 videos, $n_{shmDia1+3 + Rac1\text{-}CA}$ = 14 videos, $n_{shCTR + Rac1\text{-}DN}$ = 9 videos; $n_{shmDia1+3 + Rac1\text{-}DN}$ = 13 videos.
C: Endocytic decay constants of SypH-pHluorin traces in **A/B**: τ_{shCTR} = 12.0 ± 0.7 s, $\tau_{shmDia1+3}$ = 22.7 ± 2.0 s, $\tau_{shCTR + Rac1\text{-}CA}$ = 13.6 ± 1.2 s, $\tau_{shmDia1+3 + Rac1\text{-}CA}$ = 13.3 ± 1.4 s, $\tau_{shCTR + Rac1\text{-}DN}$ = 27.8 ± 1.3 s, $\tau_{shmDia1+3 + Rac1\text{-}DN}$= 33.4 ± 1.6 s; $p_{shCTR\ vs\ shmDia1+3}$ < 0.01; $p_{shCTR\ vs\ shCTR + Rac1\text{-}DN}$ < 0.0001, $p_{shCTR\ vs\ shmDia1+3 + Rac1\text{-}DN}$ < 0.01, $p_{shmDia1+3\ vs\ shmDia1+3 + Rac1\text{-}DN}$ < 0.01, one-way ANOVA with Tukey's post-test.
D: Maxima of background-corrected SypH-pHluorin fluorescence traces from A/B. $F_{max}/F_{0\ shCTR}$ = 1.3 ± 0.0, $F_{max}/F_{0\ shmDia1+3}$ = 1.5 ± 0.0, $F_{max}/F_{0\ shCTR + Rac1\text{-}CA}$ = 1.4 ± 0.2; $F_{max}/F_{0\ shmDia1+3 + Rac1\text{-}CA}$ = 1.5 ± 0.1, $F_{max}/F_{0\ shCTR + Rac1\text{-}DN}$ = 1.2 ± 0.1, $F_{max}/F_{0\ shmDia1+3 + Rac1\text{-}DN}$ = 1.3 ± 0.1.

Similarly, we monitored the effects of Rac1 nucleotide loading on SV endocytosis kinetics in the absence of mDia1/3. Interestingly, the expression of constitutively-active Rac1 restored normal Syph-pHluorin endocytosis kinetics in mDia1+3-depleted cultures (Figure 54), consistent with a compensatory role for Rac1 signaling when mDia formin activity is abolished. In contrast, Syph-pHluorin retrieval was delayed upon expression of dominant negative Rac1, and the loss of mDia1+3 exacerbated that phenotype (Figure 54). Expression of neither Rac1 isoform affected Syph-pH exocytosis in contrast to previous reports (Keine et al., 2022; O'neil et al., 2021) (Figure 54D).

Hence, Rac1 activity is modulated by the loss of mDia1/3 formins and is a crucial determinant for SV endocytosis kinetics.

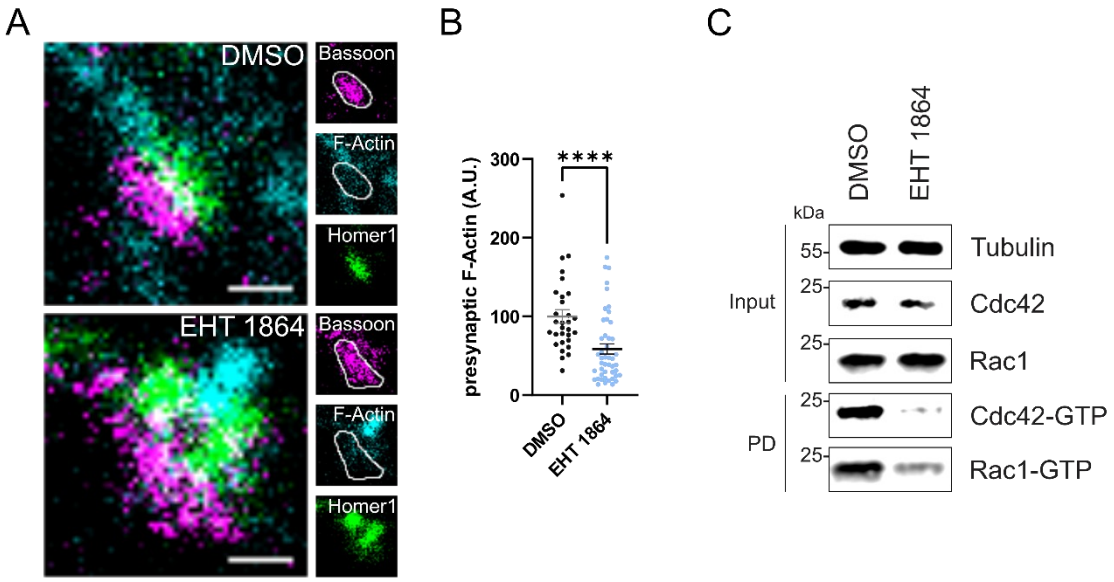

Figure 55: Rac Inhibition reduces presynaptic F-Actin Signaling.
A: Representative three-channel time-gated STED images of synapses from hippocampal cultures treated with 0.1 % DMSO or 10 µM Rac inhibitor (EHT 1864) for 2 h. Cells were fixed and stained for Bassoon (magenta), F-Actin (cyan) and Homer1 (green). Scale bar, 250 nm.
B: Presynaptic F-Actin levels in synapses of neurons treated with 0.1 % DMSO (100 ± 8.5) or 10 µM Rac1 Inhibitor (EHT 1864; 58.6 ± 6.5; $p < 0.0001$, one sample Wilcoxon test) for 2 h before fixation. Line profiles of F-Actin overlapping with Bassoon (presynapse) distribution were integrated. Data shown are normalized to DMSO (set to 100). N= 2; $n_{DMSO} = 30$, $n_{EHT\ 1864} = 46$.
C: Analysis of GTPase activity by Cdc42/Rac1-GTP pulldown (PD) from whole-cell lysates (input) of mouse hippocampal cultures upon inhibition of pan-Rac activity utilizing immobilized PAK as bait. Cells were treated with 0.1 % DMSO or 10 µM Rac inhibitor (EHT 1864) for 2 h before harvest. Samples were analyzed by immunoblotting for Cdc42, Rac1 and Tubulin using specific antibodies. Input, 10% of material used for the pulldown. Contrast of pulldown and input blots was separately adjusted for visualization purposes.

Previous experiments indicated the compensatory activation of Rac1 in response to mDia formin depletion to drive SV endocytosis, potentially via RhoA signaling. Work in non-neuronal cells has shown that the antagonism of RhoA and Rac1 activity promotes crosstalk between the GTPases to modulate compensatory Actin dynamics (Chauhana et al., 2011). We hypothesized that similar reciprocally interdependent Rho/Rac1 signaling mechanisms might govern presynaptic F-Actin assembly, thereby impacting SV endocytosis.

In support of this hypothesis, we observed a reduction in presynaptic F-Actin abundance upon application of EHT 1864 in multicolor gSTED imaging as a result of decreased GTP-bound Rac1 activity (Figure 55A/B). Interestingly, EHT 1864 treatment additionally resulted in diminished activity of Cdc42, suggesting potential crosstalk between regulatory pathways controlling Cdc42 and Rac1 activity (Figure 55C).

These results indicate that Rac1 signaling mediates F-Actin dynamics at presynaptic sites, which potentially compensates for perturbed Actin functions of mDia1/3 in mediating SV endocytosis.

We further probed this model by analyzing the ultrastructure of synapses following Rac1 inhibition alone or in combination with mDia1/3-depletion.

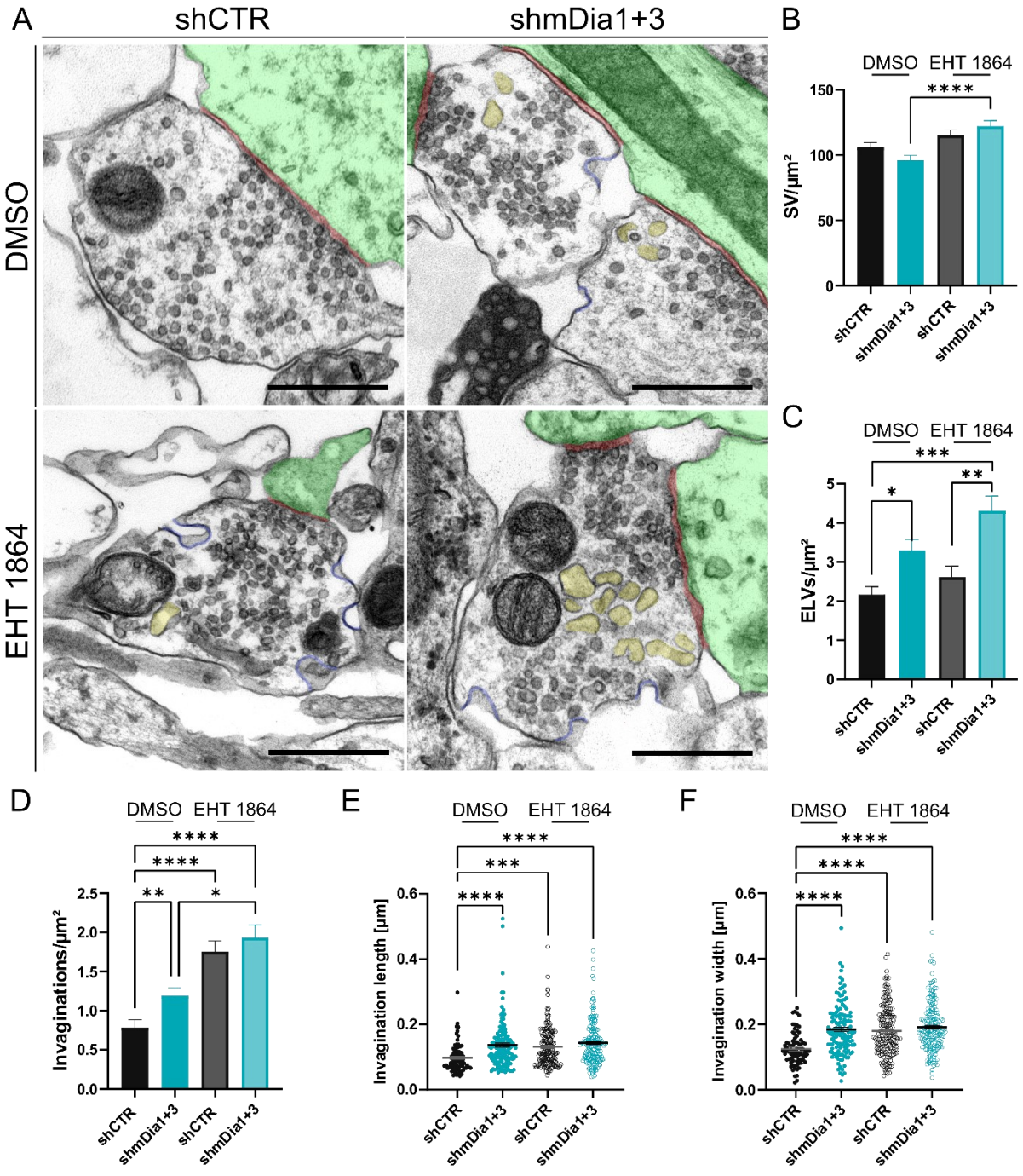

Figure 56: Inhibition of Rac Signaling alters presynaptic Ultrastructure and partially exacerbates mDia1/3 phenotypes.
A: Representative synaptic electron micrographs from hippocampal neurons transduced with lentiviral particles encoding shCTR or shmDia1+3 and treated with 0.1 % DMSO or 10 µM Rac1 Inhibitor (EHT 1864) for 2 h before fixation. Invaginations and ELVs are colored in blue and yellow, while postsynapse and synaptic cleft are colored in green and maroon, respectively. Scale bar, 250 nm.
B-E: Averaged membrane compartments of boutons exemplified in **A**. N = 1; $n_{shCTR + DMSO}$ = 144 synapses, $n_{shmDia1+3 + DMSO}$ = 143 synapses, $n_{shCTR + EHT\ 1864}$ = 136 synapses, $n_{shmDia1+3 + EHT\ 1864}$ = 153 synapses.
B: Averaged SVs/ µm² : shCTR + DMSO (106.0 ± 3.5); shmDia1+3 + DMSO (96.2 ± 3.6); shCTR + EHT 1864 (115.2 ± 4.1); shmDia1+3 + EHT 1864 (122.1 ± 4.2); $p_{shmDia1+3 + DMSO\ vs\ shmDia1+3 + EHT\ 1864} < 0.001$, Kruskal-Wallis test with Dunn's post-test. Legend continued on next page.

C: Averaged ELVs/µm²: shCTR + DMSO (2.2 ± 0.2); shmDia1+3 + DMSO (3.3 ± 0.3); shCTR + EHT 1864 (2.6 ± 0.3); shmDia1+3 + EHT 1864 (4.3 ± 0.4); $p_{shCTR + DMSO \text{ vs } shmDia1+3 + DMSO} < 0.05$; $p_{shCTR + DMSO \text{ vs } shmDia1+3 + EHT\ 1864} < 0.001$, $p_{shCTR + EHT\ 1864 \text{ vs } shmDia1+3 + EHT\ 1864} < 0.01$, Kruskal-Wallis test with Dunn's post-test.
D: Averaged Invaginations/µm²: shCTR + DMSO (0.8 ± 0.1); shmDia1+3 + DMSO (1.2 ± 0.1); shCTR + EHT 1864 (1.8 ± 0.1); shmDia1+3 + EHT 1864 (1.9 ± 0.2); $p_{shCTR + DMSO \text{ vs } shmDia1+3 + DMSO} < 0.01$, $p_{shCTR + DMSO \text{ vs } shCTR + EHT\ 1864} < 0.0001$, $p_{shCTR + DMSO \text{ vs } shmDia1+3 + EHT\ 1864} < 0.0001$, $p_{shmDia1+3 + DMSO \text{ vs } shmDia1+3 + EHT\ 1864} < 0.05$, Kruskal-Wallis test with Dunn's post-test.
E: Average invagination length: shCTR + DMSO (97.6 ± 4.5 nm); shmDia1+3 + DMSO (136.8 ± 6.0 nm); shCTR + EHT 1864 (130.9 ± 4.5 nm); shmDia1+3 + EHT 1864 (143.1 ± 4.9 nm); $p_{shCTR + DMSO \text{ vs } shmDia1+3 + DMSO} < 0.0001$, $p_{shCTR + DMSO \text{ vs } shCTR + EHT\ 1864} < 0.001$, $p_{shCTR + DMSO \text{ vs } shmDia1+3 + EHT\ 1864} < 0.0001$, Kruskal-Wallis test with Dunn's post-test. N = 1; $n_{shCTR + DMSO} = 77$ invaginations, $n_{shmDia1+3 + DMSO} = 141$ invaginations, $n_{shCTR + EHT\ 1864} = 176$ invaginations, $n_{shmDia1+3 + EHT\ 1864} = 189$ invaginations.
F: Average invagination width: shCTR + DMSO (124.5 ± 5.6 nm); shmDia1+3 + DMSO (184.1 ± 6.6 nm); shCTR + EHT 1864 (179.0 ± 5.8 nm); shmDia1+3 + EHT 1864 (191.0 ± 5.4 nm); $p_{shCTR + DMSO \text{ vs } shmDia1+3 + DMSO} < 0.000$, $p_{shCTR + DMSO \text{ vs } shCTR + EHT\ 1864} < 0.0001$, $p_{shCTR + DMSO \text{ vs } shmDia1+3 + EHT\ 1864} < 0.0001$, Kruskal-Wallis test with Dunn's post-test.
Experiments were performed together with Svea Hohensee.

Inhibition of Rac function by EHT 1864 led to the accumulation of non-coated plasma membrane invaginations (Figure 56A/D), while the number of endosome-like vacuoles and synaptic vesicles was not significantly altered (Figure 56A-*C*). Pharmacologically blocking Rac1 activity in neurons depleted of mDia1+3 further increased the number of invaginations and ELVs (Figure 56A C/D), consistent with additive phenotypes observed in CypHer and pHluorin assays (Figure 53/Figure 54). Interestingly, inhibition of Rac1 ameliorated the loss of SVs in mDia1+3-depleted neurons (Figure 56B). We further measured the length and width of membrane invaginations in our conditions to explore potential differences in their architecture between Rac perturbation and mDia formin loss. The architecture of membrane deformations (length and width) was altered in the perturbation of both Rac and mDia formins, indicating that the observed undulations differ from endocytic invaginations that are randomly found in control conditions (Figure 56E/F). Surprisingly, interference with mDia1/3 and/or Rac1 activities exhibited similar phenotypes with respect to the length and width of tubular membrane invaginations, suggesting converging pathways involving overlapping Actin-based mechanisms that modulate presynaptic membrane architecture.

Collectively, these findings demonstrate that the small Rho GTPases RhoA/B and Rac1 facilitate SV endocytosis through interconnected signaling pathways (Figure 46, Figure 50, Figure 54, and Figure 56). These pathways involve positive and negative feedback mechanisms centered around the formin effectors mDia1/3, ultimately converging on the regulation of presynaptic F-Actin dynamics (Figure 44/Figure 55).

4.3. mTORC2 couples Synaptic Vesicle Endocytosis and presynaptic Actin Dynamics

4.3.1. mDia1/3 Formins modulate mTORC2 Activity

Our study highlights the pivotal requirements for Rho proteins RhoA/B and Rac1 as well as mDia1/3 formins, in SV endocytosis. Additionally, we elucidated a reciprocal crosstalk between Rho-mDia and Rac1 signaling pathways, facilitating compensatory remodeling of the cytoskeleton. To further understand the antagonistic relationship between synaptic RhoA and Rac1, we were prompted to dissect the signaling pathways that mediate GTPase multiplexing to inversely correlate their activities. Rho GTPases, such as RhoA and Rac1 are controlled by distinct classes of regulatory proteins including guanine nucleotide exchange factors (RhoGEFs), GTPase-activating proteins (RhoGAPs) and guanine nucleotide dissociation inhibitors (RhoGDIs), that collectively shape Rho GTPase activity gradients (Boulter et al., 2010; Müller et al., 2020). This regulation often involves phosphorylation events mediated by various upstream kinases, including protein kinase A (PKA) (Qiao et al., 2008), protein kinase C (PKC) (Dovas et al., 2010; Sabbatini & Williams, 2013), Src family kinase (DerMardirossian et al., 2006) or cyclin-dependent kinase 1 (CDK1) (Whalley et al., 2015), as well as the opposing functions of phosphatases such as protein phosphatase 2 (PP2A) (Miyamoto et al., 2013).

As phosphorylation cascades are crucial determinants of Rho GTPase activity, we hypothesized that increases in Rac1 activity in mDia1/3-depleted neurons are mediated by changes in phosphorylation patterns of regulatory proteins under the control of synaptic kinases and/or phosphatases.

To test this hypothesis, we isolated phosphorylated peptides from neurons lacking mDia1/3 and subjected them to MS analysis. We identified 1442 unique phosphorylated proteins containing 973 up- and 87 down-regulated phosphorylation sites upon perturbation of mDia1/3 function in comparison to control (CTR) lysates. Indeed, we found altered phosphorylation of several Rho GTPase regulatory proteins including ARHGEF2 (GEF-H1), ARHGEF7 (β-PIX), ARHGEF12 (LARG), Intersectin1, ARHGAP21, ARHGAP34 (Srgap2), ARHGAP35 (p190RhoGAP), ARHGAP39, and RhoGDI1 in mDia1/3-depleted neurons (Table 11), indicative of alterations in the balance of Rho GTPase signaling (see Discussion).

Moreover, in neurons lacking mDia1/3, we observed increased phosphorylation of dephosphins (Cousin & Robinson, 2001), including Epsin1, Epsin2, Epsin15, SNAP91 (AP180), Amphiphysin and Synaptojanin1, as well as Synapsin1-3 (Table 11). Notably, some of the upregulated residues have been previously implicated in impairing endocytosis kinetics (S. Y. Lee et al., 2004; Verstegen et al., 2014). Hence, besides directly facilitating the reformation of SVs by mediating Actin-dependent endocytic retrieval of membranes and proteins, mDia1/3 may additionally function as signaling molecules influencing phosphorylation-dependent signaling cascades of proteins and lipids within the synaptic endocytic machinery.

To investigate signaling pathways affected by the depletion of mDia1/3, we conducted a comprehensive analysis of altered phospho-sites and proteins in the loss-of-function model. The most affected phosphorylation in our screen was the upregulation of phospho-serine$_{696}$ of the microtubule-associated protein tau, under the control of protein kinase B (AKT) (Lei et al., 2023), consistent with previous studies implicating mDia1 activity in tau pathology (Qu et al., 2017). Similarly, we found drastic increases in the phosphorylation of multiple residues in myristoylated alanine-rich C kinase substrate (MARCKS) and growth-associated protein 43 (GAP43), dependent on the activities of protein kinase C (PKC) (Heemskerk et al., 1993). Accordingly, we find increasingly phosphorylated isoforms of protein kinase C (PKCα, PKCγ, PKCε), indicating their activation (Facchinetti et al., 2008).
The phosphorylated residues we identified are regulated by intricate signaling cascades involving the mechanistic target of rapamycin complex 2 (mTORC2) (Figure 57A). Consistently, a study blocking mTORC2 function through genetic ablation of its subunit *Rictor* demonstrated the downregulation of phosphorylation of multiple PKC isoforms, and their substrates p-MARCKS and p-GAP43 in brain lysates of Rictor-KO mice (Thomanetz et al., 2013). Furthermore, we identified the mTOR kinase, Rictor, PKCα, GAP43, MARCKS, and Tau in the proximal protein environment of mDia1 at synapses following MS analysis (Figure 57B).

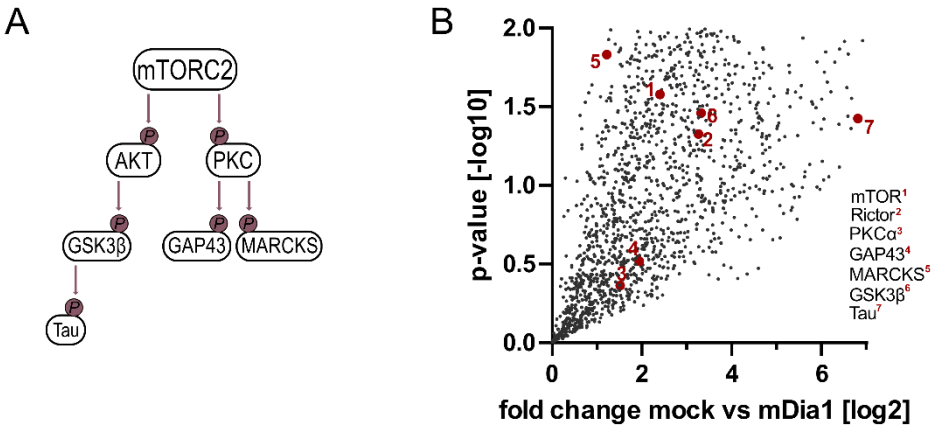

Figure 57: mDia1/3 affect mTORC2 Signaling.
A: Upregulated phospho-sites in mDia1/3-depleted neurons drive protein activities downstream of mTORC2. mTORC2 mediates phosphorylation of protein kinase B (AKT) and C (PKC) at serine$_{473}$ and threonine$_{638}$ (PKCα) (Baffi et al., 2021)**.** AKT regulates serine$_{9}$ phosphorylation of glycogen synthase kinase 3 beta (GSK3β) (Kitagishi et al., 2012). GSK3β mediates tau phosphorylation at serine$_{696}$ (Lei et al., 2023). Active PKC phophorylates GAP43 at serine$_{41}$ (Nguyen et al., 2009) and MARCKS at serine$_{25}$ and serine$_{163}$ (Heemskerk et al., 1993; Toledo et al., 2013).
B: Volcano plot of mTORC2 signalling associated proteins in the proximal environment of neuronal mDia1 analyzed by label-free proteomics of biotinylated proteins in neurons transduced with mDia1-TurboID or mock-treated cells. The logarithmic ratios of protein intensities are plotted against negative logarithmic p-values derived from two-tailed student's t-test. Each dot represents one protein. N = 3 independent experiments.
Mass spectrometry was performed by Heike Stepahnowitz.

These results indicate that formins mDia1/3 likely exert a direct influence on mTORC2 signaling pathways.

Following those findings, we investigated the role of mDia1/3 in regulating the activity of mTORC2. mTORC2 activity can be read out by phosphorylation of its downstream target protein kinase B (AKT) at serine$_{473}$ (Bayascas & Alessi, 2005), which can be experimentally assessed by utilizing specific antibodies.
Indeed, we found elevated levels of phosphorylated serine$_{473}$ AKT1 (p-AKT1) in lysates of neurons depleted of mDia1/3 (Figure 58A/B). Conversely, the activation of mDia formins by application of IMM significantly reduced the phosphorylation of AKT1 (Figure 58C/D).
Hence, mDia formins bidirectionally modulate mTORC2 activity in an antagonistic manner.

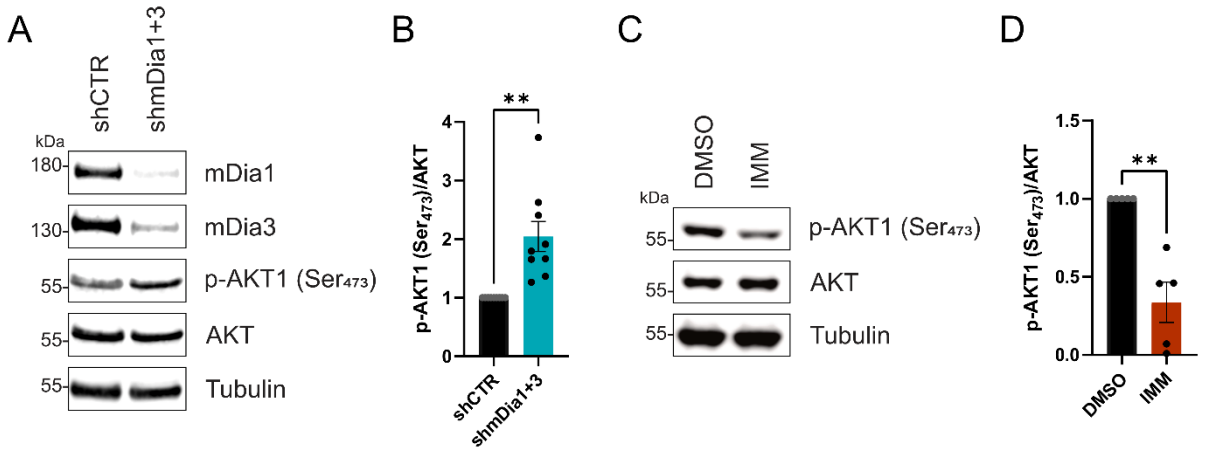

Figure 58: mDia1/3 bidirectionally drive mTORC2 Activity.
A: Analysis of mTORC2 activity in whole-cell lysates of mouse hippocampal cultures treated with lentivirus encoding shCTR or shmDia1+3. Samples were analyzed by immunoblotting against mDia1, mDia3, phosphorylated AKT1 (p-AKT1 Ser_{473}), pan-AKT and Tubulin utilising specific antibodies.
B: Phosphorylated AKT1 levels in whole-cell lysates of shmDia1+3 (2.0 ± 0.3, $p < 0.01$, one sample Wilcoxon test) compared to shCTR treated neurons exemplified in A. The ratio of phosphorylated (Ser_{473}) AKT1 to pan-AKT was calculated. Data shown is normalized to shCTR. N = 9 independent experiments.
C: Analysis of mTORC2 activity in whole-cell lysates of mouse hippocampal cultures treated with 0.1 % DMSO or 10 µM mDia activator (IMM) for 2 h. Samples were analyzed by immunoblotting against phosphorylated AKT1 (p-AKT Ser_{473}), pan-AKT and Tubulin utilising specific antibodies.
D: Phosphorylated AKT1 levels in whole-cell lysates of IMM (0.3 ± 0.1; $p < 0.01$, one-sample t-test) compared to DMSO treated neurons exemplified in C. The ratio of phosphorylated (Ser_{473}) AKT1 to pan-AKT was calculated. Data shown is normalized to DMSO. N = 5 independent experiments.

Apart from mTORC2, the mTOR kinase is also an indispensable subunit of mTOR complex 1 (mTORC1) which regulates protein synthesis in response to nutrient and amino acid availability. Interestingly, mTORC1 activity, measured by its downstream phosphorylation of $threonine_{389}$ of p70 S6 Kinase, was not affected by perturbation of mDia1/3 formins, as determined by MS analysis and immunoblotting (Data not shown).

Recent studies have highlighted the involvement of mTORC2 in both pre- and postsynaptic signaling, contributing to synaptic plasticity (Huang et al., 2013) and neurotransmission (McCabe et al., 2020; Smillie & Cousin, 2012). In addition, AKT signaling has been implicated in memory formation, synaptic plasticity and dendritic morphogenesis (Bruel-Jungerman et al., 2009; Horwood et al., 2006; Sánchez-Alegría et al., 2018; Sui et al., 2008; Waite & Eickholt, 2010). Thus, we investigated if the global increase of p-AKT1, measured in lysates of neurons depleted of mDia1/3, was attributed to the postulated pre- or postsynaptic signaling arms of mTORC2 activity.
Multicolor gSTED imaging revealed that AKT1 phosphorylation predominantly occurs at presynaptic sites marked by Bassoon (Figure 59A/C). Accordingly, presynaptic levels of p-AKT1 could be reduced by the application of AZD 3147 (Figure 59A/D), an

inhibitor of the mTOR kinase (Pike et al., 2015), indicating that phosphorylation of serine$_{347}$ of AKT1 is a *bona fide* target of synaptic mTORC2. In line with the biochemical analysis in lysates, we found elevated levels of p-AKT1 at synapses depleted of mDia1+3 (Figure 59B/E).

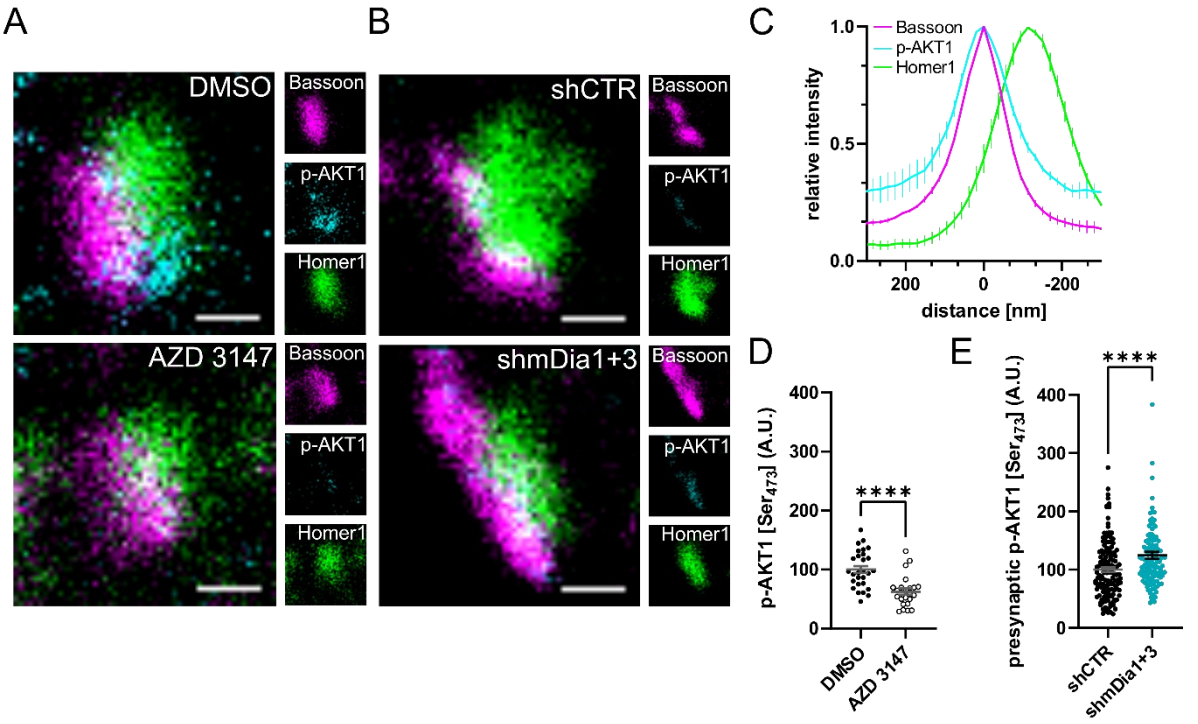

Figure 59: mDia1/3 and mTORC2 modulate presynaptic AKT1 Phosphorylation.
A: Representative three-channel time-gated STED images of synapses from hippocampal cultures treated with 0.1% DMSO or 10 nM mTORC2 inhibitor (AZD 3147) for 2 h. Cells were immunostained for Bassoon (magenta), phosphorylated AKT1 (p-AKT1; pSer$_{473}$) (cyan) and Homer1 (green). Scale bar, 250 nm.
B: Representative three-channel time-gated STED images of synapses from hippocampal cultures treated with shCTR or shmDia1+3 encoding lentivirus. Cells were immunostained for Bassoon (magenta), p-AKT1 (cyan) and Homer1 (green). Scale bar, 250 nm.
C: Averaged normalized line profiles for synaptic distribution of p-AKT1 and Homer1 relative to Bassoon (Maximum set to 0 nm). N = 3; n = 141 synapses.
D: Neuronal p-AKT1 levels in synapses from hippocampal cultures treated with 0.1% DMSO (100.0 ± 6.0) or 10 nM AZD 3147 (62.6 ± 5.6; $p < 0.0001$, one sample Wilcoxon test) for 2 h. Line profiles of p-AKT1 were integrated. Data shown are normalized to DMSO (set to 100). N = 1; n_{DMSO} = 28 synapses, $n_{AZD\ 3147}$ = 23 synapses.
E: Presynaptic p-AKT1 levels in synapses from hippocampal cultures treated with shCTR (100.0 ± 4.2) or shmDia1+3 (124.5 ± 5.9; $p < 0.0001$, one simple Wilcoxon test). Absolute line profiles of p-AKT1 overlapping with Bassoon (presynapse) distribution were integrated. Data shown are normalized to shCTR (set to 100). N = 3; n_{shCTR} = 141 synapses, $n_{shmDia1+3}$ = 131 synapses.
Experiments were performed together with Hannah Gelhaus.

Hence, mDia loss leads to increased phosphorylation of AKT1 (Figure 58) downstream of mTORC2 at presynaptic sites (Figure 59).

Taken together, these results indicate that mDia1/3 formins negatively regulate the activity of mTORC2 and its downstream signaling arms at presynapses.

4.3.2. Synaptic mTORC2 is a negative Regulator of SV Endocytosis

Both in yeast and mammalian cells, mTORC2 activity has been implicated in the control of endocytosis (Riggi et al., 2019; Smillie & Cousin, 2012). As we observed activation of mTORC2 at presynaptic sites in mDia1/3-depleted cells (Figure 58, and Figure 59), we were prompted to investigate its potential contribution to the endocytosis-related phenotypes attributed to formin perturbation (Figure 32).

To dissect the role of mTORC2 in SV endocytosis, we employed a combination of pharmacological inhibitors targeting the mTOR kinase in general or selectively mTORC1. The application of the molecule Rapamycin specifically targets mTORC1 through binding to its FKBP12/rapamycin complex binding domain (FRB), which is masked in mTORC2 (Scaiola et al., 2020). Conversely, AZD 3147 targets both mTOR complexes but exhibits higher specifity towards mTORC2 with an *in vitro* IC_{50} in the single-digit nanomolar range (Pike et al., 2015).
In line with our STED analysis, AZD 3147 application significantly decreased the phosphorylated abundance of AKT1 in lysates from both control and mDia1+3-depleted hippocampal cultures (Figure 60A/E). Interestingly, application of Rapamycin increased p-AKT1 levels in lysates of hippocampal cultures (Figure 60A/B), consistent with prior findings of activated AKT signaling as a consequence of blocking a negative feedback loop downstream of mTORC1 (Hsu et al., 2011; McCabe et al., 2020; O'Reilly et al., 2006; S. Y. Sun et al., 2005). Treatment of neurons depleted of mDia1+3 exacerbated the hyperphosphorylation of AKT1 (Figure 60B) compared to control cells.
Hence, the combination of inhibitors of the mTOR kinase (both mTORC complexes, AZD 3147) and specific-mTORC1 blockers (Rapamycin), enables the investigation of perturbation versus activation of mTORC2, providing an orthogonal approach to stimulate mTORC2 activity independent of mDia1/3 manipulation.
To assess the role of mTORC2 in SV recycling, we monitored the retrieval of vGLUT1-pHluorin when cells were treated with Rapamycin or AZD 3147 in response to stimulation with 40 APs. Blocking mTORC1 activity by Rapamycin delayed vGLUT1-pHluorin endocytosis and exacerbated phenotypes associated with the loss of mDia1+3 formins (Figure 60C/D). Conversely, the application of AZD 3147 ameliorated the endocytic phenotypes seen in the loss of mDia formins (Figure 60F/G).

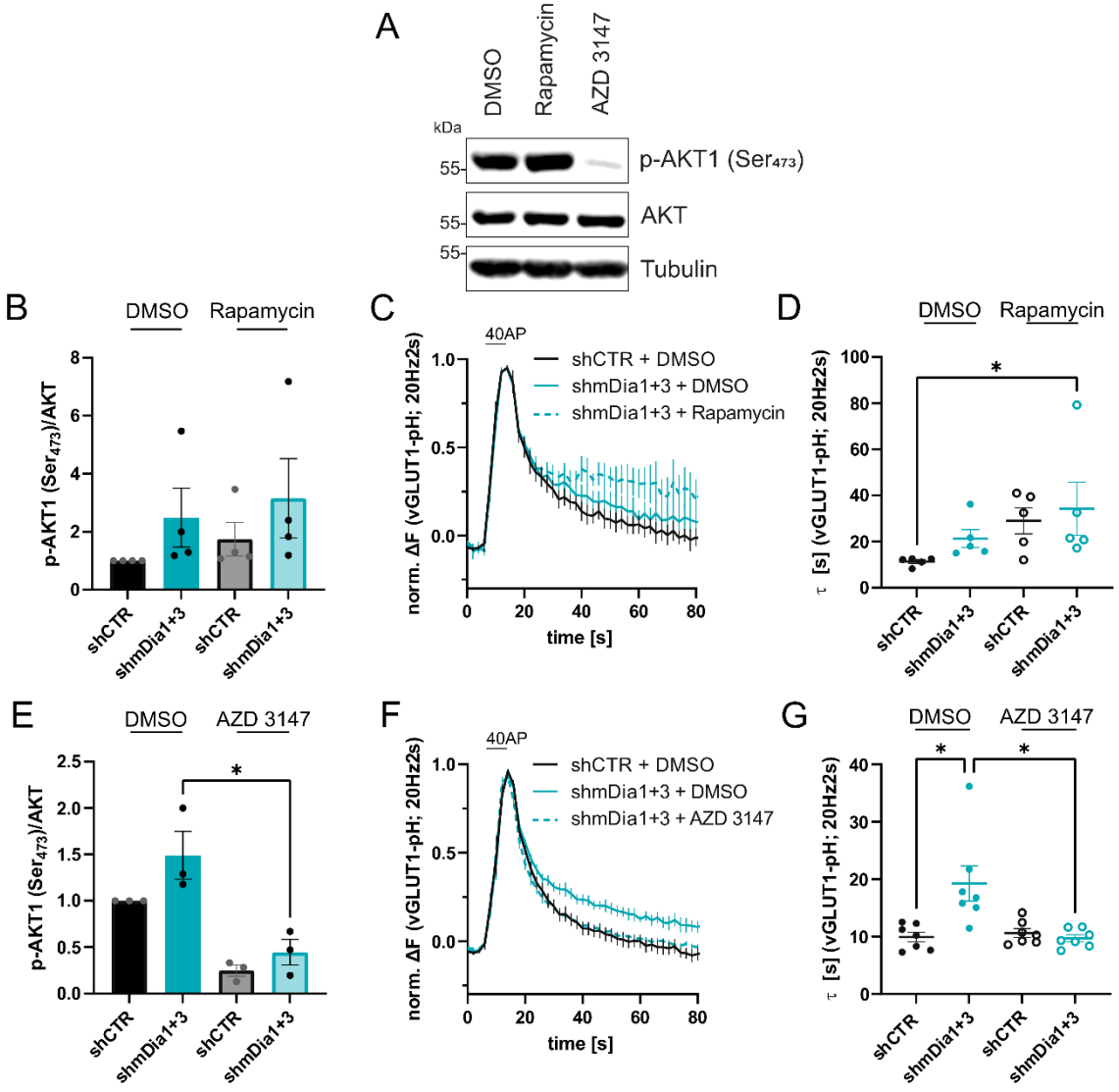

Figure 60: mTORC1 and mTORC2 differentially mediate SV Endocytosis.
A: Analysis of mTORC2 activity in whole-cell lysates of mouse hippocampal cultures treated with 0.1% DMSO, 200 nM mTORC1 inhibitor (Rapamycin), or 10 nM mTORC2 inhibitor (AZD 3147) for 2 h. Samples were analyzed by immunoblotting for phosphorylated AKT1 (p-AKT Ser_{473}), pan-AKT and Tubulin.
B: Phosphorylated AKT1 levels in lysates of neurons transduced with shCTR/shmDia1+3 and treated with 0.1% DMSO (2.5 ± 1.0 for shmDia1+3) or 200 nM Rapamycin (1.7 ± 0.6 for shCTR, 3.2 ± 1.4 for shmDia1+3) for 2 h. The ratio of p AKT1 to pan-AKT was calculated. Data is normalized to shCTR + DMSO. N = 4.
C: Averaged normalized vGLUT1-pHluorin fluorescence traces from hippocampal neurons transduced with shCTR or shmDia1+3 and treated with 0.1 % DMSO or 200 nM mTORC1 inhibitor (Rapamycin) for 2 h in response to 40 AP (20 Hz, 2 s) stimulation. N = 5; $n_{shCTR + DMSO}$ = 22 videos, $n_{shmDia1+3 + DMSO}$ = 25 videos, $n_{shCTR + Rapamycin}$ = 19 videos, $n_{shmDia1+3 + Rapamycin}$ = 22 videos.
D: Endocytic decay constants of traces in **C**: $\tau_{shCTR + DMSO}$ = 11.4 ± 0.8 s, $\tau_{shmDia1+3 + DMSO}$ = 21.4 ± 3.9 s, $\tau_{shCTR + Rapamycin}$ = 29.0 ± 5.6 s, $\tau_{shmDia1+3 + Rapamycin}$= 34.3 ± 11.5 s; $p_{shCTR+ DMSO vs shmDia1+3 + Rapamycin}$ < 0.05, Kruskal-Wallis test with Dunn's post-test).
E: Phosphorylated AKT1 levels in lysates of neurons transduced with shCTR/shmDia1+3 and treated with 0.1% DMSO (1.5 ± 0.3 for shmDia1+3) or 10 nM AZD 3147 (0.2 ± 0.1 for shCTR, $p < 0.01$, one-sample t-test; 0.4 ± 0.1 for shmDia1+3, $p_{shmDia1+3 DMSO vs shmDia1+3 AZD3147}$ < 0.05, student's t-test) for 2 h. Data is normalized to shCTR + DMSO. N = 3.
F: Averaged normalized vGLUT1-pHluorin fluorescence traces from hippocampal neurons transduced with shCTR or shmDia1+3 and treated with 0.1 % DMSO or 10 nM mTORC2 inhibitor (AZD 3147) for 2 h in response to 40 AP (20 Hz, 2 s) stimulation. N = 7; $n_{shCTR + DMSO}$ = 30 videos, $n_{shmDia1+3 + DMSO}$ = 37 videos, $n_{shCTR + AZD 3147}$ = 35 videos, $n_{shmDia1+3 + AZD 3147}$ = 41 videos.

G: Endocytic decay constants of vGLUT1-pHluorin traces in F: $\tau_{shCTR + DMSO}$ = 9.9 ± 0.8 s, $\tau_{shmDia1+3 + DMSO}$ = 19.3 ± 3.1 s, $\tau_{shCTR + AZD\ 3147}$ = 10.6 ± 0.8 s, $\tau_{shmDia1+3 + AZD\ 3147}$ = 9.7 ± 0.6 s; $p_{shCTR + DMSO\ vs\ shmDia1+3 + DMSO}$ < 0.05, $p_{shmDia1+3 + DMSO\ vs\ shmDia1+3 + AZD\ 3147}$ < 0.05, Kruskal-Wallis test with Dunn's post-test.

These results are consistent with a model in which mTORC2 activation impairs the kinetics of SV endocytosis.

To further substantiate these findings, we additionally perturbed mTORC1 and mTORC2 activity by genetic depletion of their specific subunits Raptor and Rictor, respectively, and examined corresponding effects on SV endocytosis. In contrast to previous studies (McCabe et al., 2020), we found both Raptor and Rictor subunits localized at the presynapse in close proximity to Bassoon following analysis by multicolor gSTED imaging (Figure 61). The observed localization supports the notion that both complexes may directly modulate the endocytic machinery, contributing to the observed phenotypes (Figure 60). Interestingly, Rictor was also detected at the postsynaptic membrane (Figure 61D), consistent with previous studies (Thomanetz et al., 2013).

The inhibition of mTORC1 activity via knockdown of its Raptor subunit led to an increase in the phosphorylation of AKT1 at $serine_{347}$ (Figure 62B), consistent with the effects observed following pharmacological perturbation by Rapamycin treatment (Figure 60A-D). Conversely, genetic depletion of Rictor resulted in the perturbation of mTORC2 activity, as AKT1 phosphorylation was reduced (Figure 62A/E), albeit to a lesser extent compared to the pharmacological inhibition following AZD 3147 application (Figure 60E-G). In addition, when mDia1/3 formins were co-depleted with Rictor, mTORC2 hyperactivation upon formin perturbation was rescued (Figure 62A/E), restoring AKT1 phosphorylation back to control levels.

Hence, Rictor and Raptor depletion serve as orthogonal tools to block or stimulate mTORC2 activity, respectively.

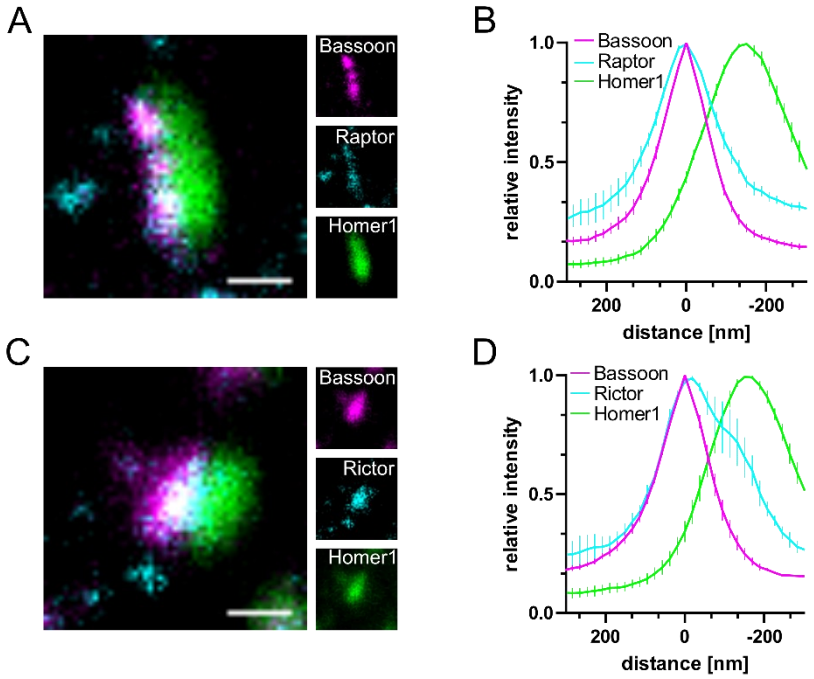

Figure 61: Raptor and Rictor are localized at presynaptic Sites.
A: Representative three-channel time-gated STED image of a synapse from hippocampal cultures fixed and immunostained for Bassoon (magenta), Rictor (cyan) and Homer1 (green). Scale bar, 250 nm.
B: Averaged normalized line profiles for synaptic distribution of Rictor and Homer1 relative to Bassoon (Maximum set to 0 nm). N = 3; n = 98 synapses.
C: Representative three-channel time-gated STED image of a synapse from hippocampal cultures fixed and immunostained for Bassoon (magenta), Raptor (cyan) and Homer1 (green). Scale bar, 250 nm.
D: Averaged normalized line profiles for synaptic distribution of Raptor and Homer1 relative to Bassoon (Maximum set to 0 nm). N = 3; n = 144 synapses.
Experiments were performed together with Hannah Gelhaus.

We further conducted single or co-depletion of Rictor/Raptor together with mDia1/3 to study the effects of mTORC2 activity on vGLUT1-pHluorin retrieval. Genetic ablation of mTORC1 activity through Raptor loss delayed SV endocytosis kinetics (Figure 62C/D), resembling effects observed with Rapamycin treatment. In contrast, loss of Rictor alone did not induce an endocytic phenotype (Figure 62F/G). Interestingly, co-depletion of Rictor and mDia1/3 mitigated the impaired kinetics of vGLUT1-pHluorin endocytosis associated with mDia1/3 perturbation, consistent with the observations following AZD 3147 treatment (Figure 60).

Taken together, our findings suggest an inverse correlation between mTORC2 activity and the kinetics of SV endocytosis. Stimulated mTORC2 activation (Figure 58, Figure 60, and Figure 62) blocks SV endocytosis, while its inhibition (Figure 60/Figure 62) is able to rescue endocytic phenotypes deriving from mDia1/3-depletion.

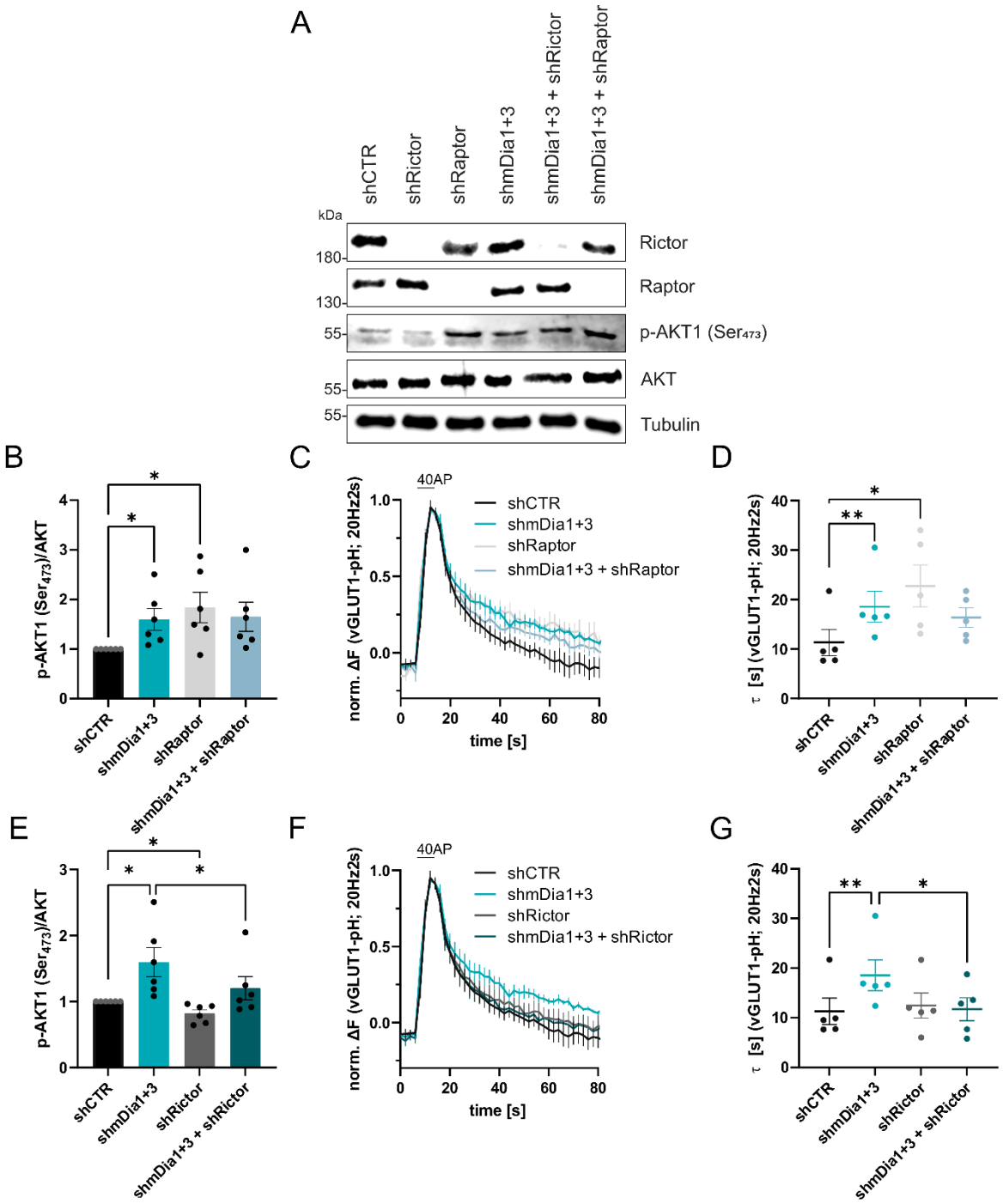

Figure 62: Genetic Ablation of mTORC1 and mTORC2 Activity differentially affects the Kinetics of SV Endocytosis.
A: Analysis of mTORC2 activity in whole-cell lysates of mouse hippocampal cultures transduced with lentivirus encoding shCTR, shRictor, shRaptor, or shmDia1+3 alone or in combination. Samples were analyzed by immunoblotting for Rictor, Raptor, phosphorylated AKT1 (p-AKT Ser_{473}), pan-AKT and Tubulin with specialized antibodies.
B: Phosphorylated AKT1 levels in whole-cell lysates of neurons transduced with shmDia1+3 (1.6 ± 0.2; $p < 0.05$) or shRaptor (1.8 ± 0.3; $p < 0.05$, one sample t-test) alone or in combination (1.7 ± 0.3) in comparison to shCTR. The ratio of phosphorylated (Ser_{473}) AKT1 to pan-AKT was calculated. N = 6.
C: Averaged normalized vGLUT1-pHluorin fluorescence traces from hippocampal neurons transduced with lentivirus encoding shCTR, shmDia1+3 and shRaptor alone or in combination in response to 40 AP (20 Hz, 2 s) stimulation. N = 5; n_{shCTR} = 24 videos, $n_{shmDia1+3}$ = 25 videos, $n_{shRaptor}$ = 21 videos, $n_{shmDia1+3 + shRaptor}$ = 23 videos. Legend continued on next page.

D: Endocytic decay constants of vGLUT1-pHluorin traces in **C**: τ_{shCTR} = 11.3 ± 2.6 s, $\tau_{shmDia1+3}$ = 18.6 ± 3.1 s; $p_{shCTR\ vs\ shmDia1+3} < 0.01$, $\tau_{shRaptor}$ = 22.8 ± 4.2 s,$\tau_{shmDia1+3\ +\ shRaptor}$ = 16.4 ± 2.0 s; $p_{shRaptor} < 0.05$, one-way ANOVA with Tukey's post-test.
E: Phosphorylated AKT1 levels in whole-cell lysates of neurons transduced with shmDia1+3 (1.6 ± 0.2; $p < 0.05$) or shRictor (0.8 ± 0.1, $p < 0.05$, one sample t-test) alone or in combination (1.2 ± 0.2; $p_{shmDia1+3\ vs\ shmDia1+3\ +\ Rictor} < 0.05$, two-tailed student's t-test). The ratio of phosphorylated (Ser_{473}) AKT1 to pan-AKT was calculated. Data shown is normalized to shCTR. N = 6.
F: Averaged normalized vGLUT1-pHluorin fluorescence traces from hippocampal neurons transduced with lentivirus encoding shCTR, shmDia1+3 and shRictor alone or in combination in response to 40 AP (20 Hz, 2 s) stimulation. N = 5; n_{shCTR} = 24 videos, $n_{shmDia1+3}$ = 25 videos, $n_{shRictor}$ = 23 videos, $n_{shmDia1+3\ +\ shRictor}$ = 22 videos.
G: Endocytic decay constants of vGLUT1-pHluorin traces in **C**: τ_{shCTR} = 11.3 ± 2.6 s, $\tau_{shmDia1+3}$ = 18.6 ± 3.1 s, $\tau_{shRictor}$ = 12.5 ± 2.5 s, $\tau_{shmDia1+3\ +\ shRictor}$ = 11.7 ± 2.3 s; $p_{shCTR\ vs\ shmDia1+3} < 0.01$, $p_{shmDia1+3\ vs\ shmDia1+3\ +\ shRictor} < 0.05$, one-way ANOVA with Tukey's post-test.

4.3.3. Interdependent mTORC2 and synaptic cytoskeletal Signaling.

4.3.3.1. Perturbation of Formin-mediated Actin Function regulates mTORC2

Previous studies identified the importance of formin activity in SV endocytosis by perturbing recycling kinetics through application of the promiscous FH2-domain inhibitor SMIFH2 (Soykan et al., 2017). Furthermore, neuronal cultures treated with SMIFH2 exhibited altered presynaptic F-Actin structures (Bingham et al., 2023). We hypothesized that if mTORC2 activation in mDia1/3-depleted neurons derives from the blockage of its Actin function, treatment of cells with SMIFH2 would induce similar phenotypes.

Indeed, we observed a significant increase in phosphorylated AKT1 levels in hippocampal lysates following SMIFH2-mediated perturbation of formin function, which could be mitigated by co-incubation with AZD 3147 (Figure 63A/B).

Next, we investigated the effects of these treatments on the retrieval of vGLUT1-pHluorin in response to stimulation with 40 APs. As previously published (Soykan et al., 2017), acute formin inhibition following SMIFH2 treatment impairs SV endocytosis (Figure 63C/D). Interestingly, co-application of AZD 3147 alleviated SMIFH2-induced phenotypes on endocytosis kinetics (Figure 63C/D), indicating that hyperactivation of mTORC2 due to formin activity perturbation blocks SV endocytosis.

Hence, interference with formin-based Actin functions through genetic or pharmacological perturbation causes mTORC2 activation, resulting in the impairment of synaptic vesicle recycling.

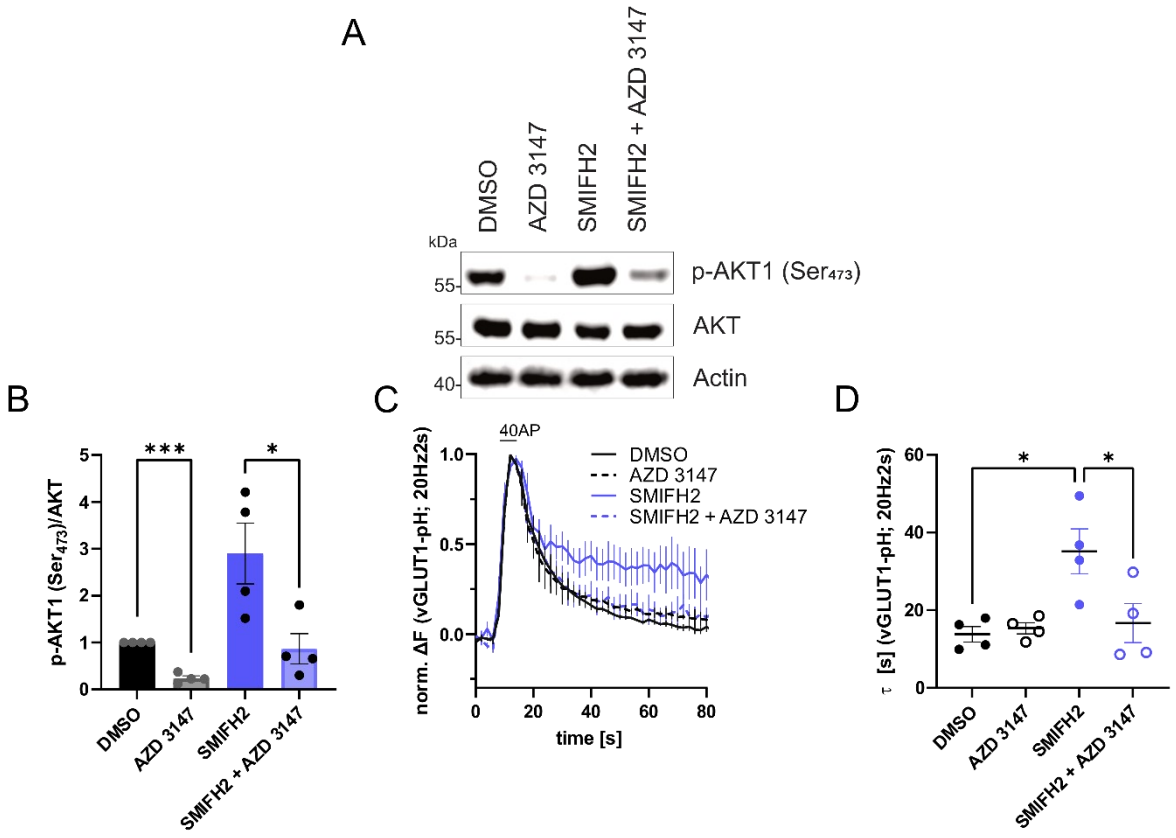

Figure 63: mTORC2 Hyperactivation drives endocytic Phenotypes of Formin Inhibition.
A: Analysis of mTORC2 activity in whole-cell lysates of mouse hippocampal cultures treated with 0.1 % DMSO, 10 nM mTORC2 inhibitor (AZD 3147) or 30 µM formin inhibitor SMIFH2 alone or in combination for 2 h. Samples were analyzed by immunoblotting for phosphorylated AKT1 (p-AKT Ser_{473}), pan-AKT and Tubulin.
B: Phosphorylated AKT1 levels in whole-cell lysates of neurons treated with AZD 3147 (0.2 ± 0.1, $p < 0.001$, one sample t-test) or 30 µM SMIFH2 (2.9 ± 0.6) or both (SMIFH2 + AZD 3147; 0.9 ± 0.3; $p_{SMIFH2 \text{ vs } SMIFH2 + AZD\ 3147} < 0.05$, one-way ANOVA with Tukey's post-test) in comparison to DMSO treated neurons exemplified in **A**. The ratio of phosphorylated (Ser_{473}) AKT1 to pan-AKT was calculated. Data shown is normalized to shCTR. N = 4.
C: Averaged normalized vGLUT1-pHluorin fluorescence traces from hippocampal neurons acutely treated with 0.1 % DMSO, 10 nM mTORC2 inhibitor (AZD 3147), or 30 µM formin inhibitor SMIFH2 alone or in combination in response to 40 AP (20 Hz, 2 s) stimulation. N = 4; $n_{DMSO} = 18$ videos, $n_{AZD\ 3147} = 17$ videos, $n_{SMIFH2} = 16$ videos, $n_{SMIFH2 + AZD\ 3147} = 14$ videos.
D: Endocytic decay constants of vGLUT1-pHluorin traces in **C**: $\tau_{DMSO} = 13.8 \pm 2.0$ s, $\tau_{AZD\ 3147} = 15.4 \pm 1.4$ s, $\tau_{SMIFH2} = 35.1 \pm 5.8$ s, $\tau_{SMIFH2 + AZD\ 3147} = 16.7 \pm 5.0$ s; $p_{DMSO \text{ vs } SMIFH2} < 0.05$, $p_{SMIFH2 \text{ vs } AZD\ 3147} < 0.05$, one-way ANOVA with Tukey's post-test.

4.3.3.2. Homeostatic Coupling of mTORC2 Activity and cytoskeletal Dynamics

Our findings suggest that mTORC2 signaling acts as a negative regulator of SV endocytosis kinetics downstream of formins. Interestingly, pharmacological inhibition of formins drives mTORC2 activation (Figure 63), while conversely, the activation of formins blocks its activity (Figure 58). Based on the results, we propose that mTORC2

activity is intricately linked to the dynamics of the Actin cytoskeleton, which are mediated by formins (Figure 44).

Consistent with this notion, we observed that increasing F-Actin levels via Jasplakinolide treatment (Oevel et al., 2024), reduced the phosphorylation of AKT1 at serine$_{347}$ (Figure 64A). Furthermore, restoring F-Actin to control levels in mDia1/3-depleted neurons through Jasplakinolide application not only ameliorated endocytosis phenotypes (Figure 45) but also reduced mTORC2 hyperactivation (Figure 64A).

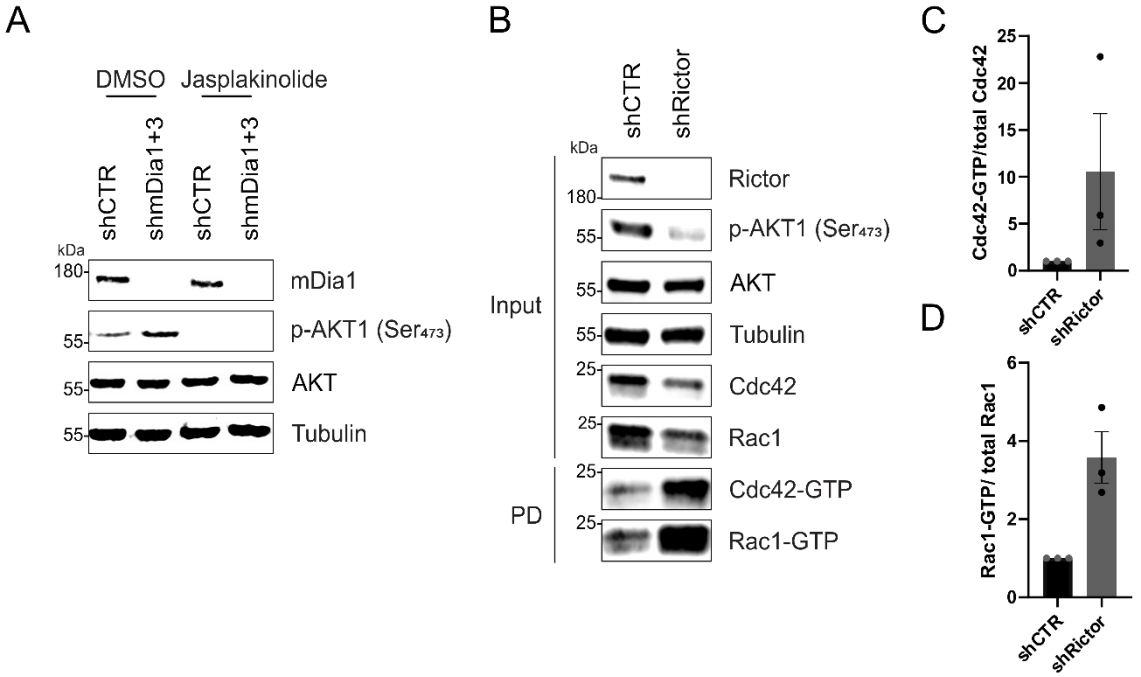

Figure 64: Interdependent mTORC2 and cytoskeletal Signaling.
A: Analysis of mTORC2 activity in whole-cell lysates of mouse hippocampal cultures transduced with lentiviral particles encoding shCTR or shmDia1+3 and treated with 0.1 % DMSO or 1 µM Jasplakinolide for 2 h. Samples were analyzed by immunoblotting for mDia1, phosphorylated AKT1 (p-AKT Ser$_{473}$), pan-AKT and Tubulin.
B: Analysis of GTPase activity by Cdc42 /Rac1-GTP pulldown (PD) from whole-cell lysates (input) of mouse hippocampal neurons expressing shCTR or shRictor utilizing immobilized PAK as a bait. Samples were analyzed by immunoblotting for Raptor, p-AKT1, pan-AKT, Cdc42, Rac1 and Tubulin using specific antibodies. Input, 10% of material used for the pulldown. Contrast of pulldown and input blots was separately adjusted for visualization purposes.
C: Densitometric quantification of Cdc42-GTP normalized to total Cdc42 levels in lysates from shRictor-transduced neurons (10.6 ± 0.8). Values for shCTR were set to 1. N = 3.
D: Densitometric quantification of Rac1-GTP normalized to total Rac1 levels (input) in lysates from neurons transduced with shRictor (3.6 ± 0.7). Values for shCTR were set to 1. N = 3.

These results suggest that the stability and abundance of Actin play a crucial role in controlling mTORC2 activity in neurons.

In addition to its regulation by cytoskeletal dynamics, mTORC2 has been implicated in controlling downstream Actin signaling in both yeast and mammalian cells (Dos et al., 2004; Huang et al., 2013; Jacinto et al., 2004; Loewith et al., 2002). Recent studies in

non-neuronal migrating cells have revealed that mTORC2 activity inhibits WAVE-mediated Actin signaling (Diz-Muñoz et al., 2016), and depletion of its specific subunit *Rictor* results in enhanced activation of the GTPase Rac1 (Saha et al., 2023). As perturbed endocytosis kinetics in mDia1/3-depleted neurons were alleviated both by mTORC2 inhibition (Figure 60/Figure 62) as well as exogenous expression of constitutively-active Rac1 (Figure 54), we investigated the activity levels of Rac1 in cells lacking the mTORC2 subunit Rictor. Consistent with earlier studies (Diz-Muñoz et al., 2016; Saha et al., 2023), we observed increased levels of GTP-bound Cdc42 and Rac1 following isolation by pulldowns utilizing an immobilized domain of their effector PAK in lysates of Rictor-depleted neurons (Figure 64B-D).

These data support a model in which mTORC2 inhibition ameliorates endocytosis phenotypes associated with mDia1/3 loss (Figure 60, Figure 62, and Figure 63) by disinhibiting downstream Actin signaling mediated by Cdc42 and Rac1 (Figure 64).

4.3.3.3. AKT drives SV Endocytosis independent of mTORC2 activity

Given the observation of increased Rac1 activity in neurons where mTORC2 was perturbed (Figure 64), we hypothesized that mTORC2 activity negatively regulates Rac1 signaling. Next, we aimed to dissect which downstream effector of mTORC2 mediates its negative role in SV endocytosis, as well as Rac1-mediated Actin modulation. mTORC2 directly phosphorylates multiple targets to initiate signaling cascades, including the activation of AKT1 (Manning & Toker, 2017).

To ascertain whether AKT1 serves as the synaptic downstream target of mTORC2, contributing to the observed phenotypes, we pharmacologically inhibited AKT function using the small molecule inhibitor MK 2206 (Pal et al., 2010). Surprisingly, inhibition of pan-AKT activity by MK 2206 treatment hindered the retrieval of vGLUT1-pHluorin following 40 AP stimulation (Figure 65), in contrast to the inhibition of its upstream kinases mTORC2 (Figure 60/Figure 62/Figure 63). Furthermore, endocytosis kinetics were exacerbated when AKT inhibition was combined with mDia1/3 formin perturbation (Figure 65).

Hence, AKT signaling drives synaptic vesicle endocytosis, consistent with previous studies (Smillie & Cousin, 2012).

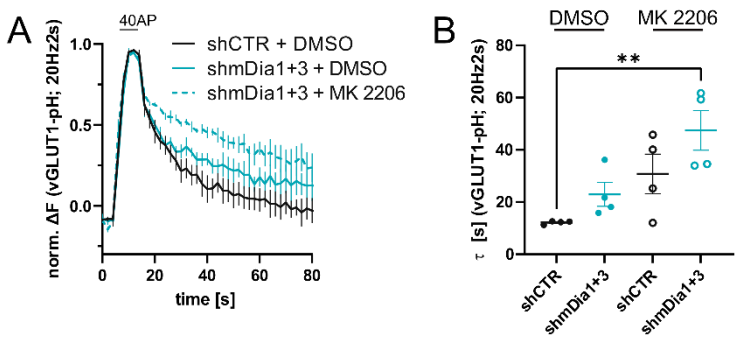

Figure 65: Pharmacological Inhibition of Protein Kinase B (AKT) inhibits SV Endocytosis.
A: Averaged normalized vGLUT1-pHluorin fluorescence traces from hippocampal neurons transduced with shCTR or shmDia1+3 and acutely treated with 0.1 % DMSO or 10 µM pan-AKT inhibitor (MK 2206) in response to 40 AP (20 Hz, 2 s) stimulation. N = 4; $n_{shCTR + DMSO}$ = 15 videos, $n_{shmDia1+3 + DMSO}$ = 18 videos, $n_{shCTR + MK\ 2206}$ = 23 videos, $n_{shmDia1+3 + MK\ 2206}$ = 18 videos.
B: Endocytic decay constants of vGLUT1-pHluorin traces in A: $\tau_{shCTR + DMSO}$ = 12.1 ± 0.3 s, $\tau_{shmDia1+3 + DMSO}$ = 23.0 ± 4.6 s, $\tau_{shCTR + MK\ 2206}$ = 30.8 ± 7.6 s, $\tau_{shmDia1+3 + MK\ 2206}$ = 47.4 ± 7.6 s; $p_{shCTR+ DMSO\ vs\ shmDia1+3 + MK\ 2206}$ < 0.01, one-way ANOVA with Tukey's post-test.

Interestingly, we observe that mTORC2-mediated phosphorylation of $serine_{473}$ does not directly modulate synaptic functions of AKT, indicating that this residue is not necessary for catalytic activity (J. Yang et al., 2002), but rather enhances downstream signaling of AKT as suggested before (Chu et al., 2018). As a consequence, distinct mTORC2 signaling pathways independent of AKT likely contribute to the amelioration of phenotypes associated with mDia1/3-depletion. One potential candidate is protein kinase C, given that the phosphorylation of multiple isoforms and downstream effectors was altered in lysates from neurons lacking mDia1/3 formins (Figure 57). Interestingly, PKC signaling has been implicated in both synaptic vesicle endocytosis (Jin et al., 2019; Plomann et al., 1998) and cytoskeletal dynamics (Larsson, 2006).

Taken together, our findings suggest that synaptic mTORC2 activity is controlled by the cytoskeleton downstream of mDia1/3 formins (Figure 58/Figure 59). Conversely, mTORC2 serves as a negative regulator of the Actin cytoskeleton (Figure 64), with modulation by the small Rho GTPases Cdc42 and Rac1 through downstream signaling independent of AKT (Figure 65), potentially mediated through PKC (Figure 57).

4.4. Plasma Membrane Tension Homeostasis drives Synaptic Vesicle Endocytosis

In our study, we identified a crucial role for interdependent Rho GTPase signaling via RhoA/B (Figure 46) and Rac1 (Figure 53/Figure 54), along with the formins mDia1/3 (Figure 32), in modulating the kinetics of synaptic vesicle endocytosis. We further

established mTORC2 as a negative regulator of SV endocytosis kinetics (Figure 60/Figure 62) and the Actin cytoskeleton (Figure 64), becoming activated upon perturbation of mDia1/3 function (Figure 58). Given our findings that mDia1/3 regulate presynaptic Actin abundance (Figure 45) and crosslink Actin filaments and the presynaptic membrane through its N-terminus (Figure 38), it is conceivable that presynaptic formins contribute to cortical tension acting on the presynaptic plasma membrane. Accordingly, inhibition of formin activity has been linked to a reduction in plasma membrane tension in non-neuronal cells (Lembo et al., 2023). Interestingly, mTORC2 has been reported to sense changes in membrane tension in both yeast and mammalian cells to mediate compensatory signaling by modulating the rates of endocytosis and cytoskeletal dynamics (Berchtold et al., 2012; Diz-Muñoz et al., 2016; Kippenberger et al., 2005; Sedding et al., 2005). Furthermore, the exo-endocytic cycling of synaptic vesicles underlies tension homeostasis of the plasma membrane (Perez et al., 2022). Thus, we were prompted to revisit the role of plasma membrane tension in neuronal mTORC2 activation downstream of mDia1/3 and its effects on the kinetics of synaptic vesicle endocytosis.

To test the consequences of tension perturbation on SV recycling, we employed palmitoylcarnitine (PalmC), a molecule known to significantly reduce tension by intercalation into the plasma membrane in *Saccharomyces cerevisiae* (Riggi et al., 2018, 2019). Furthermore, PalmC application induces phase seperation of $PI(4,5)P_2$ into clusters, resulting in sequestration and inactivation of yeast TORC2 (Riggi et al., 2018).

Contrary to expectations, we observed an increase in phosphorylation of AKT1 at $serine_{473}$ following PalmC treatment (Figure 66A), indicative of the stimulation of mTORC2 activity.

These results suggest that tension-regulation of mTORC2 at synapses differs from the well-described inhibitory pathway observed in yeast (Riggi et al., 2018). Consistently, reducing tension through the orthogonal method of hyperosmotic shocks (700 mOsm), known to cause mTORC2 inhibition in mammalian cells within seconds (Roffay et al., 2021), does not alter phosphorylation of AKT at presynaptic sites marked by Bassoon utilizing gSTED microscopy (Data not shown).

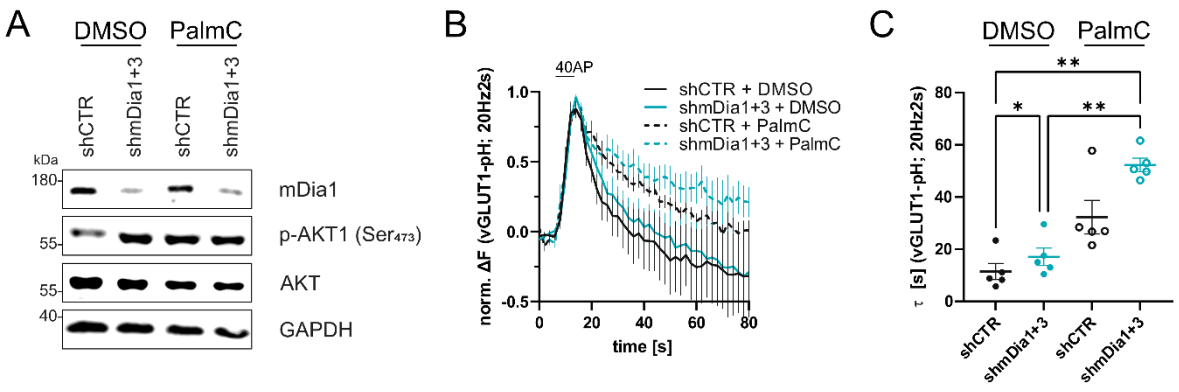

Figure 66: Reducing Membrane Tension through Palmitoylcarnitine inhibits SV Endocytosis.
A: Analysis of mTORC2 activity in whole-cell lysates of mouse hippocampal cultures transduced with lentiviral particles encoding shCTR or shmDia1+3 and treated with 0.1 % DMSO or 10 µM Palmitoylcarnitine (PalmC) for 2 h. Samples were analyzed by immunoblotting for mDia1, phosphorylated AKT1 (p-AKT Ser_{473}), pan-AKT and GAPDH.
B: Averaged normalized vGLUT1-pHluorin fluorescence traces from hippocampal neurons transduced with shCTR or shmDia1+3 and acutely treated with 0.1 % DMSO or 10 µM PalmC in response to 40 AP (20 Hz, 2 s) stimulation. N = 5; $n_{shCTR + DMSO}$ = 17 videos, $n_{shmDia1+3 + DMSO}$ = 22 videos, $n_{shCTR + PalmC}$ = 16 videos, $n_{shmDia1+3 + PalmC}$ = 16 videos.
C: Endocytic decay constants of vGLUT1-pHluorin traces in B. $\tau_{shCTR + DMSO}$ = 11.5 ± 3.1 s, $\tau_{shmDia1+3 + DMSO}$ = 17.1 ± 3.3 s, $\tau_{shCTR + PalmC}$ = 32.3 ± 6.5 s, $\tau_{shmDia1+3 + PalmC}$ = 52.3 ± 2.6 s; $p_{shCTR + DMSO vs shmDia1+3 + DMSO}$ < 0.05, $p_{shCTR+ DMSO vs shmDia1+3 + PalmC}$ < 0.01, $p_{shmDia1+3 + DMSO vs shmDia1+3 + PalmC}$ < 0.01, one-way ANOVA with Tukey's post-test.

The reduction of plasma membrane tension through acute PalmC incubation significantly perturbed the retrieval of vGLUT1-pHluorin after 40 AP stimulation trains (Figure 66B/C). Furthermore, PalmC treatment exacerbated the impairment of endocytosis kinetics following mDia1/3-depletion, indicating that plasma membrane tension crucially determines the kinetics of SV recycling.

Taken together, our findings suggest that synaptic mTORC2 is not inhibited by decreases in plasma membrane tension induced by orthogonal tools such as osmotic shocks or PalmC application, in contrast to the tension-regulation of TORC2 known from yeast. Interestingly, PalmC treatment activates mTORC2. Furthermore, the reduction of plasma membrane tension blocks the endocytic retrieval of SV proteins following PalmC incubation, in contrast to other studies (Orlando et al., 2019). This discrepancy may be attributed to the tension-dependency of Dynamin for membrane fission (Morlot et al., 2012), indicating that the coupling of tension reduction upon exocytosis with tension increases during endocytosis (Perez et al., 2022) is disrupted by PalmC treatment. Similar decoupling of membrane tension homeostasis could explain the effects of mDia1/3-depletion on the kinetics of synaptic vesicle endocytosis by the loss of cytoskeletal-membrane crosslinks, in accordance with findings by (Lembo et al., 2023).

5. Summary

In this study, we investigate the interplay between presynaptic cytoskeletal dynamics mediated by mDia1/3 formins, Rho GTPase signaling, mTORC2 activity, and plasma membrane tension in the regulation of synaptic vesicle (SV) endocytosis. Our comprehensive analysis reveals that the Actin activities (Figure 42/Figure 45) of mDia1/3 formins exert bidirectional control on the kinetics of SV endocytosis (Figure 32/Figure 33) and modulate the presynaptic ultrastructure (Figure 34) by associating with the presynaptic plasma membrane (Figure 38/Figure 39) as well as the endocytic machinery (Figure 40/Figure 41). We identify roles for the small Rho GTPases RhoA/B (Figure 46) and Rac1 (Figure 53/Figure 54) in modulating SV recycling through interdependent signaling pathways. Furthermore, we describe that localization of mDia1 is governed by the small Rho GTPase RhoA (Figure 47), although its function in endocytosis may act independently of RhoA, likely involving Cdc42 and Rac1 instead (Figure 48). Additionally, we uncover a regulatory axis involving Rho GTPases and mDia1/3 formins, in which mDia1/3 positively impacts RhoA activity (Figure 49), which subsequently downregulates Cdc42 and Rac1 signaling pathways (Figure 50). Rac1 activation can compensate for the loss of mDia1/3 formins (Figure 54) in modulating SV recycling, possibly by restoring Actin dynamics (Figure 55). Moreover, we observe that mDia1/3 formins modulate presynaptic signaling networks mediated by mTORC2 (Figure 58/Figure 59). Multiple approaches indicate that the constitutive activation of mTORC2 correlates with a block of SV endocytosis (Figure 60, Figure 62, Figure 63, and Figure 66), which can be ameliorated by increasing Actin abundance (Figure 64). Furthermore, genetic or pharmacological interference with mTORC2 activity rescues endocytosis phenotypes associated with mDia1/3 depletion (Figure 60), suggesting a negative role for mTORC2 signaling in modulating SV endocytosis (Figure 62) and the cytoskeleton (Figure 64).

In summary, our study identifies intricate signaling networks that converge on the regulation of the cytoskeleton, including mTORC2 and Rho GTPase signaling, which undergo homeostatic coupling through intricate feedback mechanisms.

While our findings provide insights on the complex regulatory pathways of SV endocytosis, several questions remain unanswered. These include elucidating the exact molecular mechanisms by which mDia1/3-mediated Actin functions control SV recycling, whether through direct Actin assembly or indirectly by regulating cortical

tension, as suggested by PalmC manipulation (Figure 66). Furthermore, exploring the pathways that facilitate crosstalk between Rho GTPases and compensatory Actin signaling (both in general and downstream of mDia1/3) at synapses is of considerable interest. Moreover, the identification of mTORC2 as a synaptic signaling module negatively regulating neurotransmission prompts inquiry into the factors contributing to synaptic mTORC2 activity and its specific role at the synapse, leading to negative regulation of the cytoskeleton and SV endocytosis. Future studies are imperative to address these unresolved questions.

6. Discussion

6.1. The role of mDia1/3 Formins in Synaptic Vesicle Endocytosis

The recycling of synaptic vesicles via endocytic pathways is a key requirement for neurotransmission. While the role of the Actin cytoskeleton in endocytosis is well established in yeast, endocytic processes in mammalian cells, in particular neurons, entail specific requirements, regarding Actin and the associated signaling molecules that modulate its dynamics. Pharmacological manipulations targeting the cytoskeleton have yielded conflicting outcomes in various studies (Babu et al., 2020; Bleckert et al., 2012; J. Bourne et al., 2006; Delvendahl et al., 2016; Eguchi et al., 2017; Holt et al., 2003; Y. Hua et al., 2011; Z. Li & Murthy, 2001; Richards et al., 2004; Sankaranarayanan et al., 2003; D. Wang et al., 2010; Q. Zhang et al., 2009), prompting further investigation into the involvement of Actin remodeling in synaptic vesicle endocytosis, and the underlying molecular mechanisms governing its dynamics.

Actin assembly is modulated by multiple regulatory proteins, including the Arp2/3 complex, which initiates branching, and formins, which facilitate linear filament nucleation and assembly (Pollard, 2007). Interestingly, previous studies demonstrated that pharmacological inhibition of Arp2/3-mediated Actin nucleation processes does not impair the retrieval of synaptic vesicle proteins during endocytosis (Ganguly et al., 2015; Soykan et al., 2017). In contrast, the perturbation of formin activity by the application of SMIFH2 impedes SV recycling (Ganguly et al., 2015; Soykan et al., 2017) (Figure 63). Here, we characterized the Diaphanous-related formins mDia1 and mDia3 as two functionally redundant isoforms, consistent with previous findings (Shinohara et al., 2012; Thumkeo et al., 2011), that are critically involved in presynaptic endocytic processes (Figure 32).

Prior studies into the roles of mDia1/3 in the brain and neurons are limited. Interestingly, homozygous loss of *DIAPH1*, the human homologue of mDia1, causes seizures, cortical blindness and microcephaly syndrome (Ercan-Sencicek et al., 2015; Esmaeilzadeh et al., 2022), underscoring the significance of Diaphanous-related formins in brain development and function. In mice, sole genetic depletion of mDia1 exhibits mild phenotypes (DeWard et al., 2009; Eisenmann et al., 2007; J. Peng et al., 2007; Sakata et al., 2007; Tanizaki et al., 2010). However, co-depletion with its closely

related isoform mDia3 induces brain dysplasia (Shinohara et al., 2012; Thumkeo et al., 2011) and aberrant locomotion (Herzog et al., 2011; Toyoda et al., 2013) by affecting interneuron migration (Shinohara et al., 2012) and axon elongation in cerebellar granule cells and cerebral cortical neurons on a molecular scale (Arakawa et al., 2003; Ohshima et al., 2008).

6.1.1. The presynaptic Localization of mDia1

In non-neuronal cells, mDia1 is localized to various cellular compartments, including the cell cortex, trafficking endosomes, and structures essential for cell division, depending on cell type and position in the cell cycle (Tominaga et al., 2000).
Within mature rodent neuronal cultures, mDia1 is observed at presynaptic terminals (Deguchi et al., 2016), however, studies have further implicated mDia formins at the axon initial segment (W. Zhang et al., 2021), along axons (Chenouard et al., 2020; Ganguly et al., 2015) and within dendrites (Qu et al., 2017). Consistent with (Deguchi et al., 2016), we identify mDia1 predominantly localized at presynaptic membranes in close proximity to active zones within mature synapses of mouse hippocampal cultures (Figure 39/Figure 67).

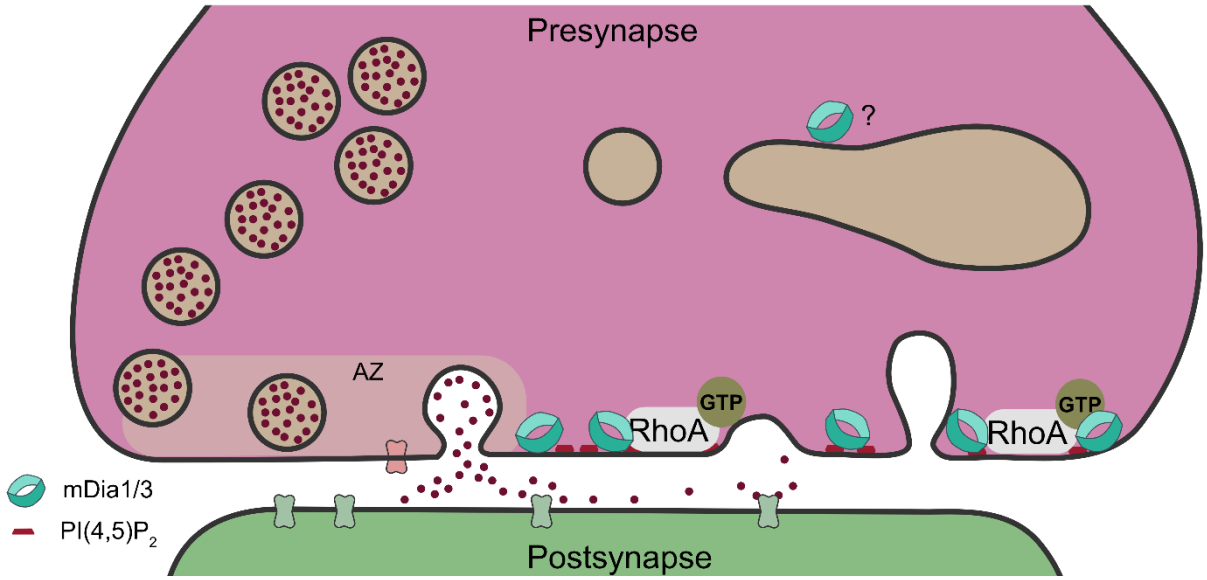

Figure 67: Synaptic Localization of mDia1/3.
At mature hippocampal mouse synapses, formins mDia1/3 predominantly localize to the presynaptic membrane in close vicinity to the active zone, dependent on RhoA and negatively charged phospholipids such as $PI(4,5)P_2$. Observed EM phenotypes suggest an additional role for mDia at endosome-like vacuoles. This action might be transient, eluding detection by fixed super-resolution microcopy.

Surprisingly, besides cytoskeletal and endocytic proteins, our analysis of the proximal protein environment of mDia1 also revealed dendritic proteins, including Homer1

(Data not shown). This suggests a potential role for mDia1 in dendritic processes (Qu et al., 2017), that are obscured from our gSTED analysis (Jung et al., 2020). However, in mature synapses, depletion of mDia1/3 does not diminish postsynaptic F-Actin abundance (Figure 44), indicating that putative dendritic roles of mDia1/3 likely occur during synapse development or are independent of Actin. Therefore, the early transduction of neurons (day in vitro 2) with biotin ligase-tagged mDia1 in our experiments enables the analysis of mDia1's proximal protein neighbors during synapse formation and maturation, where F-Actin assembly is critical (W. Zhang & Benson, 2001). Consequently, mDia1 may contribute to axon elongation (Arakawa et al., 2003) or dendrite formation (Hotulainen et al., 2009; Qu et al., 2017), as demonstrated in prior studies.

Furthermore, EM phenotypes of accumulated endosome-like vacuoles (Figure 34), suggest an essential function of mDia1/3 in the reformation of SV from ELVs, possibly requiring its localized action. Such processes may be too transient to be effectively captured using fixed super-resolution microscopic techniques.

In non-neuronal cells, the subcellular localization of mDia formins is regulated by the activity of Rho GTPases (Colucci-Guyon et al., 2005; Higashi et al., 2008; Lammers et al., 2008). Consistently, we established that mDia1 is recruited to membranes through its interaction with RhoA (Figure 47) and negatively charged phospholipids such as $PI(4,5)P_2$ and $PI(3,4,5)P_3$ via N-terminal stretches of positively charged amino acids (Figure 38;(Gorelik et al., 2011; Ramalingam et al., 2010)), both concentrated at the presynaptic plasma membrane (Figure 46,(Bolz et al., 2023)).

6.1.2. Cytoskeletal Functions of synaptic mDia1

Formins have been implicated in facilitating inter-synaptic axonal trafficking of vesicles (Chenouard et al., 2020) and regulating SV recycling dynamics at presynaptic terminals (Soykan et al., 2017) by modulating the Actin cytoskeleton (Bingham et al., 2023; Ganguly et al., 2015).

In our study, we identify a crucial role for formins mDia1/3 in governing the kinetics of endocytic membrane and protein retrieval (Figure 32). We demonstrate that the involvement of mDia1/3 in SV endocytosis is contingent upon their regulatory functions on Actin in multiple ways: a) the activation of mDia1/3 by IMM application facilitates SV recycling (Figure 33), a condition known to significantly enhance cellular

F-Actin abundance (Lash et al., 2013), b) an Actin-null mutant of mDia1 (mDia1-K994A) fails to rescue defective endocytosis upon perturbation of formin function (Figure 42), c) genetic depletion of mDia1/3 decreases presynaptic F-Actin abundance (Figure 44). Conversely, restoring presynaptic F-Actin abundance either by Jasplakinolide (Oevel et al., 2024) or constitutive Rac1 signaling alleviates endocytosis phenotypes stemming from mDia1/3 deficiency (Figure 45 and Figure 54)

These findings underscore the importance of mDia1/3-mediated Actin functions in SV endocytosis, which encompass the nucleation, elongation (Daou et al., 2014) stabilization (Xu et al., 2004) of Actin filaments: While the precise mechanism of formin-mediated filament nucleation has remained elusive, the nucleation activity of mDia1 likely relies on the nucleation promoting factor adenomatous polyposis coli protein (APC) (Okada et al., 2010). APC remains localized at nucleation sites while mDia1 processively moves along the growing barbed end to elongate the filament and shield it from capping (Breitsprecher et al., 2012). Consistently, our proximity proteomics analysis reveals significant enrichment of APC in the synaptic protein environment of mDia1 (Figure 68). Furthermore, genetic ablation of APC causes increased synaptic spine density in hippocampal neurons (Mohn et al., 2014), phenocopying the genetic perturbation of mDia1 (Qu et al., 2017), suggesting a cooperative role between mDia1 and APC in mediating Actin nucleation, albeit the consequences of perturbation phenotypically occur at postsynaptic sites.
Besides, its nucleation capacity, the formin mDia1 exhibits exceptional elongation kinetics with a gating factor close to 1 (Kovar, 2006; Shemesh & Kozlov, 2007), capable of assembling filaments at a rate of 550 subunits/s at cellular Profilin-Actin concentrations (Higashida et al., 2004). Furthermore, formins compete with capping proteins for binding to filament barbed ends (Shekhar et al., 2015), shielding filaments from disassembly (Ulrichs et al., 2023). Recent studies have indicated that mDia proteins can form complexes with capping proteins (Bombardier et al., 2015), indicating a *primed state* of mDia1 capable of rapidly switching between capping and polymerization functions by sliding along filaments. Consistent with the competitive nature of mDia1 with capping proteins (Bombardier et al., 2015), we found multiple subunits of the F-Actin capping protein (CapZ) in close proximity to mDia1 at synapses (Figure 68).

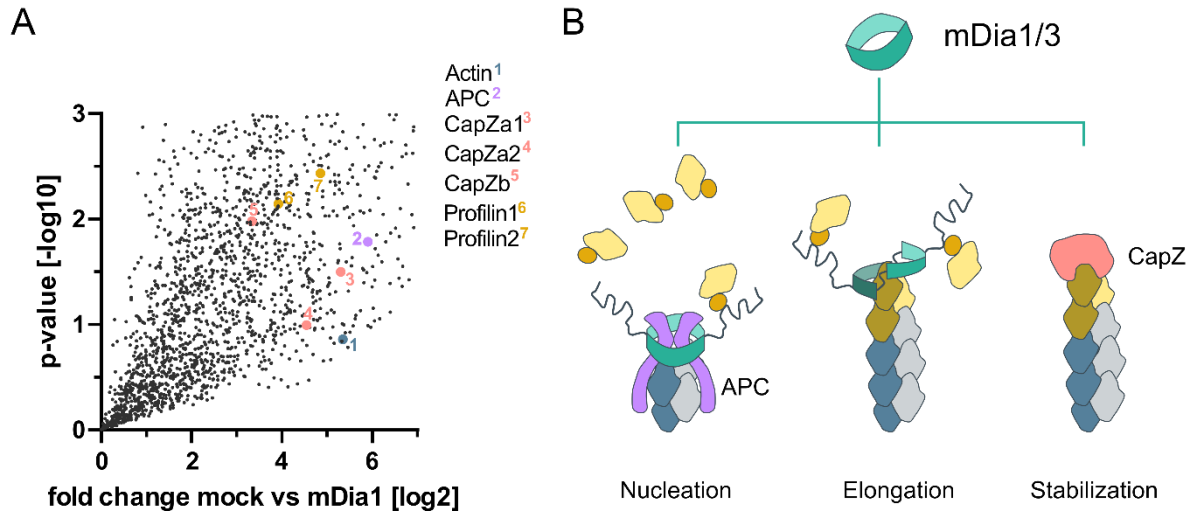

Figure 68: Actin Functions of mDia1/3 at Synapses.
A: Volcano plot of Actin assembly proteins in the proximal environment of neuronal mDia1 analyzed by label-free proteomics of biotinylated proteins in neurons transduced with mDia1-TurboID or mock-treated cells. The logarithmic ratios of protein intensities are plotted against negative logarithmic p-values derived from two-tailed student's t-test. Each dot represents one protein. N = 3 independent experiments. Mass spectrometry was performed by Heike Stepahnowitz.
B: mDia1/3 mediate the nucleation, elongation and stabilization of Actin filaments at synapses by cooperating with APC and profilin, and competing with capping proteins CapZ for barbed-end association.

Taken together, the involvement of mDia1 at synapses likely encompasses its roles in the nucleation, polymerization, and stabilization of filaments. In the following we will discuss how Actin functions are regulated and can contribute to SV endocytosis.

6.1.3. Regulation of synaptic mDia1 Activity

Both binding to phospholipids and active RhoA have been implicated in the recruitment of mDia1 to membranes (Figure 38, Figure 46, and Figure 47). In addition, RhoA-GTP levels and the phospholipid PI(4,5)P_2 can control the Actin-based activities of mDia formins:

6.1.3.1. Phospholipids

mDia1 integrates into lipid bilayers via its N-terminal domain, inducing PI(4,5)P_2 clustering (Ramalingam et al., 2010). Molecular modeling suggests that formins initially dock at membranes and cooperatively bind three or more PI(4,5)P_2 molecules to acquire Actin-nucleating activity, independent of Rho GTPase signaling (Bucki et al., 2019). Consequently, increased PI(4,5)P_2 levels following neuronal activity (Bolz et al., 2023), activate mDia1 to execute its downstream Actin functions.

6.1.3.2. Small Rho GTPases

The canonical model of mDia1 activation involves the interaction between its Rho-binding domain (RBD) and the small Rho GTPase RhoA in its GTP-bound state. This association releases mDia1 from autoinhibition, thereby facilitating downstream F-Actin assembly mediated by the mDia1-FH2 domain (Otomo et al., 2005).

In this study, we found that exogenously expressed wild-type mDia1 could not be immunoprecipitated by constitutively GTP-loaded RhoA (Figure 47A) alone, suggesting the involvement of additional factors in mDia1 activation. These factors could include phospholipids (Maiti et al., 2012; Ramalingam et al., 2010), protein interactors (Brenig et al., 2015; Mason et al., 2011), or kinase-mediated phosphorylation events (Cheng et al., 2011; Hannemann et al., 2008). Furthermore, we utilized site-directed mutagenesis to generate several mDia1 mutants: a RhoA-binding deficient (V161D + N165D), a strong RhoA-binding constitutively-active (M1182A + L1185A), and a constitutively-active Rho-binding deficient (V161D + N165D and M1182A + L1185A) mDia1 variant (Figure 47). Following our findings, we identified residues $valine_{161}$ and $asparagine_{165}$ in the RBD of mDia1 to mediate its association with RhoA (Figure 47A) and subsequent membrane recruitment (Figure 47B/C), consistent with previous studies (Lammers et al., 2005; Seth et al., 2006). Surprisingly, none of the generated mDia1 variants exhibited a dominant negative effect on the kinetics of vGLUT1-pHluorin retrieval (Figure 47A), indicating that RhoA-binding of synaptic mDia1 does not play a role in its mediation of SV endocytosis. These findings suggest two potential scenarios: a) mDia1 may act as an endocytic scaffold regardless of its activity state (see model below) or b) the activity of mDia1 can be modulated independent of RhoA, indicating the presence of alternative regulatory mechanisms that govern mDia1 function in SV endocytosis.

Many formins, including mDia1/3, share the capability to bind multiple isoforms of the Rho GTPase family (Faix & Grosse, 2006) through a mutually exclusive binding site (Lammers et al., 2008). Given that the residues in the switch regions of Rho GTPases, which mediate formin association, are conserved (Kühn & Geyer, 2014), and single amino acid substitutions can dictate the specificity of interactions between individual members of the Rho GTPase family and mDia1 (Rose et al., 2005), the most obvious candidate to regulate synaptic mDia1 activation apart from RhoA is its closely related isoform RhoB (N. Watanabe et al., 1999). Accordingly, genetic depletion of RhoA or

overexpression of dominant-negative RhoA alone does not impede SV endocytosis. Only upon co-depletion of RhoA and RhoB or expression of both dominant negative forms, SV endocytosis is stalled (Figure 46), suggesting that RhoB activity can compensate for the loss of RhoA, possibly through the action of a common effector such as Myosin IIB, consistent with (Chandrasekar et al., 2013) and (Soykan et al., 2017), or mDia formins. Furthermore, Cdc42 (J. Peng et al., 2003) and Rac1 (Lammers et al., 2005) have been implicated in binding and stimulating mDia1-mediated Actin assembly. In line with this notion, we observe elevated levels of Cdc42, Rac1 and Cdc42 effector IQGAP1 in the proximity of Rho-binding deficient mDia1 (Figure 48), suggesting that other small GTPases besides RhoA can contribute to the regulation of mDia1 (Kato et al., 2001) at synapses, in particular when RhoA binding is disrupted. Apart from Cdc42 and Rac1, we find further alterations in the proximal proteome of mDia1 dependent on its binding to RhoA (Figure 48). For example, we find increased levels of Liprin-α3 in the vicinity of Rho-binding deficient mDia1, consistent with its previously described role in competing with RhoA for mDia1 association to regulate its activity and membrane localization (Brenig et al., 2015). Furthermore, we observe elevated endocytic proteins such as Synaptophysin (S. E. Kwon & Chapman, 2011), Dynamin1/3 (Raimondi et al., 2011), Protein kinase C (PKC) (Jin et al., 2019) and ROCK2 (Zhou et al., 2009) (Figure 48), all implicated in the modulation of neurotransmission.

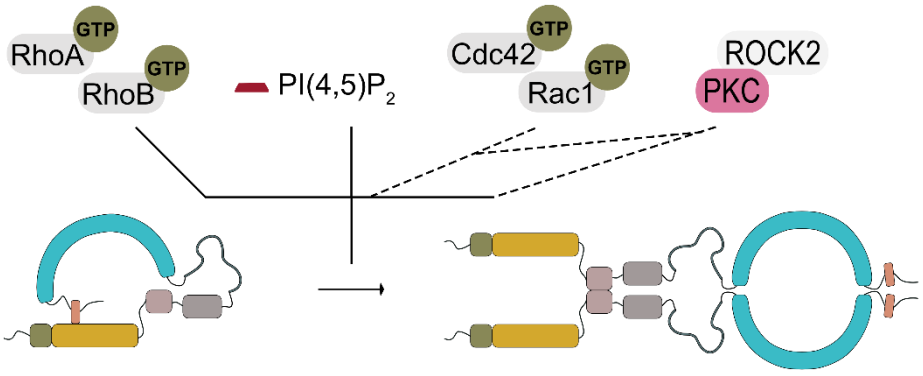

Figure 69: Model for mDia1 Activation at Synapses.
The Actin-regulatory functions of mDia1 likely necessitate its release from autoinhibition mediated by an intramolecular interaction. Contrary to the canonical view, this release may not solely depend on RhoA-GTP binding, but could require additional factors including RhoB or phospholipids, such as $PI(4,5)P_2$. Furthermore, mDia1 can orchestrate synaptic vesicle endocytosis in a RhoA-independent manner. This alternative pathway might entail the activation of mDia1 downstream of Cdc42, Rac1 and/or protein kinase C (PKC) and Rho-associated kinase 2 (ROCK2) or compensatory pathways mediated by these factors that govern synaptic vesicle endocytosis.

Our findings suggest that activation of mDia1 at synapses is more complex than solely dependent on RhoA (Figure 69). Furthermore, mDia1 can act on SV endocytosis through RhoA-independent mechanisms, likely involving Cdc42, Rac1, IQGAP1, PKC and ROCK2. These pathways might entail direct binding and activation of mDia1, and/or the activation of compensatory pathways through other formins (J. Peng et al., 2003) or Arp2/3 signaling (Higgs & Pollard, 2001) (see 4.3.2.).

6.1.4. Molecular Models for the Role of mDia1/3 in SV Endocytosis

In the following, we propose comprehensive models that integrate the findings of this study elucidating how mDia1-mediated Actin functions contribute to SV endocytosis, by exploring direct pathways involving interactions with the endocytic machinery and indirect pathways concerning mechanotransduction and biochemical signaling.

6.1.4.1. mDia-mediated Actomyosin Dynamics drive Membrane Deformation

In our study, we identified multiple PI(4,5)P_2-associated proteins of the endocytic machinery, such as the F-BAR proteins FBP17, and PACSIN1/2, N-BAR proteins Amphiphysin and Endophilin, the GTPase Dynamin1/3 and the phosphatase Synaptojanin1 in close proximity to synaptic mDia1 (Figure 40/Figure 41). In an active participation model, mDia1 collaborates with the identified machinery to facilitate synaptic vesicle endocytosis through de novo localized Actin polymerization coupled with myosin contractility, generating pushing and pulling forces, respectively (Shin et al., 2022): Following exocytosis, reduced membrane tension (Shi & Baumgart, 2015) is sensed by F-BAR proteins, initiating membrane curvature (Simunovic & Voth, 2015). Membrane associated F-BAR proteins recruit mDia formins (Aspenström, 2010), consistent with our interaction studies (Figure 40), where mDia1 binds and inserts into membranes in a PI(4,5)P_2-dependent manner (Ramalingam et al., 2010). Accordingly, we observe mDia1 localized at the presynapse, likely situated at endocytic sites on the presynaptic membrane (Figure 39, (Dani et al., 2010)). Through its membrane insertion (Figure 38), mDia1-mediated barbed end polymerization is directed towards the plasma membrane, exerting pushing forces that promote the growth of an endocytic pit (Blanchoin et al., 2014). Conversely, crosslinks of non-muscle myosin II filaments, between antiparallel Actin strands generate pulling forces by sliding

anchored filaments in opposite directions, inducing contractile forces (Carlsson & Bayly, 2014).

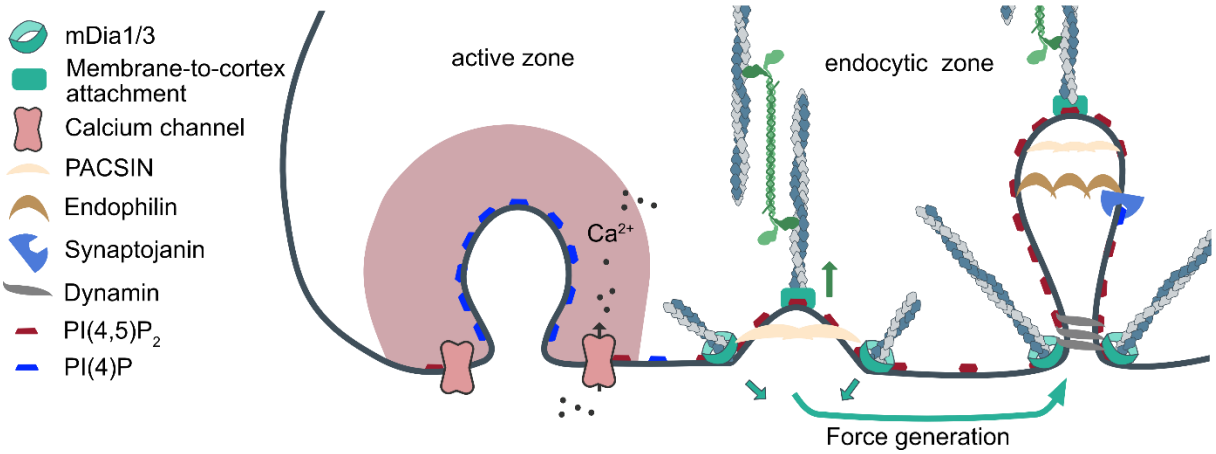

Figure 70: Model for mDia1/3-mediated Force Generation during SV Endocytosis. Following the exocytic fusion of synaptic vesicles, alterations in membrane tension at the endocytic zone are sensed by proteins of the F-BAR family such as FBP17 and PACSIN1/2. F-BAR proteins recruit mDia1 formins that insert into the presynaptic membrane via $PI(4,5)P_2$ clustering (Ramalingam et al., 2010). mDia-mediated Actin polymerization generates pushing forces against the plasma membrane. Concurrently, myosin filaments assemble and crosslink Actin filaments anchored to the plasma membrane via membrane-to-cortex attachment proteins, such as APC and/or MARCKS/GAP43. Myosin translocation towards Actin barbed ends generates pulling forces to further drive endocytic membrane deformation. Through curvature generation, N-BAR proteins such as Endophilin and Amphiphysin and Dynamin are recruited to orchestrate vesicle scission. Finally, Synaptojanin1 hydrolyses $PI(4,5)P_2$ to PI(4)P.

This myosin-mediated role in membrane invagination during SV endocytosis is consistent with (Chandrasekar et al., 2013; Soykan et al., 2017), and its cooperative action with mDia1 has been implicated in the regulation of presynaptic membrane contractility (Deguchi et al., 2016). Consequently, increased membrane curvature induces the association of N-BAR proteins that recruit Dynamin helices to surround and constrict the base of the invagination, ultimately leading to vesicle scission (L. G. Wu & Chan, 2022). This model bears striking similarities to Clathrin-mediated endocytosis in terms of the protein machinery involved. Taken together, the coordinated interplay of Actin pushing and pulling forces can govern membrane deformation independently of Clathrin (Boulant et al., 2011; Kaur et al., 2014), facilitated by mDia1-mediated actomyosin activity (Figure 70).

6.1.4.2. mDia affects synaptic Kinase/Phosphatase Signaling

The genetic ablation of mDia1/3 function results in aberrant presynaptic signaling involving synaptic kinases and phosphatases, characterized by altered phosphorylation patterns of protein regulating the cytoskeleton and endocytosis (Table 11, Figure

40/Figure 41). Furthermore, preliminary experiments revealed a reduction of synaptic PI(4,5)P_2 in neurons depleted of mDia1/3 (Figure 81), suggesting an impact on synaptic lipid signaling, consistent with findings by (C. Li et al., 2023). As phosphorylation regulates the activities of proteins within the endocytic machinery implicated in the active participation model (6.1.4.1), such as PACSINs (Senju et al., 2015), Amphiphysin (Zhao et al., 2013), Endophilin (Ambroso et al., 2014), and Dynamin (Smillie & Cousin, 2012), mDia1/3 may serve additional roles in governing synaptic signaling cascades.

For example, we observe a 10-fold increase in the phosphorylation of Synaptojanin1 residue serine$_{1144}$. This site is modulated by the opposing actions of cyclin-dependent kinase 5 (CDK5) and calcineurin, regulating its interaction with Endophilin and consecutive PI(4,5)P2 turnover (S. Y. Lee et al., 2004). This alteration suggests heightened CDK5 or diminished calcineurin signaling. Increased CDK5 activity represses SV endocytosis (G. Liu et al., 2022) as a response to defective lipid signaling (Figure 81).

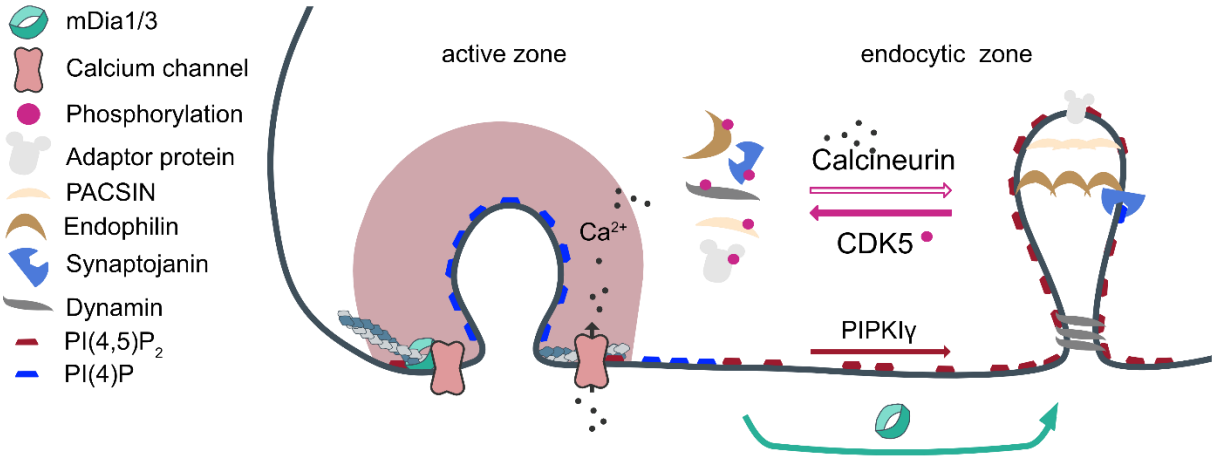

Figure 71: Model for mDia1/3-mediated Regulation of synaptic Kinases/Phosphatases. At the presynapse, plasticity is regulated by activity-dependent phosphorylation of the endocytic machinery (Clayton & Cousin, 2009). Phosphorylation of adaptor proteins AP180 and Epsin, PACSIN, Amphiphysin, Endophilin and Dynamin results in their sequestration in the cytosol. Upon exocytosis, calcium influx activates the phosphatase calcineurin, leading to dephosphorylation and induction of endocytic machinery assembly. The opposing reaction is catalyzed by cyclin-dependent kinase 5 (CDK5) among other kinases. mDia1/3 influence the phosphorylation status of many endocytic proteins, potentially by modulating calcium channel distribution and calcineurin activity. Furthermore, mDia formins likely modulate synaptic PI(4,5)P_2 levels, possibly by affecting PIPKIγ and/or Synaptojanin1 regulation.

Furthermore, the activity of calcineurin is potentiated by calcium (Cheung & Cousin, 2013). As Actin dynamics govern the density and coupling distances of voltage-gated calcium channels (Mercer et al., 2011), the loss of mDia1/3 could influence endocytosis kinetics by lowering calcium availability to activate calcineurin through modulation of

the active zone architecture (Glebov et al., 2017), as demonstrated for its potent interactor Liprin-α3 (Emperador-Melero et al., 2021). However, no significant defects in calcium-sensitive exocytic fusion of pHluorin or CypHer reporters was observed in cells lacking mDia1/3 (Figure 80).
Hence, mDia1/3 could impact synaptic vesicle endocytosis, by functioning as a signaling hub, potentially exerting localized control over intracellular calcium concentration (Figure 71), consistent with signaling roles of mDia1/3 at the immune synapse (Thumkeo et al., 2020).

6.1.4.3. mDia acts as a Scaffold to preassemble the endocytic Machinery

Recent studies indicate that the endocytic machinery identified in the mDia1 interactome (PACSIN1, Dynamin1, Endophilin-A1 and Synaptojanin1; Figure 40/Figure 41), is stored in pre-assembled molecular condensates via liquid-liquid phase separation (LLPS) at the presynaptic membrane (Sansevrino et al., 2023). Such pre-assembly facilitates ultrafast kinetics of endocytosis by bypassing the slow recruitment of endocytic factors from the cytosol, which typically takes 10-30 s for proteins like Dynamin1 (Cocucci et al., 2014). Ultrafast endocytosis is triggered by the dispersal of phase-separated condensates induced by exocytic events, such as calcium influx or changes in membrane homeostasis (Imoto et al., 2022) . Actin and Actin-regulatory proteins may play a role in forming these condensates, given the strong Actin dependence of ultrafast endocytosis at synapses (Ogunmowo et al., 2023; S. Watanabe, Rost, et al., 2013). Interestingly, mDia formins have been implicated in acting as scaffold proteins to initiate LLPS (K. Zhang et al., 2023) and in driving nanoclustering of membrane lipids (C. Li et al., 2023) and proteins with Actin-binding domains (Kalappurakkal et al., 2019).

Given the secondary role of RhoA association with mDia1 in pHluorin assays (Figure 48), formins could act as endocytic scaffolds independent of their activity state, e.g. by pre-clustering of the endocytic machinery and/or phospholipids through direct interactions (Figure 72). Consistently, decruitment of mDia1 upon stimulation in live and fixed assays (Data not shown) may suggest the disassembly of endocytic phase-separated condensates. Consequently, the loss of mDia1/3-mediated preassembled endocytic clusters could notably decelerate, though not entirely impede recycling kinetics, as demonstrated in our study (Figure 32). Further investigation is needed to

determine whether phase-separated condensates of endocytic machinery, which drive ultrafast endocytic pathways, contain the Actin cytoskeleton and/or mDia1/3.

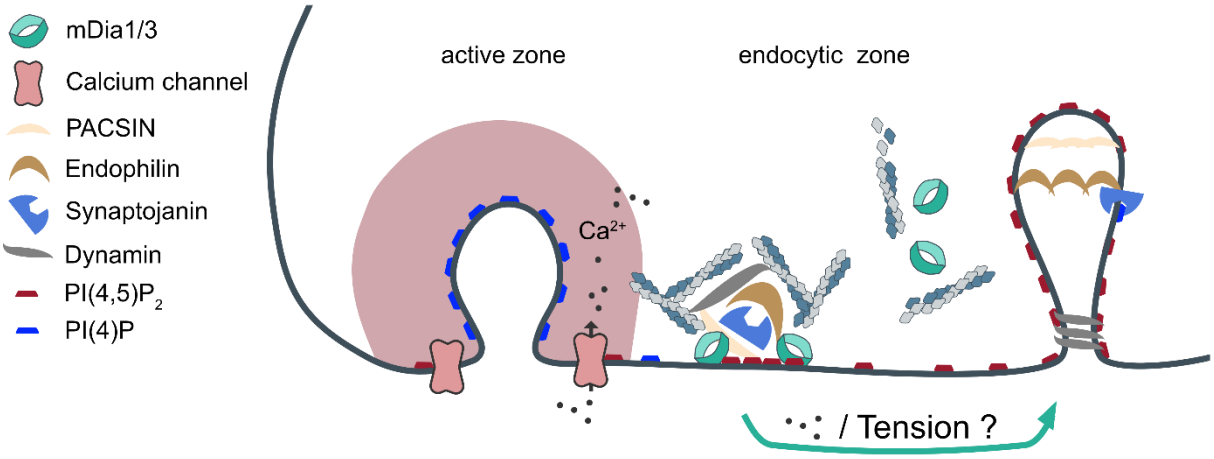

Figure 72: Model for mDia1/3-mediated Condensate Formation.
Under resting conditions, approximately 75% of Dynamin1 is dephosphorylated (Graham et al., 2007). Recent studies suggest that Dynamin1 and PACSIN1, possibly in conjunction with Endophilin and Synaptojanin, form pre-assembled condensates via liquid-liquid phase separation at the presynaptic membrane. mDia1/3 may facilitate the formation of phase-separated phases by clustering phospholipids and endocytic machinery through direct interaction dependent or independent of their unctions. Condensates are resolved upon exocytosis likely through mechanisms involving calcium signaling or tension homeostasis, initiating the assembly of the endocytic machinery.

6.1.4.4. mDia is mechanosensitive and modulates Plasma Membrane Tension

Multiple studies indicate that mDia1 is mechanosensitive and that its Actin polymerization activity is stimulated by pulling forces on the filament (Echarri et al., 2012, 2019; Jégou et al., 2013; Z. Li et al., 2020; Yu et al., 2017). In addition, mDia1-dependent actomyosin activity plays a fundamental role in maintaining the physiology and barrier function of epithelial cells, cells that routinely encounter membrane tension perturbations through osmotic fluctuations (Acharya et al., 2017; Fessenden et al., 2018). Therefore, mDia1 can likely sense mechanical forces either directly through filaments bound to the membrane or through its own membrane-insertion capability (Ramalingam et al., 2010).

mDia as a Nanogate for Tension Propagation

A theoretical study proposed that endocytosis is triggered by a reduction in membrane tension following exocytosis (Shi & Baumgart, 2015). At presynaptic terminals, tension decreases are equilibrated over several micrometers within a few seconds (Perez et al., 2022) in stark contrast to measurements of their dendritic counterparts (Shi et al.,

2018), where propagation is counteracted by the adhesive forces of the cytoskeleton. In non-neuronal cells, adhesion is regulated by Rho GTPases (Parsons et al., 2010) and mDia formins (Acharya et al., 2017). Therefore, mDia1/3 likely mediate dual roles in regulating tension propagation at presynaptic terminals: a) by modulating the abundance of the Actin cortex close to the presynaptic membrane; and b) by governing membrane-to-cortex attachments, either directly through their Actin functions (Figure 44) and membrane-binding capabilities (Figure 38) (Lembo et al., 2023) or indirectly by reducing $PI(4,5)P_2$-mediated Actin crosslinks (Figure 81), (Raucher et al., 2000; Tariq & Luikart, 2021). Observations of reduced mDia1 levels at fixed boutons and decruitment from synaptic terminals following strong stimulation in live experiments (Data not shown), suggest that mDia1-mediated membrane-to-cortex attachment may act as a barrier to enable endocytic pit formation once membrane tension drops post-exocytosis (Perez et al., 2022). This function of mDia1 is analogous to its role in regulating the tension-buffering function of caveolae (Sinha et al., 2011), likely in coordination with myosin II function (De Belly et al., 2023).

mDia Formins modulate Cortical Tension

Mechano-sensitive processes underlie reciprocal feedback loops, where mDia1 activity contributes to cortical tension by anchoring filaments to the membrane and/or promoting processive Actin assembly to generate force on membranes. Consistently, studies have shown that application of the pan-formin inhibitor SMIFH2 reduces cortical tension (Eftekharjoo et al., 2019), while activation of mDia formins by IMM treatment increases tension (Lembo et al., 2023).

In our study, we find several indications that mDia1 might modulate synaptic plasma membrane tension: a) Initial measurements using FliptR, a fluorescent membrane tension sensor (Colom et al., 2018), indicate reduced plasma membrane tension at synapses of mDia1/3-depleted neurons that respond to stimulation (Data not shown, collaboration with Agata Witkowska); b) The loss of mDia1/3 leads to accumulations of membrane folds of non-endocytic nature (Figure 36 and Figure 37), often observed as membrane reservoirs in non-neuronal cells under decreased tension (e.g., caveolae (Sinha et al., 2011) or upon disruption of the cytoskeleton (Raucher & Sheetz, 1999); c) Under steady-state conditions, cells lacking mDia1/3 exhibit reduced levels of plasma membrane stranded-vGLUT1 and vGAT (Figure 37), indicating endocytosis overshoot, a process induced by decreases in plasma membrane tension (X. S. Wu et al., 2017); and d) The application of palmitoylcarnitine, a drug shown to intercalate into

membranes to reduce tension, phenocopies mDia1/3-associated endocytosis phenotypes. Consistently, other manipulations of Actin assembly, including perturbation of the Arp2/3 complex, similarly lower tension (Diz-Muñoz et al., 2016; Lieber et al., 2013; X. S. Wu et al., 2017).

Hence, mDia1/3 play critical roles in contributing to cortical tension, serving as one determining force to either gate tension progression or directly modulate changes in global plasma membrane tension downstream of its Actin functions (Figure 73).

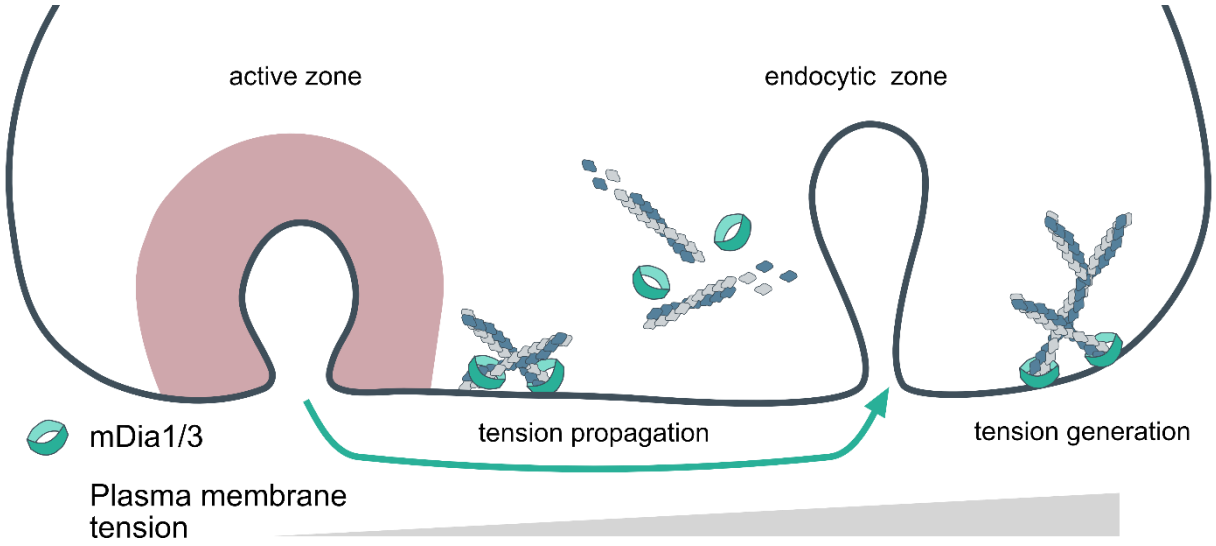

Figure 73: Model for mDia1/3-mediated synaptic Mechanotransduction.
mDia1/3 are mechanosensitive and their Actin functions are regulated by tension (Z. Li et al., 2020). Membrane tension is gated by connections between the plasma membrane and the Actin cortex via membrane-to-cortex attachment proteins, like mDia1/3, acting as a barrier to impede tension propagation (T. K. Fujiwara et al., 2016). Upon exocytosis, plasma membrane tension drops at the active zone and has to be propagated to endocytic areas to induce pit formation and recruitment of BAR proteins (Perez et al., 2022), by decruitment of mDia1/3 from membranes. In addition, outside the endocytic zone a stiff Actin corral keeps the membrane under longitudinal tension to aid membrane invagination via area constriction (Ogunmowo et al., 2023), under the control of mDia1/3 formins (Deguchi et al., 2016).

Taken together, the multifaceted roles of mDia1 in synaptic vesicle endocytosis underscore its significance as a central player in integrating biochemical signaling with mechanical cues at synapses. The various mechanisms include active Actin assembly, modulation of kinase and phosphatase activities, acting as a scaffold function to pre-assemble endocytic machinery, and/or the regulation of cortical tension with local or global consequences. These pathways may act in parallel or intersect in complex ways. For instance, the influence of mDia1 on plasma membrane tension and myosin contractility, can have downstream effects on signaling pathways. Conversely, alterations in signaling pathways can impact membrane tension and contractility. These reciprocal interactions highlight the intricate interplay between biochemical

signaling and mechanical forces mediated by mDia1. Overall, understanding the additive, parallel, or interconnected nature of these events, along with their downstream consequences and upstream regulators, presents a complex but essential aspect of elucidating the role of presynaptic Actin in synaptic vesicle endocytosis and should be subject to future investigations.

6.2. Interdependent Rho GTPase Signaling drives SV Endocytosis

The precise regulation of Actin dynamics at synapses involves the coordinated activities of the small Rho GTPase family, which act as molecular switches to translate extra- and intracellular signals into rearrangements of the cytoskeleton (H. R. Bourne et al., 1990, 1991).

Our study demonstrates that the activities of the small Rho GTPases RhoA/B and Rac1 play fundamental roles in driving the kinetics of synaptic vesicle recycling (Figure 46, Figure 53, and Figure 54) through interdependent signaling mediated by the effector proteins mDia1/3 (Figure 32). In the following, we will discuss how the RhoA effector mDia1 might influence the nucleotide switch cycle of upstream GTPases and elucidate the observed crosstalk between the GTPases Cdc42, Rac1, and RhoA at synapses and its effects on the kinetics of SV endocytosis.

6.2.1. Regulation of synaptic Rho GTPase Signaling

Cellular processes often require the staggered but concerted activity of multiple Rho GTPases, which must be tightly controlled in a spatial and temporal manner (Müller et al., 2020). This dynamic transient activation of Rho GTPase signaling pathways is achieved by modulating their regulatory proteins, such as RhoGEFs (Rho guanine exchange factors), RhoGAPs (Rho GTPase activating proteins), and RhoGDIs (Rho GDP dissociation inhibitors). Here, we identify several RhoGEFs (e.g. β-PIX, GEF-H1, LARG, Intersectin1, Trio, and *Rasgrf*2), RhoGAPs (e.g. ABR, BCR, Myo9B, and p190RhoGAP) and RhoGDI1 in the proximal protein environment of mDia1 (Figure 74) following MS analysis in line with (O'neil et al., 2021).

6.2.1.1. Feedback Regulation of Rho GTPase Activity via Formins

The regulatory proteins identified in the proximal environment of mDia1, such as leukemia-associated RhoGEF (LARG), are known to be modulated by formin activity.

Previous studies have demonstrated that mDia1 can stimulate the activity of LARG (Kitzing et al., 2007) through its FH2 domain (Chikumi et al., 2004), consistent with our results of RhoA downregulation in neurons depleted of mDia1/3 (Figure 49). Such positive feedback loops were described for other formin isoforms, including Daam1 (Habas et al., 2001) and mDia3 (Kitzing et al., 2007) which amplify the levels of active RhoA via unknown mechanisms. Hence, formins can stimulate upstream Rho GTPase activation by directly interacting with and modulating the activity of GEFs, such as LARG, at synapses.

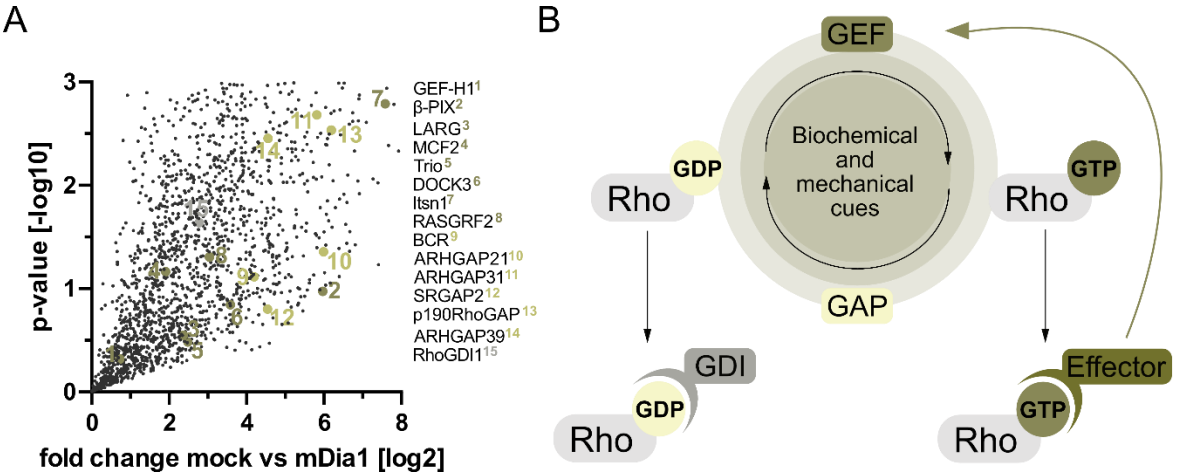

Figure 74: Regulation of synaptic Rho GTPase Signaling.
A: Volcano plot of Rho regulatory proteins in the proximal environment of neuronal mDia1 analyzed by label-free proteomics of biotinylated proteins in neurons transduced with mDia1-TurboID or mock-treated cells. Each dot represents one protein. N = 3 independent experiments. Mass spectrometry was performed by Heike Stepahnowitz.
B: The switch characteristic of Rho GTPase signaling is orchestrated by a diverse range of regulatory proteins, comprising 85 GEFs, 66 GAPs and three GDIs (Bishop & Hall, 2000; Mosaddeghzadeh & Ahmadian, 2021). This complexity integrates various chemical signals, such as kinase/phosphatase signaling, as well as physical cues, including plasma membrane tension. In their GTP-bound form, Rho GTPases activate a broad spectrum (> 70) of effector proteins including kinases, Actin-regulating proteins, and adaptor proteins, whose activities are context-dependent and exert feedback regulation on the preceding cycle.

6.2.2. Crosstalk between Rho GTPases Activities at Synapses

Crosstalk between the canonical members of the small Rho GTPases, in particular the antagonism of Rac1 and RhoA activity, has been well-documented in non-neuronal cells (Chauhana et al., 2011; MacHacek et al., 2009; Nimnual et al., 2003; Ohta et al., 2006; Rottner et al., 1999). The reciprocal relationship between RhoA and Rac1 extends to neuronal processes such as dendritic spinogenesis (Elia et al., 2006), as hyperactive RhoA decreases excitatory synapse density (Govek et al., 2004) which is phenocopied by the loss of Rac1 activity (Nakayama et al., 2000). Consistently, we find

that the attenuation of Rho activity, either pharmacologically (by Rhosin application) or via genetic depletion of formins, leads to the disinhibition of Rac1 signaling at synapses (Figure 50). The antagonistic coupling of RhoA and Rac1 activities is modulated by their regulatory proteins through distinct cellular cues, including phosphorylation and tension regulation, often regulated through feedback mechanisms by downstream effectors.

6.2.2.1. Diversity of regulatory Proteins

A myriad of identified regulators display promiscuity by acting on multiple members of the Rho GTPase family (Boulter et al., 2010; Müller et al., 2020), depending on the cellular context (Figure 74 and Table 9). For instance, Trio possesses two GEF domains capable of binding Rac1 and RhoA simultaneously (Bateman & Van Vactor, 2001), while ABR and BCR contain a GAP domain for Rac1/Cdc42 and a GEF domain for Rac, Rho, and Cdc42 (Chuang et al., 1995; Vaughan et al., 2011). This versatility can give rise to diverse (and overlapping) pathways, governing the crosstalk between the activities of Cdc42, Rac1, and RhoA at synapses downstream of mDia1/3.

6.2.2.2. Biochemical Regulation

Various regulators of the Rho GTPase switch cycle undergo programming via phosphorylation cascades that modulate their affinities toward different members of the Rho GTPase family (DerMardirossian et al., 2006; Oishi et al., 2012; Tkachenko et al., 2011). In our study, we observed increased phosphorylation of Rho GEFs, GAPs, and GDIs following enrichment and analysis of phosphorylated peptides from lysates of neurons depleted of mDia1/3: Upon perturbation of mDia1/3 function, we identified elevated levels of phosphorylated ARHGEF2 (GEF-H1) at $serine_{885}$, a modification known to suppress its GEF activity toward RhoA (Meiri et al., 2012), downstream of PKA (Meiri et al., 2009) or PAK1 (Zenke et al., 2004) signaling. In addition, phosphorylation of the Rac1 GEF, ARHGEF7 (ß-PIX, $serine_{228}$) was altered, possibly impacting its affinity towards Rac1 stimulation (Kuo et al., 2011; Vicente-Manzanares et al., 2011) (Figure 50). We further found increased levels of $tyrosine_{1105}$-phosphorylated ARHGAP35 (p19RhoGAP), implicated in memory formation and plasticity in the hippocampus (Tamura et al., 2006) through the regulation of RhoA activity (B. Yang et al., 2011).

Table 9: Selected Rho GTPase Regulators identified in the Proximity of synaptic mDia1.

Gene	Other Name	Activity for (Müller et al., 2020)			Mechanosensitive	Phospho-regulated by mDia1/3
		Cdc42	Rac1	RhoA		
GEFs						
ARHGEF2	GEF-H1	-	-	+	(Bustos et al., 2008)	+
ARHGEF7	β-PIX	+	+	-	(Boulter et al., 2006)	+
ARHGEF12	LARG	-	-	+	(Guilluy et al., 2011)	+
ARHGEF14	MCF2, Dbs	+	+	+		
ARHGEF23	TRIO	-	+	+		
DOCK3		-	+	-		-
Itsn1	Intersectin1	+	-	-		+
RASGRF2		+	+	+		
GAPs						
ARHGAP13	*SRGAP1*	-	+	-		
ARHGAP21		-	-	+		+
ARHGAP31		+	+	+		
ARHGAP34	*SRGAP2*	+	+	-		+
ARHGAP35	p190RhoGAP	-	+	+	(B. Yang et al., 2011)	+
ARHGAP39		+	+	-		+
MYO9B		+	+	+		
GDIs						
ARGHDIA	RhoGDI1	+	+	+		+

Interestingly, we observed increased levels of regulatory serine$_{34}$-phosphorylation of RhoGDI1 (Arhgdia) in lysates of mDia1+3 depleted neurons, a modification mediated by PKC isoforms downstream of mTORC2 (Dovas et al., 2010). Another PKC effector, the endocytic protein PACSIN1, a dominant interactor of synaptic mDia1 (Figure 40), has been linked to the regulation of Rac1 activity (de Kreuk et al., 2011).

These findings indicate that crosstalk between downregulated RhoA and upregulated Rac1 activity in neurons lacking mDia1/3 formins, likely stems from dysregulation of the activities of associated RhoA/Rac1GEFs (GEF-H1/β-PIX), p190RhoGAP, and RhoGDI1, among others. These changes in the phospho-proteome of RhoGTPase regulators suggest kinase/phosphatase-mediated feedback regulation of RhoA/Rac1 signaling when formins are depleted. Further investigation into the specific kinase/phosphatase networks affected by mDia1/3 knockdown, such as the mTORC2/PKC signaling axis (Dovas et al., 2010; Sabbatini & Williams, 2013) could provide valuable insights into the underlying mechanisms.

6.2.2.3. Mechanoregulation

The antagonism between RhoA and Rac1 activity is coupled to changes in plasma membrane tension (Houk et al., 2012; Katsumi et al., 2002). Cellular stress or hypertension stimulates RhoA activity via GEF-H1 (Guilluy et al., 2011) and p190RhoGAP (B. Yang et al., 2011). In turn, ROCK-mediated myosin contractility enhances Rac1 GAP activity (FILGAP, (Ehrlicher et al., 2011; Ohta et al., 2006); ARHGAP22, (Sanz-Moreno et al., 2008)) to inactivate Rac1 while simultaneously restricting access to its GEF β-PIX (Kuo et al., 2011; Shifrin et al., 2009; Vicente-Manzanares et al., 2011). Conversely, ROCK inhibition has been associated with the stimulation of Rac1 activity (Tsuji et al., 2002) in a Rho-dependent manner (Kitzing et al., 2007).
As discussed before (6.1.4.4), the depletion of mDia1/3 likely reduces cortical tension through the reduction of the Actin cortex and membrane-to-cortex attachments, which is reflected in the dysregulation of mechanosensitive GEF-H1, β-PIX and p190RhoGAP in neurons depleted of mDia1/3.

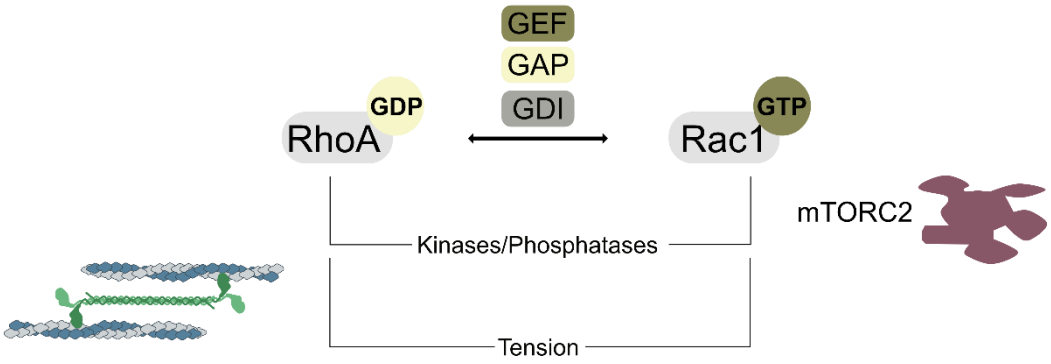

Figure 75: Crosstalk between synaptic RhoA and Rac1 Activities.
The activities of synaptic RhoA and Rac1 are inversely coupled via biochemical and mechanical signaling cascades affecting their regulatory proteins GEFs, GAPs, and GDIs. The reciprocal relationship is mediated by downstream effectors such as non-muscle myosin II and mDia1 that transduce mechanical signals to modulate the activation and/or inactivation of regulatory proteins that downregulate Rac1. Furthermore, effectors can include kinases and phosphatases, like mTORC2 (6.4.1.) that contribute to this crosstalk through phosphorylation events that alter the affinities of regulatory proteins.

In summary, the activities of synaptic RhoA and Rac1 involve their myriad of often promiscuous regulatory proteins, whose affinities are modulated by kinase/phosphatase signaling networks (Figure 57) and/or alterations in plasma membrane tension. Therein, feedback mechanisms play a crucial role in modulating the GTPase switch cycle, where effectors exert influence on specific guanine nucleotide exchange factors (GEFs) or GTPase-activating proteins (GAPs), leading to either positive or negative regulation. Disruption of the activity of Rho GTPase effector formins likely affects these pathways, resulting in the imbalance of Rho GTPase signaling, characterized by the activation of Cdc42 and Rac1 and the inhibition of RhoA in our study.

6.3. Compensation between Actin Signaling Networks

The dynamics of Actin assembly drive a myriad of cellular processes, including vesicular trafficking and cell migration, through a diverse array of Actin regulators and signaling pathways. The Arp2/3 complex, the mediator of Actin branches, has canonically been viewed as the master regulator of cell migration by forming lamellipodia (Pollard T.D. & Kholodenko, 2003). However, cells with disrupted Arp2/3 function retain migratory capability (Rotty et al., 2013; Suraneni et al., 2015), suggesting compensatory mechanisms in the migratory system. Similar redundancy between Actin signaling pathways, due to the complexity of Actin regulatory proteins, has been observed across different organisms, from yeast (Gao & Bretscher, 2008) to neurons (Bingham et al., 2023).

In our study, we observe several indications that interdependent Actin signaling networks are governed in a compensatory fashion at synapses: a) We note a significant discrepancy between acute pharmacological perturbations (SMIFH2 or EHT 1864) and long-term genetic perturbation; b) Our findings reveal redundant roles for closely-related isoforms mDia1 and mDia3 (Figure 32), as well as RhoA and RhoB (Figure 46), in regulating the kinetics of SV endocytosis; c) Depletion of mDia1/3 reduces presynaptic F-Actin abundance (Figure 44), yet mDia-independent pathways can mediate Actin assembly upon perturbation of Dynamin function (Figure 44F); d) Loss of the Rho-mDia1/3 Actin assembly axis triggers the activation of Rac1 (Figure 50), exhibits compensatory effects to ameliorate endocytosis phenotypes upon interference with mDia1/3 (Figure 54).

6.3.1. Redundancy of closely related Regulators of Actin Assembly

The depletion of mDia1/3 produces a less pronounced effect on SV endocytosis kinetics compared to acute pharmacological inhibition of formins using SMIFH2 (Soykan et al., 2017) (Figure 32 and Figure 63). This suggests that additional formins may contribute to SV recycling to compensate for mDia function, a notion supported by previous studies (J. W. Copeland et al., 2004; S. J. Copeland et al., 2007; Litschko et al., 2019; H. Sun et al., 2011). Indeed, our MS analysis identified additional formin isoforms, including DAAM1, FMN2, FMNL2, and FHOD3 (Figure 76A), in close proximity to synaptic mDia1 following MS analysis, indicating that those formins are recruited to similar cellular localizations and could act on similar membranes as mDia1/3 to drive SV endocytosis.

Redundancy among Actin-regulatory proteins is a common phenomenon. For instance, loss of the ABI1 subunit downregulates the formation of WAVE1 and WAVE2 complexes, but upregulates WAVE3 complexes containing ABI2 (Dubielecka, Cui, et al., 2010). Similarly, in neurons, Rac3 can compensate for the loss of Rac1 (Corbetta et al., 2009), RhoB for RhoA (Figure 46) and co-depletion of mDia1/3 further aggravates phenotypes *in vivo* (Thumkeo et al., 2011) and in cellular models (Figure 32) compared to the loss of mDia1 alone.

Hence, isoforms within Actin-regulatory protein families often exhibit redundancy and can compensate for the activity of related family members.

6.3.2. Compensation between Formins and Arp2/3 Signaling at Synapses

In addition to redundant isoforms within the formin family, compensation for formin signaling can occur through an antagonistic relationship with Arp2/3-mediated Actin branching, a conserved crosstalk observed from yeast (Burke et al., 2014) to mammalian cells (Bovellan et al., 2014; Isogai & Danuser, 2018; Rotty et al., 2013). Recent studies employing super-resolution microscopy on reconstituted presynaptic boutons have highlighted the inverse relationship between Arp2/3 and formin signaling in neurons: Inhibition of formins increased Arp2/3-based structures, while blocking Arp2/3 activity stimulated the formation of formin-mediated Actin rails (Bingham et al., 2023). Accordingly, we observe several indications that loss of mDia1/3 formins is partially compensated by increased Arp2/3 mediated Actin assembly, likely mediated through Rho GTPase dependent and independent signaling arms.

Independent of Rho GTPase signaling, proteins directly implicated in orchestrating crosstalk between the formin mDia1 and Arp2/3-mediated Actin nucleation include Abelson interacting proteins (ABI) (Bogdan et al., 2013), subunits of the WAVE complex. Here, we characterize ABI1 and ABI2 isoforms as potent interactors of synaptic mDia1 (Figure 40 and Table 11), localized in close proximity to the formin (Figure 41), dependent on its association with RhoA (Figure 47). This suggests a crucial role for ABI1/2 in regulating mDia1 activity at synapses, consistent with previous data (Courtney et al., 2000). Given an overlapping binding site (Ryu et al., 2009; C. Yang et al., 2007), ABI functions as a molecular switch to coordinate recruitment and activation of mDia formins or WAVE-mediated Arp2/3 signaling. Hence, in cells lacking mDia1 (and mDia3), ABI proteins are increasingly available for WAVE complexing, leading to enhanced downstream Actin branching as antagonistic competition with mDia1 association is removed. We further identify upregulated phosphorylation of $serine_{183}$ and $serine_{177}$ in ABI1 and ABI2, respectively, two residues associated with enhanced WAVE signaling (Jensen et al., 2023) and Arp2/3-based Actin nucleation (Mendoza et al., 2011).
Therefore, our findings indicate that genetic interference with mDia1/3 activity causes ABI-mediated WAVE activation (Lebensohn & Kirschner, 2009) as a compensatory mechanism.

6.3.3. Rho GTPases mediate compensatory Actin Signaling

In this study, we elucidate the dysregulation of Rho GTPase signaling in mDia1/3-depleted neurons, resulting in the stimulation of Rac1 activity as a compensatory response to mitigate endocytic deficits (Figure 54). Furthermore, the overexpression of constitutively active Rac1 can fully rescue defective SV recycling in mDia1/3-depeleted cells, indicating that Rac1 effectors mediate endocytosis in the absence of mDia formins. Given that inhibition of Rac1 reduces presynaptic F-Actin levels (Figure 55), it is likely that the constitutively active Rac1-mediated rescue involves its modulation of the cytoskeleton. Accordingly, overexpression of constitutively active Rac1 restores Actin structures in mDia1-depleted non-neuronal cells (Isogai et al., 2015).

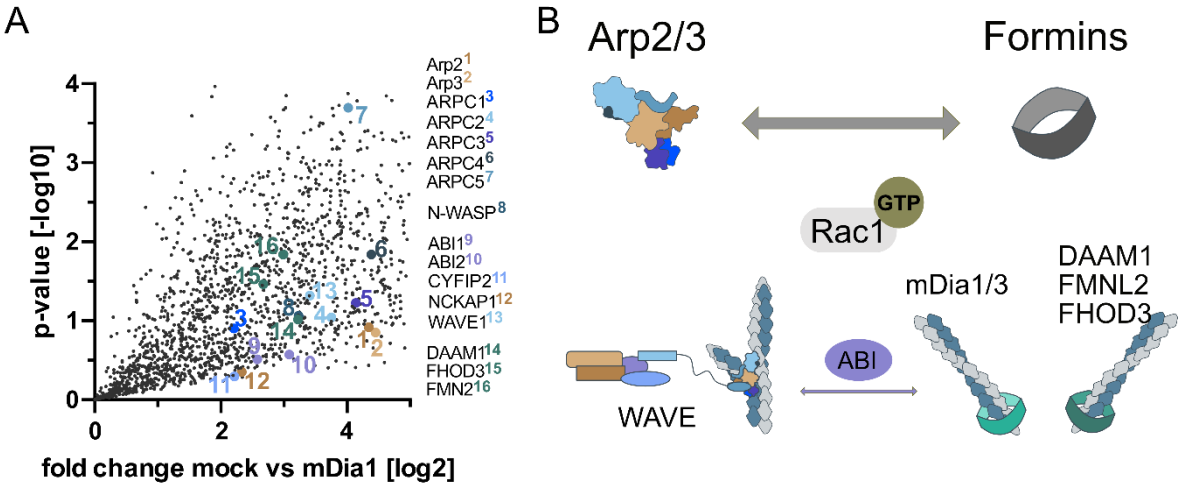

Figure 76: Compensation between Actin Signaling Pathways at Synapses.
A: Volcano plot of Actin regulatory proteins in the proximal environment of neuronal mDia1 analyzed by label-free proteomics of biotinylated proteins in neurons transduced with mDia1-TurboID or mock-treated cells. The logarithmic ratios of protein intensities are plotted against negative logarithmic p-values derived from two-tailed student's t-test. Each dot represents one protein. N = 3 independent experiments. Mass spectrometry was performed by Heike Stepahnowitz.
B: The regulation of Actin dynamics involves resilient pathways capable of compensation. Formins including DAAM1, FMNL2 and FHOD3 can compensate for Actin functions mediated by mDia1/3. This compensatory formin signaling can be modulated by Rac1 activity, which also governs Arp2/3-driven Actin nucleation via stimulation of the WAVE complex. Additionally, Rho GTPase-independent crosstalk between formin and Arp2/3 signaling is orchestrated by ABI proteins, acting as molecular switches between the WAVE complex and mDia activation.

Rac1 is known to stimulate Arp2/3-mediated branched F-Actin nucleation through activation of N-WASP (Tomasevic et al., 2007) and/or the WAVE complex (Ding et al., 2022). Consistent with this, we observe Arp2CA, a subunit of the Arp2/3 complex, and WAVE2 isoforms enriched at presynaptic terminals (Figure 76 and Figure 82). However, upon shRNA-mediated knockdown of mDia formins, we did not observe increased recruitment of Arp2C and WAVE2 to presynaptic sites (Data not shown),

suggesting the presence of additional compensatory pathways. Interestingly, Rac1 can interact with and activate several members of the formin family in mammalian cells (Kühn & Geyer, 2014) including DAAM1 (Matusek et al., 2008), FMNL1 (Favaro et al., 2013; Gomez et al., 2007; Yayoshi-Yamamoto et al., 2000) and FHOD1 (Gasteier et al., 2003; Westendorf, 2001). Therefore, the rescue of mDia1/3-associated endocytic phenotypes could be modulated by the upregulation of closely related formin family members, including DAAM1, FMNL2 and FHOD3 as identified in our MS analysis (Figure 76). Furthermore, we identify RhoGAP srGAP2 in the proximal environment of synaptic mDia1 (Table 9), which forms a complex with FMNL proteins downstream of Rac1 (Mason et al., 2011), indicating the presence of intricate Rho GTPase – formin signaling cascades at synapses. A direct compensatory pathway mediated by additional formin isoforms could substitute all mDia1/3 controlled Actin functions, such as nucleation, polymerization, and stabilization of Actin filaments, albeit at different speeds depending on their gating factors and nucleation efficiency (Harris et al., 2004; Kovar, 2006; Neidt et al., 2009; Shemesh & Kozlov, 2007).

In conclusion, Actin assembly is indispensable for cellular processes, as demonstrated by the lethality associated with the genetic knockout of its isoforms (X. S. Wu et al., 2016). Consequently, the regulatory mechanisms governing cytoskeletal dynamics are diverse and resilient, with individual signaling pathways capable of compensation. At synapses, compensatory signaling involves pathways orchestrated by Rho GTPases, WASP protein-mediated Arp2/3-driven Actin nucleation, and formin activity.

6.4. The Role of mTORC2 in coupling cytoskeleton Dynamics and SV Endocytosis

Studies in yeast have implicated the mechanistic target of rapamycin kinase complex 2 (TORC2) as a critical signaling molecule linking endocytosis and Actin dynamics (Jacinto et al., 2004; Riggi et al., 2019). Similarly, neuronal activity has been shown to activate mTORC2, with its activity scaling in response to the strength of stimulation applied to neuronal cultures (Smillie & Cousin, 2012). In our study, we find that the activity of mammalian mTORC2 is modulated by the formins mDia1/3 at the presynapse (Figure 59) and that its activation impairs the kinetics of synaptic vesicle recycling (Figure 60/Figure 62). In the following chapters, we will discuss the modulation of mTORC2 activity in response to mDia1/3 and its implications on the

synaptic vesicle cycle via its downstream substrates such as protein kinase B (AKT) and protein kinase C (PKC).

6.4.1. Regulation of synaptic mTORC2 by mDia1/3

In this study, we demonstrate that interference with formin activity, either by genetic perturbation (Figure 58) or pharmacological inhibition (Figure 63), leads to the activation of mTORC2, measured by elevated levels of AKT phosphorylation at $serine_{347,}$ at presynaptic boutons. Over the years emerging evidence has broadened our understanding of the diverse array of upstream regulators influencing mTORC2 (An et al., 2021), encompassing environmental and intracellular signals originating from the plasma membrane. These signals may include various metabolites, nutrients like insulin and growth factors, as well as Rho GTPase signaling and mechanotransduction pathways through sensing of membrane tension alterations.

6.4.1.1. Mechanoregulation

In yeast, the relationship between plasma membrane tension and mTORC2 activation is well-established: TORC2 is sequestered in membrane compartments by phase-separated $PI(4,5)P_2$ (Riggi et al., 2018). When tension increases, $PI(4,5)P_2$ is redistributed, leading to TORC2 activation via recruitment of $PI(4,5)P_2$-binding proteins (SLM1/2) from eiosomes (Berchtold & Walther, 2009) (Figure 21). Similarly, in mammalian cells, mechanical stress has been shown to stimulate mTORC2 activity, and genetic depletion of the complex itself increases plasma membrane tension (Diz-Muñoz et al., 2016) Canonically, high mTORC2 activity is associated with elevated plasma membrane tension. However, as we discussed previously (see 6.1.4.4.) the loss of mDia1/3 likely reduces presynaptic plasma membrane tension by decreasing the Actin cortex and disrupting membrane-to-cortex attachments. Therefore, the observed increase in mTORC2 activity following the perturbation of formins (Figure 58) is unlikely to be induced by elevated plasma membrane tension. In line with this notion, the application of palmitoylcarnitine (PalmC), known to decrease membrane tension in yeast (Riggi et al., 2018), stimulates mTORC2 activity in neurons. Furthermore, exposure to hyperosmotic shocks with salt concentrations known to drastically decrease membrane tension within seconds (Roffay et al., 2021) resulted in increases in synaptic AKT1 phosphorylation, albeit to a lesser extent compared to neurons

treated with hypoosmotic solutions (Data not shown). Following these observations, increased mTORC2 activity is not necessarily indicative of elevated tension in neurons. Consistently, other studies have demonstrated that AKT is phosphorylated in an activity-dependent manner at synapses (Smillie & Cousin, 2012), implying that mTORC2 is activated immediately after fusion, when tension is reduced (Perez et al., 2022). Conversely, raising F-Actin abundance by either stimulating mDia activity via IMM application (Figure 58) or treating cells with Jasplakinolide (Figure 64), two conditions known to increase cortical tension (Lembo et al., 2023; Roffay et al., 2021), result in mTORC2 inactivation.

Taken together, the regulation of synaptic mTORC2 appears to be inversely or differentially regulated by tension compared to yeast, and may rely on additional co-factors inducing its signaling, such as $PI(4,5)P_2$ as observed in yeast (Figure 21). Accordingly, studies in non-neuronal mammalian cells have shown that tension alone is insufficient to stimulate mTORC2 activity unless the co-signaling lipid $PI(3,4,5)P_3$ is present (Saha et al., 2023).

6.4.1.2. Phospholipid Regulation

Research in non-neuronal cells has highlighted the co-dependence of AKT phosphorylation at $serine_{473}$ by mTORC2 on increased $PI(3,4,5)P_3$ levels in the plasma membrane (Jacinto et al., 2004; H. Yang et al., 2013). This elevation in $PI(3,4,5)P_3$ releases the mTORC2 complex from autoinhibition (P. Liu et al., 2015). Interestingly, preliminary experiments indicate a reduction in $PI(4,5)P_2$ upon co-depletion of mDia1/3 formins (Figure 81). This reduction in $PI(4,5)P_2$ may suggest its increased conversion to $PI(3,4,5)P_3$, potentially contributing to the observed hyperactivation of mTORC2. $PI(3,4,5)P_3$ is typically generated upon insulin or growth factor stimulation via the activation of class I phosphoinositide 3-kinases (class I PI3K) and is counteracted by the phosphatidylinositol 3,4,5-trisphosphate 3-phosphatase and dual-specificity protein phosphatase (PTEN), whose inhibition enhances mTORC2 activity (Cullen et al., 2023). Consequently, synaptic mTORC2 activity may hinge on the balance between the activities of class I PI3K and PTEN, regulating synaptic $PI(3,4,5)P_3$ levels. This is supported by our findings of significantly enriched levels of the catalytic unit of class I PI3K alpha (p110) as well as its regulatory subunit (p85), as well as the phosphatase PTEN in the synaptic vicinity of mDia1 (Figure 41).

As discussed before (6.3.2.), we identified ABI1/2, a subunit of the WAVE complex, in the synaptic mDia1 interactome as one of its dominant interactors (Table 11), consistent with previous studies (Ryu et al., 2009). Besides its role in WAVE-mediated F-Actin nucleation, ABI has been implicated in modulating class I PI3K activity by directly interacting with the regulatory subunit p85 (Dubielecka, Machida, et al., 2010). This interaction sequesters p85 from inhibiting PI3K, resulting in increased $PI(3,4,5)P_3$ levels (Kotula, 2012). In cells depleted of ABI, phosphorylation levels of AKT are reduced (C. Wang et al., 2007), while elevated ABI expression correlates with increased phosphorylation of AKT (C. Wang et al., 2011) downstream of mTORC2. As mDia1 likely shares an interaction site with p85 on ABI1 (Ryu et al., 2009), the binding of these factors to ABI is mutually exclusive. Thus, the availability of ABI could link mDia1 formin perturbation to the observed increases in mTORC2 signaling, as activation of mDia1 via IMM results in decreased mTORC2 activity (Figure 58), when mDia1 is likely bound to ABI.

The putative elevation in the secondary messenger $PI(3,4,5)P_3$, resulting from the loss of mDia1/3, would likely lead to increased recruitment of proteins carrying a phosphoinositide-binding module (PH domain). Several Rho GTPase regulatory proteins carry PH-domains including Tiam (Fleming et al., 2004), P-REX1 (Hill et al., 2005) and Dbs (Rossman et al., 2002), as identified in the vicinity of synaptic mDia1 (Figure 74). Consequently, elevated $PI(3,4,5)P_3$ levels could amplify Rac1 activation (S. Srinivasan et al., 2003), as observed in our study (Figure 50). In turn, active Rac1 has been demonstrated to bind and recruit regulatory subunit p85, thereby inducing additional PI3K activation and subsequent $PI(3,4,5)P_3$ production in a positive feedback loop (Campa et al., 2015). Hence, alterations in $PI(3,4,5)P_3$ abundance are likely to result in increases in mTORC2 activity and divergent Rho GTPase signaling, consistent with the observations in mDia1/3-depleted neurons.

6.4.1.3. Rho GTPase Regulation

We previously discussed the dysregulation of Rho GTPase signaling, following genetic depletion of mDia1/3, resulting in increased activity of Rac1 and elevated levels of Rho-GDP (Figure 49 and Figure 50). Interestingly, both GTPases have been implicated in the modulation of mTORC2 activity: Insulin stimulation activates mTORC2 via a super complex involving RhoA-GDP (stabilized by phosphorylation of $serine_{188}$ by protein kinase A) facilitating glucose transporter 4 (GLUT4) translocation to the

plasma membrane (Senoo et al., 2019, 2021). Conversely, GTP-bound RhoA inhibits mTORC2 activity (Senoo et al., 2020). Consistent with these studies, the application of the pan-Rho inhibitor Rhosin, enhanced the phosphorylation of AKT at serine$_{473}$ in neuronal lysates (Data not shown), suggesting that reduced RhoA activity in mDia1/3-depleted cells may directly stimulate mTORC2 activity via super complex formation. In addition, the inversely coupled activity of Rac1 has been shown to directly interact and regulate mTORC2 independently of PI3K (Saci et al., 2011) downstream of canonical Wnt signaling (Esen et al., 2013). Accordingly, we observe that inhibition of pan-Rac signaling by treatment with EHT 1864, reduces cellular mTORC2 activity (Data not shown).

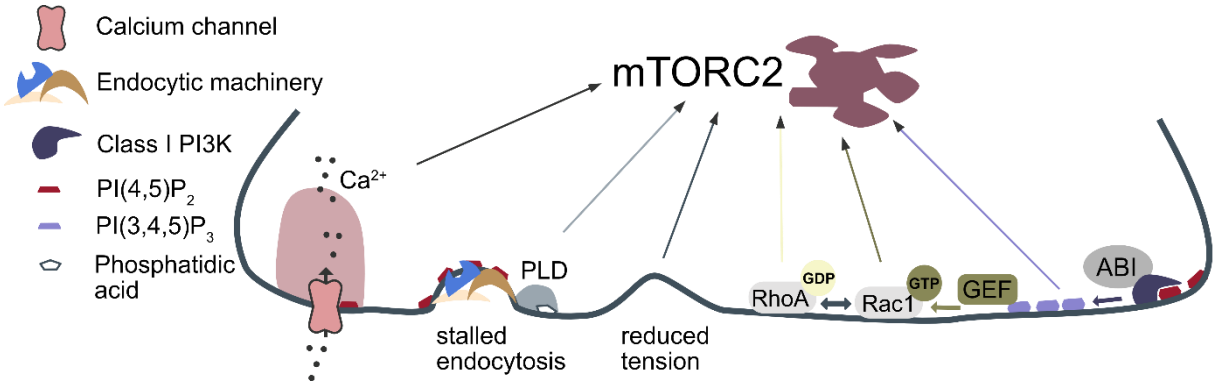

Figure 77: Factors contributing to synaptic mTORC2 Regulation.
The regulatory mechanisms governing synaptic mTORC2 differ from its mechanoregulation in yeast. At synapses, mTORC2 is multifaceted and influenced by various factors, including elevated calcium levels, tension alterations, and changes in plasma membrane composition. For instance, phospholipase D (PLD), recruited by the endocytic machinery, generates choline and phosphatidic acid, facilitating mTORC2 activation. In addition, synaptic mTORC2 is modulated by PI(3,4,5)P_3 synthesis downstream of class I phosphoinositide 3-kinase (*PI3K*) and Abelson interacting proteins (ABI). Concurrently, numerous Rac1 guanine nucleotide exchange factors (GEFs) are recruited and activated by PI(3,4,5)P_3 which stimulate GTP-loading of Rac1. Consequently, active Rac1 exerts downregulatory effects on RhoA through antagonistic feedback regulation. Notably, both Rac1-GTP and RhoA-GDP directly influence mTORC2 activity through direct interactions with the complex.

In summary, the variety of upstream regulators of mTORC2 suggests a complex interplay involving phospholipid dynamics, Rho GTPase-mediated cytoskeletal signaling, and alterations in cortical tension (Figure 77). The perturbation of mDia1/3 formins likely intersects with these pathways by impacting Actin dynamics, modulating membrane phospholipid composition, and disrupting Rho GTPase signaling. The discussed feedback and crosstalk mechanisms possibly integrate mammalian mTORC2 and Rho GTPase signaling via the co-factor PI(3,4,5)P_3, intricately linking downstream cytoskeletal dynamics and membrane tension homeostasis, diverging from tension regulation observed in yeast. Future studies are imperative to elucidate causal relationships amidst this intricate network.

6.4.2. Coupling between mTORC2 and Synaptic Vesicle Endocytosis

The yeast homolog TORC2 is known to modulate endocytosis, yet its activity is also inversely regulated by endocytosis in a negative feedback loop (Ebner et al., 2020). Similarly, we observe a negative coupling mechanism between synaptic vesicle endocytosis and mammalian mTORC2 signaling, where impaired endocytic kinetics generally coincide with increased mTORC2 activity (Figure 58, Figure 60, Figure 62, Figure 63, and Figure 66). However, whether mTORC2 activity is a consequence or the cause of the observed perturbation in endocytosis remains to be elucidated. In the following we will discuss the order of events underlying the coupling of mTORC2 regulation and endocytosis induction.

6.4.2.1. Neuronal activity-dependent Activation of mTORC2

As discussed before (see 6.1.4.3), the endocytic machinery is organized into pre-assembled molecular condensates through liquid-liquid phase separation (LLPS) (Imoto et al., 2022), facilitating ultrafast endocytosis kinetics. Interestingly, mTORC2 has been demonstrated to undergo inactivation by LLPS in yeast (Riggi et al., 2018), suggesting that similar regulatory mechanisms may operate on mTORC2 at synaptic terminals. Consistent with this idea, we find the mTORC2 specific subunit Rictor concentrated at presynaptic membranes (Figure 61). The condensates of the endocytic machinery are disassembled upon exocytosis, triggered by Ca^{2+}-influx or alterations in membrane homeostasis. In yeast, the formation of TORC2 condensates is mediated by $PI(4,5)P_2$ (Riggi et al., 2018), whose lateral distribution is known to depend on calcium concentration (Bucki et al., 2019; Y. H. Wang et al., 2012). Accordingly, mTORC2 is stimulated in a dose-dependent manner based on stimulation strength (Smillie & Cousin, 2012), underscoring that synaptic mTORC2 activation scales with Ca^{2+}-concentration in the presynaptic terminal, consistent with other studies (Merhi et al., 2017).

In such a model, mTORC2 is sequestered and inactive within presynaptic condensates at steady-state, becoming activated by exocytic fusion, which resolves LLPS of both endocytic machinery and mTORC2 (Sansevrino et al., 2023), resembling the regulation of TORC2 in yeast (Figure 20, (Riggi et al., 2018)).

6.4.2.2. The endocytic Machinery modulates mTORC2 Activity

The activation of mTORC2 in mDia1/3-depleted cells can be attributed to several factors, including ABI proteins, PI(3,4,5)P_3, and Rho GTPases. However, we also observe increased mTORC2 activity in conditions where endocytosis is blocked independent of mDia1/3 (Figure 58, Figure 60, Figure 62, Figure 63, and Figure 66), suggesting that delayed endocytosis in general stimulates mTORC2 activation. Moreover, the activation of mTORC2 correlates with the perturbation of endocytosis; specifically, more significant delays in endocytosis kinetics, result in increased activation phenotypes (Compare SMIFH2 (Figure 63) with shmDia1/3 (Figure 32 and Figure 58)). Inhibition of endocytosis leads to the accumulation of stalled endocytic machinery (Raimondi et al., 2011), potentially influencing mTORC2 indirectly via alterations in membrane composition catalyzed by Phospholipase D (PLD). The endocytic machinery, including Synaptojanin1 and Amphiphysin (Chung et al., 1997; C. Lee et al., 1997, 2000), has been shown to act on PLD1/2, converting phosphatidylcholine into choline and phosphatidic acid (PA). In turn, PLD2 and its product PA have been associated with mTORC2 activation (Diz-Muñoz et al., 2016; Hornberger et al., 2006; Toschi et al., 2009). Furthermore, PA presents an important co-factor for PI(4,5)P_2 synthesis, and depletion of its synthesizing enzyme (DAG kinase) impairs SV endocytosis (Goldschmidt et al., 2016). Interestingly, Rac1 has also been shown to mediate PLD1 activation and increase PA plasma membrane levels (Gomez-Cambronero, 2011; Momboisse et al., 2009).
In summary, PLD isoforms could act as mammalian SLM orthologs (Figure 21), linking mTORC2 and endocytic proteins at membrane invaginations analogous to yeast eisosomes (Echarri & Del Pozo, 2015). Hence, mTORC2 at synapses could be regulated by exo- and endocytic balance, which is sensed via the lipid composition of the membranes.

6.4.2.3. mTORC2 negatively regulates Synaptic Vesicle Endocytosis

Our study emphasizes the inverse coupling between mTORC2 signaling and synaptic vesicle endocytosis. As discussed above, blocked endocytosis could cause mTORC2 activation (Figure 58, Figure 60, Figure 62, Figure 63, and Figure 66). Now, we explore how mTORC2 activity can, conversely, cause the perturbation of synaptic vesicle recycling. Our findings indicate that mTORC2 can serve as an upstream regulator of

synaptic vesicle endocytosis, and its hyperactivity, following formin perturbation, impedes the kinetics of SV recycling, as pharmacological inhibition (Figure 60) or genetic depletion of mTORC2 subunit *Rictor* (Figure 62) rescues endocytosis kinetics in neurons deficient of mDia1/3. While the activity of its downstream kinase, AKT, is indispensable for SV endocytosis (Figure 65) (Smillie & Cousin, 2012), the analysis of *bona fide* targets of mTORC2 in brains of *Rictor*-KO mice revealed the most pronounced alterations in isoforms of the PKC family (PKCα, β, γ, ε) and their downstream substrates, myristoylated alanine-rich C-kinase substrate (MARCKS) and growth-associated protein 43 (GAP43) (Thomanetz et al., 2013). Consistent with these findings, we observe substantial perturbations in the phosphorylation of MARCKS and GAP43 in lysates of mDia1/3-depleted neurons, when mTORC2 activity is elevated (Table 11) highlighting the PKC family as the principal downstream substrates of mTORC2 at synapses.

Interestingly, PKC activity phosphorylates the microtubule-binding protein tau (Correas et al., 1992; Kumar et al., 2015), whose hyperphosphorylation presents a hallmark of Alzheimer's disease (Ando et al., 2021). Consequently, gain-of-function mutations of PKC cause neurodegeneration (Adachi et al., 2008; Verbeek et al., 2008; Yamamoto et al., 2010). As mDia1 has been implicated in regulating tau-mediated synaptotoxicity (Qu et al., 2017), this phenotype might be linked to its upregulation of the mTORC2-PKC signaling axis.

In the following, we will discuss how elevated PKC activity may impede SV endocytosis by acting on the endocytic machinery, in particular through the cytoskeleton, alterations in the phospholipid composition of the plasma membrane or direct modulation of other endocytic factors.

mTORC2 negatively regulates the Cytoskeleton

We observe increased phosphorylation of MARCKS and GAP43 in mDia1/3-depleted cells. MARCKS and GAP43 are Actin-crosslinking proteins that insert into lipid bilayers via myristoylation and palmitoylation, respectively (McLaughlin & Aderem, 1995). They are localized at the plasma membrane by binding and sequestering $PI(4,5)P_2$ (Laux et al., 2000) (Figure 78). Activation of PKC downstream of mTORC2 (and calcium) phosphorylates MARCKS and GAP43, leading to their dissociation from the PM into the cytosol (Figure 78). Consequently, crosslinks of the plasma membrane and the cytoskeleton are weakened (Wohnsland et al., 2000). In addition, we found hyperphosphorylation of the PKC substrates Adducins (α, β, γ; Table 11, (Thomanetz

et al., 2013) in lysates of mDia1/3-depleted neurons. Phosphorylation of Adducins modulates their capping functions and promotes free barbed-end depolymerization, resulting in decreased F-Actin abundance (Matsuoka et al., 2000), observed in presynaptic boutons lacking mDia1/3 (Figure 44).
Thus, synaptic mTORC2 likely regulates the kinetics of SV endocytosis by modulating cortical tension through reducing the Actin cortex (via Adducins) and the number of membrane-to-cortex attachments (via MARCKS/GAP43) as seen in non-neuronal mammalian cells (Diz-Muñoz et al., 2016) and yeast (Jacinto et al., 2004; Riggi et al., 2019).

mTORC2 regulates Phospholipids
The release of MARCKS and GAP43 into the cytosol upon activation of the mTORC2-PKC axis makes plasma membrane $PI(4,5)P_2$ available for various cellular processes like endocytosis (Laux et al., 2000), and class I PI3K signaling to generate $PI(3,4,5)P_3$ (Ziemba et al., 2016). Consequently, studies have shown that mTORC2 activation coincides with a decrease in $PI(4,5)P_2$ (Ono et al., 2022). Consistent with this, we observe a reduction in $PI(4,5)P_2$ in mDia1/3-depleted neurons (Figure 81), suggesting dysregulated signaling pathways involving $PI(4,5)P_2$ synthesis or conversion (Figure 4) upon mTORC2 activation at synapses. Conversely, perturbation of mTORC2 activity by genetic depletion of Rictor or AZD 3147 treatment increased synaptic PI(4,5)P2 levels in preliminary experiments (Figure 81). $PI(4,5)P_2$ serves as a critical signaling molecule driving the endocytic process at synapses (Bolz et al., 2023), by modulating interactions with the cytoskeleton or endocytic proteins (Figure 5).
Therefore, hyperactive mTORC2 could impede SV endocytosis by affecting phospholipid synthesis through the modulation of lipid kinases and/or phosphatases, leading to the reduction of $PI(4,5)P_2$.

mTORC2 signals to the endocytic Machinery
Apart from its effects on the cytoskeleton and phospholipid levels, mTORC2 may play an additional role in regulating endocytic protein activity through phosphorylation. Specifically, PKC has been implicated as a calcium sensor (Jin et al., 2019) leading to the phosphorylation of endocytic proteins, such as F-BAR proteins PACSIN1 (Plomann et al., 1998) and PACSIN2 (Senju et al., 2015), potentially modulating their recruitment to endocytic sites. Additionally, PKC isoforms, along with AKT1, can phosphorylate and inactivate glycogen synthase kinase-3β (GSK-3β) (Eng et al., 2006; Isagawa et al.,

2000), which negatively regulates Dynamin activity at the presynapse (Smillie & Cousin, 2012). The constitutive blockage of Dynamin1 re-phosphorylation following increased mTORC2 activity impairs endocytic pathways ((Smillie & Cousin, 2012), potentially disrupting the coordinated regulation of Dynamin and/or its ability to form reactive condensates, as discussed previously (Imoto et al., 2022).
Consequently, mTORC2 and its downstream substrates could influence endocytosis kinetics by modulating the activities of proteins crucial for driving membrane invagination (e.g., PACSINs) or scission (e.g., Dynamins) (Figure 78).

mTORC2 regulates Rho GTPase Signaling

As iterated above, mTORC2 serves as a negative regulator of SV endocytosis. Consequently, its inhibition can rescue defective pHluorin-retrieval in conditions where mTORC2 activity is elevated (Figure 60/Figure 62). In addition to the mechanisms discussed earlier, there is increasing evidence that inhibition of mTORC2 enhances Actin signaling via the activation of Rac1 and WAVE-mediated Actin assembly (Diz-Muñoz et al., 2016). Consistent with this, we find increased levels of Rac1-GTP in neurons depleted of the mTORC2-specific subunit *Rictor* (Figure 64). Interestingly, co-depletion of *Rictor* together with mDia1/3 further elevated Rac1-GTP levels (Data not shown), indicating that mDia1/3 or *Rictor* loss activates Rac1 through distinct pathways. Since overexpression of constitutively active Rac1 ameliorates phenotypes of SV retrieval in Synaptophysin-pHluorin assays in cells depleted of mDia1/3 (Figure 54), inhibition of mTORC2 could similarly rescue defective SV endocytosis by enhancing Rac1 activation and Actin abundance (Diz-Muñoz et al., 2016). Hence, Rac1 activity might be the crucial component to drive the restoration of SV endocytosis kinetics upon mTORC2 inhibition in mDia1/3-deficient neurons.
The literature indicates that mTORC2 signaling influences several key members of the Rho GTPase family, including Cdc42 (Martinez-Lopez et al., 2023), Rac1 (Saha et al., 2023) and RhoA (L. Liu et al., 2010; Saha et al., 2023), either through direct interactions or by indirectly stimulating GTPase regulatory proteins, such as guanosine exchange factors Tiam1 (Huang et al., 2013) and P-Rex1 (Hernández-Negrete et al., 2007), as well as RhoGDI1 (Mehta et al., 2001) and RhoGDI2 (Agarwal et al., 2013).

Furthermore, the mTORC2 substrate AKT has been shown to directly phosphorylate Rac1 at serine$_{71}$, inducing conformational changes that sterically hinder its binding to GTP (T. Kwon et al., 2000). Consequently, Rac1 activity is enhanced in cells depleted of the mTORC2-specific subunit *Rictor* (Saha et al., 2023). Moreover, the

neuron-specific loss of *Rictor* increases dendritic complexity (Thomanetz et al., 2013), a phenotype associated with the hyperactivation of Rac1 (Z. Li et al., 2000). Conversely, high mTORC2 activity can reduce dendritic arborization through PKC-mediated phosphorylation of MARCKS (A. M. Garrett et al., 2012; Z. Li et al., 2000) affecting Arp2/3 localization and Actin assembly (Q. Yang et al., 2013), highlighting the bidirectional control of Rac1 activity by mTORC2.

In addition to its role in cytoskeletal regulation, Rac1 has been implicated in the regulation of various endocytic factors including class I PI3Kinases, Endophilins (Tyckaert et al., 2022), Synaptojanin2 (Malecz et al., 2000), IQGAP1 and Phospholipase D1. Therefore, an mTORC2-Rac1 axis could contribute to SV endocytosis independently of Actin signaling.

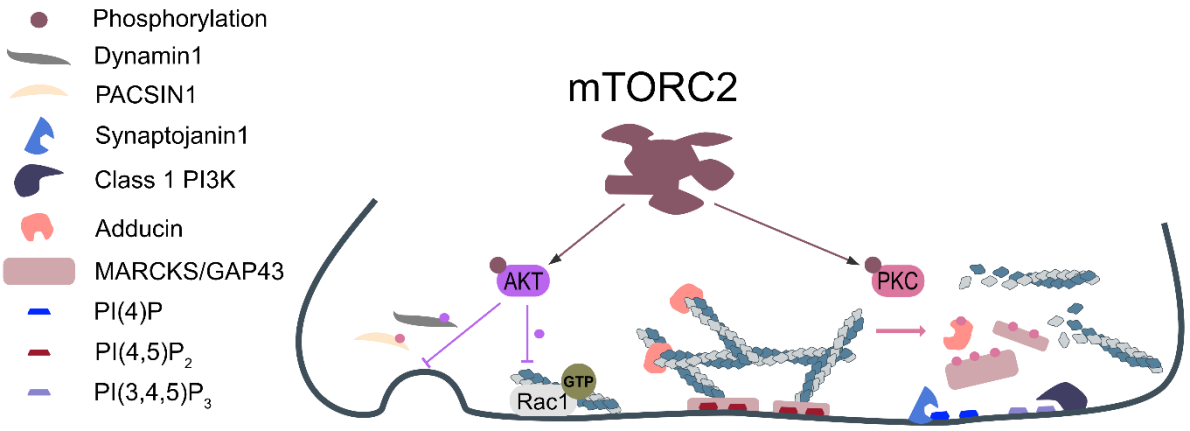

Figure 78: mTORC2 negatively regulates Synaptic Vesicle Endocytosis.
Synaptic mTORC2 influences synaptic vesicle endocytosis by acting on its downstream effectors protein kinase B (AKT) and protein kinase C (PKC). Through direct phosphorylation, mTORC2 activation inhibits endocytic membrane scission by modulating the activity of PACSIN1 (via PKC) and Dynamin1 (via AKT and its downstream kinase GSK3β). The mTORC2 signaling pathway also impacts Rac1-mediated Actin cytoskeleton remodeling by phosphorylating Rac1 directly (downstream of AKT) and/or regulating the activities of its regulatory GEFs and GDIs (downstream of PKC). In addition, hyperactive PKC phosphorylates membrane-to-cortex attachment proteins MARCKS and GAP43 resulting in their dissociation from the membrane. This liberation of $PI(4,5)P_2$ facilitates its uptake via endocytosis or conversionto $PI(3,4,5)P_3$ or PI(4)P by class I PI3K or Synaptojanin1, respectively. Furthermore, constitutive PKC activity likely causes disassembly of the Actin cortex by inactivating Actin-capping proteins, such as Adducins, thereby contributing to the sustained perturbation of endocytosis.

In summary, mTORC2 activity potentially contributes to endocytosis at synapses through multiple mechanisms: a) Regulation of the Actin cytoskeleton via Rho GTPase signaling and membrane-to-cortex attachments; b) Modulation of phospholipid identity and membrane composition affecting protein interactions (Ono et al., 2022); and/or c) Phosphorylation-mediated dysregulation of endocytic proteins. Similar to yeast, where TORC2 regulates endocytosis through both rapid phosphorylation cascades of endocytic proteins (Bourgoint et al., 2018; Roelants et al., 2017) and slower

alterations in plasma membrane biophysical properties (Rispal et al., 2015), neuronal mTORC2 may employ parallel pathways to control synaptic endocytosis.

Our study highlights mTORC2 as a crucial mediator linking the dynamics of synaptic vesicle endocytosis with the cytoskeleton. In healthy cells, mTORC2 activity correlates with neurotransmitter release, likely orchestrating the synchronization of exocytic fusion and endocytosis induction. This process involves calcium-mediated modulation of phospholipid composition via its downstream effector PKC. Active PKC promotes the liberation of $PI(4,5)P_2$, facilitating the recruitment of the endocytic machinery and/or cytoskeletal regulatory proteins. Throughout our investigation, we have uncovered a tightly interconnected network involving regulators of the cytoskeleton, such as mDia1/3 and Rho GTPases, phospholipids, and mTORC2, orchestrated through intricate crosstalk mechanisms. Perturbations in any of these factors can have profound effects on the activities of others, leading to the establishment of positive and negative feedback loops. Ultimately, these interactions play a crucial role in modulating the endocytosis of synaptic vesicles and highlight the resilience that exists within the Actin cytoskeleton at synapses.

7. Conclusion and Outlook

Towards a Model for presynaptic Actin in Synaptic Vesicle Endocytosis

To understand the role of Actin dynamics in synaptic vesicle endocytosis, we contextualize the findings of this study with previous data.

7.1. Distinct pools of presynaptic Actin

Emerging evidence indicates that Actin governs the synaptic vesicle cycle in multiple ways by forming distinct cytoskeletal structures found at the active zone, the endocytic zone, in the cytosol, and between the pools as connecting modules (Figure 79). At the active zone, an Actin mesh (Bingham et al., 2023) is mediated by Arp2/3 activity (O'neil et al., 2021), but independent of Rac1 (Figure 54). This mesh modulates active zone architecture (Hirokawa et al., 1989) and functions as a barrier to restrict vesicle mobility (Rothman et al., 2016) and exocytosis (Aunis & Bader, 1988; Morales et al., 2000). Linear Actin filaments form rails (Siksou et al., 2007) that connect the presynaptic membrane and pools of synaptic vesicles in the presynaptic cytosol (Figure

79). These rails are formin-dependent (Bingham et al., 2023) and mediate vesicle trafficking via myosin activity (González-Forero et al., 2012; Maschi et al., 2018; A. Peng et al., 2012; G. Srinivasan et al., 2008) between the endocytic zone and storage pools, as well as the reserve pool and the active zone (Bloom et al., 2003; Sakaba & Neher, 2003). Around the reserve pool, Actin acts as a scaffold (Sankaranarayanan et al., 2003) to cluster synaptic vesicles together via synapsins governing vesicle replenishment and synaptic depression downstream of Rac1 (Keine et al., 2022; O'neil et al., 2021). A rigid cluster at the periactive zone (Ogunmowo et al., 2023), resembling a branched Actin corral (Y. C. Li et al., 2010) is anchored to the plasma membrane to constrain, shape, and retain its components (Deguchi et al., 2016) by keeping it under longitudinal tension, which might also serve as a clustering machinery of endocytic proteins (6.1.4.4).

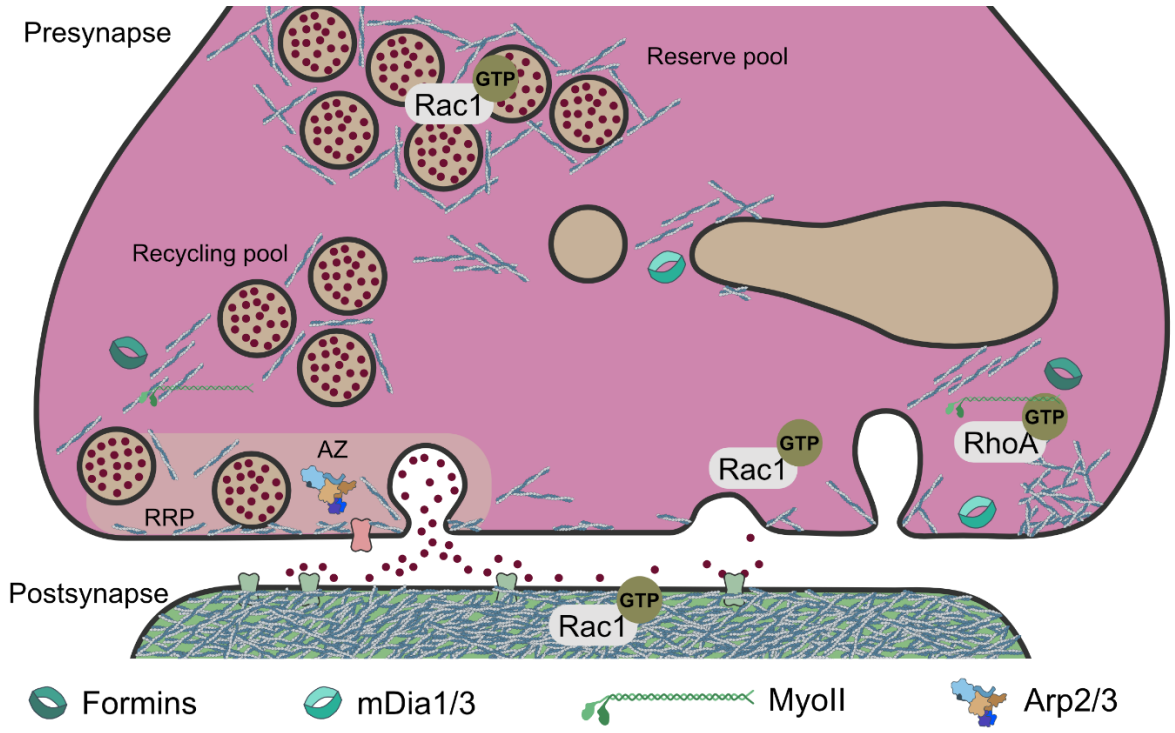

Figure 79: Regulation of presynaptic F-Actin Pools by Rho GTPases, Formins and the Arp2/3 Complex.
Presynaptic Actin forms distinct pools that participate in the SV cycle. At the active zone an Arp2/3-mediated network modulates a barrier function for SV fusion. Linear rails connect the presynaptic membrane (the active and endocytic zone) with synaptic vesicle pools, which are dependent on formin and non-muscle myosin II (MyoII) activity downstream of RhoA signaling. Conversely, Rac1 can be found at the post- and presynapse regulating Actin at the reserve pool and at the endocytic zone. RhoA and mDia1/3 act on the presynaptic membrane to modulate the rigid endocytic Actin corral keeping the membrane under tension and likely regulate transient endocytic Actin assembly pools.

Lastly, a transient pool of Actin that can be targeted by pharmacological manipulation (Soykan et al., 2017), controls SV endocytosis independent of Arp2/3 (O'neil et al., 2021), to provide mechanical force for the scission of endocytic vesicles from the

plasma membrane and/or from endosome-like vacuoles (ELVs). However, detecting this transient pool proves challenging due to its rapid turnover. Interestingly, this pool becomes observable only upon inhibition of endocytosis, e.g., by perturbing Dynamin function (Figure 43).
Following our results, we anticipate mDia1/3 to contribute to the assembly of the transient F-Actin pool and the maintenance of the rigid corral, which regulates plasma membrane tension homeostasis and bouton architecture (Figure 34 and Figure 35). In contrast, acute manipulation of formin activity through SMIFH2 application likely impacts solely the dynamics of the transient endocytic assembly pool, offering a potential explanation for the differential phenotypes observed (Soykan et al., 2017).

7.2. Compensation between Actin Signaling Pathways

In our study, we demonstrate that synaptic Actin signaling operates through interconnected pathways capable of compensating for perturbations in individual components. Specifically, we show that formin signaling, mediated by mDia1/3 activity, regulates the activation status of Rho GTPase regulators that can govern compensatory Actin responses. The presence of numerous regulatory proteins within synapses (Figure 74) underscores the redundancy and diversity inherent in the Rho GTPase signaling network. Various guanine nucleotide exchange factors (GEFs) and GTPase-activating proteins (GAPs) are likely present within the discrete presynaptic Actin pools, forming context-specific signaling cascades that modulate morphology and the synaptic vesicle cycle. Compensatory responses between Actin networks are likely facilitated by pivotal molecules enabling the crosstalk between Rho GTPases on the molecular level (such as ABI), but further investigation is required for a comprehensive dissection of such pathways.

7.3. Controversy of Actin Manipulation revisited

Our findings delineate the presence of distinct pools of Actin and the effective compensatory coupling between components of cytoskeletal remodeling, thereby shedding light on the longstanding controversy surrounding the role of Actin in the synaptic vesicle cycle (Babu et al., 2020; J. Bourne et al., 2006; Cole et al., 2000;

Delvendahl et al., 2016; Z. Hua et al., 2011; Z. Li & Murthy, 2001; Morales et al., 2000; Ogunmowo et al., 2023; Rampérez et al., 2019; Richards et al., 2004; Sakaba & Neher, 2003; Sankaranarayanan et al., 2003; Soykan et al., 2017; S. Watanabe, Rost, et al., 2013; L. G. Wu & Chan, 2022). Pharmacological interventions lead to widespread disturbances in global Actin dynamics, yet specific Actin pools act locally. Hence, we envision the conflicting results to stem from the differential accessibility of chemicals to enter distinct Actin subsynaptic structures and/or from differences in the duration of perturbation (acute versus long-term manipulation) impacting compensatory signaling.

For example, phenomena such as liquid-liquid phase separation observed in the reserve pool (Song & Augustine, 2023; M. Zhang & Augustine, 2021) and at the presynaptic membrane (Imoto et al., 2022; Sansevrino et al., 2023) could impede the penetrance of chemicals into local pools (Bleckert et al., 2012) resulting in varying degrees of Actin disruption across different experimental setups (Cingolani & Goda, 2008; Papandréou & Leterrier, 2018).

Moreover, the duration of pharmacological manipulation likely contributes to the strength and precision of compensatory signaling. Consistently, we observe more drastic effects on SV recycling by acute pharmacological perturbation (Figure 63) compared to long-term genetic interference (incubation with viral particles expressing shmDia1+3 for > 12 days, Figure 32), indicating that compensatory adaption is not instantaneous but requires time to fine-tune resilient Actin signaling responses. Shorter adaptation periods likely also account for differences in ultrastructural phenotypes observed in EM. For instance, acute perturbation of Rac1 or formins leads to accumulations of invaginations due to blocked endocytosis, while genetic perturbation results in additional phenotypes, such as enhanced numbers of endosome-like vacuoles (Figure 34/Figure 35, (Soykan et al., 2017)). Furthermore, the timing of perturbation (age of culture) contributes to the efficiency of compensatory Actin signaling, as cytoskeletal disruption is more severe in young cultures (DIV 5-6) (Hori et al., 2022; W. Zhang & Benson, 2001).

The redundancy identified in this study is possibly one of the origins of the varying outcomes of pharmacological manipulations that were observed before. Such compensatory mechanisms elucidate the difference between studies employing pharmacological interference with Actin regulators versus the direct genetic depletion of cytoskeletal Actin monomers (Ling Gang Wu, 2016).

Future advances in microscopic technology, combined with induced genetic or pharmacological manipulation techniques, enabling the modulation and visualization of specific presynaptic Actin structures in a temporally and spatially controlled manner, including the transient endocytic pool, will be essential for further elucidating the role of Actin in synaptic vesicle endocytosis.

7.4. Mechanical and biochemical Cues drive Synaptic Vesicle Endocytosis

In our work, we elucidate that the Actin cytoskeleton contributes to the kinetics of SV recycling by integrating biochemical and mechanical cues involving phospholipids, Rho GTPases and kinase/phosphatase signaling pathways. Specifically, the cytoskeleton modulates plasma membrane homeostasis by active force generation or passive cortical tension regulation (Figure 73) and presynaptic signaling networks via the mechanistic target of rapamycin complex 2 (mTORC2) (Figure 77).

7.4.1. Actin Contributions to Plasma Membrane Homeostasis

Here, we identify significant roles for the activities of Rac1 and RhoA/B in modulating the kinetics of synaptic vesicle endocytosis (Figure 46 and Figure 53). Interestingly, their canonical downstream Actin structures, lamellipodia and stress fibers, respectively (Figure 16), are visually absent in presynaptic boutons. Instead, presynaptic membrane-associated Actin structures form a thin layer underneath the plasma membrane (Figure 16), resembling the Actin cortex in non-neuronal cells, consisting of three to five filaments of Actin (Shirai et al., 2017). Accordingly, neuronal membrane tension is in the range of 0.01 mN/m (Hochmuth et al., 1996), comparably low with respect to other cell types, likely as a result of limited cortical Actin and membrane-to-cortex attachment proteins. Reduced tension of the neuronal plasma membrane might be an essential paradigm for exo- and endocytic coupling at synapses with membrane reservoirs enabling the ultrafast and efficient initiation of endocytosis. Further literature supports such notion, as even under dramatic osmotic pressure, neuronal plasma membrane tension only moderately increases (Dai et al., 1997; Wan et al., 1995), indicating a high capacity for osmotic resilience.

Alterations in tension downstream of perturbations of Actin may dictate the predominant pathway of endocytosis, as supported by findings from (Boulant et al., 2011). Notably, ultrafast endocytosis induced by 1 AP stimulation exhibits a strong

dependence on the Actin cytoskeleton in mouse hippocampal cultures (S. Watanabe et al., 2014), while action potential trains do not affect other forms of endocytosis in the same model system (Y. Hua et al., 2011; Z. Li & Murthy, 2001; Sankaranarayanan et al., 2003). Consistently, we find that perturbation of mDia1/3 activity yields more pronounced kinetic phenotypes with reduced stimuli (Figure 32). Hence, the depletion of F-Actin in mDia1/3-deficient cells impedes ultrafast endocytosis kinetics (6.1.4.3), while facilitating activity-dependent bulk endocytosis as a compensatory pathway on a slower timescale due to reduced tension (6.1.4.4) and increased Rac1/Cdc42 signaling, consistent with (Kokotos et al., 2018). This model also provides insights into the accumulation of ELVs as the predominant intermediates derived from bulk endocytosis (Figure 34 and Figure 35) in electron microscopy, in contrast to findings from acute perturbation (Soykan et al., 2017).

7.4.2. Actin Contributions to biochemical Signaling via mTORC2

In addition to the possible mechanical effects of Actin manipulation on SV kinetics, our study reveals that the interference with Actin regulatory factors mDia1/3 modulates presynaptic signaling cascades (Figure 57 and Table 11). We identify that mDia1/3 negatively regulate the signaling network mediated by the mechanistic target of rapamycin complex 2 (mTORC2). This negative regulation is conducive to the kinetics of SV endocytosis, as constitutive mTORC2 activation impairs SV recycling and Actin remodeling (Figure 60 and Figure 64). However, mTORC2 might also play an important role in coupling neurotransmitter release and the induction of endocytosis (6.4.2.1).

While the TORC2-mediated Actin axis is well described in yeast, tissue-specific deletion of the mTORC2 subunit *Rictor* did not result in significant Actin phenotypes in skeletal muscle (Bentzinger et al., 2008), adipocytes (Cybulski et al., 2009), liver (Hagiwara et al., 2012), or kidney (Gödel et al., 2011). In contrast, *Rictor* and mTORC2 play a pivotal role in brain function (Shiota et al., 2006), by regulating neuronal morphology (Thomanetz et al., 2013) and synaptic plasticity through rearrangements of the Actin cytoskeleton (Huang et al., 2013). Synaptic mTORC2 likely acts through its main downstream effector protein kinase C (Baffi et al., 2021; Rüegg, 2013), whose role as a calcium sensor explains its specialized role at synapses, e.g. by regulating the SV cycle.

Actin is crucial for synaptic plasticity at the postsynaptic dendrite, e.g., via exo- and endocytic coupling of receptors regulated by differential Rho GTPase signaling and their regulatory proteins (e.g., long-term potentiation via Rasgrf2 (Kesavapany et al., 2004) and Trio; long-term depression via P-Rex1 and Tiam-1 (Duman et al., 2022)). We envision Actin and its regulatory proteins to play an analogous role in the synaptic vesicle cycle and presynaptic plasticity (Chéreau et al., 2017; Monday et al., 2020). Since the reformation of SVs is also impacted by neurodegenerative disorders, a comprehensive analysis of the roles and actions of specific components, including the cytoskeleton, may contribute to a better understanding of disease pathology in the future.

In conclusion, the significance of neurotransmission to survival has driven the development of a resilient and intricately interconnected cytoskeletal Actin network. This network encompasses multiple compensatory modes that can be concurrently induced to uphold the fidelity of neurotransmission and synaptic vesicle endocytosis. In doing so, this network ensures that perturbations can be readily accommodated to adapt to both internal and external cues.
This study elucidates the previously uncharacterized and conserved regulation of presynaptic Actin, and creates a novel framework for understanding how presynaptic morphology and function are coupled through mechanical and biochemical signaling pathways following the remodeling of the cytoskeleton.

8. References

Acharya, B. R., Wu, S. K., Lieu, Z. Z., Parton, R. G., Grill, S. W., Bershadsky, A. D., Gomez, G. A., & Yap, A. S. (2017). Mammalian Diaphanous 1 Mediates a Pathway for E-cadherin to Stabilize Epithelial Barriers through Junctional Contractility. *Cell Reports*, *18*(12). https://doi.org/10.1016/j.celrep.2017.02.078

Adachi, N., Kobayashi, T., Takahashi, H., Kawasaki, T., Shirai, Y., Ueyama, T., Matsuda, T., Seki, T., Sakai, N., & Saito, N. (2008). Enzymological analysis of mutant protein kinase Cγ causing spinocerebellar ataxia type 14 and dysfunction in Ca2+ homeostasis. *Journal of Biological Chemistry*, *283*(28). https://doi.org/10.1074/jbc.M801492200

Adie, E. J., Francis, M. J., Davies, J., Smith, L., Marenghi, A., Hather, C., Hadingham, K., Michael, N. P., Milligan, G., & Game, S. (2003). CypHer 5: a generic approach for measuring the activation and trafficking of G protein-coupled receptors in live cells. *Assay and Drug Development Technologies*, *1*(2). https://doi.org/10.1089/15406580360545062

Agarwal, N. K., Chen, C. H., Cho, H., Boulbès, D. R., Spooner, E., & Sarbassov, D. D. (2013). Rictor regulates cell migration by suppressing RhoGDI2. *Oncogene*, *32*(20). https://doi.org/10.1038/onc.2012.287

Aghamohammadzadeh, S., & Ayscough, K. R. (2009). Differential requirements for Actin during yeast and mammalian endocytosis. *Nature Cell Biology*, *11*(8). https://doi.org/10.1038/ncb1918

Allison, D. W., Gelfand, V. I., Spector, I., & Craig, A. M. (1998). Role of Actin in anchoring postsynaptic receptors in cultured hippocampal neurons: Differential attachment of NMDA versus AMPA receptors. *Journal of Neuroscience*, *18*(7). https://doi.org/10.1523/jneurosci.18-07-02423.1998

Ambroso, M. R., Hegde, B. G., & Langen, R. (2014). Endophilin A1 induces different membrane shapes using a conformational switch that is regulated by phosphorylation. *Proceedings of the National Academy of Sciences of the United States of America*, *111*(19). https://doi.org/10.1073/pnas.1402233111

An, P., Xu, W., Luo, J., & Luo, Y. (2021). Expanding TOR Complex 2 Signaling: Emerging Regulators and New Connections. In *Frontiers in Cell and Developmental Biology* (Vol. 9). https://doi.org/10.3389/fcell.2021.713806

Andersson, F., Jakobsson, J., Löw, P., Shupliakov, O., & Brodin, L. (2008). Perturbation of syndapin/PACSIN impairs synaptic vesicle recycling evoked by intense stimulation. *Journal of Neuroscience*, *28*(15). https://doi.org/10.1523/JNEUROSCI.1754-07.2008

Ando, K., Houben, S., Homa, M., de Fisenne, M. A., Potier, M. C., Erneux, C., Brion, J. P., & Leroy, K. (2021). Alzheimer's Disease: Tau Pathology and Dysfunction of Endocytosis. *Frontiers in Molecular Neuroscience*, *13*. https://doi.org/10.3389/fnmol.2020.583755

Apodaca, G. (2002). Modulation of membrane traffic by mechanical stimuli. In *American Journal of Physiology - Renal Physiology* (Vol. 282, Issues 2 51-2). https://doi.org/10.1152/ajprenal.2002.282.2.f179

Arakawa, Y., Bito, H., Furuyashiki, T., Tsuji, T., Takemoto-Kimura, S., Kimura, K., Nozaki, K., Hashimoto, N., & Narumiya, S. (2003). Control of axon elongation via an SDF-1α/Rho/mDia pathway in cultured cerebellar granule neurons. *Journal of Cell Biology*, *161*(2). https://doi.org/10.1083/jcb.200210149

Aronova, S., Wedaman, K., Aronov, P. A., Fontes, K., Ramos, K., Hammock, B. D., & Powers, T. (2008). Regulation of Ceramide Biosynthesis by TOR Complex 2. *Cell Metabolism*, *7*(2). https://doi.org/10.1016/j.cmet.2007.11.015

Aspenström, P. (2010). Formin-binding proteins: Modulators of formin-dependent Actin polymerization. In *Biochimica et Biophysica Acta - Molecular Cell Research* (Vol. 1803, Issue 2). https://doi.org/10.1016/j.bbamcr.2009.06.002

Aunis, D., & Bader, M. F. (1988). The cytoskeleton as a barrier to exocytosis in secretory cells. In *Journal of Experimental Biology* (Vol. 139). https://doi.org/10.1242/jeb.139.1.253

Ayscough, K. R. (2000). Endocytosis and the development of cell polarity in yeast require a dynamic F-Actin cytoskeleton. *Current Biology*, *10*(24). https://doi.org/10.1016/S0960-9822(00)00859-9

Babu, L. P. A., Wang, H. Y., Eguchi, K., Guillaud, L., & Takahashi, T. (2020). Microtubule and Actin differentially regulate synaptic vesicle cycling to maintain high-frequency neurotransmission. *Journal of Neuroscience*, *40*(1). https://doi.org/10.1523/JNEUROSCI.1571-19.2019

8. References

Bacaj, T., Wu, D., Yang, X., Morishita, W., Zhou, P., Xu, W., Malenka, R. C., & Südhof, T. C. (2013). Synaptotagmin-1 and Synaptotagmin-7 Trigger Synchronous and Asynchronous Phases of Neurotransmitter Release. *Neuron*, *80*(4). https://doi.org/10.1016/j.neuron.2013.10.026

Baffi, T. R., Lorden, G., Wozniak, J. M., Feichtner, A., Yeung, W., Kornev, A. P., King, C. C., Rio, J. C. D., Limaye, A. J., Bogomolovas, J., Gould, C. M., Chen, J., Kennedy, E. J., Kannan, N., Gonzalez, D. J., Stefan, E., Taylor, S. S., & Newton, A. C. (2021). TORC2 controls the activity of PKC and Akt by phosphorylating a conserved TOR interaction motif. *Science Signaling*, *14*(678). https://doi.org/10.1126/scisignal.abe4509

Bartolini, F., Ramalingam, N., & Gundersen, G. G. (2012). Actin-capping protein promotes microtubule stability by antagonizing the Actin activity of mDia1. *Molecular Biology of the Cell*, *23*(20). https://doi.org/10.1091/mbc.E12-05-0338

Bateman, J., & Van Vactor, D. (2001). The Trio family of guanine-nucleotide-exchange factors: Regulators of axon guidance. *Journal of Cell Science*, *114*(11). https://doi.org/10.1242/jcs.114.11.1973

Baumgart, T., Capraro, B. R., Zhu, C., & Das, S. L. (2011). Thermodynamics and mechanics of membrane curvature generation and sensing by proteins and lipids. *Annual Review of Physical Chemistry*, *62*. https://doi.org/10.1146/annurev.physchem.012809.103450

Bayascas, J. R., & Alessi, D. R. (2005). Regulation of Akt/PKB Ser473 phosphorylation. In *Molecular Cell* (Vol. 18, Issue 2). https://doi.org/10.1016/j.molcel.2005.03.020

Bellacosa, A., Chan, T. O., Ahmed, N. N., Datta, K., Malstrom, S., Stokoe, D., McCormick, F., Feng, J., & Tsichlis, P. (1998). Akt activation by growth factors is a multiple-step process: The role of the PH domain. *Oncogene*, *17*(3). https://doi.org/10.1038/sj.onc.1201947

Bentzinger, C. F., Romanino, K., Cloëtta, D., Lin, S., Mascarenhas, J. B., Oliveri, F., Xia, J., Casanova, E., Costa, C. F., Brink, M., Zorzato, F., Hall, M. N., & Rüegg, M. A. (2008). Skeletal Muscle-Specific Ablation of Raptor, but Not of Rictor, Causes Metabolic Changes and Results in Muscle Dystrophy. *Cell Metabolism*, *8*(5). https://doi.org/10.1016/j.cmet.2008.10.002

Berchtold, D., Piccolis, M., Chiaruttini, N., Riezman, I., Riezman, H., Roux, A., Walther, T. C., & Loewith, R. (2012). Plasma membrane stress induces relocalization of Slm proteins and activation of TORC2 to promote sphingolipid synthesis. *Nature Cell Biology*, *14*(5). https://doi.org/10.1038/ncb2480

Berchtold, D., & Walther, T. C. (2009). TORC2 plasma membrane localization is essential for cell viability and restricted to a distinct domain. *Molecular Biology of the Cell*, *20*(5). https://doi.org/10.1091/mbc.E08-10-1001

Bingham, D., Jakobs, C. E., Wernert, F., Boroni-Rueda, F., Jullien, N., Schentarra, E. M., Friedl, K., Da Costa Moura, J., van Bommel, D. M., Caillol, G., Ogawa, Y., Papandréou, M. J., & Leterrier, C. (2023). Presynapses contain distinct Actin nanostructures. *Journal of Cell Biology*, *222*(10). https://doi.org/10.1083/jcb.202208110

Binotti, B., Jahn, R., & Pérez-Lara, Á. (2021). An overview of the synaptic vesicle lipid composition. In *Archives of Biochemistry and Biophysics* (Vol. 709). https://doi.org/10.1016/j.abb.2021.108966

Bishop, A. L., & Hall, A. (2000). Rho GTPases and their effector proteins. In *Biochemical Journal* (Vol. 348, Issue 2). https://doi.org/10.1042/0264-6021:3480241

Blanchoin, L., Boujemaa-Paterski, R., Sykes, C., & Plastino, J. (2014). Actin dynamics, architecture, and mechanics in cell motility. *Physiological Reviews*, *94*(1). https://doi.org/10.1152/physrev.00018.2013

Blanchoin, L., Pollard, T. D., & Mullins, R. D. R. D. (2000). Interactions of ADF/cofilin, Arp2/3 complex, capping protein and profilin in remodeling of branched Actin filament networks. *Current Biology*, *10*(20). https://doi.org/10.1016/S0960-9822(00)00749-1

Bleckert, A., Photowala, H., & Alford, S. (2012). Dual pools of Actin at presynaptic terminals. *Journal of Neurophysiology*, *107*(12). https://doi.org/10.1152/jn.00789.2011

Bloom, O., Evergren, E., Tomilin, N., Kjaerulff, O., Löw, P., Brodin, L., Pieribone, V. A., Greengard, P., & Shupliakov, O. (2003). Colocalization of synapsin and Actin during synaptic vesicle recycling. *Journal of Cell Biology*, *161*(4). https://doi.org/10.1083/jcb.200212140

Bogdan, S., Schultz, J., & Grosshans, J. (2013). Formin' cellular structures. *Communicative & Integrative Biology*, *6*(6). https://doi.org/10.4161/cib.27634

Bolz, S., Kaempf, N., Puchkov, D., Krauss, M., Russo, G., Soykan, T., Schmied, C., Lehmann, M., Müller, R., Schultz, C., Perrais, D., Maritzen, T., & Haucke, V. (2023). Synaptotagmin 1-triggered lipid signaling facilitates coupling of exo- and endocytosis. *Neuron*, *111*(23). https://doi.org/10.1016/j.neuron.2023.08.016

Bombardier, J. P., Eskin, J. A., Jaiswal, R., Corrêa, I. R., Xu, M. Q., Goode, B. L., & Gelles, J. (2015). Single-molecule visualization of a formin-capping protein "decision complex" at the Actin filament barbed end. *Nature Communications*, *6*. https://doi.org/10.1038/ncomms9707

Bos, J. L., Rehmann, H., & Wittinghofer, A. (2007). GEFs and GAPs: Critical Elements in the Control of Small G Proteins. In *Cell* (Vol. 129, Issue 5). https://doi.org/10.1016/j.cell.2007.05.018

Boucrot, E., Ferreira, A. P. A., Almeida-Souza, L., Debard, S., Vallis, Y., Howard, G., Bertot, L., Sauvonnet, N., & McMahon, H. T. (2015). Endophilin marks and controls a clathrin-independent endocytic pathway. *Nature*, *517*(7535). https://doi.org/10.1038/nature14067

Boulant, S., Kural, C., Zeeh, J. C., Ubelmann, F., & Kirchhausen, T. (2011). Actin dynamics counteract membrane tension during clathrin-mediated endocytosis. *Nature Cell Biology*, *13*(9). https://doi.org/10.1038/ncb2307

Boulter, E., Garcia-Mata, R., Guilluy, C., Dubash, A., Rossi, G., Brennwald, P. J., & Burridge, K. (2010). Regulation of Rho GTPase crosstalk, degradation and activity by RhoGDI1. *Nature Cell Biology*, *12*(5). https://doi.org/10.1038/ncb2049

Boulter, E., Grall, D., Cagnol, S., Van Obberghen-Schilling, E., Boulter, E., Grall, D., Cagnol, S., & Van Obberghen-Schilling, E. (2006). Regulation of cell-matrix adhesion dynamics and Rac-1 by integrin linked kinase. *The FASEB Journal*, *20*(9). https://doi.org/10.1096/fj.05-4579fje

Bourgoint, C., Rispal, D., Berti, M., Filipuzzi, I., Helliwell, S. B., Prouteau, M., & Loewith, R. (2018). Target of rapamycin complex 2– dependent phosphorylation of the coat protein Pan1 by Akl1 controls endocytosis dynamics in Saccharomyces cerevisiae. *Journal of Biological Chemistry*, *293*(31). https://doi.org/10.1074/jbc.RA117.001615

Bourne, H. R., Sanders, D. A., & McCormick, F. (1990). The GTPase superfamily: A conserved switch for diverse cell functions. In *Nature* (Vol. 348, Issue 6297). https://doi.org/10.1038/348125a0

Bourne, H. R., Sanders, D. A., & McCormick, F. (1991). The GTPase superfamily: conserved structure and molecular mechanism. In *Nature* (Vol. 349, Issue 6305). https://doi.org/10.1038/349117a0

Bourne, J., Morgan, J. R., & Pieribone, V. A. (2006). Actin polymerization regulates clathrin coat maturation during early stages of synaptic vesicle recycling at lamprey synapses. *Journal of Comparative Neurology*, *497*(4). https://doi.org/10.1002/cne.21006

Bovellan, M., Romeo, Y., Biro, M., Boden, A., Chugh, P., Yonis, A., Vaghela, M., Fritzsche, M., Moulding, D., Thorogate, R., Jégou, A., Thrasher, A. J., Romet-Lemonne, G., Roux, P. P., Paluch, E. K., & Charras, G. (2014). Cellular control of cortical Actin nucleation. *Current Biology*, *24*(14). https://doi.org/10.1016/j.cub.2014.05.069

Branon, T. C., Bosch, J. A., Sanchez, A. D., Udeshi, N. D., Svinkina, T., Carr, S. A., Feldman, J. L., Perrimon, N., & Ting, A. Y. (2018). Efficient proximity labeling in living cells and organisms with TurboID. *Nature Biotechnology*, *36*(9). https://doi.org/10.1038/nbt.4201

Brazil, D. P., Yang, Z. Z., & Hemmings, B. A. (2004). Advances in protein kinase B signalling: AKTion on multiple fronts. In *Trends in Biochemical Sciences* (Vol. 29, Issue 5). https://doi.org/10.1016/j.tibs.2004.03.006

Breitsprecher, D., & Goode, B. L. (2013). Formins at a glance. In *Journal of Cell Science* (Vol. 126, Issue 1). https://doi.org/10.1242/jcs.107250

Breitsprecher, D., Jaiswal, R., Bombardier, J. P., Gould, C. J., Gelles, J., & Goode, B. L. (2012). Rocket launcher mechanism of collaborative Actin assembly defined by single-molecule imaging. *Science*, *336*(6085). https://doi.org/10.1126/science.1218062

Brenig, J., De Boor, S., Knyphausen, P., Kuhlmann, N., Wroblowski, S., Baldus, L., Scislowski, L., Artz, O., Trauschies, P., Baumann, U., Neundorf, I., & Lammers, M. (2015). Structural and biochemical basis for the inhibitory effect of liprin-α3 on mouse diaphanous 1 (mDia1) Function. *Journal of Biological Chemistry*, *290*(23). https://doi.org/10.1074/jbc.M114.621946

Bruel-Jungerman, E., Veyrac, A., Dufour, F., Horwood, J., Laroche, S., & Davis, S. (2009). Inhibition of PI3K-Akt signaling

blocks exercise-mediated enhancement of adult neurogenesis and synaptic plasticity in the dentate gyrus. *PLoS ONE*, *4*(11). https://doi.org/10.1371/journal.pone.0007901

Brunger, A. T., Choi, U. B., Lai, Y., Leitz, J., & Zhou, Q. (2018). Molecular Mechanisms of Fast Neurotransmitter Release. In *Annual Review of Biophysics* (Vol. 47). https://doi.org/10.1146/annurev-biophys-070816-034117

Bucki, R., Wang, Y. H., Yang, C., Kandy, S. K., Fatunmbi, O., Bradley, R., Pogoda, K., Svitkina, T., Radhakrishnan, R., & Janmey, P. A. (2019). Lateral distribution of phosphatidylinositol 4,5-bisphosphate in membranes regulates formin- and ARP2/3-mediated Actin nucleation. *Journal of Biological Chemistry*, *294*(12). https://doi.org/10.1074/jbc.RA118.005552

Bugyi, B., & Carlier, M. F. (2010). Control of Actin filament treadmilling in cell motility. In *Annual Review of Biophysics* (Vol. 39, Issue 1). https://doi.org/10.1146/annurev-biophys-051309-103849

Burgoyne, R. D., Fisher, R. J., & Graham, M. E. (2001). Regulation of kiss-and-run exocytosis [1]. In *Trends in Cell Biology* (Vol. 11, Issue 10). https://doi.org/10.1016/S0962-8924(01)02089-X

Burke, T. A., Christensen, J. R., Barone, E., Suarez, C., Sirotkin, V., & Kovar, D. R. (2014). Homeostatic Actin cytoskeleton networks are regulated by assembly factor competition for monomers. *Current Biology*, *24*(5). https://doi.org/10.1016/j.cub.2014.01.072

Burridge, K., & Wennerberg, K. (2004). Rho and Rac Take Center Stage. In *Cell* (Vol. 116, Issue 2). https://doi.org/10.1016/S0092-8674(04)00003-0

Bustos, R. I., Forget, M. A., Settleman, J. E., & Hansen, S. H. (2008). Coordination of Rho and Rac GTPase Function via p190B RhoGAP. *Current Biology*, *18*(20). https://doi.org/10.1016/j.cub.2008.09.019

Campa, C. C., Ciraolo, E., Ghigo, A., Germena, G., & Hirsch, E. (2015). Crossroads of PI3K and Rac pathways. *Small GTPases*, *6*(2). https://doi.org/10.4161/21541248.2014.989789

Campellone, K. G., & Welch, M. D. (2010). A nucleator arms race: Cellular control of Actin assembly. In *Nature Reviews Molecular Cell Biology* (Vol. 11, Issue 4). https://doi.org/10.1038/nrm2867

Carlsson, A. E., & Bayly, P. V. (2014). Force generation by endocytic Actin patches in budding yeast. *Biophysical Journal*, *106*(8). https://doi.org/10.1016/j.bpj.2014.02.035

Carson, R. P., Fu, C., Winzenburger, P., & Ess, K. C. (2013). Deletion of Rictor in neural progenitor cells reveals contributions of mTORC2 signaling to tuberous sclerosis complex. *Human Molecular Genetics*, *22*(1). https://doi.org/10.1093/hmg/dds414

Ceccarelli, B., Hurlbut, W. P., & Mauro, A. (1973). Turnover of transmitter and synaptic vesicles at the prog neuromuscular junction. *Journal of Cell Biology*, *57*(2). https://doi.org/10.1083/jcb.57.2.499

Chanaday, N. L., & Kavalali, E. T. (2018a). Optical detection of three modes of endocytosis at hippocampal synapses. *ELife*, *7*. https://doi.org/10.7554/eLife.36097

Chanaday, N. L., & Kavalali, E. T. (2018b). Presynaptic origins of distinct modes of neurotransmitter release. In *Current Opinion in Neurobiology* (Vol. 51). https://doi.org/10.1016/j.conb.2018.03.005

Chanaday, N. L., & Kavalali, E. T. (2018c). Time course and temperature dependence of synaptic vesicle endocytosis. In *FEBS Letters* (Vol. 592, Issue 21). https://doi.org/10.1002/1873-3468.13268

Chandrasekar, I., Huettner, J. E., Turney, S. G., & Bridgman, P. C. (2013). Myosin II regulates activity dependent compensatory endocytosis at central synapses. *Journal of Neuroscience*, *33*(41). https://doi.org/10.1523/JNEUROSCI.2229-13.2013

Chauhana, B. K., Louc, M., Zhengd, Y., & Langa, R. A. (2011). Balanced Rac1 and RhoA activities regulate cell shape and drive invagination morphogenesis in epithelia. *Proceedings of the National Academy of Sciences of the United States of America*, *108*(45). https://doi.org/10.1073/pnas.1108993108

Chen, Z., Borek, D., Padrick, S. B., Gomez, T. S., Metlagel, Z., Ismail, A. M., Umetani, J., Billadeau, D. D., Otwinowski, Z., & Rosen, M. K. (2010). Structure and control of the Actin regulatory WAVE complex. *Nature*, *468*(7323). https://doi.org/10.1038/nature09623

Cheng, L., Zhang, J., Ahmad, S., Rozier, L., Yu, H., Deng, H., & Mao, Y. (2011). Aurora B Regulates Formin mDia3 in Achieving Metaphase Chromosome Alignment. *Developmental Cell*, *20*(3). https://doi.org/10.1016/j.devcel.2011.01.008

Chenouard, N., Xuan, F., & Tsien, R. W. (2020). Synaptic vesicle traffic is supported by transient Actin filaments and regulated by PKA and NO. *Nature Communications*, *11*(1). https://doi.org/10.1038/s41467-020-19120-1

Chéreau, R., Saraceno, G. E., Angibaud, J., Cattaert, D., & Nägerl, U. V. (2017). Superresolution imaging reveals activity-dependent plasticity of axon morphology linked to changes in action potential conduction velocity. *Proceedings of the National Academy of Sciences of the United States of America*, *114*(6). https://doi.org/10.1073/pnas.1607541114

Cherfils, J., & Zeghouf, M. (2013). Regulation of small GTPases by GEFs, GAPs, and GDIs. In *Physiological Reviews* (Vol. 93, Issue 1). https://doi.org/10.1152/physrev.00003.2012

Chesarone, M. A., Dupage, A. G., & Goode, B. L. (2010). Unleashing formins to remodel the Actin and microtubule cytoskeletons. In *Nature Reviews Molecular Cell Biology* (Vol. 11, Issue 1). https://doi.org/10.1038/nrm2816

Chesarone, M. A., & Goode, B. L. (2009). Actin nucleation and elongation factors: mechanisms and interplay. In *Current Opinion in Cell Biology* (Vol. 21, Issue 1). https://doi.org/10.1016/j.ceb.2008.12.001

Chesarone, M., Gould, C. J., Moseley, J. B., & Goode, B. L. (2009). Displacement of Formins from Growing Barbed Ends by Bud14 Is Critical for Actin Cable Architecture and Function. *Developmental Cell*, *16*(2). https://doi.org/10.1016/j.devcel.2008.12.001

Cheung, G., & Cousin, M. A. (2013). Synaptic vesicle generation from activity-dependent bulk endosomes requires calcium and calcineurin. *Journal of Neuroscience*, *33*(8). https://doi.org/10.1523/JNEUROSCI.4697-12.2013

Chikumi, H., Barac, A., Behbahani, B., Gao, Y., Teramoto, H., Zheng, Y., & Gutkind, J. S. (2004). Homo- and hetero-oligomerization of PDZ-RhoGEF, LARG and p115RhoGEF by their C-terminal region regulates their in vivo Rho GEF activity and transforming potential. *Oncogene*, *23*(1). https://doi.org/10.1038/sj.onc.1207012

Cho, K. F., Branon, T. C., Udeshi, N. D., Myers, S. A., Carr, S. A., & Ting, A. Y. (2020). Proximity labeling in mammalian cells with TurboID and split-TurboID. *Nature Protocols*, *15*(12). https://doi.org/10.1038/s41596-020-0399-0

Chrzanowska-Wodnicka, M., & Burridge, K. (1996). Rho-stimulated contractility drives the formation of stress fibers and focal adhesions. *Journal of Cell Biology*, *133*(6). https://doi.org/10.1083/jcb.133.6.1403

Chu, N., Salguero, A. L., Liu, A. Z., Chen, Z., Dempsey, D. R., Ficarro, S. B., Alexander, W. M., Marto, J. A., Li, Y., Amzel, L. M., Gabelli, S. B., & Cole, P. A. (2018). Akt Kinase Activation Mechanisms Revealed Using Protein Semisynthesis. *Cell*, *174*(4). https://doi.org/10.1016/j.cell.2018.07.003

Chuang, T. H., Xu, X., Kaartinen, V., Heisterkamp, N., Groffen, J., & Bokoch, G. M. (1995). Abr and Bcr are multifunctional regulators of the Rho GTP-binding protein family. *Proceedings of the National Academy of Sciences of the United States of America*, *92*(22). https://doi.org/10.1073/pnas.92.22.10282

Chung, J. K., Sekiya, F., Kang, H. S., Lee, C., Han, J. S., Kim, S. R., Bae, Y. S., Morris, A. J., & Rhee, S. G. (1997). Synaptojanin inhibition of phospholipase D activity by hydrolysis of phosphatidylinositol 4,5-Bisphosphate. *Journal of Biological Chemistry*, *272*(25). https://doi.org/10.1074/jbc.272.25.15980

Cingolani, L. A., & Goda, Y. (2008). Actin in action: The interplay between the Actin cytoskeleton and synaptic efficacy. In *Nature Reviews Neuroscience* (Vol. 9, Issue 5). https://doi.org/10.1038/nrn2373

Clarke, D. N., & Martin, A. C. (2021). Actin-based force generation and cell adhesion in tissue morphogenesis. In *Current Biology* (Vol. 31, Issue 10). https://doi.org/10.1016/j.cub.2021.03.031

Clayton, E. L., & Cousin, M. A. (2009). The molecular physiology of activity-dependent bulk endocytosis of synaptic vesicles. In *Journal of Neurochemistry* (Vol. 111, Issue 4). https://doi.org/10.1111/j.1471-4159.2009.06384.x

Cocucci, E., Gaudin, R., & Kirchhausen, T. (2014). Dynamin recruitment and membrane scission at the neck of a clathrin-coated pit. *Molecular Biology of the Cell*, *25*(22). https://doi.org/10.1091/mbc.E14-07-1240

Cole, J. C., Villa, B. R. S., & Wilkinson, R. S. (2000). Disruption of Actin impedes transmitter release in snake motor terminals. *Journal of Physiology*, *525*(3). https://doi.org/10.1111/j.1469-7793.2000.t01-2-00579.x

Colicos, M. A., Collins, B. E., Sailor, M. J., & Goda, Y. (2001). Remodeling of synaptic Actin induced by photoconductive stimulation. *Cell*, *107*(5). https://doi.org/10.1016/S0092-8674(01)00579-7

Colom, A., Derivery, E., Soleimanpour, S., Tomba, C., Molin, M. D., Sakai, N., González-Gaitán, M., Matile, S., & Roux, A.

(2018). A fluorescent membrane tension probe. *Nature Chemistry*, *10*(11). https://doi.org/10.1038/s41557-018-0127-3

Colucci-Guyon, E., Niedergang, F., Wallar, B. J., Peng, J., Alberts, A. S., & Chavrier, P. (2005). A role for mammalian diaphanous-related formins in complement receptor (CR3)-mediated phagocytosis in macrophages. *Current Biology*, *15*(22). https://doi.org/10.1016/j.cub.2005.09.051

Copeland, J. W., Copeland, S. J., & Treisman, R. (2004). Homo-oligomerization is essential for F-Actin assembly by the formin family FH2 domain. *Journal of Biological Chemistry*, *279*(48). https://doi.org/10.1074/jbc.M404429200

Copeland, S. J., Green, B. J., Burchat, S., Papalia, G. A., Banner, D., & Copeland, J. W. (2007). The diaphanous inhibitory domain/diaphanous autoregulatory domain interaction is able to mediate heterodimerization between mDia1 and mDia2. *Journal of Biological Chemistry*, *282*(41). https://doi.org/10.1074/jbc.M703834200

Corbetta, S., Gualdoni, S., Ciceri, G., Monari, M., Zuccaro, E., Tybulewicz, V. L. J., & De Curtis, I. (2009). Essential role of Rac1 and Rac3 GTPases in neuronal development. *The FASEB Journal*, *23*(5). https://doi.org/10.1096/fj.08-121574

Correas, I., Díaz-Nido, J., & Avila, J. (1992). Microtubule-associated protein tau is phosphorylated by protein kinase C on its tubulin binding domain. *Journal of Biological Chemistry*, *267*(22). https://doi.org/10.1016/s0021-9258(19)49595-1

Courtemanche, N. (2018). Mechanisms of formin-mediated Actin assembly and dynamics. In *Biophysical Reviews* (Vol. 10, Issue 6). https://doi.org/10.1007/s12551-018-0468-6

Courtemanche, N., & Pollard, T. D. (2012). Determinants of formin homology 1 (FH1) domain function in Actin filament elongation by formins. *Journal of Biological Chemistry*, *287*(10). https://doi.org/10.1074/jbc.M111.322958

Courtney, K. D., Grove, M., Vandongen, H., Vandongen, A., LaMantia, A. S., & Pendergast, A. M. (2000). Localization and phosphorylation of AbI-interactor proteins, Abi-1 and Abi-2, in the developing nervous system. *Molecular and Cellular Neurosciences*, *16*(3). https://doi.org/10.1006/mcne.2000.0865

Cousin, M. A., & Robinson, P. J. (2001). The dephosphins: Dephosphorylation by calcineurin triggers synaptic vesicle endocytosis. In *Trends in Neurosciences* (Vol. 24, Issue 11). https://doi.org/10.1016/S0166-2236(00)01930-5

Crawford, D. C., & Kavalali, E. T. (2015). Molecular underpinnings of synaptic vesicle pool heterogeneity. In *Traffic* (Vol. 16, Issue 4). https://doi.org/10.1111/tra.12262

Cremona, O., Di Paolo, G., Wenk, M. R., Lüthi, A., Kim, W. T., Takei, K., Daniell, L., Nemoto, Y., Shears, S. B., Flavell, R. A., McCormick, D. A., & De Camilli, P. (1999). Essential role of phosphoinositide metabolism in synaptic vesicle recycling. *Cell*, *99*(2). https://doi.org/10.1016/S0092-8674(00)81649-9

Cullen, E. R., Safari, M., Mittelstadt, I., & Weston, M. C. (2023). Hyperactivity of mTORC1 and mTORC2-dependent signaling mediate epilepsy downstream of somatic PTEN loss. *BioRxiv*. https://doi.org/https://doi.org/10.1101/2023.08.18.553856

Cybulski, N., Polak, P., Auwerx, J., Rüegg, M. A., & Hall, M. N. (2009). mTOR complex 2 in adipose tissue negatively controls whole-body growth. *Proceedings of the National Academy of Sciences of the United States of America*, *106*(24). https://doi.org/10.1073/pnas.0811321106

Dai, J., Ping Ting-Beall, H., & Sheetz, M. P. (1997). The secretion-coupled endocytosis correlates with membrane tension changes in RBL 2H3 cells. *Journal of General Physiology*, *110*(1). https://doi.org/10.1085/jgp.110.1.1

Dai, J., & Sheetz, M. P. (1995). Regulation of endocytosis, exocytosis, and shape by membrane tension. *Cold Spring Harbor Symposia on Quantitative Biology*, *60*. https://doi.org/10.1101/SQB.1995.060.01.060

Dani, A., Huang, B., Bergan, J., Dulac, C., & Zhuang, X. (2010). Superresolution Imaging of Chemical Synapses in the Brain. *Neuron*, *68*(5). https://doi.org/10.1016/j.neuron.2010.11.021

Daou, P., Hasan, S., Breitsprecher, D., Baudelet, E., Camoin, L., Audebert, S., Goode, B. L., & Badache, A. (2014). Essential and nonredundant roles for Diaphanous formins in cortical microtubule capture and directed cell migration. *Molecular Biology of the Cell*, *25*(5). https://doi.org/10.1091/mbc.E13-08-0482

De Belly, H., Yan, S., Borja da Rocha, H., Ichbiah, S., Town, J. P., Zager, P. J., Estrada, D. C., Meyer, K., Turlier, H., Bustamante, C., & Weiner, O. D. (2023). Cell protrusions and contractions generate long-range membrane tension propagation. *Cell*, *186*(14). https://doi.org/10.1016/j.cell.2023.05.014

de Kreuk, B. J., Nethe, M., Fernandez-Borja, M., Anthony, E. C., Hensbergen, P. J., Deelder, A. M., Plomann, M., & Hordijk, P. L. (2011). The F-BAR domain protein PACSIN2 associates with Rac1 and regulates cell spreading and migration. *Journal of Cell Science*, *124*(14). https://doi.org/10.1242/jcs.080630

Deguchi, Y., Harada, M., Shinohara, R., Lazarus, M., Cherasse, Y., Urade, Y., Yamada, D., Sekiguchi, M., Watanabe, D., Furuyashiki, T., & Narumiya, S. (2016). mDia and ROCK Mediate Actin-Dependent Presynaptic Remodeling Regulating Synaptic Efficacy and Anxiety. *Cell Reports*, *17*(9). https://doi.org/10.1016/j.celrep.2016.10.088

Delvendahl, I., Vyleta, N. P., von Gersdorff, H., & Hallermann, S. (2016). Fast, Temperature-Sensitive and Clathrin-Independent Endocytosis at Central Synapses. *Neuron*, *90*(3). https://doi.org/10.1016/j.neuron.2016.03.013

Denker, A., & Rizzoli, S. O. (2010). Synaptic vesicle pools: An update. In *Frontiers in Synaptic Neuroscience* (Issue OCT). https://doi.org/10.3389/fnsyn.2010.00135

Derivery, E., & Gautreau, A. (2010). Generation of branched Actin networks: Assembly and regulation of the N-WASP and WAVE molecular machines. In *BioEssays* (Vol. 32, Issue 2). https://doi.org/10.1002/bies.200900123

DerMardirossian, C., Rocklin, G., Seo, J. Y., & Bokoch, G. M. (2006). Phosphorylation of RhoGDI by Src regulates Rho GTPase binding and cytosol-membrane cycling. *Molecular Biology of the Cell*, *17*(11). https://doi.org/10.1091/mbc.E06-06-0533

DeWard, A. D., Leali, K., West, R. A., Prendergast, G. C., & Alberts, A. S. (2009). Loss of RhoB expression enhances the myelodysplastic phenotype of mammalian diaphanous-related formin mDia1 knockout mice. *PLoS ONE*, *4*(9). https://doi.org/10.1371/journal.pone.0007102

Ding, B., Yang, S., Schaks, M., Liu, Y., Brown, A. J., Rottner, K., Chowdhury, S., & Chen, B. (2022). Structures reveal a key mechanism of WAVE regulatory complex activation by Rac1 GTPase. *Nature Communications*, *13*(1). https://doi.org/10.1038/s41467-022-33174-3

Diz-Muñoz, A., Thurley, K., Chintamen, S., Altschuler, S. J., Wu, L. F., Fletcher, D. A., & Weiner, O. D. (2016). Membrane Tension Acts Through PLD2 and mTORC2 to Limit Actin Network Assembly During Neutrophil Migration. *PLoS Biology*, *14*(6). https://doi.org/10.1371/journal.pbio.1002474

Dmitrieff, S., & Nédélec, F. (2015). Membrane Mechanics of Endocytosis in Cells with Turgor. *PLoS Computational Biology*, *11*(10). https://doi.org/10.1371/journal.pcbi.1004538

Dos, D. S., Ali, S. M., Kim, D. H., Guertin, D. A., Latek, R. R., Erdjument-Bromage, H., Tempst, P., & Sabatini, D. M. (2004). Rictor, a novel binding partner of mTOR, defines a rapamycin-insensitive and Raptor-independent pathway that regulates the cytoskeleton. *Current Biology*, *14*(14). https://doi.org/10.1016/j.cub.2004.06.054

Dovas, A., Choi, Y., Yoneda, A., Multhaupt, H. A. B., Kwon, S. H., Kang, D., Oh, E. S., & Couchman, J. R. (2010). Serine 34 phosphorylation of Rho guanine dissociation inhibitor (RhoGDIα) links signaling from conventional protein kinase C to RhoGTPase in cell adhesion. *Journal of Biological Chemistry*, *285*(30). https://doi.org/10.1074/jbc.M109.098129

Dubielecka, P. M., Cui, P., Xiong, X., Hossain, S., Heck, S., Angelov, L., & Kotula, L. (2010). Differential regulation of macropinocytosis by Abi1/Hssh3bp1 isoforms. *PLoS ONE*, *5*(5). https://doi.org/10.1371/journal.pone.0010430

Dubielecka, P. M., Machida, K., Xiong, X., Hossain, S., Ogiue-Ikeda, M., Carrera, A. C., Mayer, B. J., & Kotula, L. (2010). Abi1/Hssh3bp1 pY213 links Abl kinase signaling to p85 regulatory subunit of PI-3 kinase in regulation of macropinocytosis in LNCaP cells. *FEBS Letters*, *584*(15). https://doi.org/10.1016/j.febslet.2010.06.029

Duman, J. G., Blanco, F. A., Cronkite, C. A., Ru, Q., Erikson, K. C., Mulherkar, S., Saifullah, A. Bin, Firozi, K., & Tolias, K. F. (2022). Rac-maninoff and Rho-vel: The symphony of Rho-GTPase signaling at excitatory synapses. In *Small GTPases* (Vol. 13, Issue 1). https://doi.org/10.1080/21541248.2021.1885264

Dvorsky, R., & Ahmadian, M. R. (2004). Always look on the bright site of Rho: Structural implications for a conserved intermolecular interface. In *EMBO Reports* (Vol. 5, Issue 12). https://doi.org/10.1038/sj.embor.7400293

Echarri, A., & Del Pozo, M. A. (2015). Caveolae - mechanosensitive membrane invaginations linked to Actin filaments. In *Journal of Cell Science* (Vol. 128, Issue 15). https://doi.org/10.1242/jcs.153940

Echarri, A., Muriel, O., Pavón, D. M., Azegrouz, H., Escolar, F., Terrón, M. C., Sanchez-Cabo, F., Martínez, F., Montoya, M. C., Llorca, O., & del Pozo, M. A. (2012). Caveolar domain organization and trafficking is regulated by Abl kinases and mDia1. *Journal of Cell Science*, *125*(13). https://doi.org/10.1242/jcs.090134

Echarri, A., Pavón, D. M., Sánchez, S., García-García, M., Calvo, E., Huerta-López, C., Velázquez-Carreras, D., Viaris de Lesegno, C., Ariotti, N., Lázaro-Carrillo, A., Strippoli, R., De Sancho, D., Alegre-Cebollada, J., Lamaze, C., Parton, R. G., & Del Pozo, M. A. (2019). An Abl-FBP17 mechanosensing system couples local plasma membrane curvature and stress fiber remodeling during mechanoadaptation. *Nature Communications*, *10*(1). https://doi.org/10.1038/s41467-019-13782-2

Eden, S., Rohatgi, R., Podtelejnikov, A. V., Mann, M., & Kirschner, M. W. (2002). Mechanism of regulation of WAVE1-induced Actin nucleation by Rac1 and Nck. *Nature*, *418*(6899). https://doi.org/10.1038/nature00859

Eftekharjoo, M., Palmer, D., McCoy, B., & Maruthamuthu, V. (2019). Fibrillar force generation by fibroblasts depends on formin. *Biochemical and Biophysical Research Communications*, *510*(1). https://doi.org/10.1016/j.bbrc.2019.01.035

Eguchi, K., Taoufiq, Z., Thorn-Seshold, O., Trauner, D., Hasegawa, M., & Takahashi, T. (2017). Wild-type monomeric α-synuclein can impair vesicle endocytosis and synaptic fidelity via tubulin polymerization at the calyx of held. *Journal of Neuroscience*, *37*(25). https://doi.org/10.1523/JNEUROSCI.0179-17.2017

Ehrlicher, A. J., Nakamura, F., Hartwig, J. H., Weitz, D. A., & Stossel, T. P. (2011). Mechanical strain in Actin networks regulates FilGAP and integrin binding to filamin A. *Nature*, *478*(7368). https://doi.org/10.1038/nature10430

Eisenmann, K. M., West, R. A., Hildebrand, D., Kitchen, S. M., Peng, J., Sigler, R., Zhang, J., Siminovitch, K. A., & Alberts, A. S. (2007). T cell responses in mammalian diaphanous-related formin mDia1 knock-out mice. *Journal of Biological Chemistry*, *282*(34). https://doi.org/10.1074/jbc.M703243200

Elia, L. P., Yamamoto, M., Zang, K., & Reichardt, L. F. (2006). p120 Catenin Regulates Dendritic Spine and Synapse Development through Rho-Family GTPases and Cadherins. *Neuron*, *51*(1). https://doi.org/10.1016/j.neuron.2006.05.018

Emperador-Melero, J., Wong, M. Y., Wang, S. S. H., de Nola, G., Nyitrai, H., Kirchhausen, T., & Kaeser, P. S. (2021). PKC-phosphorylation of Liprin-α3 triggers phase separation and controls presynaptic active zone structure. *Nature Communications*, *12*(1). https://doi.org/10.1038/s41467-021-23116-w

Eng, C. H., Huckaba, T. M., & Gundersen, G. G. (2006). The formin mDia regulates GSK3β through novel PKCs to promote microtubule stabilization but not MTOC reorientation in migrating fibroblasts. *Molecular Biology of the Cell*, *17*(12). https://doi.org/10.1091/mbc.E05-10-0914

Engqvist-Goldstein, Å. E. Y., & Drubin, D. G. (2003). Actin Assembly and Endocytosis: From Yeast to Mammals. *Annual Review of Cell and Developmental Biology*, *19*. https://doi.org/10.1146/annurev.cellbio.19.111401.093127

Ercan-Sencicek, A. G., Jambi, S., Franjic, D., Nishimura, S., Li, M., El-Fishawy, P., Morgan, T. M., Sanders, S. J., Bilguvar, K., Suri, M., Johnson, M. H., Gupta, A. R., Yuksel, Z., Mane, S., Grigorenko, E., Picciotto, M., Alberts, A. S., Gunel, M., Šestan, N., & State, M. W. (2015). Homozygous loss of DIAPH1 is a novel cause of microcephaly in humans. *European Journal of Human Genetics*, *23*(2). https://doi.org/10.1038/ejhg.2014.82

Esen, E., Chen, J., Karner, C. M., Okunade, A. L., Patterson, B. W., & Long, F. (2013). WNT-LRP5 signaling induces warburg effect through mTORC2 activation during osteoblast differentiation. *Cell Metabolism*, *17*(5). https://doi.org/10.1016/j.cmet.2013.03.017

Esmaeilzadeh, H., Noeiaghdam, R., Johari, L., Hosseini, S. A., Nabavizadeh, S. H., & Alyasin, S. S. (2022). Homozygous Autosomal Recessive DIAPH1 Mutation Associated with Central Nervous System Involvement and Aspergillosis: A Rare Case. *Case Reports in Genetics*, *2022*. https://doi.org/10.1155/2022/4142214

Facchinetti, V., Ouyang, W., Wei, H., Soto, N., Lazorchak, A., Gould, C., Lowry, C., Newton, A. C., Mao, Y., Miao, R. Q., Sessa, W. C., Qin, J., Zhang, P., Su, B., & Jacinto, E. (2008). The mammalian target of rapamycin complex 2 controls folding and stability of Akt and protein kinase C. *EMBO Journal*, *27*(14). https://doi.org/10.1038/emboj.2008.120

Faix, J., & Grosse, R. (2006). Staying in Shape with Formins. In *Developmental Cell* (Vol. 10, Issue 6). https://doi.org/10.1016/j.devcel.2006.05.001

Farsi, Z., Jahn, R., & Woehler, A. (2017). Proton electrochemical gradient: Driving and regulating neurotransmitter uptake. In *BioEssays* (Vol. 39, Issue 5). https://doi.org/10.1002/bies.201600240

Favaro, P., Traina, F., Machado-Neto, J. A., Lazarini, M., Lopes, M. R., Pereira, J. K. N., Costa, F. F., Infante, E., Ridley, A. J., & Saad, S. T. O. (2013). FMNL1 promotes proliferation and migration of leukemia cells. *Journal of Leukocyte Biology*, *94*(3). https://doi.org/10.1189/jlb.0113057

Ferguson, S., Raimondi, A., Paradise, S., Shen, H., Mesaki, K., Ferguson, A., Destaing, O., Ko, G., Takasaki, J., Cremona, O., O' Toole, E., & De Camilli, P. (2009). Coordinated Actions of Actin and BAR Proteins Upstream of Dynamin at Endocytic Clathrin-Coated Pits. *Developmental Cell*, *17*(6). https://doi.org/10.1016/j.devcel.2009.11.005

Fessenden, T. B., Beckham, Y., Perez-Neut, M., Juan, G. R. S., Chourasia, A. H., Macleod, K. F., Oakes, P. W., & Gardel, M. L. (2018). Dia1-dependent adhesions are required by epithelial tissues to initiate invasion. *Journal of Cell Biology*, *217*(4). https://doi.org/10.1083/jcb.201703145

Fidyk, N. J., & Cerione, R. A. (2002). Understanding the catalytic mechanism of GTPase-activating proteins: Demonstration of the importance of switch domain stabilization in the stimulation of GTP hydrolysis. *Biochemistry*, *41*(52). https://doi.org/10.1021/bi026413p

Finer, J. T., Mehta, A. D., Spudich, J. A., Lombardi, V., Kinosita, K., Block, S., Gilford, Cooke, R., Brenner, B., & Highsmith, S. (1995). Characterization of single Actin-myosin interactions. *Biophysical Journal*, *68*(4 SUPPL.).

Fleming, I. N., Batty, I. H., Prescott, A. R., Gray, A., Kular, G. S., Stewart, H., & Downes, C. P. (2004). Inositol phospholipids regulate the guanine-nucleotide-exchange factor Tiam1 by facilitating its binding to the plasma membrane and regulating GDP/GTP exchange on Rac1. *Biochemical Journal*, *382*(3). https://doi.org/10.1042/BJ20040916

Frost, N. A., Shroff, H., Kong, H., Betzig, E., & Blanpied, T. A. (2010). Single-molecule discrimination of discrete perisynaptic and distributed sites of Actin filament assembly within dendritic spines. *Neuron*, *67*(1). https://doi.org/10.1016/j.neuron.2010.05.026

Fujisawa, K., Fujita, A., Ishizaki, T., Saito, Y., & Narumiya, S. (1996). Identification of the Rho-binding domain of p160(ROCK), a Rho-associated coiled-coil containing protein kinase. *Journal of Biological Chemistry*, *271*(38). https://doi.org/10.1074/jbc.271.38.23022

Fujiwara, I., Vavylonis, D., & Pollard, T. D. (2007). Polymerization kinetics of ADP- and ADP-Pi-Actin determined by fluorescence microscopy. *Proceedings of the National Academy of Sciences of the United States of America*, *104*(21). https://doi.org/10.1073/pnas.0702510104

Fujiwara, T. K., Iwasawa, K., Kalay, Z., Tsunoyama, T. A., Watanabe, Y., Umemura, Y. M., Murakoshi, H., Suzuki, K. G. N., Nemoto, Y. L., Morone, N., & Kusumi, A. (2016). Confined diffusion of transmembrane proteins and lipids induced by the same Actin meshwork lining the plasma membrane. *Molecular Biology of the Cell*, *27*(7). https://doi.org/10.1091/mbc.E15-04-0186

Galletta, B. J., Mooren, O. L., & Cooper, J. A. (2010). Actin dynamics and endocytosis in yeast and mammals. In *Current Opinion in Biotechnology* (Vol. 21, Issue 5). https://doi.org/10.1016/j.copbio.2010.06.006

Gandhl, S. P., & Stevens, C. F. (2003). Three modes of synaptic vesicular recycling revealed by single-vesicle imaging. *Nature*, *423*(6940). https://doi.org/10.1038/nature01677

Ganguly, A., Tang, Y., Wang, L., Ladt, K., Loi, J., Dargent, B., Leterrier, C., & Roy, S. (2015). A dynamic formin-dependent deep F-Actin network in axons. *Journal of Cell Biology*, *210*(3). https://doi.org/10.1083/jcb.201506110

Gao, L., & Bretscher, A. (2008). Analysis of unregulated formin activity reveals how yeast can balance F-Actin assembly between different microfilament-based organizations. *Molecular Biology of the Cell*, *19*(4). https://doi.org/10.1091/mbc.E07-05-0520

Garcia-Mata, R., Boulter, E., & Burridge, K. (2011). The "invisible hand": Regulation of RHO GTPases by RHOGDIs. In *Nature Reviews Molecular Cell Biology* (Vol. 12, Issue 8). https://doi.org/10.1038/nrm3153

Garrett, A. M., Schreiner, D., Lobas, M. A., & Weiner, J. A. (2012). γ-Protocadherins Control Cortical Dendrite Arborization by Regulating the Activity of a FAK/PKC/MARCKS Signaling Pathway. *Neuron*, *74*(2). https://doi.org/10.1016/j.neuron.2012.01.028

Garrett, W. S., Chen, L. M., Kroschewski, R., Ebersold, M., Turley, S., Trombetta, S., Galán, J. E., & Mellman, I. (2000). Developmental control of endocytosis in dendritic cells by Cdc42. *Cell*, *102*(3). https://doi.org/10.1016/S0092-8674(00)00038-6

Gasteier, J. E., Madrid, R., Krautkrämer, E., Schröder, S., Muranyi, W., Benichou, S., & Fackler, O. T. (2003). Activation of the Rac-binding partner FHOD1 induces Actin stress fibers via a ROCK-dependent mechanism. *Journal of Biological*

Chemistry, *278*(40). https://doi.org/10.1074/jbc.M306229200

Gauthier, N. C., Fardin, M. A., Roca-Cusachs, P., & Sheetz, M. P. (2011). Temporary increase in plasma membrane tension coordinates the activation of exocytosis and contraction during cell spreading. *Proceedings of the National Academy of Sciences of the United States of America*, *108*(35). https://doi.org/10.1073/pnas.1105845108

Gerth, F., Jäpel, M., Sticht, J., Kuropka, B., Schmitt, X. J., Driller, J. H., Loll, B., Wahl, M. C., Pagel, K., Haucke, V., & Freund, C. (2019). Exon Inclusion Modulates Conformational Plasticity and Autoinhibition of the Intersectin 1 SH3A Domain. *Structure*, *27*(6). https://doi.org/10.1016/j.str.2019.03.020

Gibbs, J. B., Marshall, M. S., Scolnick, E. M., Dixon, R. A. F., & Vogel, U. S. (1990). Modulation of guanine nucleotides bound to Ras in NIH3T3 cells by oncogenes, growth factors, and the GTPase activating protein (GAP). *Journal of Biological Chemistry*, *265*(33). https://doi.org/10.1016/s0021-9258(17)30523-9

Gimber, N., Tadeus, G., Maritzen, T., Schmoranzer, J., & Haucke, V. (2015). Diffusional spread and confinement of newly exocytosed synaptic vesicle proteins. *Nature Communications*, *6*. https://doi.org/10.1038/ncomms9392

Gitler, D., Cheng, Q., Greengard, P., & Augustine, G. J. (2008). Synapsin IIa controls the reserve pool of glutamatergic synaptic vesicles. *Journal of Neuroscience*, *28*(43). https://doi.org/10.1523/JNEUROSCI.0924-08.2008

Glebov, O. O., Jackson, R. E., Winterflood, C. M., Owen, D. M., Barker, E. A., Doherty, P., Ewers, H., & Burrone, J. (2017). Nanoscale Structural Plasticity of the Active Zone Matrix Modulates Presynaptic Function. *Cell Reports*, *18*(11). https://doi.org/10.1016/j.celrep.2017.02.064

Gödel, M., Hartleben, B., Herbach, N., Liu, S., Zschiedrich, S., Lu, S., Debreczeni-Mór, A., Lindenmeyer, M. T., Rastaldi, M. P., Hartleben, G., Wiech, T., Fornoni, A., Nelson, R. G., Kretzler, M., Wanke, R., Pavenstädt, H., Kerjaschki, D., Cohen, C. D., Hall, M. N., … Huber, T. B. (2011). Role of mTOR in podocyte function and diabetic nephropathy in humans and mice. *Journal of Clinical Investigation*, *121*(6). https://doi.org/10.1172/JCI44774

Goldschmidt-Clermont, P. J., Furman, M. I., Wachsstock, D., Safer, D., Nachmias, V. T., & Pollard, T. D. (1992). The control of Actin nucleotide exchange by thymosinβ4 and profilin. A potential regulatory mechanism for Actin polymerization in cells. *Molecular Biology of the Cell*, *3*(9). https://doi.org/10.1091/mbc.3.9.1015

Goldschmidt, H. L., Tu-Sekine, B., Volk, L., Anggono, V., Huganir, R. L., & Raben, D. M. (2016). DGKθ Catalytic Activity Is Required for Efficient Recycling of Presynaptic Vesicles at Excitatory Synapses. *Cell Reports*, *14*(2). https://doi.org/10.1016/j.celrep.2015.12.022

Goley, E. D., & Welch, M. D. (2006). The ARP2/3 complex: An Actin nucleator comes of age. In *Nature Reviews Molecular Cell Biology* (Vol. 7, Issue 10). https://doi.org/10.1038/nrm2026

Gomez-Cambronero, J. (2011). The exquisite regulation of PLD2 by a wealth of interacting proteins: S6K, Grb2, Sos, WASp and Rac2 (And a surprise discovery: PLD2 is a GEF). In *Cellular Signalling* (Vol. 23, Issue 12). https://doi.org/10.1016/j.cellsig.2011.06.017

Gomez, T. S., Kumar, K., Medeiros, R. B., Shimizu, Y., Leibson, P. J., & Billadeau, D. D. D. (2007). Formins Regulate the Actin-Related Protein 2/3 Complex-Independent Polarization of the Centrosome to the Immunological Synapse. *Immunity*, *26*(2). https://doi.org/10.1016/j.immuni.2007.01.008

Gonschior, H., Schmied, C., Van der Veen, R. E., Eichhorst, J., Himmerkus, N., Piontek, J., Günzel, D., Bleich, M., Furuse, M., Haucke, V., & Lehmann, M. (2022). Nanoscale segregation of channel and barrier claudins enables paracellular ion flux. *Nature Communications*, *13*(1). https://doi.org/10.1038/s41467-022-32533-4

González-Forero, D., Montero, F., García-Morales, V., Domínguez, G., Gómez-Pérez, L., García-Verdugo, J. M., & Moreno-López, B. (2012). Endogenous rho-kinase signaling maintains synaptic strength by stabilizing the size of the readily releasable pool of synaptic vesicles. *Journal of Neuroscience*, *32*(1). https://doi.org/10.1523/JNEUROSCI.3215-11.2012

Gorelik, R., Yang, C., Kameswaran, V., Dominguez, R., & Svitkina, T. (2011). Mechanisms of plasma membrane targeting of formin mDia2 through its amino terminal domains. *Molecular Biology of the Cell*, *22*(2). https://doi.org/10.1091/mbc.E10-03-0256

Govek, E. E., Newey, S. E., Akerman, C. J., Cross, J. R., Der Veken, L. Van, & Van Aelst, L. (2004). The X-linked mental retardation protein oligophrenin-1 is required for dendritic spine morphogenesis. *Nature Neuroscience*, *7*(4).

https://doi.org/10.1038/nn1210

Graham, M. E., Anggono, V., Bache, N., Larsen, M. R., Craft, G. E., & Robinson, P. J. (2007). The in vivo phosphorylation sites of rat brain dynamin I. *Journal of Biological Chemistry*, *282*(20). https://doi.org/10.1074/jbc.M609713200

Granseth, B., Odermatt, B., Royle, S. J. J., & Lagnado, L. (2006). Clathrin-Mediated Endocytosis Is the Dominant Mechanism of Vesicle Retrieval at Hippocampal Synapses. *Neuron*, *51*(6). https://doi.org/10.1016/j.neuron.2006.08.029

Graziano, B. R., DuPage, A. G., Michelot, A., Breitsprecher, D., Moseley, J. B., Sagot, I., Blanchoin, L., & Goode, B. L. (2011). Mechanism and cellular function of Bud6 as an Actin nucleation-promoting factor. *Molecular Biology of the Cell*, *22*(21). https://doi.org/10.1091/mbc.E11-05-0404

Guilluy, C., Swaminathan, V., Garcia-Mata, R., O'Brien, E. T., Superfine, R., & Burridge, K. (2011). The Rho GEFs LARG and GEF-H1 regulate the mechanical response to force on integrins. *Nature Cell Biology*, *13*(6). https://doi.org/10.1038/ncb2254

Guo, J., Ge, J. L., Hao, M., Sun, Z. C., Wu, X. S., Zhu, J. B., Wang, W., Yao, P. T., Lin, W., & Xue, L. (2015). A Three-Pool Model Dissecting Readily Releasable Pool Replenishment at the Calyx of Held. *Scientific Reports*, *5*. https://doi.org/10.1038/srep09517

Guzman, G. A., Guzman, R. E., Jordan, N., & Hidalgo, P. (2019). A tripartite interaction among the calcium channel α1- and β-subunits and f-Actin increases the readily releasable pool of vesicles and its recovery after depletion. *Frontiers in Cellular Neuroscience*, *13*. https://doi.org/10.3389/fncel.2019.00125

Habas, R., Kato, Y., & He, X. (2001). Wnt/Frizzled activation of Rho regulates vertebrate gastrulation and requires a novel formin homology protein Daam1. *Cell*, *107*(7). https://doi.org/10.1016/S0092-8674(01)00614-6

Hagiwara, A., Cornu, M., Cybulski, N., Polak, P., Betz, C., Trapani, F., Terracciano, L., Heim, M. H., Rüegg, M. A., & Hall, M. N. (2012). Hepatic mTORC2 activates glycolysis and lipogenesis through Akt, glucokinase, and SREBP1c. *Cell Metabolism*, *15*(5). https://doi.org/10.1016/j.cmet.2012.03.015

Hannemann, S., Madrid, R., Stastna, J., Kitzing, T., Gasteier, J., Schönichen, A., Bouchet, J., Jimenez, A., Geyer, M., Grosse, R., Benichou, S., & Fackler, O. T. (2008). The diaphanous-related formin FHOD1 associates with ROCK1 and promotes Src-dependent plasma membrane blebbing. *Journal of Biological Chemistry*, *283*(41). https://doi.org/10.1074/jbc.M801800200

Harris, E. S., Li, F., & Higgs, H. N. (2004). The Mouse Formin, FRLα, Slows Actin Filament Barbed End Elongation, Competes with Capping Protein, Accelerates Polymerization from Monomers, and Severs Filaments. *Journal of Biological Chemistry*, *279*(19). https://doi.org/10.1074/jbc.M312718200

Hassinger, J. E., Oster, G., Drubin, D. G., & Rangamani, P. (2017). Design principles for robust vesiculation in clathrin-mediated endocytosis. *Proceedings of the National Academy of Sciences of the United States of America*, *114*(7). https://doi.org/10.1073/pnas.1617705114

Haucke, V., Neher, E., & Sigrist, S. J. (2011). Protein scaffolds in the coupling of synaptic exocytosis and endocytosis. In *Nature Reviews Neuroscience* (Vol. 12, Issue 3). https://doi.org/10.1038/nrn2948

He, L., & Wu, L. G. (2007). The debate on the kiss-and-run fusion at synapses. In *Trends in Neurosciences* (Vol. 30, Issue 9). https://doi.org/10.1016/j.tins.2007.06.012

Heemskerk, F. M. J., Chen, H. C., & Huang, F. L. (1993). Protein kinase C phosphorylates Ser152, Ser156 and Ser163 but not Ser160 of MARCKS in rat brain. *Biochemical and Biophysical Research Communications*, *190*(1). https://doi.org/10.1006/bbrc.1993.1036

Hernández-Negrete, I., Carretero-Ortega, J., Rosenfeldt, H., Hernández-García, R., Calderón-Salinas, J. V., Reyes-Cruz, G., Gutkind, J. S., & Vázquez-Prado, J. (2007). P-Rex1 links mammalian target of rapamycin signaling to Rac activation and cell migration. *Journal of Biological Chemistry*, *282*(32). https://doi.org/10.1074/jbc.M703771200

Herzog, D., Loetscher, P., van Hengel, J., Knüsel, S., Brakebusch, C., Taylor, V., Suter, U., & Relvas, J. B. (2011). The small GTpase RhoA is required to maintain spinal cord neuroepithelium organization and the neural stem cell pool. *Journal of Neuroscience*, *31*(13). https://doi.org/10.1523/JNEUROSCI.4807-10.2011

Heuser, J. E., & Reese, T. S. (1973). Evidence for recycling of synaptic vesicle membrane during transmitter release at the frog

neuromuscular junction. *Journal of Cell Biology*, *57*(2). https://doi.org/10.1083/jcb.57.2.315

Higashi, T., Ikeda, T., Shirakawa, R., Kondo, H., Kawato, M., Horiguchi, M., Okuda, T., Okawa, K., Fukai, S., Nureki, O., Kita, T., & Horiuchi, H. (2008). Biochemical characterization of the Rho GTPase-regulated Actin assembly by diaphanous-related formins, mDia1 and Daam1, in platelets. *Journal of Biological Chemistry*, *283*(13). https://doi.org/10.1074/jbc.M707839200

Higashida, C., Miyoshi, T., Fujita, A., Oceguera-Yanez, F., Monypenny, J., Andou, Y., Narumiya, S., & Watanabe, N. (2004). Actin Polymerization-Driven Molecular Movement of mDia1 in Living Cells. *Science*, *303*(5666). https://doi.org/10.1126/science.1093923

Higgs, H. N., & Pollard, T. D. (2001). Regulation of Actin filament network formation through Arp2/3 complex: Activation by a diverse array of proteins. In *Annual Review of Biochemistry* (Vol. 70). https://doi.org/10.1146/annurev.biochem.70.1.649

Hill, K., Krugmann, S., Andrews, S. R., Coadwell, W. J., Finan, P., Welch, H. C. E., Hawkins, P. T., & Stephens, L. R. (2005). Regulation of P-Rex1 by phosphatidylinositol (3,4,5)-trisphosphate and Gβγ subunits. *Journal of Biological Chemistry*, *280*(6). https://doi.org/10.1074/jbc.M411262200

Hirokawa, N., Sobue, K., Kanda, K., Harada, A., & Yorifuji, H. (1989). The cytoskeletal architecture of the presynaptic terminal and molecular structure of synapsin 1. *Journal of Cell Biology*, *108*(1). https://doi.org/10.1083/jcb.108.1.111

Hochmuth, R. M., Shao, J. Y., Dai, J., & Sheetz, M. P. (1996). Deformation and flow of membrane into tethers extracted from neuronal growth cones. *Biophysical Journal*, *70*(1). https://doi.org/10.1016/S0006-3495(96)79577-2

Holderith, N., Lorincz, A., Katona, G., Rózsa, B., Kulik, A., Watanabe, M., & Nusser, Z. (2012). Release probability of hippocampal glutamatergic terminals scales with the size of the active zone. *Nature Neuroscience*, *15*(7). https://doi.org/10.1038/nn.3137

Holt, M., Cooke, A., Wu, M. M., & Lagnado, L. (2003). Bulk membrane retrieval in the synaptic terminal of retinal bipolar cells. *Journal of Neuroscience*, *23*(4). https://doi.org/10.1523/jneurosci.23-04-01329.2003

Hori, T., Eguchi, K., Wang, H. Y., Miyasaka, T., Guillaud, L., Taoufiq, Z., Mahapatra, S., Yamada, H., Takei, K., & Takahashi, T. (2022). Microtubule assembly by soluble tau impairs vesicle endocytosis and excitatory neurotransmission via dynamin sequestration in Alzheimer's disease mice synapse model. *ELife*, *11*. https://doi.org/10.7554/eLife.73542

Hornberger, T. A., Chu, W. K., Mak, Y. W., Hsiung, J. W., Huang, S. A., & Chien, S. (2006). The role of phospholipase D and phosphatidic acid in the mechanical activation of mTOR signaling in skeletal muscle. *Proceedings of the National Academy of Sciences of the United States of America*, *103*(12). https://doi.org/10.1073/pnas.0600678103

Horvath, P. M., Piazza, M. K., Monteggia, L. M., & Kavalali, E. T. (2020). Spontaneous and evoked neurotransmission are partially segregated at inhibitory synapses. *ELife*, *9*. https://doi.org/10.7554/eLife.52852

Horwood, J. M., Dufour, F., Laroche, S., & Davis, S. (2006). Signalling mechanisms mediated by the phosphoinositide 3-kinase/Akt cascade in synaptic plasticity and memory in the rat. *European Journal of Neuroscience*, *23*(12). https://doi.org/10.1111/j.1460-9568.2006.04859.x

Hotulainen, P., Llano, O., Smirnov, S., Tanhuanpää, K., Faix, J., Rivera, C., & Lappalainen, P. (2009). Defning mechanisms of Actin polymerization and depolymerization during Dendritic spine morphogenesis. *Journal of Cell Biology*, *185*(2). https://doi.org/10.1083/jcb.200809046

Houk, A. R., Jilkine, A., Mejean, C. O., Boltyanskiy, R., Dufresne, E. R., Angenent, S. B., Altschuler, S. J., Wu, L. F., & Weiner, O. D. (2012). Membrane tension maintains cell polarity by confining signals to the leading edge during neutrophil migration. *Cell*, *148*(1–2). https://doi.org/10.1016/j.cell.2011.10.050

Hsu, P. P., Kang, S. A., Rameseder, J., Zhang, Y., Ottina, K. A., Lim, D., Peterson, T. R., Choi, Y., Gray, N. S., Yaffe, M. B., Marto, J. A., & Sabatini, D. M. (2011). The mTOR-regulated phosphoproteome reveals a mechanism of mTORC1-mediated inhibition of growth factor signaling. *Science*, *332*(6035). https://doi.org/10.1126/science.1199498

Hua, Y., Sinha, R., Thiel, C. S., Schmidt, R., Hüve, J., Martens, H., Hell, S. W., Egner, A., & Klingauf, J. (2011). A readily retrievable pool of synaptic vesicles. *Nature Neuroscience*, *14*(7). https://doi.org/10.1038/nn.2838

Hua, Z., Leal-Ortiz, S., Foss, S. M., Waites, C. L., Garner, C. C., Voglmaier, S. M., & Edwards, R. H. (2011). V-SNARE

composition distinguishes synaptic vesicle pools. *Neuron*, *71*(3). https://doi.org/10.1016/j.neuron.2011.06.010

Huang, W., Zhu, P. J., Zhang, S., Zhou, H., Stoica, L., Galiano, M., Krnjević, K., Roman, G., & Costa-Mattioli, M. (2013). MTORC2 controls Actin polymerization required for consolidation of long-term memory. *Nature Neuroscience*, *16*(4). https://doi.org/10.1038/nn.3351

Hunter, T. (1995). Protein kinases and phosphatases: The Yin and Yang of protein phosphorylation and signaling. In *Cell* (Vol. 80, Issue 2). https://doi.org/10.1016/0092-8674(95)90405-0

Imamura, H., Tanaka, K., Hihara, T., Umikawa, M., Kamei, T., Takahashi, K., Sasaki, T., & Takai, Y. (1997). Bni1p and Bnr1p: Downstream targets of the Rho family small G-proteins which interact with profilin and regulate Actin cytoskeleton in Saccharomyces cerevisiae. *EMBO Journal*, *16*(10). https://doi.org/10.1093/emboj/16.10.2745

Imoto, Y., Raychaudhuri, S., Ma, Y., Fenske, P., Sandoval, E., Itoh, K., Blumrich, E. M., Matsubayashi, H. T., Mamer, L., Zarebidaki, F., Söhl-Kielczynski, B., Trimbuch, T., Nayak, S., Iwasa, J. H., Liu, J., Wu, B., Ha, T., Inoue, T., Jorgensen, E. M., … Watanabe, S. (2022). Dynamin is primed at endocytic sites for ultrafast endocytosis. *Neuron*, *110*(17). https://doi.org/10.1016/j.neuron.2022.06.010

Isagawa, T., Mukai, H., Oishi, K., Taniguchi, T., Hasegawa, H., Kawamata, T., Tanaka, C., & Ono, Y. (2000). Dual effects of PKNα and protein kinase C on phosphorylation of tau protein by glycogen synthase kinase-3β. *Biochemical and Biophysical Research Communications*, *273*(1). https://doi.org/10.1006/bbrc.2000.2926

Isogai, T., & Danuser, G. (2018). Discovery of functional interactions among Actin regulators by analysis of image fluctuations in an unperturbed motile cell system. *Philosophical Transactions of the Royal Society B: Biological Sciences*, *373*(1747). https://doi.org/10.1098/rstb.2017.0110

Isogai, T., van der Kammen, R., Leyton-Puig, D., Kedziora, K. M., Jalink, K., & Innocenti, M. (2015). Initiation of lamellipodia and ruffles involves cooperation between mDia1 and the Arp2/3 complex. *Journal of Cell Science*, *128*(20). https://doi.org/10.1242/jcs.176768

Jacinto, E., Loewith, R., Schmidt, A., Lin, S., Rüegg, M. A., Hall, A., & Hall, M. N. (2004). Mammalian TOR complex 2 controls the Actin cytoskeleton and is rapamycin insensitive. *Nature Cell Biology*, *6*(11). https://doi.org/10.1038/ncb1183

Jaiswal, R., Breitsprecher, D., Collins, A., Corrêa, I. R., Xu, M. Q., & Goode, B. L. (2013). The formin daam1 and fascin directly collaborate to promote filopodia formation. *Current Biology*, *23*(14). https://doi.org/10.1016/j.cub.2013.06.013

Jégou, A., Carlier, M. F., & Romet-Lemonne, G. (2013). Formin mDia1 senses and generates mechanical forces on Actin filaments. *Nature Communications*, *4*. https://doi.org/10.1038/ncomms2888

Jensen, C. C., Clements, A. N., Liou, H., Ball, L. E., Bethard, J. R., Langlais, P. R., Toth, R. K., Chauhan, S. S., Casillas, A. L., Daulat, S. R., Kraft, A. S., Cress, A. E., Miranti, C. K., Mouneimne, G., Rogers, G. C., & Warfel, N. A. (2023). PIM1 phosphorylates ABI2 to enhance Actin dynamics and promote tumor invasion. *Journal of Cell Biology*, *222*(6). https://doi.org/10.1083/jcb.202208136

Jia, D., Gomez, T. S., Metlagel, Z., Umetani, J., Otwinowski, Z., Rosen, M. K., & Billadeau, D. D. (2010). WASH and WAVE Actin regulators of the Wiskott-Aldrich syndrome protein (WASP) family are controlled by analogous structurally related complexes. *Proceedings of the National Academy of Sciences of the United States of America*, *107*(23). https://doi.org/10.1073/pnas.0913293107

Jin, Y. H., Wu, X. S., Shi, B., Zhang, Z., Guo, X., Gan, L., Chen, Z., & Wu, L. G. (2019). Protein kinase C and calmodulin serve as calcium sensors for calcium-stimulated endocytosis at synapses. *Journal of Neuroscience*, *39*(48). https://doi.org/10.1523/JNEUROSCI.0182-19.2019

Job, C., & Lagnado, L. (1998). Calcium and protein kinase C regulate the Actin cytoskeleton in the synaptic terminal of retinal bipolar cells. *Journal of Cell Biology*, *143*(6). https://doi.org/10.1083/jcb.143.6.1661

Jung, M., Kim, D., & Mun, J. Y. (2020). Direct Visualization of Actin Filaments and Actin-Binding Proteins in Neuronal Cells. In *Frontiers in Cell and Developmental Biology* (Vol. 8). https://doi.org/10.3389/fcell.2020.588556

Kabrawala, S., Zimmer, M. D., & Campellone, K. G. (2020). WHIMP links the Actin nucleation machinery to Src-family kinase signaling during protrusion and motility. *PLoS Genetics*, *16*(3). https://doi.org/10.1371/journal.pgen.1008694

Kaibuchi, K., Kuroda, S., & Amano, M. (1999). Regulation of the cytoskeleton and cell adhesion by the Rho family GTPases in

mammalian cells. In *Annual Review of Biochemistry* (Vol. 68). https://doi.org/10.1146/annurev.biochem.68.1.459

Kaksonen, M., Toret, C. P., & Drubin, D. G. (2006). Harnessing Actin dynamics for clathrin-mediated endocytosis. In *Nature Reviews Molecular Cell Biology* (Vol. 7, Issue 6). https://doi.org/10.1038/nrm1940

Kalappurakkal, J. M., Anilkumar, A. A., Patra, C., van Zanten, T. S., Sheetz, M. P., & Mayor, S. (2019). Integrin Mechano-chemical Signaling Generates Plasma Membrane Nanodomains that Promote Cell Spreading. *Cell*, *177*(7). https://doi.org/10.1016/j.cell.2019.04.037

Kato, T., Watanabe, N., Morishima, Y., Fujita, A., Ishizaki, T., & Narumiya, S. (2001). Localization of a mammalian homolog of diaphanous, mDia1, to the mitotic spindle in HeLa cells. *Journal of Cell Science*, *114*(4). https://doi.org/10.1242/jcs.114.4.775

Katsumi, A., Milanini, J., Kiosses, W. B., Del Pozo, M. A., Kaunas, R., Chien, S., Hahn, K. M., & Schwartz, M. A. (2002). Effects of cell tension on the small GTPase Rac. *Journal of Cell Biology*, *158*(1). https://doi.org/10.1083/jcb.200201105

Katz, B. (1950). Action potentials from a sensory nerve ending. *The Journal of Physiology*, *111*(3–4). https://doi.org/10.1113/jphysiol.1950.sp004478

Kaur, S., Fielding, A. B., Gassner, G., Carter, N. J., & Royle, S. J. (2014). An unmet Actin requirement explains the mitotic inhibition of clathrin-mediated endocytosis. *ELife*, *3*. https://doi.org/10.7554/elife.00829

Kavalali, E. T. (2015). The mechanisms and functions of spontaneous neurotransmitter release. In *Nature Reviews Neuroscience* (Vol. 16, Issue 1). https://doi.org/10.1038/nrn3875

Keine, C., Al-Yaari, M., Radulovic, T., Thomas, C. I., Ramos, P. V., Guerrero-Given, D., Ranjan, M., Taschenberger, H., Kamasawa, N., & Young, S. M. (2022). Presynaptic Rac1 controls synaptic strength through the regulation of synaptic vesicle priming. *ELife*, *11*. https://doi.org/10.7554/eLife.81505

Kennedy, M. B. (2016). Synaptic signaling in learning and memory. *Cold Spring Harbor Perspectives in Biology*, *8*(2). https://doi.org/10.1101/cshperspect.a016824

Kesavapany, S., Amin, N., Zheng, Y. L., Nijhara, R., Jaffe, H., Sihag, R., Gutkind, J. S., Takahashi, S., Kulkarni, A., Grant, P., & Pant, H. C. (2004). p35/Cyclin-Dependent Kinase 5 Phosphorylation of Ras Guanine Nucleotide Releasing Factor 2 (RasGRF2) Mediates Rac-Dependent Extracellular Signal-Regulated Kinase 1/2 Activity, Altering RasGRF2 and Microtubule-Associated Protein 1b Distribution in Neurons. *Journal of Neuroscience*, *24*(18). https://doi.org/10.1523/JNEUROSCI.0690-04.2004

Kessels, M. M., & Qualmann, B. (2004). The syndapin protein family: Linking membrane trafficking with the cytoskeleton. In *Journal of Cell Science* (Vol. 117, Issue 15). https://doi.org/10.1242/jcs.01290

Khandelwal, P., Ruiz, W. G., & Apodaca, G. (2010). Compensatory endocytosis in bladder umbrella cells occurs through an integrin-regulated and RhoA-and dynamin-dependent pathway. *EMBO Journal*, *29*(12). https://doi.org/10.1038/emboj.2010.91

Kim, A. S., Kakalis, L. T., Abdul-Manan, N., Liu, G. A., & Rosen, M. K. (2000). Autoinhibition and activation mechanisms of the Wiskott-Aldrich syndrome protein. *Nature*, *404*(6774). https://doi.org/10.1038/35004513

Kippenberger, S., Loitsch, S., Guschel, M., Müller, J., Knies, Y., Kaufmann, R., & Bernd, A. (2005). Mechanical stretch stimulates protein kinase B/Akt phosphorylation in epidermal cells via angiotensin II type 1 receptor and epidermal growth factor receptor. *Journal of Biological Chemistry*, *280*(4). https://doi.org/10.1074/jbc.M409590200

Kitagishi, Y., Kobayashi, M., Kikuta, K., & Matsuda, S. (2012). Roles of PI3K/AKT/GSK3/mTOR pathway in cell signaling of mental illnesses. In *Depression Research and Treatment* (Vol. 2012). https://doi.org/10.1155/2012/752563

Kitzing, T. M., Sahadevan, A. S., Brandt, D. T., Knieling, H., Hannemann, S., Fackler, O. T., Großhans, J., & Grosse, R. (2007). Positive feedback between Dia1, LARG, and RhoA regulates cell morphology and invasion. *Genes and Development*, *21*(12). https://doi.org/10.1101/gad.424807

Kokotos, A. C., Peltier, J., Davenport, E. C., Trost, M., & Cousin, M. A. (2018). Activity-dependent bulk endocytosis proteome reveals a key presynaptic role for the monomeric GTPase Rab11. *Proceedings of the National Academy of Sciences of the United States of America*, *115*(43). https://doi.org/10.1073/pnas.1809189115

Kononenko, N. L., & Haucke, V. (2015). Molecular mechanisms of presynaptic membrane retrieval and synaptic vesicle reformation. In *Neuron* (Vol. 85, Issue 3). https://doi.org/10.1016/j.neuron.2014.12.016

Kononenko, N. L., Puchkov, D., Classen, G. A., Walter, A. M., Pechstein, A., Sawade, L., Kaempf, N., Trimbuch, T., Lorenz, D., Rosenmund, C., Maritzen, T., & Haucke, V. (2014). Clathrin/AP-2 mediate synaptic vesicle reformation from endosome-like vacuoles but are not essential for membrane retrieval at central synapses. *Neuron*, *82*(5). https://doi.org/10.1016/j.neuron.2014.05.007

Körber, C., Horstmann, H., Sätzler, K., & Kuner, T. (2012). Endocytic structures and synaptic vesicle recycling at a central synapse in awake rats. *Traffic*, *13*(12). https://doi.org/10.1111/tra.12007

Korobova, F., & Svitkina, T. M. (2010). Molecular architecture of synaptic Actin cytoskeleton in hippocampal neurons reveals a mechanism of dendritic spine morphogenesis. *Molecular Biology of the Cell*, *21*(1). https://doi.org/10.1091/mbc.E09-07-0596

Kotula, L. (2012). Abi1, a critical molecule coordinating Actin cytoskeleton reorganization with PI-3 kinase and growth signaling. In *FEBS Letters* (Vol. 586, Issue 17). https://doi.org/10.1016/j.febslet.2012.05.015

Kovar, D. R. (2006). Molecular details of formin-mediated Actin assembly. In *Current Opinion in Cell Biology* (Vol. 18, Issue 1). https://doi.org/10.1016/j.ceb.2005.12.011

Kovar, D. R., Harris, E. S., Mahaffy, R., Higgs, H. N., & Pollard, T. D. (2006). Control of the assembly of ATP- and ADP-Actin by formins and profilin. In *Cell* (Vol. 124, Issue 2). https://doi.org/10.1016/j.cell.2005.11.038

Kozlov, M. M., & Bershadsky, A. D. (2004). Processive capping by formin suggests a force-driven mechanism of Actin polymerization. *Journal of Cell Biology*, *167*(6). https://doi.org/10.1083/jcb.200410017

Krause, M., Dent, E. W., Bear, J. E., Loureiro, J. J., & Gertler, F. B. (2003). Ena/VASP Proteins: Regulators of the Actin Cytoskeleton and Cell Migration. *Annual Review of Cell and Developmental Biology*, *19*. https://doi.org/10.1146/annurev.cellbio.19.050103.103356

Kühn, S., & Geyer, M. (2014). Formins as effector proteins of rho GTPases. In *Small GTPases* (Vol. 5, Issue JUNE). https://doi.org/10.4161/sgtp.29513

Kumar, P., Jha, N. K., Jha, S. K., Ramani, K., & Ambasta, R. K. (2015). Tau phosphorylation, molecular chaperones, and ubiquitin E3 Ligase: Clinical relevance in Alzheimer's disease. In *Journal of Alzheimer's Disease* (Vol. 43, Issue 2). https://doi.org/10.3233/JAD-140933

Kuo, J. C., Han, X., Hsiao, C. Te, Yates, J. R., & Waterman, C. M. (2011). Analysis of the myosin-II-responsive focal adhesion proteome reveals a role for β-Pix in negative regulation of focal adhesion maturation. *Nature Cell Biology*, *13*(4). https://doi.org/10.1038/ncb2216

Kwon, S. E., & Chapman, E. R. (2011). Synaptophysin Regulates the Kinetics of Synaptic Vesicle Endocytosis in Central Neurons. *Neuron*, *70*(5). https://doi.org/10.1016/j.neuron.2011.04.001

Kwon, T., Kwon, D. Y., Chun, J., Kim, J. H., & Kang, S. S. (2000). Akt protein kinase inhibits Rac1-GTP binding through phosphorylation at serine 71 of Rac1. *Journal of Biological Chemistry*, *275*(1). https://doi.org/10.1074/jbc.275.1.423

Lacy, M. M., Ma, R., Ravindra, N. G., & Berro, J. (2018). Molecular mechanisms of force production in clathrin-mediated endocytosis. In *FEBS Letters* (Vol. 592, Issue 21). https://doi.org/10.1002/1873-3468.13192

Lamaze, C., Chuang, T. H., Terlecky, L. J., Bokoch, G. M., & Schmid, S. L. (1996). Regulation of receptor-mediated endocytosis by Rho and Rac. *Nature*, *382*(6587). https://doi.org/10.1038/382177a0

Lammers, M., Meyer, S., Kühlmann, D., & Wittinghofer, A. (2008). Specificity of interactions between mDia isoforms and Rho proteins. *Journal of Biological Chemistry*, *283*(50). https://doi.org/10.1074/jbc.M805634200

Lammers, M., Rose, R., Scrima, A., & Wittinghofer, A. (2005). The regulation of mDia1 by autoinhibition and its release by Rho•GTP. *EMBO Journal*, *24*(23). https://doi.org/10.1038/sj.emboj.7600879

Larsson, C. (2006). Protein kinase C and the regulation of the Actin cytoskeleton. In *Cellular Signalling* (Vol. 18, Issue 3). https://doi.org/10.1016/j.cellsig.2005.07.010

Lash, L. L., Wallar, B. J., Turner, J. D., Vroegop, S. M., Kilkuskie, R. E., Kitchen-Goosen, S. M., Xu, H. E., & Alberts, A. S. (2013).

Small-molecule intramimics of formin autoinhibition: A new strategy to target the cytoskeletal remodeling machinery in cancer cells. *Cancer Research*, *73*(22). https://doi.org/10.1158/0008-5472.CAN-13-1593

Lauwers, E., Goodchild, R., & Verstreken, P. (2016). Membrane Lipids in Presynaptic Function and Disease. In *Neuron* (Vol. 90, Issue 1). https://doi.org/10.1016/j.neuron.2016.02.033

Laux, T., Fukami, K., Thelen, M., Golub, T., Frey, D., & Caroni, P. (2000). GAP43, MARCKS, and CAP23 modulate PI(4,5)P2 at plasmalemmal rafts, and regulate cell cortex Actin dynamics through a common mechanism. *Journal of Cell Biology*, *149*(7). https://doi.org/10.1083/jcb.149.7.1455

Lawson, C. D., & Ridley, A. J. (2018). Rho GTPase signaling complexes in cell migration and invasion. In *Journal of Cell Biology* (Vol. 217, Issue 2). https://doi.org/10.1083/jcb.201612069

Lebensohn, A. M., & Kirschner, M. W. (2009). Activation of the WAVE Complex by Coincident Signals Controls Actin Assembly. *Molecular Cell*, *36*(3). https://doi.org/10.1016/j.molcel.2009.10.024

Lee, C., Kang, H. S., Chung, J. K., Sekiya, F., Kim, J. R., Han, J. S., Kim, S. R., Bae, Y. S., Morris, A. J., & Rhee, S. G. (1997). Inhibition of phospholipase D by clathrin assembly protein 3 (AP3). *Journal of Biological Chemistry*, *272*(25). https://doi.org/10.1074/jbc.272.25.15986

Lee, C., Kim, S. R., Chung, J. K., Frohman, M. A., Kilimann, M. W., & Rhee, S. G. (2000). Inhibition of phospholipase D by amphiphysins. *Journal of Biological Chemistry*, *275*(25). https://doi.org/10.1074/jbc.M001695200

Lee, S. Y., Wenk, M. R., Kim, Y., Nairn, A. C., & De Camilli, P. (2004). Regulation of synaptojanin 1 by cyclin-dependent kinase 5 at synapses. *Proceedings of the National Academy of Sciences of the United States of America*, *101*(2). https://doi.org/10.1073/pnas.0307813100

Lei, L., Luo, Y., Kang, D., Yang, F., Meng, D., Wang, J.-Z., Liu, R., Wang, X., & Li, H.-L. (2023). Gypenoside IX restores Akt/GSK-3β pathway and alleviates Alzheimer's disease-like neuropathology and cognitive deficits. *Aging*, *12*(15), 14172–1419. https://doi.org/https://doi.org/10.18632/aging.205295

Lembo, S., Strauss, L., Cheng, W. C. D., Vermeil, J., Siggel, M., Toro-Nahuelpan, M., Chan, C. J., Kosinski, J., Piel, M., Roure, O. Du, Heuvingh, J., Mahamid, J., & Diz-Muñoz, A. (2023). The distance between the plasma membrane and the actomyosin cortex acts as a nanogate to control cell surface mechanics. *BioRxiv*.

Lenzen, C., Cool, R. H., Prinz, H., Kuhlmann, J., & Wittinghofer, A. (1998). Kinetic analysis by fluorescence of the interaction between Ras and the catalytic domain of the guanine nucleotide exchange factor Cdc25(Mm). *Biochemistry*, *37*(20). https://doi.org/10.1021/bi972621j

Leonard, T. A., Róycki, B., Saidi, L. F., Hummer, G., & Hurley, J. H. (2011). Crystal structure and allosteric activation of protein kinase C βiI. *Cell*, *144*(1). https://doi.org/10.1016/j.cell.2010.12.013

Li, C., Hamon, Y., Mazaud, D., Troncoso, P. G., Dessar, M., Lamaze, C., & Blouin, C. M. (2023). Dia2 formin controls receptor activity by organizing plasma membrane lipid partitioning at the nanoscale. *BioRxiv*.

Li, Y. C., Bai, W. Z., Zhou, L., Sun, L. K., & Hashikawa, T. (2010). Nonhomogeneous distribution of filamentous Actin in the presynaptic terminals on the spinal motoneurons. *Journal of Comparative Neurology*, *518*(16). https://doi.org/10.1002/cne.22374

Li, Z., Lee, H., Eskin, S. G., Ono, S., Zhu, C., & McIntire, L. V. (2020). Mechanochemical coupling of formin-induced Actin interaction at the level of single molecular complex. *Biomechanics and Modeling in Mechanobiology*, *19*(5). https://doi.org/10.1007/s10237-019-01284-5

Li, Z., & Murthy, V. N. (2001). Visualizing postendocytic traffic of synaptic vesicles at hippocampal synapses. *Neuron*, *31*(4). https://doi.org/10.1016/S0896-6273(01)00398-1

Li, Z., Van Aelst, L., & Cline, H. T. (2000). Rho GTPases regulate distinct aspects of dendritic arbor growth in Xenopus central neurons in vivo. *Nature Neuroscience*, *3*(3). https://doi.org/10.1038/72920

Lieber, A. D., Yehudai-Resheff, S., Barnhart, E. L., Theriot, J. A., & Keren, K. (2013). Membrane tension in rapidly moving cells is determined by cytoskeletal forces. *Current Biology*, *23*(15). https://doi.org/10.1016/j.cub.2013.05.063

Litschko, C., Brühmann, S., Csiszár, A., Stephan, T., Dimchev, V., Damiano-Guercio, J., Junemann, A., Körber, S., Winterhoff,

M., Nordholz, B., Ramalingam, N., Peckham, M., Rottner, K., Merkel, R., & Faix, J. (2019). Functional integrity of the contractile Actin cortex is safeguarded by multiple Diaphanous-related formins. *Proceedings of the National Academy of Sciences of the United States of America*, *116*(9). https://doi.org/10.1073/pnas.1821638116

Liu, G., Kochlamazashvili, G., Puchkov, D., Müller, R., Schultz, C., Mackintosh, A. I., Vollweiter, D., Haucke, V., & Soykan, T. (2022). Endosomal phosphatidylinositol 3-phosphate controls synaptic vesicle cycling and neurotransmission. *The EMBO Journal*, *41*(9). https://doi.org/10.15252/embj.2021109352

Liu, L., Das, S., Losert, W., & Parent, C. A. (2010). MTORC2 Regulates Neutrophil Chemotaxis in a cAMP- and RhoA-Dependent Fashion. *Developmental Cell*, *19*(6). https://doi.org/10.1016/j.devcel.2010.11.004

Liu, P., Gan, W., Chin, Y. R., Ogura, K., Guo, J., Zhang, J., Wang, B., Blenis, J., Cantley, L. C., Toker, A., Su, B., & Wei, W. (2015). Ptdins(3,4,5) P3 -dependent activation of the mTORC2 kinase complex. *Cancer Discovery*, *5*(11). https://doi.org/10.1158/2159-8290.CD-15-0460

Loewith, R., Jacinto, E., Wullschleger, S., Lorberg, A., Crespo, J. L., Bonenfant, D., Oppliger, W., Jenoe, P., & Hall, M. N. (2002). Two TOR complexes, only one of which is rapamycin sensitive, have distinct roles in cell growth control. *Molecular Cell*, *10*(3). https://doi.org/10.1016/S1097-2765(02)00636-6

López-Hernández, T., Takenaka, K., Mori, Y., Kongpracha, P., Nagamori, S., Haucke, V., & Takamori, S. (2022). Clathrin-independent endocytic retrieval of SV proteins mediated by the clathrin adaptor AP-2 at mammalian central synapses. *ELife*, *11*. https://doi.org/10.7554/eLife.71198

Maas, R. L., Zeller, R., Woychik, R. P., Vogt, T. F., & Leder, P. (1990). Disruption of formin-encoding transcripts in two mutant limb deformity alleles. *Nature*, *346*(6287). https://doi.org/10.1038/346853a0

MacHacek, M., Hodgson, L., Welch, C., Elliott, H., Pertz, O., Nalbant, P., Abell, A., Johnson, G. L., Hahn, K. M., & Danuser, G. (2009). Coordination of Rho GTPase activities during cell protrusion. *Nature*, *461*(7260). https://doi.org/10.1038/nature08242

Machesky, L. M., & Hall, A. (1997). Role of Actin polymerization and adhesion to extracellular matrix in Rac- and Rho-induced cytoskeletal reorganization. *Journal of Cell Biology*, *138*(4). https://doi.org/10.1083/jcb.138.4.913

Macia, E., Ehrlich, M., Massol, R., Boucrot, E., Brunner, C., & Kirchhausen, T. (2006). Dynasore, a Cell-Permeable Inhibitor of Dynamin. *Developmental Cell*, *10*(6). https://doi.org/10.1016/j.devcel.2006.04.002

Maiti, S., Michelot, A., Gould, C., Blanchoin, L., Sokolova, O., & Goode, B. L. (2012). Structure and activity of full-length formin mDia1. *Cytoskeleton*, *69*(6). https://doi.org/10.1002/cm.21033

Malecz, N., McCabe, P. C., Spaargaren, C., Qiu, R. G., Chuang, Y. yu, & Symons, M. (2000). Synaptojanin 2, a novel Rac1 effector that regulates clathrin-mediated endocytosis. *Current Biology*, *10*(21). https://doi.org/10.1016/S0960-9822(00)00778-8

Manning, B. D., & Cantley, L. C. (2007). AKT/PKB Signaling: Navigating Downstream. In *Cell* (Vol. 129, Issue 7). https://doi.org/10.1016/j.cell.2007.06.009

Manning, B. D., & Toker, A. (2017). AKT/PKB Signaling: Navigating the Network. In *Cell* (Vol. 169, Issue 3). https://doi.org/10.1016/j.cell.2017.04.001

Maritzen, T., & Haucke, V. (2018). Coupling of exocytosis and endocytosis at the presynaptic active zone. In *Neuroscience Research* (Vol. 127). https://doi.org/10.1016/j.neures.2017.09.013

Martin, T. F. J. (2012). Role of PI(4,5)P 2 in Vesicle Exocytosis and Membrane Fusion NIH Public Access Author Manuscript. In *Subcellular Biochemistry* (Vol. 59).

Martinez-Lopez, N., Mattar, P., Toledo, M., Bains, H., Kalyani, M., Aoun, M. L., Sharma, M., McIntire, L. B. J., Gunther-Cummins, L., Macaluso, F. P., Aguilan, J. T., Sidoli, S., Bourdenx, M., & Singh, R. (2023). mTORC2–NDRG1–CDC42 axis couples fasting to mitochondrial fission. *Nature Cell Biology*, *25*(7). https://doi.org/10.1038/s41556-023-01163-3

Maschi, D., Gramlich, M. W., & Klyachko, V. A. (2018). Myosin V functions as a vesicle tether at the plasma membrane to control neurotransmitter release in central synapses. *ELife*, *7*. https://doi.org/10.7554/eLife.39440

Mason, F. M., Heimsath, E. G., Higgs, H. N., & Soderling, S. H. (2011). Bi-modal regulation of a formin by srGAP2. *Journal of Biological Chemistry*, *286*(8). https://doi.org/10.1074/jbc.M110.190397

Matsuoka, Y., Li, X., & Bennett, V. (2000). Adducin: Structure, function and regulation. In *Cellular and Molecular Life Sciences* (Vol. 57, Issue 6). https://doi.org/10.1007/PL00000731

Matusek, T., Gombos, R., Szécsényi, A., Sánchez-Soriano, N., Czibula, Á., Pataki, C., Gedai, A., Prokop, A., Raskó, I., & Mihály, J. (2008). Formin proteins of the DAAM subfamily play a role during axon growth. *Journal of Neuroscience*, *28*(49). https://doi.org/10.1523/JNEUROSCI.2727-08.2008

Maufront, J., Guichard, B., Cao, L. Y., Di Cicco, A., Jégou, A., Romet-Lemonne, G., & Bertin, A. (2023). Direct observation of the conformational states of formin mDia1 at Actin filament barbed ends and along the filament. *Molecular Biology of the Cell*, *34*(1). https://doi.org/10.1091/mbc.E22-10-0472

McCabe, M. P., Cullen, E. R., Barrows, C. M., Shore, A. N., Tooke, K. I., Laprade, K. A., Stafford, J. M., & Weston, M. C. (2020). Genetic inactivation of mTORC1 or mTORC2 in neurons reveals distinct functions in glutamatergic synaptic transmission. *ELife*, *9*. https://doi.org/10.7554/eLife.51440

McLaughlin, S., & Aderem, A. (1995). The myristoyl-electrostatic switch: a modulator of reversible protein-membrane interactions. In *Trends in Biochemical Sciences* (Vol. 20, Issue 7). https://doi.org/10.1016/S0968-0004(00)89042-8

McMahon, H. T., & Boucrot, E. (2011). Molecular mechanism and physiological functions of clathrin-mediated endocytosis. In *Nature Reviews Molecular Cell Biology* (Vol. 12, Issue 8). https://doi.org/10.1038/nrm3151

Mehta, D., Rahman, A., & Malik, A. B. (2001). Protein Kinase C-α Signals Rho-Guanine Nucleotide Dissociation Inhibitor Phosphorylation and Rho Activation and Regulates the Endothelial Cell Barrier Function. *Journal of Biological Chemistry*, *276*(25). https://doi.org/10.1074/jbc.M101927200

Meiri, D., Greeve, M. A., Brunet, A., Finan, D., Wells, C. D., LaRose, J., & Rottapel, R. (2009). Modulation of Rho Guanine Exchange Factor Lfc Activity by Protein Kinase A-Mediated Phosphorylation. *Molecular and Cellular Biology*, *29*(21). https://doi.org/10.1128/mcb.01268-08

Meiri, D., Marshall, C. B., Greeve, M. A., Kim, B., Balan, M., Suarez, F., Wu, C., LaRose, J., Fine, N., Ikura, M., & Rottapel, R. (2012). Mechanistic Insight into the Microtubule and Actin Cytoskeleton Coupling through Dynein-Dependent RhoGEF Inhibition. *Molecular Cell*, *45*(5). https://doi.org/10.1016/j.molcel.2012.01.027

Mendoza, M. C., Er, E. E., Zhang, W., Ballif, B. A., Elliott, H. L., Danuser, G., & Blenis, J. (2011). ERK-MAPK Drives Lamellipodia Protrusion by Activating the WAVE2 Regulatory Complex. *Molecular Cell*, *41*(6). https://doi.org/10.1016/j.molcel.2011.02.031

Mercer, A. J., Chen, M., & Thoreson, W. B. (2011). Lateral mobility of presynaptic L-Type calcium channels at photoreceptor ribbon synapses. *Journal of Neuroscience*, *31*(12). https://doi.org/10.1523/JNEUROSCI.5921-10.2011

Merhi, A., Delrée, P., & Marini, A. M. (2017). The metabolic waste ammonium regulates mTORC2 and mTORC1 signaling. *Scientific Reports*, *7*. https://doi.org/10.1038/srep44602

Merrifield, C. J., Perrais, D., & Zenisek, D. (2005). Coupling between clathrin-coated-pit invagination, cortActin recruitment, and membrane scission observed in live cells. *Cell*, *121*(4). https://doi.org/10.1016/j.cell.2005.03.015

Miesenböck, G., De Angelis, D. A., & Rothman, J. E. (1998). Visualizing secretion and synaptic transmission with pH-sensitive green fluorescent proteins. *Nature*, *394*(6689). https://doi.org/10.1038/28190

Milosevic, I., Giovedi, S., Lou, X., Raimondi, A., Collesi, C., Shen, H., Paradise, S., O'Toole, E., Ferguson, S., Cremona, O., & De Camilli, P. (2011). Recruitment of endophilin to clathrin-coated pit necks is required for efficient vesicle uncoating after fission. *Neuron*, *72*(4). https://doi.org/10.1016/j.neuron.2011.08.029

Miya Fujimoto, L., Roth, R., Heuser, J. E., & Schmid, S. L. (2000). Actin assembly plays a variable, but not obligatory role in receptor-mediated endocytosis in mammalian cells. *Traffic*, *1*(2). https://doi.org/10.1034/j.1600-0854.2000.010208.x

Miyamoto, Y., Torii, T., Yamamori, N., Ogata, T., Tanoue, A., & Yamauchi, J. (2013). Akt and PP2A reciprocally regulate the guanine nucleotide exchange factor Dock6 to control axon growth of sensory neurons. *Science Signaling*, *6*(265). https://doi.org/10.1126/scisignal.2003661

Mizuno, H., Higashida, C., Yuan, Y., Ishizaki, T., Narumiya, S., & Watanabe, N. (2011). Rotational movement of the formin mDia1 along the double helical strand of an Actin filament. *Science*, *331*(6013). https://doi.org/10.1126/science.1197692

Mohn, J. L., Alexander, J., Pirone, A., Palka, C. D., Lee, S. Y., Mebane, L., Haydon, P. G., & Jacob, M. H. (2014). Adenomatous polyposis coli protein deletion leads to cognitive and autism-like disabilities. *Molecular Psychiatry*, *19*(10). https://doi.org/10.1038/mp.2014.61

Molloy, J. E., Burns, J. E., Kendrick-Jones, B., Tregear, R. T., & White, D. C. S. (1995). Movement and force produced by a single myosin head. *Nature*, *378*(6553). https://doi.org/10.1038/378209a0

Molnár, G., Dagher, M. C., Geiszt, M., Settleman, J., & Ligeti, E. (2001). Role of prenylation in the interaction of RHO-family small GTPases with GTPpase activating proteins. *Biochemistry*, *40*(35). https://doi.org/10.1021/bi011158e

Momboisse, F., Londcamp, E., Calco, V., Ceridono, M., Vitale, N., Bader, M. F., & Gasman, S. (2009). βPIX-activated Rac1 stimulates the activation of phospholipase D, which is associated with exocytosis in neuroendocrine cells. *Journal of Cell Science*, *122*(6). https://doi.org/10.1242/jcs.038109

Monday, H. R., Bourdenx, M., Jordan, B. A., & Castillo, P. E. (2020). Cb1-receptor-mediated inhibitory ltd triggers presynaptic remodeling via protein synthesis and ubiquitination. *ELife*, *9*. https://doi.org/10.7554/ELIFE.54812

Moon, S. Y., & Zheng, Y. (2003). Rho GTPase-activating proteins in cell regulation. *Trends in Cell Biology*, *13*(1). https://doi.org/10.1016/S0962-8924(02)00004-1

Morales, M., Colicos, M. A., & Goda, Y. (2000). Actin-dependent regulation of neurotransmitter release at central synapses. *Neuron*, *27*(3). https://doi.org/10.1016/S0896-6273(00)00064-7

Morgan, J. R., Skye Comstra, H., Cohen, M., & Faundez, V. (2013). Presynaptic membrane retrieval and endosome biology: Defining molecularly heterogeneous synaptic vesicles. *Cold Spring Harbor Perspectives in Biology*, *5*(10). https://doi.org/10.1101/cshperspect.a016915

Morlot, S., Galli, V., Klein, M., Chiaruttini, N., Manzi, J., Humbert, F., Dinis, L., Lenz, M., Cappello, G., & Roux, A. (2012). Membrane shape at the edge of the dynamin helix sets location and duration of the fission reaction. *Cell*, *151*(3). https://doi.org/10.1016/j.cell.2012.09.017

Mosaddeghzadeh, N., & Ahmadian, M. R. (2021). The rho family gtpases: Mechanisms of regulation and signaling. In *Cells* (Vol. 10, Issue 7). https://doi.org/10.3390/cells10071831

Moseley, J. B., Sagot, I., Manning, A. L., Xu, Y., Eck, M. J., Pellman, D., & Goode, B. L. (2004). A Conserved Mechanism for Bni1- and mDia1-induced Actin Assembly and Dual Regulation of Bni1 by Bud6 and Profilin. *Molecular Biology of the Cell*, *15*(2). https://doi.org/10.1091/mbc.E03-08-0621

Müller, P. M., Rademacher, J., Bagshaw, R. D., Wortmann, C., Barth, C., van Unen, J., Alp, K. M., Giudice, G., Eccles, R. L., Heinrich, L. E., Pascual-Vargas, P., Sanchez-Castro, M., Brandenburg, L., Mbamalu, G., Tucholska, M., Spatt, L., Czajkowski, M. T., Welke, R. W., Zhang, S., … Rocks, O. (2020). Systems analysis of RhoGEF and RhoGAP regulatory proteins reveals spatially organized RAC1 signalling from integrin adhesions. *Nature Cell Biology*, *22*(4). https://doi.org/10.1038/s41556-020-0488-x

Nakayama, A. Y., Harms, M. B., & Luo, L. (2000). Small GTPases Rac and Rho in the maintenance of dendritic spines and branches in hippocampal pyramidal neurons. *Journal of Neuroscience*, *20*(14). https://doi.org/10.1523/jneurosci.20-14-05329.2000

Neher, E., & Brose, N. (2018). Dynamically Primed Synaptic Vesicle States: Key to Understand Synaptic Short-Term Plasticity. In *Neuron* (Vol. 100, Issue 6). https://doi.org/10.1016/j.neuron.2018.11.024

Neidt, E. M., Scott, B. J., & Kovar, D. R. (2009). Formin differentially utilizes profilin isoforms to rapidly assemble Actin filaments. *Journal of Biological Chemistry*, *284*(1). https://doi.org/10.1074/jbc.M804201200

Newton, A. C. (2018). Protein kinase C: perfectly balanced. In *Critical Reviews in Biochemistry and Molecular Biology* (Vol. 53, Issue 2). https://doi.org/10.1080/10409238.2018.1442408

Nezami, A., Poy, F., Toms, A., Zheng, W., & Eck, M. J. (2010). Crystal structure of a complex between amino and carboxy terminal fragments of mDia1: Insights into autoinhibition of diaphanous-related formins. *PLoS ONE*, *5*(9). https://doi.org/10.1371/journal.pone.0012992

Nguyen, L., He, Q., & Meiri, K. F. (2009). Regulation of GAP-43 at serine 41 acts as a switch to modulate both intrinsic and extrinsic behaviors of growing neurons, via altered membrane distribution. *Molecular and Cellular Neuroscience*, *41*(1).

https://doi.org/10.1016/j.mcn.2009.01.011

Ni, Q., & Papoian, G. A. (2019). Turnover versus treadmilling in Actin network assembly and remodeling. *Cytoskeleton*, *76*(11–12). https://doi.org/10.1002/cm.21564

Niles, B. J., & Powers, T. (2012). Plasma membrane proteins Slm1 and Slm2 mediate activation of the AGC kinase Ypk1 by TORC2 and sphingolipids in S. cerevisiae. In *Cell Cycle* (Vol. 11, Issue 20). https://doi.org/10.4161/cc.21752

Nimnual, A. S., Taylor, L. J., & Bar-Sagi, D. (2003). Redox-dependent downregulation of Rho by Rac. *Nature Cell Biology*, *5*(3). https://doi.org/10.1038/ncb938

Nobes, C. D., & Hall, A. (1995). Rho, Rac, and Cdc42 GTPases regulate the assembly of multimolecular focal complexes associated with Actin stress fibers, lamellipodia, and filopodia. *Cell*, *81*(1). https://doi.org/10.1016/0092-8674(95)90370-4

Nosov, G., Kahms, M., & Klingauf, J. (2020). The Decade of Super-Resolution Microscopy of the Presynapse. In *Frontiers in Synaptic Neuroscience* (Vol. 12). https://doi.org/10.3389/fnsyn.2020.00032

O'neil, S. D., Rácz, B., Brown, W. E., Gao, Y., Soderblom, E. J., Yasuda, R., & Soderling, S. H. (2021). Action potential-coupled rho gtpase signaling drives presynaptic plasticity. *ELife*, *10*. https://doi.org/10.7554/eLife.63756

O'Reilly, K. E., Rojo, F., She, Q. B., Solit, D., Mills, G. B., Smith, D., Lane, H., Hofmann, F., Hicklin, D. J., Ludwig, D. L., Baselga, J., & Rosen, N. (2006). mTOR inhibition induces upstream receptor tyrosine kinase signaling and activates Akt. *Cancer Research*, *66*(3). https://doi.org/10.1158/0008-5472.CAN-05-2925

Oevel, K., Hohensee, S., Kumar, A., Rosas-Brugada, I., Bartolini, F., Soykan, T., & Haucke, V. (2024). Rho GTPase signaling and mDia facilitate endocytosis via presynaptic Actin. *ELife*, *12*(RP92755). https://doi.org/https://doi.org/10.7554/eLife.92755.3

Ogunmowo, T. H., Jing, H., Raychaudhuri, S., Kusick, G. F., Imoto, Y., Li, S., Itoh, K., Ma, Y., Jafri, H., Dalva, M. B., Chapman, E. R., Ha, T., Watanabe, S., & Liu, J. (2023). Membrane compression by synaptic vesicle exocytosis triggers ultrafast endocytosis. *Nature Communications*, *14*(1). https://doi.org/10.1038/s41467-023-38595-2

Oh, D., Han, S., Seo, J., Lee, J. R., Choi, J., Groffen, J., Kim, K., Cho, Y. S., Choi, H. S., Shin, H., Woo, J., Won, H., Park, S. K., Kim, S. Y., Jo, J., Whitcomb, D. J., Cho, K., Kim, H., Bae, Y. C., … Kim, E. (2010). Regulation of synaptic Rac1 activity, long-term potentiation maintenance, and learning and memory by BCR and ABR Rac GTPase-activating proteins. *Journal of Neuroscience*, *30*(42). https://doi.org/10.1523/JNEUROSCI.1711-10.2010

Ohshima, Y., Kubo, T., Koyama, R., Ueno, M., Nakagawa, M., & Yamashita, T. (2008). Regulation of axonal elongation and pathfinding from the entorhinal cortex to the dentate gyrus in the hippocampus by the chemokine stromal cell-derived factor 1α. *Journal of Neuroscience*, *28*(33). https://doi.org/10.1523/JNEUROSCI.1670-08.2008

Ohta, Y., Hartwig, J. H., & Stossel, T. P. (2006). FilGAP, a Rho- and ROCK-regulated GAP for Rac binds filamin A to control Actin remodelling. *Nature Cell Biology*, *8*(8). https://doi.org/10.1038/ncb1437

Oikawa, T., Yamaguchi, H., Itoh, T., Kato, M., Ijuin, T., Yamazaki, D., Suetsugu, S., & Takenawa, T. (2004). PtdIns(3,4,5)P3 binding is necessary for WAVE2-induced formation of lamellipodia. *Nature Cell Biology*, *6*(5). https://doi.org/10.1038/ncb1125

Oishi, A., Makita, N., Sato, J., & Iiri, T. (2012). Regulation of RhoA signaling by the cAMP-dependent phosphorylation of RhoGDIα. *Journal of Biological Chemistry*, *287*(46). https://doi.org/10.1074/jbc.M112.401547

Okada, K., Bartolini, F., Deaconescu, A. M., Moseley, J. B., Dogic, Z., Grigorieff, N., Gundersen, G. G., & Goode, B. L. (2010). Adenomatous polyposis coli protein nucleates Actin assembly and synergizes with the formin mDia1. *Journal of Cell Biology*, *189*(7). https://doi.org/10.1083/jcb.201001016

Olivera-Couto, A., & Aguilar, P. S. (2012). Eisosomes and plasma Membrane organization. In *Molecular Genetics and Genomics* (Vol. 287, Issue 8). https://doi.org/10.1007/s00438-012-0706-8

Onesto, C., Shutes, A., Picard, V., Schweighoffer, F., & Der, C. J. (2008). Characterization of EHT 1864, a Novel Small Molecule Inhibitor of Rac Family Small GTPases. In *Methods in Enzymology* (Vol. 439). https://doi.org/10.1016/S0076-6879(07)00409-0

Ono, Y., Matsuzawa, K., & Ikenouchi, J. (2022). mTORC2 suppresses cell death induced by hypo-osmotic stress by promoting sphingomyelin transport. *Journal of Cell Biology*, *221*(4). https://doi.org/10.1083/jcb.202106160

Onoa, B., Li, H., Gagnon-Bartsch, J. A., Elias, L. A. B., & Edwards, R. H. (2010). Vesicular monoamine and glutamate transporters select distinct synaptic vesicle recycling pathways. *Journal of Neuroscience*, *30*(23). https://doi.org/10.1523/JNEUROSCI.5298-09.2010

Orlando, M., Schmitz, D., Rosenmund, C., & Herman, M. A. (2019). Calcium-Independent Exo-endocytosis Coupling at Small Central Synapses. *Cell Reports*, *29*(12). https://doi.org/10.1016/j.celrep.2019.11.060

Otomo, T., Otomo, C., Tomchick, D. R., Machius, M., & Rosen, M. K. (2005). Structural basis of Rho GTPase-mediated activation of the formin mDia1. *Molecular Cell*, *18*(3). https://doi.org/10.1016/j.molcel.2005.04.002

Otomo, T., Tomchick, D. R., Otomo, C., Machius, M., & Rosen, M. K. (2010). Crystal structure of the formin mDIA1 in autoinhibited conformation. *PLoS ONE*, *5*(9). https://doi.org/10.1371/journal.pone.0012896

Pal, S. K., Reckamp, K., Yu, H., & Figlin, R. A. (2010). Akt inhibitors in clinical development for the treatment of cancer. In *Expert Opinion on Investigational Drugs* (Vol. 19, Issue 11). https://doi.org/10.1517/13543784.2010.520701

Panatier, A., Arizono, M., & Valentin Nägerl, U. (2014). Dissecting tripartite synapses with STED microscopy. *Philosophical Transactions of the Royal Society B: Biological Sciences*, *369*(1654). https://doi.org/10.1098/rstb.2013.0597

Papandréou, M. J., & Leterrier, C. (2018). The functional architecture of axonal Actin. In *Molecular and Cellular Neuroscience* (Vol. 91). https://doi.org/10.1016/j.mcn.2018.05.003

Parsons, J. T., Horwitz, A. R., & Schwartz, M. A. (2010). Cell adhesion: Integrating cytoskeletal dynamics and cellular tension. In *Nature Reviews Molecular Cell Biology* (Vol. 11, Issue 9). https://doi.org/10.1038/nrm2957

Paul, A. S., & Pollard, T. D. (2009). Review of the mechanism of processive Actin filament elongation by formins. In *Cell Motility and the Cytoskeleton* (Vol. 66, Issue 8). https://doi.org/10.1002/cm.20379

Peng, A., Rotman, Z., Deng, P. Y., & Klyachko, V. A. (2012). Differential Motion Dynamics of Synaptic Vesicles Undergoing Spontaneous and Activity-Evoked Endocytosis. *Neuron*, *73*(6). https://doi.org/10.1016/j.neuron.2012.01.023

Peng, G. E., Wilson, S. R., & Weiner, O. D. (2011). A pharmacological cocktail for arresting Actin dynamics in living cells. *Molecular Biology of the Cell*, *22*(21). https://doi.org/10.1091/mbc.E11-04-0379

Peng, J., Kitchen, S. M., West, R. A., Sigler, R., Eisenmann, K. M., & Alberts, A. S. (2007). Myeloproliferative defects following targeting of the Drf1 gene encoding the mammalian diaphanous-related formin mDia1. *Cancer Research*, *67*(16). https://doi.org/10.1158/0008-5472.CAN-07-1467

Peng, J., Wallar, B. J., Flanders, A., Swiatek, P. J., & Alberts, A. S. (2003). Disruption of the Diaphanous-related formin Drf1 gene encoding mDia1 reveals a role for Drf3 as an effector for Cdc42. *Current Biology*, *13*(7). https://doi.org/10.1016/S0960-9822(03)00170-2

Perez, C. G., Dudzinski, N. R., Rouches, M., Landajuela, A., Machta, B., Zenisek, D., & Karatekin, E. (2022). Rapid propagation of membrane tension at retinal bipolar neuron presynaptic terminals. *Science Advances*, *8*(1). https://doi.org/10.1126/sciadv.abl4411

Pieribone, V. A., Shupliakov, O., Brodin, L., Hilfiker-Rothenfluh, S., Czernik, A. J., & Greengard, P. (1995). Distinct pools of synaptic vesicles in neurotransmitter release. *Nature*, *375*(6531). https://doi.org/10.1038/375493a0

Pike, K. G., Morris, J., Ruston, L., Pass, S. L., Greenwood, R., Williams, E. J., Demeritt, J., Culshaw, J. D., Gill, K., Pass, M., Finlay, M. R. V., Good, C. J., Roberts, C. A., Currie, G. S., Blades, K., Eden, J. M., & Pearson, S. E. (2015). Discovery of AZD3147: A potent, selective dual inhibitor of mTORC1 and mTORC2. *Journal of Medicinal Chemistry*, *58*(5). https://doi.org/10.1021/jm501778s

Plomann, M., Lange, R., Vopper, G., Cremer, H., Heinlein, U. A. O., Scheff, S., Baldwin, S. A., Leitges, M., Cramer, M., Paulsson, M., & Barthels, D. (1998). PACSIN, a brain protein that is upregulated upon differentiation into neuronal cells. *European Journal of Biochemistry*, *256*(1). https://doi.org/10.1046/j.1432-1327.1998.2560201.x

Pollard, T. D. (1986). Rate constants for the reactions of ATP- and ADP-Actin with the ends of Actin filaments. *Journal of Cell Biology*, *103*(6). https://doi.org/10.1083/jcb.103.6.2747

Pollard, T. D. (2007). Regulation of Actin filament assembly by Arp2/3 complex and formins. In *Annual Review of Biophysics and Biomolecular Structure* (Vol. 36). https://doi.org/10.1146/annurev.biophys.35.040405.101936

Pollard T.D., & Kholodenko, B. N. (2003). Cellular Motility Driven by Assembly and Disassembly of Actin Filaments. In *Cell* (Vol. 7, Issue 1).

Posor, Y., Jang, W., & Haucke, V. (2022). Phosphoinositides as membrane organizers. In *Nature Reviews Molecular Cell Biology* (Vol. 23, Issue 12). https://doi.org/10.1038/s41580-022-00490-x

Pring, M., Evangelista, M., Boone, C., Yang, C., & Zigmond, S. H. (2003). Mechanism of formin-induced nucleation of Actin filaments. *Biochemistry*, *42*(2). https://doi.org/10.1021/bi026520j

Pruyne, D., Evangelista, M., Yang, C., Bi, E., Zigmond, S., Bretscher, A., & Boone, C. (2002). Role of formins in Actin assembly: Nucleation and barbed-end association. *Science*, *297*(5581). https://doi.org/10.1126/science.1072309

Qiao, J., Holian, O., Lee, B. S., Huang, F., Zhang, J., & Lum, H. (2008). Phosphorylation of GTP dissociation inhibitor by PKA negatively regulates RhoA. *American Journal of Physiology - Cell Physiology*, *295*(5). https://doi.org/10.1152/ajpcell.00139.2008

Qu, X., Yuan, F. N., Corona, C., Pasini, S., Pero, M. E., Gundersen, G. G., Shelanski, M. L., & Bartolini, F. (2017). Stabilization of dynamic microtubules by mDia1 drives Tau-dependent Aβ1-42 synaptotoxicity. *Journal of Cell Biology*, *216*(10). https://doi.org/10.1083/jcb.201701045

Quinlan, M. E., Hilgert, S., Bedrossian, A., Mullins, R. D., & Kerkhoff, E. (2007). Regulatory interactions between two Actin nucleators, Spire and Cappuccino. *Journal of Cell Biology*, *179*(1). https://doi.org/10.1083/jcb.200706196

Rafelski, S. M., & Theriot, J. A. (2004). Crawling toward a unified model of cell motility: Spatial and temporal regulation of Actin dynamics. In *Annual Review of Biochemistry* (Vol. 73). https://doi.org/10.1146/annurev.biochem.73.011303.073844

Raimondi, A., Ferguson, S. M., Lou, X., Armbruster, M., Paradise, S., Giovedi, S., Messa, M., Kono, N., Takasaki, J., Cappello, V., O'Toole, E., Ryan, T. A., & De Camilli, P. (2011). Overlapping Role of Dynamin Isoforms in Synaptic Vesicle Endocytosis. *Neuron*, *70*(6). https://doi.org/10.1016/j.neuron.2011.04.031

Ramalingam, N., Zhao, H., Breitsprecher, D., Lappalainen, P., Faix, J., & Schleicher, M. (2010). Phospholipids regulate localization and activity of mDia1 formin. *European Journal of Cell Biology*, *89*(10). https://doi.org/10.1016/j.ejcb.2010.06.001

Rampérez, A., Bartolomé-Martín, D., García-Pascual, A., Sánchez-Prieto, J., & Torres, M. (2019). Photoconversion of FM1-43 Reveals Differences in Synaptic Vesicle Recycling and Sensitivity to Pharmacological Disruption of Actin Dynamics in Individual Synapses. *ACS Chemical Neuroscience*, *10*(4). https://doi.org/10.1021/acschemneuro.8b00712

Raucher, D., & Sheetz, M. P. (1999). Characteristics of a membrane reservoir buffering membrane tension. *Biophysical Journal*, *77*(4). https://doi.org/10.1016/S0006-3495(99)77040-2

Raucher, D., Stauffer, T., Chen, W., Shen, K., Guo, S., York, J. D., Sheetz, M. P., & Meyer, T. (2000). Phosphatidylinositol 4,5-bisphosphate functions as a second messenger that regulates cytoskeleton-plasma membrane adhesion. *Cell*, *100*(2). https://doi.org/10.1016/S0092-8674(00)81560-3

Raynaud, F., Moutin, E., Schmidt, S., Dahl, J., Bertaso, F., Boeckers, T. M., Homburger, V., & Fagni, L. (2014). Rho-GTPase-activating Protein Interacting with Cdc-42-interacting Protein 4 Homolog 2 (Rich2). *Journal of Biological Chemistry*, *289*(5). https://doi.org/10.1074/jbc.m113.534636

Reid, T., Furuyashiki, T., Ishizaki, T., Watanabe, G., Watanabe, N., Fujisawa, K., Morii, N., Madaule, P., & Narumiya, S. (1996). Rhotekin, a new putative target for Rho bearing homology to a serine/threonine kinase, PKN, and rhophilin in the Rho-binding domain. *Journal of Biological Chemistry*, *271*(23). https://doi.org/10.1074/jbc.271.23.13556

Renard, H. F., Simunovic, M., Lemiere, J., Boucrot, E., Garcia-Castillo, M. D., Arumugam, S., Chambon, V., Lamaze, C., Wunder, C., Kenworthy, A. K., Schmidt, A. A., McMahon, H. T., Sykes, C., Bassereau, P., & Johannes, L. (2015). Endophilin-A2 functions in membrane scission in clathrin-independent endocytosis. *Nature*, *517*(7535). https://doi.org/10.1038/nature14064

Richards, D. A., Guatimosim, C., & Betz, W. J. (2000). Two endocytic recycling routes selectively fill two vesicle pools in frog motor nerve terminals. *Neuron*, *27*(3). https://doi.org/10.1016/S0896-6273(00)00065-9

Richards, D. A., Rizzoli, S. O., & Betz, W. J. (2004). Effects of wortmannin and latrunculin A on slow endocytosis at the frog neuromuscular junction. *Journal of Physiology*, *557*(1). https://doi.org/10.1113/jphysiol.2004.062158

Ridley, A. J., & Hall, A. (1992). The small GTP-binding protein rho regulates the assembly of focal adhesions and Actin stress fibers in response to growth factors. *Cell*, *70*(3). https://doi.org/10.1016/0092-8674(92)90163-7

Ridley, A. J., Paterson, H. F., Johnston, C. L., Diekmann, D., & Hall, A. (1992). The small GTP-binding protein rac regulates growth factor-induced membrane ruffling. *Cell*, *70*(3). https://doi.org/10.1016/0092-8674(92)90164-8

Riggi, M., Bourgoint, C., Macchione, M., Matile, S., Loewith, R., & Roux, A. (2019). TORC2 controls endocytosis through plasma membrane tension. *Journal of Cell Biology*, *218*(7). https://doi.org/10.1083/jcb.201901096

Riggi, M., Niewola-Staszkowska, K., Chiaruttini, N., Colom, A., Kusmider, B., Mercier, V., Soleimanpour, S., Stahl, M., Matile, S., Roux, A., & Loewith, R. (2018). Decrease in plasma membrane tension triggers PtdIns(4,5)P 2 phase separation to inactivate TORC2. *Nature Cell Biology*, *20*(9). https://doi.org/10.1038/s41556-018-0150-z

Rispal, D., Eltschinger, S., Stahl, M., Vaga, S., Bodenmiller, B., Abraham, Y., Filipuzzi, I., Movva, N. R., Aebersold, R., Helliwell, S. B., & Loewith, R. (2015). Target of rapamycin complex 2 regulates Actin polarization and endocytosis via multiple pathways. *Journal of Biological Chemistry*, *290*(24). https://doi.org/10.1074/jbc.M114.627794

Ritter, B., Ferguson, S. M., De Camilli, P., & McPherson, P. S. (2017). A lentiviral system for efficient knockdown of proteins in neuronal cultures. *MNI Open Research*, *1*. https://doi.org/10.12688/mniopenres.12766.1

Robinson, M. S. (2015). Forty Years of Clathrin-coated Vesicles. In *Traffic* (Vol. 16, Issue 12). https://doi.org/10.1111/tra.12335

Roelants, F. M., Leskoske, K. L., Pedersen, R. T. A., Muir, A., Liu, J. M.-H., Finnigan, G. C., & Thorner, J. (2017). TOR Complex 2-Regulated Protein Kinase Fpk1 Stimulates Endocytosis via Inhibition of Ark1/Prk1-Related Protein Kinase Akl1 in Saccharomyces cerevisiae . *Molecular and Cellular Biology*, *37*(7). https://doi.org/10.1128/mcb.00627-16

Roffay, C., Molinard, G., Kim, K., Urbanska, M., Andrade, V., Barbarasa, V., Nowak, P., Mercier, V., García-Calvo, J., Matile, S., Loewith, R., Echard, A., Guck, J., Lenz, M., & Roux, A. (2021). Passive coupling of membrane tension and cell volume during active response of cells to osmosis. *Proceedings of the National Academy of Sciences of the United States of America*, *118*(47). https://doi.org/10.1073/pnas.2103228118

Romero, S., Le Clainche, C., Didry, D., Egile, C., Pantaloni, D., & Carlier, M. F. (2004). Formin is a processive motor that requires profilin to accelerate Actin assembly and associated ATP hydrolysis. *Cell*, *119*(3). https://doi.org/10.1016/j.cell.2004.09.039

Rose, R., Weyand, M., Lammers, M., Ishizaki, T., Ahmadian, M. R., & Wittinghofer, A. (2005). Structural and mechanistic insights into the interaction between Rho and mammalian Dia. *Nature*, *435*(7041). https://doi.org/10.1038/nature03604

Rosenbloom, A. D., Kovar, E. W., Kovar, D. R., Loew, L. M., & Pollard, T. D. (2021). Mechanism of Actin filament nucleation. *Biophysical Journal*, *120*(20). https://doi.org/10.1016/j.bpj.2021.09.006

Rossman, K. L., Worthylake, D. K., Snyder, J. T., Siderovski, D. P., Campbell, S. L., & Sondek, J. (2002). A crystallographic view of interactions between Dbs and Cdc42: PH domain-assisted guanine nucleotide exchange. *EMBO Journal*, *21*(6). https://doi.org/10.1093/emboj/21.6.1315

Rothman, J. S., Kocsis, L., Herzog, E., Nusser, Z., & Silver, R. A. (2016). Physical determinants of vesicle mobility and supply at a central synapse. *ELife*, *5*(AUGUST). https://doi.org/10.7554/eLife.15133

Rottner, K., Faix, J., Bogdan, S., Linder, S., & Kerkhoff, E. (2017). Actin assembly mechanisms at a glance. *Journal of Cell Science*, *130*(20). https://doi.org/10.1242/jcs.206433

Rottner, K., Hall, A., & Small, J. V. (1999). Interplay between Rac and Rho in the control of substrate contact dynamics. *Current Biology*, *9*(12). https://doi.org/10.1016/S0960-9822(99)80286-3

Rotty, J. D., Wu, C., & Bear, J. E. (2013). New insights into the regulation and cellular functions of the ARP2/3 complex. *Nature Reviews Molecular Cell Biology*, *14*(1). https://doi.org/10.1038/nrm3492

Roux, A., Uyhazi, K., Frost, A., & De Camilli, P. (2006). GTP-dependent twisting of dynamin implicates constriction and tension in membrane fission. *Nature*, *441*(7092). https://doi.org/10.1038/nature04718

Rüegg, M. A. (2013). In vivo evidence for mTORC2-mediated Actin cytoskeleton rearrangement in neurons. *Bioarchitecture*,

3(4). https://doi.org/10.4161/bioa.26497

Ryu, J. R., Echarri, A., Li, R., & Pendergast, A. M. (2009). Regulation of Cell-Cell Adhesion by Abi/Diaphanous Complexes. *Molecular and Cellular Biology*, *29*(7). https://doi.org/10.1128/mcb.01483-08

Sabbatini, M. E., & Williams, J. A. (2013). Cholecystokinin-Mediated RhoGDI Phosphorylation via PKCα Promotes both RhoA and Rac1 Signaling. *PLoS ONE*, *8*(6). https://doi.org/10.1371/journal.pone.0066029

Saci, A., Cantley, L. C., & Carpenter, C. L. (2011). Rac1 Regulates the Activity of mTORC1 and mTORC2 and Controls Cellular Size. *Molecular Cell*, *42*(1). https://doi.org/10.1016/j.molcel.2011.03.017

Saffarian, S., Cocucci, E., & Kirchhausen, T. (2009). Distinct dynamics of endocytic clathrin-coated pits and coated plaques. *PLoS Biology*, *7*(9). https://doi.org/10.1371/journal.pbio.1000191

Saha, S., Town, J. P., & Weiner, O. D. (2023). Mechanosensitive mTORC2 independently coordinates leading and trailing edge polarity programs during neutrophil migration. *Molecular Biology of the Cell*, *34*(5). https://doi.org/10.1091/MBC.E22-05-0191

Sakaba, T., & Neher, E. (2003). Involvement of Actin polymerization in vesicle recruitment at the calyx of held synapse. *Journal of Neuroscience*, *23*(3). https://doi.org/10.1523/jneurosci.23-03-00837.2003

Sakamoto, S., Thumkeo, D., Ohta, H., Zhang, Z., Huang, S., Kanchanawong, P., Fuu, T., Watanabe, S., Shimada, K., Fujihara, Y., Yoshida, S., Ikawa, M., Watanabe, N., Saitou, M., & Narumiya, S. (2018). mDia1/3 generate cortical F-Actin meshwork in Sertoli cells that is continuous with contractile F-Actin bundles and indispensable for spermatogenesis and male fertility. *PLoS Biology*, *16*(9). https://doi.org/10.1371/journal.pbio.2004874

Sakata, D., Taniguchi, H., Yasuda, S., Adachi-Morishima, A., Hamazaki, Y., Nakayama, R., Miki, T., Minato, N., & Narumiya, S. (2007). Impaired T lymphocyte trafficking in mice deficient in an Actin-nucleating protein, mDia1. *Journal of Experimental Medicine*, *204*(9). https://doi.org/10.1084/jem.20062647

Saleem, M., Morlot, S., Hohendahl, A., Manzi, J., Lenz, M., & Roux, A. (2015). A balance between membrane elasticity and polymerization energy sets the shape of spherical clathrin coats. *Nature Communications*, *6*. https://doi.org/10.1038/ncomms7249

Sánchez-Alegría, K., Flores-León, M., Avila-Muñoz, E., Rodríguez-Corona, N., & Arias, C. (2018). PI3K signaling in neurons: A central node for the control of multiple functions. In *International Journal of Molecular Sciences* (Vol. 19, Issue 12). https://doi.org/10.3390/ijms19123725

Sankaranarayanan, S., Atluri, P. P., & Ryan, T. A. (2003). Actin has a molecular scaffolding, not propulsive, role in presynaptic function. *Nature Neuroscience*, *6*(2). https://doi.org/10.1038/nn1002

Sankaranarayanan, S., De Angelis, D., Rothman, J. E., & Ryan, T. A. (2000). The use of pHluorins for optical measurements of presynaptic activity. *Biophysical Journal*, *79*(4). https://doi.org/10.1016/S0006-3495(00)76468-X

Sansevrino, R., Hoffmann, C., & Milovanovic, D. (2023). Condensate biology of synaptic vesicle clusters. In *Trends in Neurosciences* (Vol. 46, Issue 4). https://doi.org/10.1016/j.tins.2023.01.001

Sanz-Moreno, V., Gadea, G., Ahn, J., Paterson, H., Marra, P., Pinner, S., Sahai, E., & Marshall, C. J. (2008). Rac Activation and Inactivation Control Plasticity of Tumor Cell Movement. *Cell*, *135*(3). https://doi.org/10.1016/j.cell.2008.09.043

Sasaki, T., Kato, M., & Takai, Y. (1993). Consequences of weak interaction of rho GDI with the GTP-bound forms of rho p21 and rac p21. *Journal of Biological Chemistry*, *268*(32). https://doi.org/10.1016/s0021-9258(20)80478-5

Scaiola, A., Mangia, F., Imseng, S., Boehringer, D., Berneiser, K., Shimobayashi, M., Stuttfeld, E., Hall, M. N., Ban, N., & Maier, T. (2020). The 3.2-Å resolution structure of human mTORC2. *Science Advances*, *6*(45). https://doi.org/10.1126/SCIADV.ABC1251

Schafer, D. A. (2004). Regulating Actin dynamics at membranes: A focus on dynamin. In *Traffic* (Vol. 5, Issue 7). https://doi.org/10.1111/j.1600-0854.2004.00199.x

Schmied, C., Soykan, T., Bolz, S., Haucke, V., & Lehmann, M. (2021). SynActJ: Easy-to-Use Automated Analysis of Synaptic Activity. *Frontiers in Computer Science*, *3*. https://doi.org/10.3389/fcomp.2021.777837

Sedding, D. G., Hermsen, J., Seay, U., Eickelberg, O., Kummer, W., Schwencke, C., Strasser, R. H., Tillmanns, H., & Braun-

Dullaeus, R. C. (2005). Caveolin-1 facilitates mechanosensitive protein kinase B (Akt) signaling in vitro and in vivo. *Circulation Research*, *96*(6). https://doi.org/10.1161/01.RES.0000160610.61306.0f

Senju, Y., Rosenbaum, E., Shah, C., Hamada-Nakahara, S., Itoh, Y., Yamamoto, K., Hanawa-Suetsugu, K., Daumke, O., & Suetsugu, S. (2015). Phosphorylation of PACSIN2 by protein kinase C triggers the removal of caveolae from the plasma membrane. *Journal of Cell Science*, *128*(15). https://doi.org/10.1242/jcs.167775

Senoo, H., Kamimura, Y., Kimura, R., Nakajima, A., Sawai, S., Sesaki, H., & Iijima, M. (2019). Phosphorylated Rho–GDP directly activates mTORC2 kinase towards AKT through dimerization with Ras–GTP to regulate cell migration. *Nature Cell Biology*, *21*(7). https://doi.org/10.1038/s41556-019-0348-8

Senoo, H., Murata, D., Wai, M., Arai, K., Iwata, W., Sesaki, H., & Iijima, M. (2021). KARATE: PKA-induced KRAS4B-RHOA-mTORC2 supercomplex phosphorylates AKT in insulin signaling and glucose homeostasis. *Molecular Cell*, *81*(22). https://doi.org/10.1016/j.molcel.2021.09.001

Senoo, H., Wai, M., Matsubayashi, H. T., Sesaki, H., & Iijima, M. (2020). Hetero-oligomerization of Rho and Ras GTPases Connects GPCR Activation to mTORC2-AKT Signaling. *Cell Reports*, *33*(8). https://doi.org/10.1016/j.celrep.2020.108427

Sept, D., & McCammon, J. A. (2001). Thermodynamics and kinetics of Actin filament nucleation. *Biophysical Journal*, *81*(2). https://doi.org/10.1016/S0006-3495(01)75731-1

Seth, A., Otomo, C., & Rosen, M. K. (2006). Autoinhibition regulates cellular localization and Actin assembly activity of the diaphanous-related formins FRLα and mDia1. *Journal of Cell Biology*, *174*(5). https://doi.org/10.1083/jcb.200605006

Shang, X., Marchioni, F., Sipes, N., Evelyn, C. R., Jerabek-Willemsen, M., Duhr, S., Seibel, W., Wortman, M., & Zheng, Y. (2012). Rational design of small molecule inhibitors targeting rhoa subfamily rho GTPases. *Chemistry and Biology*, *19*(6). https://doi.org/10.1016/j.chembiol.2012.05.009

Shekhar, S., Kerleau, M., Kühn, S., Pernier, J., Romet-Lemonne, G., Jégou, A., & Carlier, M. F. (2015). Formin and capping protein together embrace the Actin filament in a ménage à trois. *Nature Communications*, *6*. https://doi.org/10.1038/ncomms9730

Shemesh, T., & Kozlov, M. M. (2007). Actin polymerization upon processive capping by formin: A model for slowing and acceleration. *Biophysical Journal*, *92*(5). https://doi.org/10.1529/biophysj.106.098459

Shi, Z., & Baumgart, T. (2015). Membrane tension and peripheral protein density mediate membrane shape transitions. *Nature Communications*, *6*. https://doi.org/10.1038/ncomms6974

Shi, Z., Graber, Z. T., Baumgart, T., Stone, H. A., & Cohen, A. E. (2018). Cell Membranes Resist Flow. *Cell*, *175*(7). https://doi.org/10.1016/j.cell.2018.09.054

Shifrin, Y., Arora, P. D., Ohta, Y., Calderwood, D. A., & McCulloch, C. A. (2009). The role of filGAP-filamin a interactions in mechanoprotection. *Molecular Biology of the Cell*, *20*(5). https://doi.org/10.1091/mbc.E08-08-0872

Shin, W., Zucker, B., Kundu, N., Lee, S. H., Shi, B., Chan, C. Y., Guo, X., Harrison, J. T., Turechek, J. M., Hinshaw, J. E., Kozlov, M. M., & Wu, L. G. (2022). Molecular mechanics underlying flat-to-round membrane budding in live secretory cells. *Nature Communications*, *13*(1). https://doi.org/10.1038/s41467-022-31286-4

Shinohara, R., Thumkeo, D., Kamijo, H., Kaneko, N., Sawamoto, K., Watanabe, K., Takebayashi, H., Kiyonari, H., Ishizaki, T., Furuyashiki, T., & Narumiya, S. (2012). A role for mDia, a Rho-regulated Actin nucleator, in tangential migration of interneuron precursors. *Nature Neuroscience*, *15*(3). https://doi.org/10.1038/nn.3020

Shiota, C., Woo, J. T., Lindner, J., Shelton, K. D., & Magnuson, M. A. (2006). Multiallelic Disruption of the Rictor Gene in Mice Reveals that mTOR Complex 2 Is Essential for Fetal Growth and Viability. *Developmental Cell*, *11*(4). https://doi.org/10.1016/j.devcel.2006.08.013

Shirai, Y. M., Tsunoyama, T. A., Hiramoto-Yamaki, N., Hirosawa, K. M., Shibata, A. C. E., Kondo, K., Tsurumune, A., Ishidate, F., Kusumi, A., & Fujiwara, T. K. (2017). Cortical Actin nodes: Their dynamics and recruitment of podosomal proteins as revealed by super-resolution and single-molecule microscopy. *PLoS ONE*, *12*(11). https://doi.org/10.1371/journal.pone.0188778

Shupliakov, O., Löw, P., Grabs, D., Gad, H., Chen, H., David, C., Takei, K., De Camilli, P., & Brodin, L. (1997). Synaptic vesicle

endocytosis impaired by disruption of dynamin-SH3 domain interactions. *Science*, *276*(5310). https://doi.org/10.1126/science.276.5310.259

Siksou, L., Rostaing, P., Lechaire, J. P., Boudier, T., Ohtsuka, T., Fejtová, A., Kao, H. T., Greengard, P., Gundelfinger, E. D., Triller, A., & Marty, S. (2007). Three-dimensional architecture of presynaptic terminal cytomatrix. *Journal of Neuroscience*, *27*(26). https://doi.org/10.1523/JNEUROSCI.1773-07.2007

Silm, K., Yang, J., Marcott, P. F., Asensio, C. S., Eriksen, J., Guthrie, D. A., Newman, A. H., Ford, C. P., & Edwards, R. H. (2019). Synaptic Vesicle Recycling Pathway Determines Neurotransmitter Content and Release Properties. *Neuron*, *102*(4). https://doi.org/10.1016/j.neuron.2019.03.031

Simunovic, M., & Voth, G. A. (2015). Membrane tension controls the assembly of curvature-generating proteins. *Nature Communications*, *6*. https://doi.org/10.1038/ncomms8219

Sinha, B., Köster, D., Ruez, R., Gonnord, P., Bastiani, M., Abankwa, D., Stan, R. V., Butler-Browne, G., Vedie, B., Johannes, L., Morone, N., Parton, R. G., Raposo, G., Sens, P., Lamaze, C., & Nassoy, P. (2011). Cells respond to mechanical stress by rapid disassembly of caveolae. *Cell*, *144*(3). https://doi.org/10.1016/j.cell.2010.12.031

Siuta, M. A., Robertson, S. D., Kocalis, H., Saunders, C., Gresch, P. J., Khatri, V., Shiota, C., Philip Kennedy, J., Lindsley, C. W., Daws, L. C., Polley, D. B., Veenstra-Vanderweele, J., Stanwood, G. D., Magnuson, M. A., Niswender, K. D., & Galli, A. (2010). Dysregulation of the norepinephrine transporter sustains cortical hypodopaminergia and schizophrenialike behaviors in neuronal Rictor null mice. *PLoS Biology*, *8*(6). https://doi.org/10.1371/journal.pbio.1000393

Smillie, K. J., & Cousin, M. A. (2012). Akt/PKB Controls the Activity-Dependent Bulk Endocytosis of Synaptic Vesicles. *Traffic*, *13*(7). https://doi.org/10.1111/j.1600-0854.2012.01365.x

Smith, S. M., Renden, R., & von Gersdorff, H. (2008). Synaptic vesicle endocytosis: fast and slow modes of membrane retrieval. *Trends in Neurosciences*, *31*(11). https://doi.org/10.1016/j.tins.2008.08.005

Song, S. H., & Augustine, G. J. (2023). Different mechanisms of synapsin-induced vesicle clustering at inhibitory and excitatory synapses. *Cell Reports*, *42*(8). https://doi.org/10.1016/j.celrep.2023.113004

Sossey-Alaoui, K., Li, X., Ranalli, T. A., & Cowell, J. K. (2005). WAVE3-mediated cell migration and lamellipodia formation are regulated downstream of phosphatidylinositol 3-kinase. *Journal of Biological Chemistry*, *280*(23). https://doi.org/10.1074/jbc.M500503200

Soulet, F., Yarar, D., Leonard, M., & Schmid, S. L. (2005). SNX9 regulates dynamin assembly and is required for efficient clathrin-mediated endocytosis. *Molecular Biology of the Cell*, *16*(4). https://doi.org/10.1091/mbc.E04-11-1016

Soykan, T., Kaempf, N., Sakaba, T., Vollweiter, D., Goerdeler, F., Puchkov, D., Kononenko, N. L., & Haucke, V. (2017). Synaptic Vesicle Endocytosis Occurs on Multiple Timescales and Is Mediated by Formin-Dependent Actin Assembly. *Neuron*, *93*(4). https://doi.org/10.1016/j.neuron.2017.02.011

Srinivasan, G., Jun, H. K., & Von Gersdorff, H. (2008). The pool of fast releasing vesicles is augmented by myosin light chain kinase inhibition at the calyx of held synapse. *Journal of Neurophysiology*, *99*(4). https://doi.org/10.1152/jn.00949.2007

Srinivasan, S., Wang, F., Glavas, S., Ott, A., Hofmann, F., Aktories, K., Kalman, D., & Bourne, H. R. (2003). Rac and Cdc42 play distinct roles in regulating PI(3,4,5)P3 and polarity during neutrophil chemotaxis. *Journal of Cell Biology*, *160*(3). https://doi.org/10.1083/jcb.200208179

Staal, R. G. W., Mosharov, E. V., & Sulzer, D. (2004). Dopamine neurons release transmitter via a flickering fusion pore. *Nature Neuroscience*, *7*(4). https://doi.org/10.1038/nn1205

Stovold, C. F., Millard, T. H., & Machesky, L. M. (2005). Inclusion of Scar/WAVE3 in a similar complex to Scar/WAVE1 and 2. *BMC Cell Biology*, *6*. https://doi.org/10.1186/1471-2121-6-11

Stradal, T. E. B., Rottner, K., Disanza, A., Confalonieri, S., Innocenti, M., & Scita, G. (2004). Regulation of Actin dynamics by WASP and WAVE family proteins. In *Trends in Cell Biology* (Vol. 14, Issue 6). https://doi.org/10.1016/j.tcb.2004.04.007

Subauste, M. C., Von Herrath, M., Benard, V., Chamberlain, C. E., Chuang, T. H., Chu, K., Bokoch, G. M., & Hahn, K. M. (2000). Rho family proteins modulate rapid apoptosis induced by cytotoxic T lymphocytes and Fas. *Journal of Biological Chemistry*, *275*(13). https://doi.org/10.1074/jbc.275.13.9725

Südhof, T. C. (2013). Neurotransmitter release: The last millisecond in the life of a synaptic vesicle. In *Neuron* (Vol. 80, Issue 3). https://doi.org/10.1016/j.neuron.2013.10.022

Sui, L., Wang, J., & Li, B. M. (2008). Role of the phosphoinositide 3-kinase-Akt-mammalian target of the rapamycin signaling pathway in long-term potentiation and trace fear conditioning memory in rat medial prefrontal cortex. *Learning and Memory*, *15*(10). https://doi.org/10.1101/lm.1067808

Sun, H., Schlondorff, J. S., Brown, E. J., Higgs, H. N., & Pollak, M. R. (2011). Rho activation of mDia formins is modulated by an interaction with inverted formin 2 (INF2). *Proceedings of the National Academy of Sciences of the United States of America*, *108*(7). https://doi.org/10.1073/pnas.1017010108

Sun, S. Y., Rosenberg, L. M., Wang, X., Zhou, Z., Yue, P., Fu, H., & Khuri, F. R. (2005). Activation of Akt and eIF4E survival pathways by rapamycin-mediated mammalian target of rapamycin inhibition. *Cancer Research*, *65*(16). https://doi.org/10.1158/0008-5472.CAN-05-0917

Suraneni, P., Fogelson, B., Rubinstein, B., Noguera, P., Volkmann, N., Hanein, D., Mogilner, A., & Li, R. (2015). A mechanism of leading-edge protrusion in the absence of Arp2/3 complex. *Molecular Biology of the Cell*, *26*(5). https://doi.org/10.1091/mbc.E14-07-1250

Surviladze, Z., Waller, A., Strouse, J. J., Bologa, C., Ursu, O., Salas, V., Parkinson, J. F., Phillips, G. K., Romero, E., Wandinger-Ness, A., Sklar, L. A., Schroeder, C., Simpson, D., Nöth, J., Wang, J., Golden, J., & Aubé, J. (2010). A Potent and Selective Inhibitor of Cdc42 GTPase. In *Probe Reports from the NIH Molecular Libraries Program*.

Takamori, S., Holt, M., Stenius, K., Lemke, E. A., Grønborg, M., Riedel, D., Urlaub, H., Schenck, S., Brügger, B., Ringler, P., Müller, S. A., Rammner, B., Gräter, F., Hub, J. S., De Groot, B. L., Mieskes, G., Moriyama, Y., Klingauf, J., Grubmüller, H., … Jahn, R. (2006). Molecular Anatomy of a Trafficking Organelle. *Cell*, *127*(4). https://doi.org/10.1016/j.cell.2006.10.030

Takei, K., Mundigl, O., Daniell, L., & De Camilli, P. (1996). The synaptic vesicle cycle: A single vesicle budding step involving clathrin and dynamin. *Journal of Cell Biology*, *133*(6). https://doi.org/10.1083/jcb.133.6.1237

Takenawa, T., & Suetsugu, S. (2007). The WASP-WAVE protein network: Connecting the membrane to the cytoskeleton. In *Nature Reviews Molecular Cell Biology* (Vol. 8, Issue 1). https://doi.org/10.1038/nrm2069

Tamura, H., Fukada, M., Fujikawa, A., & Noda, M. (2006). Protein tyrosine phosphatase receptor type Z is involved in hippocampus-dependent memory formation through dephosphorylation at Y1105 on p190 RhoGAP. *Neuroscience Letters*, *399*(1–2). https://doi.org/10.1016/j.neulet.2006.01.045

Tanaka, K., Takeda, S., Mitsuoka, K., Oda, T., Kimura-Sakiyama, C., Maéda, Y., & Narita, A. (2018). Structural basis for cofilin binding and Actin filament disassembly. *Nature Communications*, *9*(1). https://doi.org/10.1038/s41467-018-04290-w

Tanizaki, H., Egawa, G., Inaba, K., Honda, T., Nakajima, S., Moniaga, C. S., Otsuka, A., Ishizaki, T., Tomura, M., Watanabe, T., Miyachi, Y., Narumiya, S., Okada, T., & Kabashima, K. (2010). Rho-mDial pathway is required for adhesion, migration, and T-cell stimulation in dendritic cells. *Blood*, *116*(26). https://doi.org/10.1182/blood-2010-01-264150

Tariq, K., & Luikart, B. W. (2021). Striking a balance: PIP2 and PIP3 signaling in neuronal health and disease. *Exploration of Neuroprotective Therapy*, *1*(2). https://doi.org/10.37349/ent.2021.00008

Thomanetz, V., Angliker, N., Cloëtta, D., Lustenberger, R. M., Schweighauser, M., Oliveri, F., Suzuki, N., & Rüegg, M. A. (2013). Ablation of the mTORC2 component Rictor in brain or Purkinje cells affects size and neuron morphology. *Journal of Cell Biology*, *201*(2). https://doi.org/10.1083/jcb.201205030

Thottacherry, J. J., Kosmalska, A. J., Kumar, A., Vishen, A. S., Elosegui-Artola, A., Pradhan, S., Sharma, S., Singh, P. P., Guadamillas, M. C., Chaudhary, N., Vishwakarma, R., Trepat, X., del Pozo, M. A., Parton, R. G., Rao, M., Pullarkat, P., Roca-Cusachs, P., & Mayor, S. (2018). Mechanochemical feedback control of dynamin independent endocytosis modulates membrane tension in adherent cells. *Nature Communications*, *9*(1). https://doi.org/10.1038/s41467-018-06738-5

Thumkeo, D., Katsura, Y., Nishimura, Y., Kanchanawong, P., Tohyama, K., Ishizaki, T., Kitajima, S., Takahashi, C., Hirata, T., Watanabe, N., Krummel, M. F., & Narumiya, S. (2020). MDia1/3-dependent Actin polymerization spatiotemporally controls LAT phosphorylation by Zap70 at the immune synapse. *Science Advances*, *6*(1).

https://doi.org/10.1126/sciadv.aay2432

Thumkeo, D., Shinohara, R., Watanabe, K., Takebayashi, H., Toyoda, Y., Tohyama, K., Ishizaki, T., Furuyashiki, T., & Narumiya, S. (2011). Deficiency of mDia, an Actin nucleator, disrupts integrity of neuroepithelium and causes periventricular dysplasia. *PLoS ONE*, *6*(9). https://doi.org/10.1371/journal.pone.0025465

Tkachenko, E., Sabouri-Ghomi, M., Pertz, O., Kim, C., Gutierrez, E., MacHacek, M., Groisman, A., Danuser, G., & Ginsberg, M. H. (2011). Protein kinase A governs a RhoA-RhoGDI protrusion-retraction pacemaker in migrating cells. *Nature Cell Biology*, *13*(6). https://doi.org/10.1038/ncb2231

Toei, M., Saum, R., & Forgac, M. (2010). Regulation and isoform function of the V-ATPases. In *Biochemistry* (Vol. 49, Issue 23). https://doi.org/10.1021/bi100397s

Toledo, A., Zolessi, F. R., & Arruti, C. (2013). A Novel Effect of MARCKS Phosphorylation by Activated PKC: The Dephosphorylation of Its Serine 25 in Chick Neuroblasts. *PLoS ONE*, *8*(4). https://doi.org/10.1371/journal.pone.0062863

Tomasevic, N., Jia, Z., Russell, A., Fujii, T., Hartman, J. J., Clancy, S., Wang, M., Beraud, C., Wood, K. W., & Sakowicz, R. (2007). Differential regulation of WASP and N-WASP by Cdc42, Rac1, Nck, and PI(4,5)P2. *Biochemistry*, *46*(11). https://doi.org/10.1021/bi062152y

Tominaga, T., Sahai, E., Chardin, P., McCormick, F., Courtneidge, S. A., & Alberts, A. S. (2000). Diaphanous-related formins bridge Rho GTPase and Src tyrosine kinase signaling. *Molecular Cell*, *5*(1). https://doi.org/10.1016/S1097-2765(00)80399-8

Toschi, A., Lee, E., Xu, L., Garcia, A., Gadir, N., & Foster, D. A. (2009). Regulation of mTORC1 and mTORC2 Complex Assembly by Phosphatidic Acid: Competition with Rapamycin. *Molecular and Cellular Biology*, *29*(6). https://doi.org/10.1128/mcb.00782-08

Toyoda, Y., Shinohara, R., Thumkeo, D., Kamijo, H., Nishimaru, H., Hioki, H., Kaneko, T., Ishizaki, T., Furuyashiki, T., & Narumiya, S. (2013). EphA4-dependent axon retraction and midline localization of Ephrin-B3 are disrupted in the spinal cord of mice lacking mDia1 and mDia3 in combination. *Genes to Cells*, *18*(10). https://doi.org/10.1111/gtc.12081

Tsuji, T., Ishizaki, T., Okamoto, M., Higashida, C., Kimura, K., Furuyashiki, T., Arakawa, Y., Birge, R. B., Nakamoto, T., Hirai, H., & Narumiya, S. (2002). ROCK and mDia1 antagonize in Rho-dependent Rac activation in Swiss 3T3 fibroblasts. *Journal of Cell Biology*, *157*(5). https://doi.org/10.1083/jcb.200112107

Tyckaert, F., Zanin, N., Morsomme, P., & Renard, H. F. (2022). Rac1, the Actin cytoskeleton and microtubules are key players in clathrin-independent endophilin-A3-mediated endocytosis. *Journal of Cell Science*, *135*(14). https://doi.org/10.1242/jcs.259623

Ulrichs, H., Gaska, I., & Shekhar, S. (2023). Multicomponent regulation of Actin barbed end assembly by twinfilin, formin and capping protein. *Nature Communications*, *14*(1). https://doi.org/10.1038/s41467-023-39655-3

Van Den Bogaart, G., Meyenberg, K., Risselada, H. J., Amin, H., Willig, K. I., Hubrich, B. E., Dier, M., Hell, S. W., Grubmüller, H., Diederichsen, U., & Jahn, R. (2011). Membrane protein sequestering by ionic protein-lipid interactions. *Nature*, *479*(7374). https://doi.org/10.1038/nature10545

Van der Kloot, W. (1991). The regulation of quantal size. In *Progress in Neurobiology* (Vol. 36, Issue 2). https://doi.org/10.1016/0301-0082(91)90019-W

Vaughan, E. M., Miller, A. L., Yu, H. Y. E., & Bement, W. M. (2011). Control of local Rho GTPase crosstalk by Abr. *Current Biology*, *21*(4). https://doi.org/10.1016/j.cub.2011.01.014

Verbeek, D. S., Goedhart, J., Bruinsma, L., Sinke, R. J., & Reits, E. A. (2008). PKCγ mutations in spinocerebellar ataxia type 14 affect C1 domain accessibility and kinase activity leading to aberrant MAPK signaling. *Journal of Cell Science*, *121*(14). https://doi.org/10.1242/jcs.027698

Verstegen, A. M. J., Tagliatti, E., Lignani, G., Marte, A., Stolero, T., Atias, M., Corradi, A., Valtorta, F., Gitler, D., Onofri, F., Fassio, A., & Benfenati, F. (2014). Phosphorylation of synapsin I by cyclin-dependent kinase-5 sets the ratio between the resting and recycling pools of synaptic vesicles at hippocampal synapses. *Journal of Neuroscience*, *34*(21). https://doi.org/10.1523/JNEUROSCI.3973-13.2014

Verstreken, P., Koh, T. W., Schulze, K. L., Zhai, R. G., Hiesinger, P. R., Zhou, Y., Mehta, S. Q., Cao, Y., Roos, J., & Bellen, H. J. (2003). Synaptojanin is recruited by endophilin to promote synaptic vesicle uncoating. *Neuron*, *40*(4). https://doi.org/10.1016/S0896-6273(03)00644-5

Vicente-Manzanares, M., Ma, X., Adelstein, R. S., & Horwitz, A. R. (2009). Non-muscle myosin II takes centre stage in cell adhesion and migration. In *Nature Reviews Molecular Cell Biology* (Vol. 10, Issue 11). https://doi.org/10.1038/nrm2786

Vicente-Manzanares, M., Newell-Litwa, K., Bachir, A. I., Whitmore, L. A., & Horwitz, A. R. (2011). Myosin IIA/IIB restrict adhesive and protrusive signaling to generate front-back polarity in migrating cells. *Journal of Cell Biology*, *193*(2). https://doi.org/10.1083/jcb.201012159

Vicidomini, G., Bianchini, P., & Diaspro, A. (2018). STED super-resolved microscopy. In *Nature Methods* (Vol. 15, Issue 3). https://doi.org/10.1038/nmeth.4593

Vidali, L., Van Gisbergen, P. A. C., Guérin, C., Franco, P., Li, M., Burkart, G. M., Augustine, R. C., Blanchoin, L., & Bezanilla, M. (2009). Rapid formin-mediated Actin-filament elongation is essential for polarized plant cell growth. *Proceedings of the National Academy of Sciences of the United States of America*, *106*(32). https://doi.org/10.1073/pnas.0901170106

Waite, K., & Eickholt, B. J. (2010). The neurodevelopmental implications of PI3K signaling. *Current Topics in Microbiology and Immunology*, *346*(1). https://doi.org/10.1007/82-2010-82

Wallar, B. J., & Alberts, A. S. (2003). The formins: Active scaffolds that remodel the cytoskeleton. In *Trends in Cell Biology* (Vol. 13, Issue 8). https://doi.org/10.1016/S0962-8924(03)00153-3

Walter, A. M., Müller, R., Tawfik, B., Wierda, K. D., Pinheiro, P. S., Nadler, A., McCarthy, A. W., Ziomkiewicz, I., Kruse, M., Reither, G., Rettig, J., Lehmann, M., Haucke, V., Hille, B., Schultz, C., & Sørensen, J. B. (2017). Phosphatidylinositol 4,5-bisphosphate optical uncaging potentiates exocytosis. *ELife*, *6*. https://doi.org/10.7554/eLife.30203

Walther, T. C., Brickner, J. H., Aguilar, P. S., Bernales, S., Pantoja, C., & Walter, P. (2006). Eisosomes mark static sites of endocytosis. *Nature*, *439*(7079). https://doi.org/10.1038/nature04472

Wan, X., Harris, J. A., & Morris, C. E. (1995). Responses of neurons to extreme osmomechanical stress. *The Journal of Membrane Biology*, *145*(1). https://doi.org/10.1007/BF00233304

Wang, C., Navab, R., Iakovlev, V., Leng, Y., Zhang, J., Tsao, M. S., Siminovitch, K., McCready, D. R., & Done, S. J. (2007). Abelson interactor protein-1 positively regulates breast cancer cell proliferation, migration, and invasion. *Molecular Cancer Research*, *5*(10). https://doi.org/10.1158/1541-7786.MCR-06-0391

Wang, C., Tran-Thanh, D., Moreno, J. C., Cawthorn, T. R., Jacks, L. M., Wang, D. Y., McCready, D. R., & Done, S. J. (2011). Expression of Abl interactor 1 and its prognostic significance in breast cancer: A tissue-array-based investigation. *Breast Cancer Research and Treatment*, *129*(2). https://doi.org/10.1007/s10549-010-1241-0

Wang, D., Zhang, L., Zhao, G., Wahlström, G., Heino, T. I., Chen, J., & Zhang, Y. Q. (2010). Drosophila twinfilin is required for cell migration and synaptic endocytosis. *Journal of Cell Science*, *123*(9). https://doi.org/10.1242/jcs.060251

Wang, Y. H., Collins, A., Guo, L., Smith-Dupont, K. B., Gai, F., Svitkina, T., & Janmey, P. A. (2012). Divalent cation-induced cluster formation by polyphosphoinositides in model membranes. *Journal of the American Chemical Society*, *134*(7). https://doi.org/10.1021/ja208640t

Wang, Z., Guo, W., Li, L., Luk'Yanchuk, B., Khan, A., Liu, Z., Chen, Z., & Hong, M. (2011). Optical virtual imaging at 50 nm lateral resolution with a white-light nanoscope. *Nature Communications*, *2*(1). https://doi.org/10.1038/ncomms1211

Watanabe, N., Kato, T., Fujita, A., Ishizaki, T., & Narumiya, S. (1999). Cooperation between mDia1 and ROCK in Rho-induced Actin reorganization. *Nature Cell Biology*, *1*(3). https://doi.org/10.1038/11056

Watanabe, S., Liu, Q., Davis, M. W., Hollopeter, G., Thomas, N., Jorgensen, N. B., & Jorgensen, E. M. (2013). Ultrafast endocytosis at Caenorhabditis elegans neuromuscular junctions. *ELife*, *2013*(2). https://doi.org/10.7554/eLife.00723

Watanabe, S., Mamer, L. E., Raychaudhuri, S., Luvsanjav, D., Eisen, J., Trimbuch, T., Söhl-Kielczynski, B., Fenske, P., Milosevic, I., Rosenmund, C., & Jorgensen, E. M. (2018). Synaptojanin and Endophilin Mediate Neck Formation during Ultrafast Endocytosis. *Neuron*, *98*(6). https://doi.org/10.1016/j.neuron.2018.06.005

Watanabe, S., Rost, B. R., Camacho-Pérez, M., Davis, M. W., Söhl-Kielczynski, B., Rosenmund, C., & Jorgensen, E. M. (2013).

Ultrafast endocytosis at mouse hippocampal synapses. *Nature*, *504*(7479). https://doi.org/10.1038/nature12809

Watanabe, S., Trimbuch, T., Camacho-Pérez, M., Rost, B. R., Brokowski, B., Söhl-Kielczynski, B., Felies, A., Davis, M. W., Rosenmund, C., & Jorgensen, E. M. (2014). Clathrin regenerates synaptic vesicles from endosomes. *Nature*, *515*(7526). https://doi.org/10.1038/nature13846

Waugh, R. E., & Bauserman, R. G. (1995). Physical measurements of bilayer-skeletal separation forces. *Annals of Biomedical Engineering*, *23*(3). https://doi.org/10.1007/BF02584431

Wenk, M. R., & De Camilli, P. (2004). Protein-lipid interactions and phosphoinositide metabolism in membrane traffic: Insights from vesicle recycling in nerve terminals. In *Proceedings of the National Academy of Sciences of the United States of America* (Vol. 101, Issue 22). https://doi.org/10.1073/pnas.0401874101

Westendorf, J. J. (2001). The Formin/Diaphanous-related Protein, FHOS, Interacts with Rac1 and Activates Transcription from the Serum Response Element. *Journal of Biological Chemistry*, *276*(49). https://doi.org/10.1074/jbc.M105162200

Whalley, H. J., Porter, A. P., Diamantopoulou, Z., White, G. R. M., Castañeda-Saucedo, E., & Malliri, A. (2015). Cdk1 phosphorylates the Rac activator Tiam1 to activate centrosomal Pak and promote mitotic spindle formation. *Nature Communications*, *6*. https://doi.org/10.1038/ncomms8437

Wilhelm, B. G., Mandad, S., Truckenbrodt, S., Kroḧnert, K., Schäfer, C., Rammner, B., Koo, S. J., Claßen, G. A., Krauss, M., Haucke, V., Urlaub, H., & Rizzoli, S. O. (2014). Composition of isolated synaptic boutons reveals the amounts of vesicle trafficking proteins. *Science*, *344*(6187). https://doi.org/10.1126/science.1252884

Wittinghofer, A., & Vetter, I. R. (2011). Structure-function relationships of the G domain, a canonical switch motif. *Annual Review of Biochemistry*, *80*. https://doi.org/10.1146/annurev-biochem-062708-134043

Wohnsland, F., Schmitz, A. A. P., Steinmetz, M. O., Aebi, U., & Vergères, G. (2000). Interaction between Actin and the effector peptide of MARCKS-related protein. Identification of functional amino acid segments. *Journal of Biological Chemistry*, *275*(27). https://doi.org/10.1074/jbc.M910298199

Wong, K. W., Mohammadi, S., & Isberg, R. R. (2006). Disruption of RhoGDI and RhoA regulation by a Rac1 specificity switch mutant. *Journal of Biological Chemistry*, *281*(52). https://doi.org/10.1074/jbc.M605387200

Wu, L. G., & Chan, C. Y. (2022). Multiple Roles of Actin in Exo- and Endocytosis. In *Frontiers in Synaptic Neuroscience* (Vol. 14). https://doi.org/10.3389/fnsyn.2022.841704

Wu, L. G., Hamid, E., Shin, W., & Chiang, H. C. (2014). Exocytosis and endocytosis: Modes, functions, and coupling mechanisms*. In *Annual Review of Physiology* (Vol. 76). https://doi.org/10.1146/annurev-physiol-021113-170305

Wu, X. S., Elias, S., Liu, H., Heureaux, J., Wen, P. J., Liu, A. P., Kozlov, M. M., & Wu, L. G. (2017). Membrane Tension Inhibits Rapid and Slow Endocytosis in Secretory Cells. *Biophysical Journal*, *113*(11). https://doi.org/10.1016/j.bpj.2017.09.035

Wu, X. S., Lee, S. H., Sheng, J., Zhang, Z., Zhao, W. D., Wang, D., Jin, Y., Charnay, P., Ervasti, J. M., & Wu, L. G. (2016). Actin Is Crucial for All Kinetically Distinguishable Forms of Endocytosis at Synapses. *Neuron*, *92*(5). https://doi.org/10.1016/j.neuron.2016.10.014

Wu, X. S., Zhang, Z., Zhao, W. D., Wang, D., Luo, F., & Wu, L. G. (2014). Calcineurin is universally involved in vesicle endocytosis at neuronal and nonneuronal secretory cells. *Cell Reports*, *7*(4). https://doi.org/10.1016/j.celrep.2014.04.020

Xu, Y., Moseley, J. B., Sagot, I., Poy, F., Pellman, D., Goode, B. L., & Eck, M. J. (2004). Crystal structures of a formin homology-2 domain reveal a tethered dimer architecture. *Cell*, *116*(5). https://doi.org/10.1016/S0092-8674(04)00210-7

Yamamoto, K., Seki, T., Adachi, N., Takahashi, T., Tanaka, S., Hide, I., Saito, N., & Sakai, N. (2010). Mutant protein kinase C gamma that causes spinocerebellar ataxia type 14 (SCA14) is selectively degraded by autophagy. *Genes to Cells*, *15*(5). https://doi.org/10.1111/j.1365-2443.2010.01395.x

Yang, B., Radel, C., Hughes, D., Kelemen, S., & Rizzo, V. (2011). P190 RhoGTPase-activating protein links the β1 integrin/caveolin-1 mechanosignaling complex to RhoA and Actin remodeling. *Arteriosclerosis, Thrombosis, and Vascular Biology*, *31*(2). https://doi.org/10.1161/ATVBAHA.110.217794

Yang, C., Czech, L., Gerboth, S., Kojima, S. I., Scita, G., & Svitkina, T. (2007). Novel roles of formin mDia2 in lamellipodia and

filopodia formation in motile cells. *PLoS Biology*, *5*(11). https://doi.org/10.1371/journal.pbio.0050317

Yang, F., Moss, L. G., & Phillips, G. N. (1996). The Molecular Structure of Green Fluorescent Protein. *Nature Biotechnology*, *14*(10). https://doi.org/10.1038/nbt1096-1246

Yang, H., Rudge, D. G., Koos, J. D., Vaidialingam, B., Yang, H. J., & Pavletich, N. P. (2013). MTOR kinase structure, mechanism and regulation. *Nature*, *497*(7448). https://doi.org/10.1038/nature12122

Yang, J., Cron, P., Thompson, V., Good, V. M., Hess, D., Hemmings, B. A., & Barford, D. (2002). Molecular mechanism for the regulation of protein kinase B/Akt by hydrophobic motif phosphorylation. *Molecular Cell*, *9*(6). https://doi.org/10.1016/S1097-2765(02)00550-6

Yang, Q., Zhang, X. F., Van Goor, D., Dunn, A. P., Hyland, C., Medeiros, N., & Forscher, P. (2013). Protein kinase C activation decreases peripheral Actin network density and increases central nonmuscle myosin II contractility in neuronal growth cones. *Molecular Biology of the Cell*, *24*(19). https://doi.org/10.1091/mbc.E13-05-0289

Yao, L. H., Rao, Y., Bang, C., Kurilova, S., Varga, K., Wang, C. Y., Weller, B. D., Cho, W., Cheng, J., & Gong, L. W. (2013). Actin polymerization does not provide direct mechanical forces for vesicle fission during clathrin-mediated endocytosis. *Journal of Neuroscience*, *33*(40). https://doi.org/10.1523/JNEUROSCI.2171-13.2013

Yayoshi-Yamamoto, S., Taniuchi, I., & Watanabe, T. (2000). FRL, a Novel Formin-Related Protein, Binds to Rac and Regulates Cell Motility and Survival of Macrophages. *Molecular and Cellular Biology*, *20*(18). https://doi.org/10.1128/mcb.20.18.6872-6881.2000

Yu, M., Yuan, X., Lu, C., Le, S., Kawamura, R., Efremov, A. K., Zhao, Z., Kozlov, M. M., Sheetz, M., Bershadsky, A., & Yan, J. (2017). MDia1 senses both force and torque during F-Actin filament polymerization. *Nature Communications*, *8*(1). https://doi.org/10.1038/s41467-017-01745-4

Yuan, J., & Fang, X. (2014). Super-resolved fluorescence microscopy-nanoscopy. *Chemistry Bulletin / Huaxue Tongbao*, *77*(11).

Zenke, F. T., Krendel, M., DerMardirossian, C., King, C. C., Bohl, B. P., & Bokoch, G. M. (2004). p21-activated Kinase 1 Phosphorylates and Regulates 14-3-3 Binding to GEF-H1, a Microtubule-localized Rho Exchange Factor. *Journal of Biological Chemistry*, *279*(18). https://doi.org/10.1074/jbc.M400084200

Zhang, B., & Zheng, Y. (1998). Regulation of RhoA GTP hydrolysis by the GTPase-activating proteins p190, p50RhoGAP, Bcr, and 3BP-1. *Biochemistry*, *37*(15). https://doi.org/10.1021/bi9718447

Zhang, K., Huang, M., Li, A., Wen, J., Yan, L., Li, Y., Guo, L., Senthil, K. S., Zhou, Y., Chen, G., Liu, Y., Zhang, X., Yao, X., Qin, D., & Su, H. (2023). DIAPH3 condensates formed by liquid-liquid phase separation act as a regulatory hub for stress-induced Actin cytoskeleton remodeling. *Cell Reports*, *42*(1). https://doi.org/10.1016/j.celrep.2022.111986

Zhang, M., & Augustine, G. J. (2021). Synapsins and the synaptic vesicle reserve pool: Floats or anchors? In *Cells* (Vol. 10, Issue 3). https://doi.org/10.3390/cells10030658

Zhang, Q., Li, Y., & Tsien, R. W. (2009). The dynamic control of kiss-and-run and vesicular reuse probed with single nanoparticles. *Science*, *323*(5920). https://doi.org/10.1126/science.1167373

Zhang, W., & Benson, D. L. (2001). Stages of synapse development defined by dependence on F-Actin. *Journal of Neuroscience*, *21*(14). https://doi.org/10.1523/jneurosci.21-14-05169.2001

Zhang, W., Ciorraga, M., Mendez, P., Retana, D., Boumedine-Guignon, N., Achón, B., Russier, M., Debanne, D., & Garrido, J. J. (2021). Formin Activity and mDia1 Contribute to Maintain Axon Initial Segment Composition and Structure. *Molecular Neurobiology*, *58*(12). https://doi.org/10.1007/s12035-021-02531-6

Zhao, X., Wang, D., Liu, X., Liu, L., Song, Z., Zhu, T., Adams, G., Gao, X., Tian, R., Huang, Y., Chen, R., Wang, F., Liu, D., Yu, X., Chen, Y., Chen, Z., Teng, M., Ding, X., & Yao, X. (2013). Phosphorylation of the Bin, Amphiphysin, and RSV161/167 (BAR) domain of ACAP4 regulates membrane tubulation. *Proceedings of the National Academy of Sciences of the United States of America*, *110*(27). https://doi.org/10.1073/pnas.1217727110

Zhou, Z., Meng, Y., Asrar, S., Todorovski, Z., & Jia, Z. (2009). A critical role of Rho-kinase ROCK2 in the regulation of spine and synaptic function. *Neuropharmacology*, *56*(1). https://doi.org/10.1016/j.neuropharm.2008.07.031

Zhu, Y., Xu, J., & Heinemann, S. F. (2009). Two Pathways of Synaptic Vesicle Retrieval Revealed by Single-Vesicle Imaging.

Neuron, *61*(3). https://doi.org/10.1016/j.neuron.2008.12.024

Ziemba, B. P., Burke, J. E., Masson, G., Williams, R. L., & Falke, J. J. (2016). Regulation of PI3K by PKC and MARCKS: Single-Molecule Analysis of a Reconstituted Signaling Pathway. *Biophysical Journal*, *110*(8). https://doi.org/10.1016/j.bpj.2016.03.001

Zigmond, S. H., Evangelists, M., Boone, C., Yang, C., Dar, A. C., Sicheri, F., Forkey, J., & Pring, M. (2003). Formin Leaky Cap Allows Elongation in the Presence of Tight Capping Proteins. *Current Biology*, *13*(20). https://doi.org/10.1016/j.cub.2003.09.057

9. Appendix

9.1. Supplemental Figures

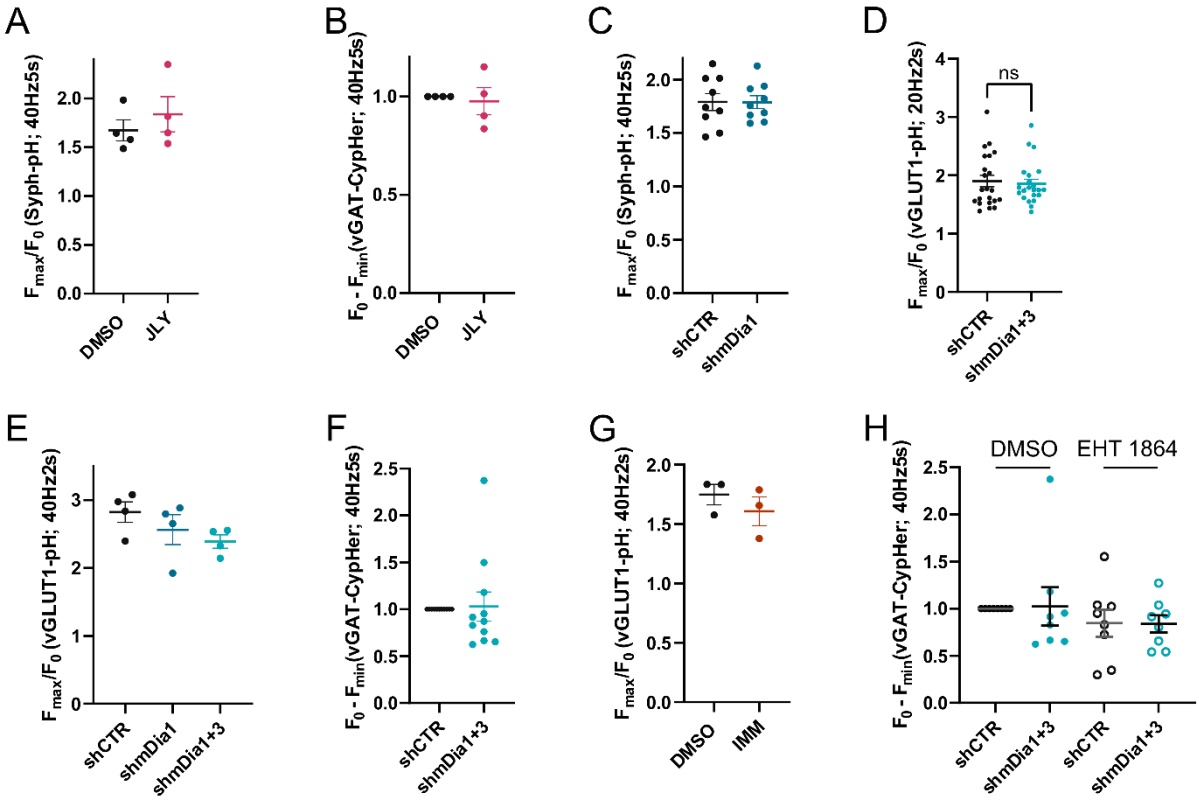

Figure 80: Exocytosis is not altered upon Actin Perturbation.
A: Maxima of background-corrected Syph-pHluorin fluorescence traces (surface normalized) for neurons treated with 0.1 % DMSO (1.7 ± 0.1) or JLY cocktail (1.8 ± 0.2) in response to 200 AP stimulation (40 Hz, 5 s). N = 4; n_{DMSO} = 23 videos; n_{JLY} = 36 videos.
B: Minima of background-corrected vGAT-CypHer fluorescence traces (surface normalization) for neurons treated with 0.1 % DMSO or JLY cocktail (1.0 ± 0.1) in response to 200 AP stimulation (40 Hz, 5 s). Values for DMSO were set to 1. N = 4; n_{DMSO} = 23 videos; n_{JLY} = 29 videos.
Legend continued on next page.

C: Maxima of background-corrected Syph-pHluorin fluorescence traces (surface normalized) for neurons transfected with shCTR (1.8 ± 0.1) or shmDia1 (1.8 ± 0.1) in response to 200 AP stimulation (40 Hz, 5 s). N = 9; n_{shCTR} = 49 videos; $n_{shmDia1}$ = 42 videos.
D: Maxima of background-corrected vGLUT1-pHluorin fluorescence traces (surface normalized) for neurons transduced with shCTR (1.9 ± 0.1) or shmDia1+3 (1.9 ± 0.1) in response to 40 AP stimulation (20 Hz, 2 s). N = 22; n_{shCTR} = 105 videos and $n_{shmDia1+3}$ = 128 videos.
E: Maxima of background-corrected vGLUT1-pHluorin fluorescence traces (surface normalized) for neurons transduced with shCTR (2.8 ± 0.2), shmDia1 (2.6 ± 0.2), or shmDia1+3 (2.4 ± 0.1) in response to 80 AP stimulation (40 Hz, 2 s). N = 4; n_{shCTR} = 12 videos; $n_{shmDia1}$ = 15 videos and $n_{shmDia1+3}$ = 18 videos.
F: Minima of background-corrected vGAT-CypHer fluorescence traces (surface normalized) for neurons transduced with shCTR or shmDia1+3 (1.0 ± 0.2) in response to 200 AP stimulation (40 Hz, 5 s). Values for shCTR were set to 1. N = 11; n_{shCTR} = 45 videos and $n_{shmDia1+3}$ = 42 videos.
G: Maxima of background-corrected vGLUT1-pHluorin fluorescence traces (surface normalized) for neurons treated with 0.1 % DMSO (1.7 ± 0.1) or mDia activator (IMM; 1.6 ± 0.1) in response to 80 AP stimulation (40 Hz, 2 s). N = 3; n_{DMSO} = 18 videos; n_{IMM} = 16 videos.
H: Minima of background-corrected vGAT-CypHer fluorescence traces (surface normalized) for neurons treated with 0.1 % DMSO (1.0 ± 0.2 for shmDia1+3) or 10 µM Rac1 Inhibitor (EHT 1864; 0.8 ± 0.1 for shCTR; 0.8 ± 0.1 for shmDia1+3) in response to 200 AP stimulation (40 Hz, 5 s). Data represent mean ± SEM. Values were normalised to DMSO treated shCTR (set to 1). N = 8; $n_{shCTR + DMSO}$ = 46 videos, $n_{shmDia1+3 + DMSO}$ = 45 videos, $n_{shCTR + EHT\ 1864}$ = 42 videos, $n_{shmDia1+3 + EHT\ 1864}$ = 43 videos.

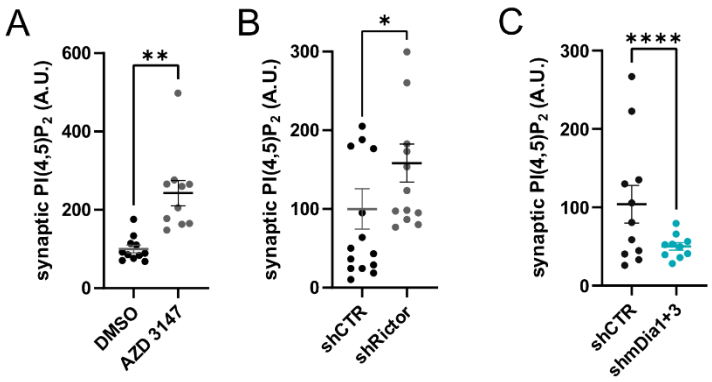

Figure 81: Inverse Alterations in PI(4,5)P_2 Signaling induced by mDia1/3 and mTORC2.
A: Analysis of synaptic PI(4,5)P_2 abundance using the recombinant PI(4,5)P_2-binding domain eGFP-PH-PLCδ1 in a mask of vGLUT1 staining in neurons treated with 0.1% DMSO (100.0 ± 9.7) or 10 nM AZD 3147 (242.5 ± 32.4; $p < 0.01$ one sample t-test) for 2h. N =1, n =10 images.
B: Analysis of synaptic PI(4,5)P_2 abundance in neurons transduced with shCTR (100.0 ± 25.7) or shRictor (158.2± 24.2; $p < 0.05$ one sample t-test). N =1, n =12 images.
C: Analysis of synaptic PI(4,5)P_2 abundance in neurons transduced with shCTR (100.0 ± 13.1) or shmDia1+3 ((48.2± 4.6) $p < 0.0001$ one sample t-test). N =1, n =10 images.
Experiments and analysis were performed as described in (Bolz et al., 2023)

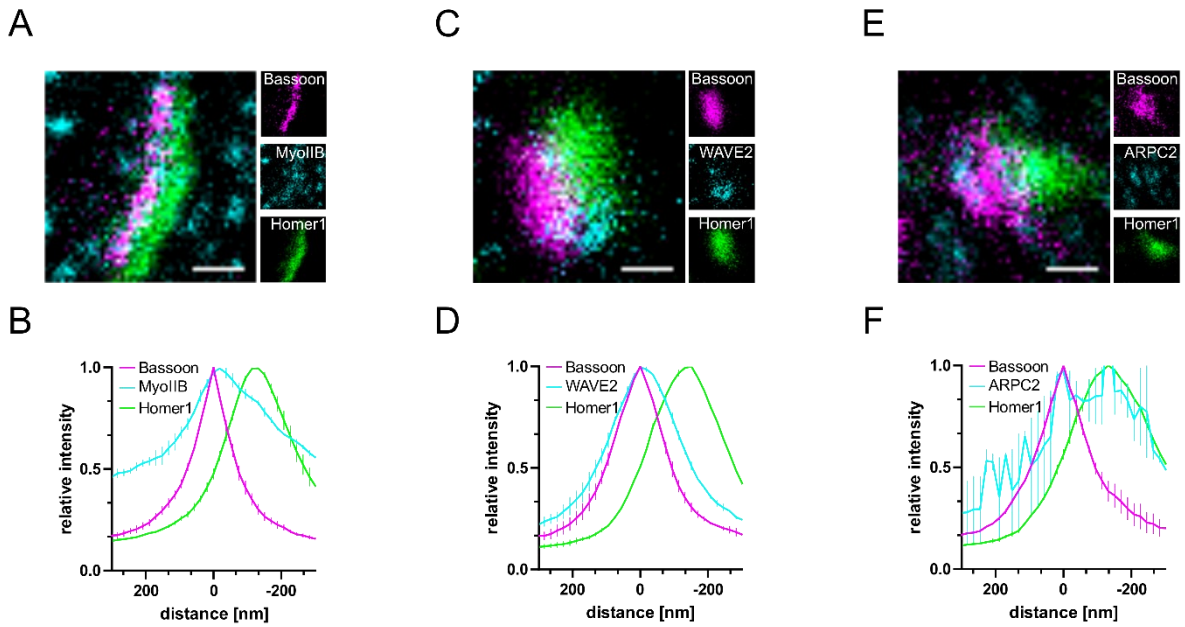

Figure 82: Cytoskeletal Proteins localize at the presynaptic Bouton.
A: Representative three-channel time-gated STED image of a synapse from hippocampal cultures fixed and immunostained for Bassoon (presynaptic marker, magenta), Myosin IIB (cyan) and Homer1 (postsynaptic marker, green). Scale bar, 250 nm.
B: Averaged normalized line profiles for synaptic distribution of Myosin IIB and Homer1 relative to Bassoon (Maximum set to 0 nm). N = 3, n = 267 synapses.
C: Representative three-channel time-gated STED image of a synapse from hippocampal cultures fixed and immunostained for Bassoon (presynaptic marker, magenta), WAVE2 (cyan) and Homer1 (postsynaptic marker, green). Scale bar, 250 nm.
D: Averaged normalized line profiles for synaptic distribution of WAVE2 and Homer1 relative to Bassoon (Maximum set to 0 nm). N = 2, n = 71 synapses.
E: Representative three-channel time-gated STED image of a synapse from hippocampal cultures fixed and immunostained for Bassoon (presynaptic marker, magenta), ARPC2 (cyan) and Homer1 (postsynaptic marker, green). Scale bar, 250 nm.
F: Averaged normalized line profiles for synaptic distribution of ARPC2 and Homer1 relative to Bassoon (Maximum set to 0 nm). N = 2, n = 66 synapses.

9.2. Supplemental Tables

Table 10: Selected Protein Hits from mDia1 Immunoprecipitates.

Gene/protein	Fold change [log2]	p-value [-log10]
mDia1	7.49	3.04
Eno2	3.03	1.25
Fasn	2.99	1.95
Got2	2.96	1.06
Ppia	2.95	1.11
Dsp	2.82	1.66
Rab1;Rab1A	2.67	1.47
Dynamin1	2.63	1.00
Pacsin1	2.62	1.14
Atp6v1a	2.57	1.12
Gstm1;Gstm7;Gstm2	2.51	2.37
Aco2	2.51	1.19

Ckb	2.50	0.77
Gnao1	2.50	0.85
Calm1	2.45	1.00
Cycs	2.44	1.03
Aldoa;Aldoart1	2.44	0.99
Dync1h1	2.41	1.10
Ywhaz	2.39	0.98
Ighg1	2.33	1.62
Pkp1	2.33	1.20
Pgk1	2.27	1.00
Hsp90aa1	2.26	1.23
Jup	2.25	1.58
Cnp	2.25	0.98
Ywhab	2.24	0.96
Amphiphysin	2.24	1.37
Cdc42bpa	2.23	1.62
Macf1	2.23	1.21
Gnb1	2.23	0.67
Anp32a;Anp32c	2.23	1.03
Tomm70a	2.22	1.50
Map1a	2.22	1.38
Map1b	2.21	1.09
Snca	2.20	1.74
Stip1	2.20	1.44
Dnajc6	2.20	1.75
Ap2a2	2.18	1.35
Hsp90b1	2.17	1.20
Rab3a	2.16	0.92
Sep 07	2.15	0.93
Itpr1	2.14	1.36
Cadm2	2.13	0.99
Set	2.12	1.04
Capza2	2.12	1.13
Ap2a1	2.00	1.36
Stx1b	2.00	1.03
Tnr	2.00	0.77
Abi1	1.99	1.07

Table 11: Selected altered Phospho-sites in lysates of mDia1/3-depleted Neurons.

Gene names	Phospho-sites	Enrichment (shmDia1+3/shCTR)
Abi1	183	infinite
Abi2	177	3.18
Abi2	221	infinite

Abl2	621	12.98
Abl2	785	infinite
Add1	358	1.85
Add1	610	1.97
Add1	12	6.13
Add2	60	0.59
Add2	594	5.23
Add2	532	8.18
Add2	700	infinite
Add2	11	infinite
Add3	12	3.26
Add3	681	4.97
Add3	673	infinite
Add3	423	infinite
Add3;Add2;Add1	693;712;724	2.39
Amph	310	4.07
Amph	500	9.72
Amph	262	infinite
Apc	1359	3.65
Apc	2713	4.00
Apc	2260	4.48
Apc	1040	7.58
Appl1	401	1.64
Arfgap1	342	infinite
Arhgap1	51	6.21
Arhgap21	609	infinite
Arhgap21	453	infinite
Arhgap32	892	infinite
Arhgap35	1105	infinite
Arhgap39	597	infinite
Arhgdia	7	2.75
Arhgdia	34	infinite
Arhgef12	736	1.60
Arhgef2	885	2.43
Arhgef7	228	infinite
Cfl1	3	1.71
Cfl2	3	3.71
Fmn2	724	4.54
Fmnl1	1021	12.67
Fmnl1	509	infinite
Gap43	142	0.52

Gap43	41	5.95
Gap43	172	6.00
Gap43	96	6.59
Gap43	95	12.87
Gsk3a;Gsk3b	279;216	2.56
Gsk3a;Gsk3b	278;215	infinite
Gsk3b	9	2.40
Itsn1	897;906	2.66
Itsn1	203	infinite
Itsn1	971	infinite
Mapt	502	1.34
Mapt	648	2.12
Mapt	509	2.34
Mapt	708	2.44
Mapt	491	5.17
Mapt	554	5.42
Mapt	527	5.62
Mapt	473	6.06
Mapt	523	6.50
Mapt	490	6.64
Mapt	470	18.37
Mapt	494	infinite
Mapt	506	infinite
Mapt	696	infinite
Marcks	163	1.38
Marcks	138	5.93
Marcks	27	8.20
Marcks	29	11.44
Marcks	113	11.99
Marcks	141	infinite
Prkca	638	1.35
Prkca	319	3.75
Prkce	346	4.41
Prkce	388	4.81
Prkce	710	5.80
Prkce	368	7.82
Prkce	329	infinite
Prkcg	655	1.97
Srgap2	1013	1.73
Sv2a	127	6.24
Syn1	510	1.28

Syn1	67	1.63
Syn1	62	1.82
Syn1	666	2.52
Syn1	427	2.77
Syn1	553	3.40
Syn1	568	5.88
Syn1	437	infinite
Syn1	684	infinite
Syn1	682	infinite
Syn2	546	2.06
Syn2	426	2.47
Syn2	422	infinite
Syn2	420	infinite
Syn3	540	1.84
Synj1	1147	2.67
Synj1	1084	4.25
Synj1	1160	9.13

* infinite: peptide was not found in shCTR

9.3. Abbreviations

ABI	Abelson interactor
ADBE	Activity-dependent bulk endocytosis
ADP	Adenosine diphosphate
AKT	Protein kinase B
AP	Action potential
APC	Adenomatous polyposis coli protein
Arp	Actin-related protein
ATP	Adenosine triphosphate
ATPase	ATP hydrolyzing enzyme
AZ	Active zone
BAR	Bin-amphiphysin-rvs
BCA	Bicinchoninic acid
CA	Consitutively active
Ca^{2+}	Calcium ions
CaN	Calcineurin
CapZ	Capping protein
Cdc42	Cell division cycle 42
CDK5	Cyclin-dependent kinase 5
CIE	Clathrin-independent endocytosis
CME	Clathrin-mediated endocytosis
CTR	Control
DAAM	Dishevelled-associated activator of morphogenesis

DAD	Diaphanous autoregulatory domain
DID	Diaphanous inhibitory domain
DIV	Day in vitro
DMSO	Dimethyl sulfoxide
DN	Dominant negative
Dynamin1-K44A	$Lysine_{44}$ to alanine Dynamin1 variant (GTPase-inactive)
ELVs	Endosome-like vacuoles
EM	Electron microscopy
F	Fluorescence
F_0	Basal fluorescence
F-Actin	Filamentous Actin
FH1	Formin homology 1
FH2	Formin homology 2
FHOD	Formin Homology Domain-containing Protein
F_{max}	Fold increase after stimulation
FMN	Formin
FMNL	Formin-related proteins identified in leukocytes
GABA	gamma-aminobutyric acid
G-Actin	Globular Actin
GAP	GTPase-activating proteins
GAP43	Growth-associated protein 43
GDI	Guanine nucleotide dissociation inhibitors
GDP	Guanosie diphosphate
GEF	Guanine nucleotide exchange factors
GEF-H1	ARHGEF2
GFP	Green fluorescent protein
GSK3β	Glycogen synthase kinase 3 beta
GTP	Guanosine triphosphate
GTPase	GTP hydrolyzing enzyme
HEK293T	Human embryonic kidney 293T cells
IB	Immunoblot
IC	Immunocytochemistry
IMM	Intramimic mDia activator
INF	Inverted Formin
IP	Immunoprecipitation
J	Jasplakinolide
KO	Genetic knockout
L	Latrunculin A
LARG	Leukemia-associated RhoGEF, ARHGEF12
LLPS	Liquid-liquid phase seperation
MARCKS	Myristotylated alanine-rich C kinase substrate
mDia1	Mammalian diaphanous 1, DIAPH1
mDia1-ML	$Methionine_{1182}$ and $leucine_{1185}$ to alanine mDia1 mutant (M1182A + L1185A)
mDia1-VN	$Valine_{161}$ and $asparagine_{165}$ to aspartate mDia1 mutant (V161D + N165D)
mDia1-VNML	mDia1 mutant (V161D + N165D M1182A + L1185A)
mDia3	Mammalian diaphanous 3, DIAPH2

Mock	Non-infected control
MS	Mass spectrometry
mTOR	Mechanistic target of Rapamycin
mTORC1	mTOR complex 1
mTORC2	mTOR complex 2
MyoII	Non-muscle myosin II
norm ΔF	$F\text{-}F_0$ and normalized to ΔF_{max}
NPF	Nucleation-promoting factor
nRFP	Nuclear red fluorescent protein
p190RhoGAP	ARHGAP35
P2'	Synaptosomes
PACSIN	Protein kinase C and casein kinase substrate in neurons
PAK	p21-activated kinase
p-AKT1	$Serine_{347}$-phosphorylated AKT1
PBD	PAK-binding domain
pHluorin	Superecliptic pH-sensitive GFP variant
PI	Posphoinositide
$PI(3,4,5)P_2$	Phosphatidylinositol-3,4,5-bisphosphate
PI(4)P	Phosphatidylinositol-4-phosphate
$PI(4,5)P_2$	Phosphatidylinositol-4,5-bisphosphate
PI3K	Class I phosphoinositide 3-kinases
PKC	Protein kinase C
PSD	Postsynaptic density
PTEN	Phosphatase and tension homolog
Rac1	Ras-related C3 botulinum toxin substrate 1
Rac1-CA	$Glutamine_{44}$ to leucine GTP-locked Rac1 mutant (Q61L)
Rac1-DN	$Threonine_{17}$ to asparagine dominant negative Rac1 mutant (Q61L)
Raptor	Regulatory-associated protein of mTOR
Ras	Rat sarcoma
RBD	Rho-bindng domain
Rho	Ras homologous
RhoA-CA	$Glutamine_{44}$ to leucine GTP-locked RhoA mutant (Q63L)
RhoGDI1	Arhgdia
Rictor	Rapamycin insensitive companion of mTOR
ROCK	Rho-associated kinase
ROI	Region of interest
RRP	Ready-releasable pool
RT	Room temperature
SDS-PAGE	Sodium dodecyl sulfate polyacrylamide gel electrophoresis
SEM	Standard error of the mean
SMIFH2	Small molecule inhibitor of FH2 domain
Srgap2	ARHGAP34
STED	Stimulated emission depletion
SV	Synaptic vesicle
Syph	Synaptophysin

TTX	Tetrodotoxin
UFE	Ultrafast endocytosis
vATPase	vacuolar proton ATPase
vGAT	vesicular GABA transporter
vGLUT1	vesicular glutamate transporter 1
WASP	Wiskott-Aldrich syndrome protein
WAVE	WASP and verprolin homolog
WT	Wild-type
Y	ROCK inhibitor Y-27632
β-PIX	ARHGEF7
τ	Endocytic decay constant; 1/e

9.4. List of Figures

9.5. List of Tables

9.6. Publications

Oevel, K., Hohensee, S., Kumar, A., Rosas-Brugada, I., Bartolini, F., Soykan, T., & Haucke, V. (2024).
Rho GTPase signaling and mDia facilitate endocytosis via presynaptic Actin.
ELife, *12*(RP92755). https://doi.org/10.7554/eLife.92755.3

Oevel, K., Calandra, I., Park, H., Renz, M., Cornelis, R., Hendawy, M., Koeksoy, E., Plajer, V., Roosen, D., Scheu, L., & Stolze, K. (2023).
Sustainable Leibniz – Transforming research practices towards environmental sustainability.
Zenodo. https://doi.org/10.5281/zenodo.7714680